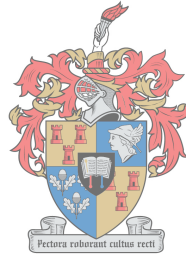


Design of an Electrochemically Reactive HIV DNA Biosensor by use of Hairpin DNA Probes on Carbon Nanofibers.

by

Nicholas Lawrenson



UNIVERSITEIT
iYUNIVESITHI
STELLENBOSCH
UNIVERSITY

Thesis presented in partial fulfilment of the requirements for the degree of Master of Engineering in Electronic Engineering in the Faculty of Engineering at Stellenbosch University

Supervisors: Prof. W.J. Perold
Prof. G. Van Zyl

March 2018

Declaration

By submitting this thesis electronically, I declare that the entirety of the work contained therein is my own, original work, that I am the sole author thereof (save to the extent explicitly otherwise stated), that reproduction and publication thereof by Stellenbosch University will not infringe any third party rights and that I have not previously in its entirety or in part submitted it for obtaining any qualification.

Date: March 2018

Copyright © 2018 Stellenbosch University
All rights reserved

Abstract

A low cost, electrochemical HIV DNA biosensor was investigated using hairpin DNA probes immobilized on carbon nanofibers. The basic biosensor model, as well as electrochemical and optical based biosensor techniques, were explored. The electrochemical and optical techniques were evaluated for use in low-cost HIV DNA detection.

A resistive based electrochemical technique was chosen to detect the presence of HIV single stranded DNA. A carbon nanofiber mat was used as the selected transducer, with hairpin probe DNA immobilized by self assembled monolayers. The self assembled monolayers were formed by gold-thiol bonding where gold was sputter coated onto the carbon nanofibers. The immobilization of the hairpin probe was validated by use of a fluorescent label and confocal microscopy.

A high precision and low current sensing circuit was designed to detect the change in resistance of the transducer during a hybridization event. A user friendly graphic user interface was designed to conduct, display and record all data during testing. A ferrocene labelled hairpin probe was used for all electronic based testing. It is believed that a ferrocene modification will increase electrochemical reactions in biosensors.

It was found that the designed hairpins operated as expected during fluorescent based testing, but it was not possible to obtain an electronic signal. Various post processing methods were explored to increase the chance of detection of HIV DNA and it was found that the sensor was able to detect the addition of a sample solution, but not necessarily HIV DNA.

Various optimizations and alternative solutions were suggested and it is believed that, with some minor changes, a resistive based biosensor to detect HIV DNA is very possible.

Opsomming

'n Lae-koste elektrochemiese MIV DNS biosensor is ondersoek deur middel van haarnaald DNS probes wat aan koolstof nanovesels vasgeheg was. Basiese biosensor modelle, insluitende elektrochemiese en optiese tegnieke, was ondersoek. Die elektrochemiese en optiese tegnieke is geëvalueer vir lae-koste MIV DNS herkenning.

Dit was gekies om gebruik te maak van 'n elektriese weerstand-gebaseerde elektrochemiese meet tegniek om die teenwoordigheid van enkelstring MIV DNS te bepaal. 'n Laag van koolstof nanovesels is gekies as koppelvlak, met DNS haarnaald probes daaraan geheg deur middel van 'n molekulere enkellaag. Die enkellaag is gevorm deur middel van goud-tiol bindings, waar die goud deur 'n plasma deponeringsproses op die nanovesels neergele is. Fluoresente merkers en gefokusde fluoressensie mikroskopie is gebruik om die suksesvolle aanhegting van die haarnaald probes te ondersoek en verifieer.

'n Hoe-akkuraatheid en laestroom meetbaan is ontwerp om die weerstandsverandering in die nanovesel laag waar te neem gedurende die hibridisering-proses. 'n Gebruikersvriendelike grafiese koppelvlak is ook ontwerp om alle gemete data aan 'n gebruiker te vertoon en te stoor vir latere verwerking. Alle elektroniese toetse het gebruik gemaak van ferroseen-germekte haarnaald probes omdat daar geglo word dat elektrochemiese reaksies in biosensors verhoog word deur ferroseen aanpassings.

Die ontwerpte haarnaald probes het soos verwag opgetree gedurende fluoressensie-gebaseerde toetse, maar geen ooreenstemmende elektriese verandering kon gemeet word nie. Verskeie verwerkingsprosesse is ondersoek om die waarskynlikheid dat MIV DNS opgemerk word te verhoog, maar daar is gevind dat die sensor die toevoeging van 'n monster oplossing kon meet, maar nie noodwendig die teenwoordigheid van MIV DNS nie.

Verskeie optimerings en alternatiewe oplossings is voorgestel en daar word geglo dat dit baie moontlik is om met klein veranderings 'n effektiewe weerstand sensor vir MIV DNS te realiseer.

Acknowledgements

The author of this report, Nicholas Lawrenson would like to thank the following people for their contribution to this project.

- Prof Perold, for his enthusiasm and encouragement over the past 2 years, as well as all the advice given regarding designs, report writing and editing.
- Prof van Zyl, for all the help with the biological aspect of the project, countless emails and DNA designs necessary for the project.
- Wessel Croukamp, for all the time spent machining testing baths and other accessories.
- Wynand van Eeden for advice, discussing ideas and many hours helping with PCB and 3D printing designs.
- Christiaan Viviers for all the team work and collaborations in designing the biosensor baths.
- Deon Neveling for the help and training in the microbiology labs and for after hour work.
- Prof Dicks for allowing me to work at the Microbiology Department.
- Alvera Vorster from the CAF DNA Sequencing Unit for initial help and advice with qPCR and DNA based issues.
- Shahieda Isaacs and Mary Grace Katusiime for the many hours spent at Virology doing qPCR validation and sample preparation.
- The CAF SEM Unit for help and training with regard to SEM and EDX.
- The CAF Confocal Unit for hours spent imaging fluorescent probes.
- To my mother and David, for all the help and support they have given me throughout the years, both emotionally and financially.
- Peter Thorrington-Smith, for providing the opportunity to study further and get an Engineering degree and further still, for a Masters degree.

Contents

| | |
|--|------------|
| Declaration | i |
| Abstract | ii |
| Opsomming | iii |
| Acknowledgements | iv |
| Contents | v |
| List of Figures | xii |
| Abbreviations | xvi |
| 1 Introduction | 1 |
| 1.1 HIV (Human Immunodeficiency Virus) | 1 |
| 1.2 Biosensors | 2 |
| 1.3 Thesis Overview | 3 |
| 2 Literature Review | 4 |
| 2.1 Biosensors | 4 |
| 2.1.1 Introduction | 4 |
| 2.1.2 Biosensor Model | 5 |
| 2.1.3 Biorecognition Elements | 6 |
| 2.1.3.1 Enzymes | 6 |
| 2.1.3.2 Antibodies | 6 |
| 2.1.3.3 Aptamers | 6 |
| 2.1.3.4 Hybridization Probes | 7 |
| 2.1.4 Label vs Label-Free Biorecognition | 8 |
| 2.1.5 Immobilization Techniques | 8 |
| 2.1.5.1 Adsorption | 9 |
| 2.1.5.2 SAM (Self-assembled Monolayer) | 9 |
| 2.1.5.3 The Biotin-(Strept)Avidin System | 10 |
| 2.1.5.4 Entrapment | 11 |
| 2.1.6 Blocking | 11 |

| | | |
|----------|--|-----------|
| 2.1.7 | Transducers | 11 |
| 2.1.7.1 | Optical Biosensors | 12 |
| 2.1.7.2 | Electrochemical Biosensors | 14 |
| 2.1.8 | Electrochemical Detection Techniques | 16 |
| 2.1.8.1 | Voltammetry | 16 |
| 2.1.8.2 | EIS (Electrochemical Impedance Spectroscopy) | 18 |
| 2.1.8.3 | Nanowires | 20 |
| 2.1.9 | Biosensor Testing and Standards | 20 |
| 2.1.9.1 | Types of Microbial Testing Performed | 20 |
| 2.1.9.2 | Biosensor "Gold" Standards | 21 |
| 2.2 | Human Immunodeficiency Virus (HIV) | 21 |
| 2.2.1 | HIV Diagnosis | 24 |
| 2.2.1.1 | HIV Screening Tests | 24 |
| 2.3 | DNA Introduction | 30 |
| 2.3.1 | DNA Definition | 30 |
| 2.3.1.1 | DNA Structure | 30 |
| 2.3.1.2 | DNA Directionality | 32 |
| 2.3.1.3 | DNA Size Comparison | 33 |
| 2.3.1.4 | DNA Temperature of Melting (T_m) | 33 |
| 2.3.1.5 | DNA Self Dimers | 34 |
| 2.3.2 | DNA Based Biosensors | 34 |
| 2.4 | HIV DNA Biosensor Research | 35 |
| 2.4.1 | A label-free electrochemical biosensor for detection of HIV related gene based on interaction between DNA and protein | 35 |
| 2.4.2 | Coupling of a Reagentless Electrochemical DNA Bio- sensor with Conducting Polymer Film and Nanocom- posite as Matrices for the Detection of the HIV DNA Sequences | 36 |
| 2.4.3 | Label-free DNA biosensor based on resistance change of platinum nanoparticles assemblies | 37 |
| 2.5 | Conclusion | 39 |
| 3 | Research Background | 41 |
| 3.1 | Current Biosensor Research at Stellenbosch University | 41 |
| 3.1.1 | Superconductors Advanced materials and Nano Devices (SAND) Research group | 41 |
| 3.1.2 | Development of a Resistive Microfluidic Sensing Device for Pathogen Detection | 41 |
| 3.1.3 | Low Cost and Portable <i>E. coli</i> Biosensor | 42 |
| 3.2 | Conclusion | 45 |
| 4 | Proposed Project Design | 46 |

| | | |
|----------|--|-----------|
| 4.1 | Transducer | 47 |
| 4.1.1 | Conductive Fibers | 48 |
| 4.2 | Immobilization Technique | 49 |
| 4.2.1 | Deposition of Gold | 49 |
| 4.3 | Biorecognition Element | 49 |
| 4.3.1 | DNA Hairpin Probe | 50 |
| 4.4 | Electronic Measurement Design | 51 |
| 4.4.1 | Design Investigation | 52 |
| 4.4.2 | Proposed Electronic Design | 55 |
| 4.5 | Conclusion | 56 |
| 5 | Carbon Nanofibers | 57 |
| 5.1 | Nanofiber Characteristics | 57 |
| 5.2 | Cutting of Nanofibers | 62 |
| 5.2.1 | Laser Cutting Nanofibers | 62 |
| 5.2.1.1 | Blue Laser Diode Cutting | 63 |
| 5.2.1.2 | Yag Laser Cutting | 63 |
| 5.2.1.3 | Gebrateq CO ₂ Laser Cutting | 64 |
| 5.2.1.4 | Boyd and Ogier CO ₂ Laser Cutting | 66 |
| 5.2.1.5 | Backing for Materials during Laser Cutting | 66 |
| 5.3 | Gold Sputter Coating | 68 |
| 5.4 | Conclusion | 72 |
| 6 | DNA Hairpin Probe Design | 73 |
| 6.1 | Target DNA Sequence | 73 |
| 6.1.1 | Hybridized Target T _m | 73 |
| 6.1.2 | Target Self-Dimer | 74 |
| 6.2 | Fluorescent Labeled Probe Design | 74 |
| 6.2.1 | Fluorescent Probe DNA Sequence | 74 |
| 6.2.1.1 | 5DTPA | 75 |
| 6.2.1.2 | iCy3 | 75 |
| 6.2.1.3 | iSpC3 | 75 |
| 6.2.1.4 | 3IAbRQSp | 76 |
| 6.2.2 | Fluorescent Hairpin Probe Operation | 76 |
| 6.2.3 | Hairpin Structure T _m | 77 |
| 6.2.4 | Self Dimers | 77 |
| 6.3 | Ferrocene Labeled Probe Design | 78 |
| 6.3.1 | Ferrocene Probe DNA Sequence | 78 |
| 6.3.1.1 | dT-Ferrocene | 79 |
| 6.3.2 | Ferrocene Hairpin Probe Operation | 80 |
| 6.3.3 | Hairpin Structure T _m | 81 |
| 6.3.4 | Self Dimers | 81 |
| 6.4 | Conclusion | 81 |

| | | |
|----------|---|------------|
| 7 | Electronic Sensor Design | 82 |
| 7.1 | Design Considerations | 83 |
| 7.1.1 | Constant Current Value | 83 |
| 7.1.2 | ADC Resolution | 84 |
| 7.1.3 | Signal Amplification and Filtering | 84 |
| 7.2 | Spice Simulations | 87 |
| 7.3 | Circuit Design | 91 |
| 7.3.1 | Arduino Leonardo Microprocessor | 91 |
| 7.3.2 | External Power Supply Regulation | 92 |
| 7.3.2.1 | 5 V Precision Regulator | 92 |
| 7.3.3 | Constant Current | 94 |
| 7.3.3.1 | Setting Constant Current Value | 95 |
| 7.3.4 | Sample Switch and Connection | 96 |
| 7.3.5 | Voltage Follower and Low Pass Filtering | 97 |
| 7.3.6 | Analogue to Digital Converter | 98 |
| 7.3.6.1 | External Serial Clock, Single Cycle Operation | 99 |
| 7.3.6.2 | ADC Supply | 99 |
| 7.3.6.3 | Voltage Reference Input | 99 |
| 7.3.6.4 | Adjustable Voltage Reference ADP123 | 100 |
| 7.3.6.5 | Conversion Clock Oscillator | 101 |
| 7.3.6.6 | Serial Peripheral Interface (SPI) | 101 |
| 7.4 | PCB Routing and Manufacture | 102 |
| 7.5 | User Interface Software | 103 |
| 7.6 | Conclusion | 106 |
| 8 | Mechanical Design | 107 |
| 8.1 | Test Bath | 107 |
| 8.1.1 | Test Bath Lid | 107 |
| 8.1.2 | Test Bath Base | 110 |
| 8.2 | Biosensor Mount | 112 |
| 8.3 | Immobilization Bath | 114 |
| 8.4 | Conclusion | 116 |
| 9 | System Validation and Testing | 117 |
| 9.1 | Software Testing and Validation | 117 |
| 9.2 | Circuit Accuracy and Precision | 119 |
| 9.2.1 | USB Powered, Averaging Data vs. No Averaging | 120 |
| 9.2.2 | External PSU Powered, Averaging Data vs. No Averaging | 123 |
| 9.3 | Carbon Nanofiber Resistance | 125 |
| 9.4 | Gold Coating Effect on Resistance | 125 |
| 9.4.1 | Addition of Liquid to Fibers | 126 |
| 9.4.2 | Temperature Testing | 129 |
| 9.5 | Conclusion | 130 |

| | |
|---|------------|
| 10 Hairpin Probe Validation | 131 |
| 10.1 SYBR Green | 132 |
| 10.2 qPCR Measurements | 133 |
| 10.2.1 qPCR Experiment Setup | 133 |
| 10.2.2 Target DNA qPCR Measurements | 134 |
| 10.2.3 Fluorescent Hairpin DNA qPCR Measurements | 135 |
| 10.2.3.1 Fluorescent Hairpin Probe Measurements Alone | 135 |
| 10.2.3.2 Fluorescent Probe and Target DNA Measure- | |
| ments | 137 |
| 10.2.4 Ferrocene vs Fluorescent Hairpin DNA qPCR Measure- | |
| ments | 139 |
| 10.2.4.1 Ferrocene vs Fluorescent Hairpin DNA, no Tar- | |
| get DNA | 140 |
| 10.2.4.2 Ferrocene vs Fluorescent Hairpin DNA with | |
| Target DNA | 141 |
| 10.3 Conclusion | 142 |
| 11 Hairpin Probe Immobilization Validation | 143 |
| 11.1 Confocal Microscopy | 143 |
| 11.1.1 Fluorescent Hairpin Probe Confocal Imaging | 144 |
| 11.1.2 Ferrocene Hairpin Probe Confocal Imaging with SYBR | |
| Green | 146 |
| 11.2 Conclusion | 147 |
| 12 Biosensor Results | 148 |
| 12.1 Tris Resistive Measurements | 148 |
| 12.2 10 μM FE Probe and 10 μM Target DNA Resistive Measurements | 149 |
| 12.3 20 μM FE Probe and 10 μM Target DNA Resistive Measurements | 151 |
| 12.4 Circuit Adjustments | 153 |
| 12.4.1 Tris Resistive Measurements | 153 |
| 12.4.2 20 μM Fe Probe and 10 μM Target DNA Resistive Meas- | |
| urements | 154 |
| 12.5 Data Processing | 156 |
| 12.5.1 Trend Line Fitting | 156 |
| 12.5.2 Derivative Curve | 157 |
| 12.5.3 Averaging of Polynomial Fit Curves | 158 |
| 12.5.4 Averaging of Derivative Fit Curves | 159 |
| 12.6 Conclusion | 159 |
| 13 Optimizations and Alternative Solutions | 161 |
| 13.1 Optimizations | 161 |
| 13.1.1 Biosensor Miniaturization | 161 |
| 13.1.1.1 Sensor Miniaturization | 161 |
| 13.1.1.2 Electronic Miniaturization | 161 |

| | | |
|-----------|--|------------|
| 13.1.2 | On-Chip Technology | 162 |
| 13.1.2.1 | On-Chip Heating | 162 |
| 13.1.2.2 | On-Chip PCR Amplification | 162 |
| 13.1.3 | Electronic Filtering | 162 |
| 13.1.4 | Fluorescent Label | 162 |
| 13.1.5 | Post-Processing Algorithms | 163 |
| 13.2 | Alternative Solutions | 163 |
| 13.2.1 | Nanofibers | 163 |
| 13.2.2 | Electrolytic Interfaced Experiments | 164 |
| 13.2.2.1 | Screen-Printed Electrodes | 165 |
| 13.2.2.2 | Interdigitated Electrodes | 166 |
| 13.3 | Conclusion | 166 |
| 14 | Conclusion | 168 |
| | Appendices | 171 |
| A | Datasheets | 173 |
| A.1 | Rapid Anti-HIV test | 173 |
| A.2 | Target DNA Sequence Datasheet | 175 |
| A.3 | Fluorescent DNA Probe Datasheets | 176 |
| A.4 | Ferrocene DNA Probe Datasheet | 179 |
| B | Electronic Component Datasheets | 180 |
| B.1 | ON Semiconductor, 9V Regulator, MC7800 | 180 |
| B.2 | Texas Instruments, 5V Precision Regulator, LM4120 | 180 |
| B.3 | Microchip, 3.3V Precision Regulator, MCP1501 | 180 |
| B.4 | Texas Instruments, Adjustable Constant Current Source, LM334 | 180 |
| B.5 | Analog Devices, Single-Supply Input/Output Operational Amplifier, AD8629 | 181 |
| B.6 | Linear Technology, 24-bit-2 channel-Analogue to Digital Converter, LTC2402 | 181 |
| B.7 | Analog Devices, Programmable CMOS linear regulator, ADP123 | 181 |
| B.8 | Texas Instruments, Precision Timers, NE555PWR | 181 |
| B.9 | Harwin, 3mm Pitch Spring Test Probe with Concave Tip | 181 |
| C | Failed Hairpin Probe Experiments | 182 |
| D | Protocols | 186 |
| D.1 | Immobilization Protocol | 186 |
| D.2 | Stock Reagents | 187 |
| D.2.1 | Nuclease-Free Water | 187 |
| D.2.2 | Tris Buffer Protocol | 187 |
| D.3 | TE Buffer Protocol | 187 |
| D.4 | Fluorescent Probe DNA Resuspension | 188 |

CONTENTS

xi

| | |
|---|-----|
| D.5 Ferrocene Probe DNA Resuspension | 189 |
| D.6 Stock Solution Dilutions | 189 |
| D.7 Bath Wash Protocol | 189 |
| D.8 Electronic Test Protocol | 190 |
| D.9 qPCR Preparation Protocol | 191 |
| D.9.0.1 SYBR Green Master Mix | 192 |
| D.9.0.2 Fluorescent Hairpin Probe DNA | 192 |
| D.9.0.3 Ferrocene Hairpin Probe DNA | 192 |
| D.9.0.4 Target DNA | 193 |
| D.9.0.5 Target PCR Product | 193 |
| D.9.0.6 Genomic Control dsDNA | 193 |

Bibliography**194**

List of Figures

| | | |
|------|--|----|
| 2.1 | Typical Biosensor Model | 5 |
| 2.2 | Different examples of biomolecule immobilization strategies. | 9 |
| 2.3 | Typical fluorescent biosensor output when the target analyte is present. | 13 |
| 2.4 | Bioluminescence emitted from individual colonies. | 13 |
| 2.5 | Different Voltammetry methods. | 16 |
| 2.6 | Representation of a simple Voltammetry setup with two electrode cell. | 17 |
| 2.7 | Representation of a modern voltammetric setup. | 17 |
| 2.8 | An overview of selected cyclic voltammograms. | 18 |
| 2.9 | A representation of what HIV looks like. | 22 |
| 2.10 | The HIV life cycle. | 23 |
| 2.11 | Common ELISA formats. | 25 |
| 2.12 | Typical examples of Western blot reactions. | 26 |
| 2.13 | The structure of DNA and RNA. | 31 |
| 2.14 | Representation of DNA nucleotides and their directionality. | 32 |
| 2.15 | A size comparison of different biological elements. | 33 |
| 2.16 | A basic example of a DNA based electrochemical biosensor. | 35 |
| 2.17 | Schematic illustration of biosensor proposed. | 36 |
| 2.18 | Schematic of stepwise fabrication process of biosensor. | 37 |
| 2.19 | Gold interdigitated electrodes on silicon wafer substrate. | 38 |
| 2.20 | Cross section of the sensing device (schematic) after the target to probe DNA hybridization event. | 39 |
| 3.1 | Imaging of microfiber at different steps of fabrication. | 43 |
| 3.2 | Project results. | 44 |
| 4.1 | Biosensor design block diagram. | 47 |
| 4.2 | Hairpin probe representation. | 51 |
| 4.3 | Voltage division circuit in order to calculate resistance. | 53 |
| 4.4 | Auto ranging circuit using multiple inputs. | 54 |
| 4.5 | Proposed new electronic design. | 55 |
| 5.1 | Transmission electron micrograph of the PR-19 product. | 57 |

| | | |
|------|--|-----|
| 5.2 | Carbon nanofiber imaging. | 59 |
| 5.3 | Non-woven carbon backing. | 60 |
| 5.4 | Carbon nanofiber EDX elemental map. | 61 |
| 5.5 | Energy Dispersive X-Ray Spectroscopy (EDX) analysis of Carbon Nanofibers. | 62 |
| 5.6 | Blue laser diode results. | 63 |
| 5.7 | Yag laser cutter results. | 64 |
| 5.8 | Beyond CNC CO ₂ laser cutter: 12% power rating results. | 65 |
| 5.9 | Beyond CNC CO ₂ laser cutter: 20% power rating results. | 65 |
| 5.10 | Speedy 300 Trotec CO ₂ laser cutter: 15% power rating results. | 66 |
| 5.11 | Laser cutting on ceramic backing. | 67 |
| 5.12 | Laser cutting on stainless steel backing. | 68 |
| 5.13 | 60k times magnification SEM of gold deposited on nanofibers | 69 |
| 5.14 | 15k times magnification SEM of gold deposited on nanofibers | 70 |
| 6.1 | The most likely self dimer formed by two ssDNA target sequences. | 74 |
| 6.2 | Dithiol (DTPA) linker providing two thiol (SH) functional groups that bind to gold. | 75 |
| 6.3 | FL probe design when closed. | 76 |
| 6.4 | FL probe design when open and hybridized to target DNA. | 76 |
| 6.5 | The most likely self dimer formed by the FL probe. | 77 |
| 6.6 | Ferrocene modification. | 79 |
| 6.7 | FE probe design when closed. | 80 |
| 6.8 | FE probe design when open and hybridized to target DNA. | 80 |
| 6.9 | The most likely self dimer formed by the FL probe. | 81 |
| 7.1 | Electronic measurement block diagram. | 83 |
| 7.2 | Electronic measurement schematic. | 86 |
| 7.3 | 3.3 V Supply LtSpice simulation with real time noise. | 87 |
| 7.4 | Spice Simulation Results | 88 |
| 7.5 | Spice Simulation Results | 89 |
| 7.6 | Transducer voltage LtSpice with real time noise. | 89 |
| 7.7 | Spice simulation results. | 90 |
| 7.8 | External voltage supply regulation. | 92 |
| 7.9 | Constant current design. | 94 |
| 7.10 | Sample switch and connection. | 96 |
| 7.11 | Voltage Follower and Low Pass Filtering | 97 |
| 7.12 | ADC design. | 98 |
| 7.13 | External serial clock, single cycle operation. | 99 |
| 7.14 | PCB board layout. | 102 |
| 7.15 | PCBWay results. | 103 |
| 7.16 | Test detail form. | 104 |
| 7.17 | GUI plotting tab. | 105 |

| | | |
|------|--|-----|
| 8.1 | Spring test probe. | 108 |
| 8.2 | Test bath lid. | 108 |
| 8.3 | Test bath lid design. | 109 |
| 8.4 | Test bath base, side view with clamp. | 110 |
| 8.5 | Test bath base design. | 111 |
| 8.6 | Full system on mount. | 112 |
| 8.7 | System mount CAD sketch. | 113 |
| 8.8 | Immobilization bath. | 114 |
| 8.9 | Immobilization bath CAD sketch. | 115 |
| 9.1 | GUI output. | 118 |
| 9.2 | Dummy point added to reduce scaling effect. | 119 |
| 9.3 | Typical 56 Ω resistance test. USB powered, no averaging. | 120 |
| 9.4 | Typical 56 Ω resistance test. USB powered, with averaging. | 120 |
| 9.5 | 56 Ω resistor, USB powered, max deviance comparison of software averaging (3 values) vs no averaging. | 121 |
| 9.6 | 100 Ω resistor, USB powered, max deviance comparison of software averaging (3 values) vs no averaging. | 122 |
| 9.7 | 1 k Ω resistor, USB powered, max deviance comparison of software averaging (3 values) vs no averaging. | 122 |
| 9.8 | 4.6 k Ω resistor, USB powered, max deviance comparison of software averaging (3 values) vs no averaging. | 123 |
| 9.9 | 100 Ω resistor, external PSU power, max deviance comparison of software averaging (3 values) vs no averaging. | 124 |
| 9.10 | 1 k Ω resistor, external PSU power, max deviance comparison of software averaging (3 values) vs no averaging. | 124 |
| 9.11 | Carbon fiber resistance tests (averaging used). | 125 |
| 9.12 | Gold coated carbon fiber resistance tests (averaging used). Gold deposit thicknesses of 5, 10, 15, 20 and 25nm. | 126 |
| 9.13 | Dry fibers, results when 50 μ L TE buffer added to the fibers at different stages. | 127 |
| 9.14 | Previously wet fibers, results when 40 μ L TE buffer added to the fibers at different stages. | 128 |
| 9.14 | Previously wet fibers, results when 40 μ L TE buffer added to the fibers at different stages. | 129 |
| 9.15 | Results of temperature tests in 37 $^{\circ}$ C environment. Both dry and wet fibers were tested. | 130 |
| 10.1 | SYBR Green. | 132 |
| 10.2 | Melt Curve Setup | 134 |
| 10.3 | Melt curve 13 $^{\circ}$ C to 93 $^{\circ}$ C of target DNA (3 μ M), SYBR Green measurements. | 135 |
| 10.4 | Melt curve 13 $^{\circ}$ C to 93 $^{\circ}$ C of FL probe (1 μ M), Cal Orange measurements. | 137 |

| | | |
|------|---|-----|
| 10.5 | Melt curve 13°C to 93°C of FL probe (1 μ M) with target DNA (3 μ M), Cal Orange measurements. | 138 |
| 10.6 | Melt curve 13°C to 93°C of FL probe (1 μ M) with target DNA (3 μ M), SYBR Green measurements. | 139 |
| 10.7 | Melt curve 13°C to 93°C of 1 μ M FL probe (red) and 1 μ M FE probe (pink) , SYBR Green measurements. | 140 |
| 10.8 | Melt curve 13°C to 93°C of 1 μ M FL probe (red) and 1 μ M FE probe (blue) with 3 μ M target DNA, SYBR Green measurements. | 141 |
| 11.1 | Confocal imaging of Fl probe on various thicknesses of gold coated CNFs. | 145 |
| 11.2 | FE probe validation, SYBR Green confocal imaging | 146 |
| 11.2 | FE probe validation, SYBR Green confocal imaging | 147 |
| 12.1 | Resistive measurements of CNF during addition of 50 μ L Tris buffer. | 149 |
| 12.2 | Resistive measurements of CNF during addition of 50 μ L of 10 μ M target DNA with 10 μ M immobilized FE probe with 10 μ M immobilized FE probe. | 150 |
| 12.2 | Resistive measurements of CNF during addition of 50 μ L of 10 μ M target DNA with 10 μ M immobilized FE probe. | 151 |
| 12.3 | Resistive measurements of CNF during addition of 50 μ L of 10 μ M target DNA with 20 μ M immobilized FE probe. | 152 |
| 12.4 | Resistive measurements of CNF during addition of 50 μ L of Tris buffer. | 153 |
| 12.4 | Resistive measurements of CNF during addition of Tris buffer. | 154 |
| 12.5 | Resistive measurements of CNF during addition of 50 μ L of 10 μ M target DNA with 20 μ M immobilized FE probe. | 155 |
| 12.5 | Resistive measurements of CNF during addition of 50 μ L of 10 μ M target DNA with 20 μ M immobilized FE probe. | 156 |
| 12.6 | 6 th order polynomial trend line fit. | 157 |
| 12.7 | Derivative Curve | 158 |
| 12.8 | 6 th order polynomial averages of 4 experiments each. | 158 |
| 12.9 | Derivative curve averages of 4 experiments each. | 159 |
| 13.1 | Electrolytic Interface Electronic Model. | 165 |
| 13.2 | Screen printed carbon electrodes. | 166 |
| C.1 | Failed confocal experiment, FL probe only, incubated at 37°C. | 183 |
| C.2 | Failed confocal experiment, FL probe and target, incubated at 37°C. | 183 |
| C.3 | Failed qPCR experiment, FL probe only | 184 |
| C.4 | Failed qPCR experiment, FL probe and target DNA | 185 |

Abbreviations

| | |
|----------------|---|
| /CS | Active Low Chip Select |
| 3D | Three-Dimensional |
| <i>E. coli</i> | <i>Escherichia coli</i> |
| A | Adenine |
| AC | Alternating Current |
| ADC | Analogue to Digital Converter |
| AIDS | Acquired Immunodeficiency Syndrome |
| BJT | Bipolar Junction Transistor |
| C | Cytosine |
| CAD | Computer Aided Design |
| CAF | Charities Aid Foundation |
| CD4 | Cluster of Differentiation 4 |
| CE | Conformite Europeene or European Conformity |
| CEO | Chief Executive Officer |
| CFU | Colony Forming Units |
| CNF | Carbon Nanofiber |
| CNT | Carbon Nanotube |
| CS | Chip Select |
| CV | Cyclic Voltammetry |
| CVD | Chemically Vapor Deposited |

| | |
|----------|--|
| DC | Direct Current |
| DNA | Deoxyribonucleic Acid |
| dsDNA | double stranded DNA |
| EDX | Energy Dispersive X-Ray |
| EIS | Electrochemical Impedance Spectroscopy |
| ELISA | Enzyme-Linked Immunosorbent Assays |
| FDA | Food and Drug Administration |
| FE probe | Ferrocene hairpin probe DNA |
| FL probe | Flourescent hairpin probe DNA |
| G | Guanine |
| GUI | Graphic User Interface |
| HIV | Human Immunodeficiency Virus |
| I/O | Input/Output |
| IDE | InterDigitated Electrode |
| kD | kilo Daltons |
| LCD | Liquid Crystal Display |
| LED | Light Emitting Diode |
| LOD | Limit of Detection |
| LPF | Low Pass Filter |
| LSPR | Localized Surface Plasmon Resonance |
| MISO | Master In Slave Out |
| MM | Mismatched |
| MOSI | Master Out Slave In |
| opamp | operational amplifier |
| PANI | Polyaniline |
| PB | Prussian Blue |
| PCB | Printed Circuit Board |

| | |
|----------------|---|
| PCR | Polymerase Chain Reaction |
| pH | Potential of Hydrogen |
| ppm | Parts per million |
| PSU | Power Supply Unit |
| QCM | Quartz Crystal Microbalance |
| R.E | Reference Electrode |
| RFU | Relative Fluorescent Unit |
| RIfS | Reflectometric interference Spectroscopy |
| RNA | Ribonucleic acid |
| SAM | Self Assembled Monolayers |
| SAND | Superconductors Advanced materials and Nano Devices |
| SCK | Transfer Clock |
| SDO | Three State Digital Output |
| SELEX | Systematic Evolution of Ligands by EXponential enrichment |
| SEM | Scanning Electron Microscope |
| SERS | Surface-Enhanced Raman Scattering |
| SIV | Simian Immunodeficiency Virus |
| SMD | Surface Mount Devices |
| SPI | Serial Peripheral Interface |
| SPR | Surface Plasmon Resonance |
| ssDNA | single stranded DNA |
| T | Thymine |
| TIA | Technology Innovation Agency |
| T _m | Temperature of melting |
| UART | Universal Asynchronous Receiver-Transmitter |
| UNAIDS | The Joint United Nations Programme on HIV and AIDS |
| USB | Universal Serial Bus |

LIST OF FIGURES

xix

| | |
|-------|-------------------------------------|
| UV | Ultraviolet |
| VACNF | Verically Aligned Carbon Nanofibers |
| W.E | Working Electrode |
| WHO | World Health Organization |
| YSI | Yellow Spring Instruments |

Chapter 1

Introduction

1.1 HIV (Human Immunodeficiency Virus)

"According to UNAIDS (The Joint United Nations Programme on HIV and AIDS), there are approximately 7 million people living with HIV in South Africa and whilst diagnosis rates have improved significantly since 2000, approximately 1.7 million people remain undiagnosed. Early HIV diagnosis is vital, so that effective treatment can be administered to protect your health and to prevent onward transmission. Most people lead long and normal lives with early detection and appropriate treatment. Late diagnosis can result in unnecessary illness and reduce your life expectancy. People who remain unaware of their HIV status are unknowingly the source of the majority of new infections."[1].

An advisory panel that is part of UNAIDS established a revolutionary target called, "cascade" in order to beat AIDS (Acquired Immunodeficiency Syndrome) by 2030. The target consists of the "90, 90, 90 Goals" which aim to be achieved by 2020. The "90, 90, 90 Goals" to be achieved are:

- 90% of all people living with HIV will know their HIV status.
- 90% of all people with diagnosed HIV infection will receive sustained antiretroviral therapy.
- 90% of all people receiving antiretroviral therapy will have viral suppression.

By achieving these goals and ensuring diagnosis of HIV as soon as possible, treatment can be used to prevent any further transmission. In doing so, UNAIDS target may be achieved and by 2030, HIV will no longer be a global health threat[1].

In the past HIV and AIDS were considered a massive threat to world health which then socially created a stigma when dealing with HIV or AIDS. In reality, HIV no longer poses such a great threat and treatment is readily and cheaply available worldwide. Bridget Bard, founder and CEO (Chief Executive Officer) of BioSure is quoted as saying, "HIV is three letters, not a sentence.". What this means is that if a patient contracts HIV, it is no longer a death sentence if detected early enough and proper treatment begins immediately.

Bridget Bard also stated that 30 years ago, the simple pregnancy test was considered taboo and there was much debate as to whether patients should be allowed to use such tests in the comfort of their own homes. Today, the same debate has resurfaced when referring to at-home HIV self-tests. In 2016 the South African government decided to allow the use of at-home HIV self-testing. By changing the law regarding HIV tests, this has allowed any person in the country, the ability to test and monitor their HIV status in the privacy of their own home. This has now opened a very important market in the pharmaceutical industry and it has become vitally important that highly accurate and reliable tests become available.

BioSure has stated that they are the first and only company to provide HIV self-tests that are FDA (Food and Drug Administration) approved, CE marked (Conformite Europeene or European Conformity) and boast 99.7% accurate readings after 3 months of potential infection. Most HIV self-tests are very similar to pregnancy tests, in that the results are displayed as simple lines consisting of a control line and a positive line that detect the presence of HIV antibodies. A complete literature review of HIV is detailed in Section 2.2.

1.2 Biosensors

The devices used to detect HIV, pregnancy or even body temperature to name a few are termed *biosensors*. A biosensor which is fully detailed in Section 2.1 is any device that couples a biological recognition element to a signal transducer which in turn creates a measurable signal.

The history of biosensors originates as far back as 1906 but was not defined until 1956 when Leland C. Clark, considered the father of biosensors, developed the first "true" biosensor that detected oxygen. Most biosensors are chemical or optical in nature but the first electrochemical based biosensor developed was by Clark in 1962 and eventually the first commercial biosensor was developed by YSI (Yellow Spring Instruments) in 1975[2]. This implies that biosensing and especially electrochemical biosensing is a relatively new field and only recently, became an emerging research and commercial field in South Africa.

1.3 Thesis Overview

An investigation into the possibility of designing an electrochemically reactive biosensor by use of hairpin DNA (Deoxyribonucleic Acid) probes to detect the presence of HIV was proposed and conducted. The electrochemical signal to be measured is a change in resistance of a conductive carbon nanofiber substrate.

Due to the emerging research field of electrochemical biosensors in South Africa, and the impact HIV has world wide, there is great interest in HIV detection especially as a low cost, portable system. In Section 2.1, research is conducted into what biosensors are, where they are used and the various implementation methods of biosensors are discussed. HIV and AIDS is then discussed in Section 2.2, where the standard HIV tests and the ethical concerns of at home testing (rapid tests) are explained. HIV antibodies are generally only detectable after three months of infection, termed the "window period" and so it was decided that the direct detection of HIV DNA is investigated in the hopes that the "window period" may be shortened. Section 2.3 covers a brief introduction to DNA and DNA based biosensors. As mentioned, the common rapid HIV tests generally produce a visible line to indicate infection or no infection with no further information. By using modern electrochemical techniques, there is a possibility that a rapid test may be able to produce more than a binary "infected" or "not infected" result. Using electrochemical techniques there may be a simple biosensor that can not only indicate infection, but also quantify the level of infection in comparison to measured signal strength. By being able to quantify infection, enables the commercial use of biosensors to be greatly increased because a patient would be able to use the biosensor to monitor their status throughout their antiretroviral treatment. Another benefit of electrochemical biosensors is that it may be cheaper than optical sensors to scale up production. Section 2.4 reviews a few DNA and electrochemical specific research articles in order to get a better understanding of the current research field.

A brief background into the current research team and project outputs completed at Stellenbosch University is found in Chapter 3, which includes an *E. coli* (*Escherichia coli*) prototype biosensor completed before research into the current biosensor thesis began. Chapter 4 covers the theoretical proposed project design and thereafter, all design procedures, characterizations and results are fully detailed.

Chapter 2

Literature Review

2.1 Biosensors

2.1.1 Introduction

A biosensor is defined as :

An analytical device composed of a biological recognition element directly interfaced to a signal transducer, which together relate the concentration of an analyte (or group of related analytes) to a measurable response. Biosensors for bacterial detection involve biological recognition components such as a receptor, nucleic acid, or antibodies attached to an appropriate transducer [3].

In short, a biosensor is used to detect and indicate the presence of a biological element such as a disease, virus or specific DNA in a measurable and sensitive manner. Biosensors have a wide range of applications from clinical through to environmental and agricultural uses.

Industry examples of biosensors are:

- General health-care monitoring.
- Screening for disease.
- Clinical analysis and diagnosis of disease.
- Veterinary and agricultural applications.
- Industrial processing and monitoring.
- Environmental pollution control.

In the medical and clinical industry biosensors are used in everyday applications such as checking blood sugar levels in diabetes patients or detecting

life threatening diseases, bacteria or viruses such as *E. coli* or HIV. Biosensors can be used in the food industry to measure carbohydrates, alcohols and acids. Quality control processing to detect pathogens in fresh meat, poultry or, fish is one example [4].

2.1.2 Biosensor Model

Figure 2.1 depicts the basic components of a biosensor model. The first component is the bio-receptor or biorecognition element, which is typically an enzyme, antibody, microorganism or nucleic acid. The biorecognition element is the component that reacts with the target analyte that is to be detected. The second element of the biosensor model is the transducer. The most frequently used transducer types are optical/light, surface potential, mass change or electrochemical (current, voltage, resistance). The transducer is the component that converts energy from the biorecognition element into a signal which can be measured when the target analyte is present. The final component is the processing of the measurable signal provided by the transducer. In some cases the transducer and the measurable signal may be the same component (i.e a transducer that changes colour visible to the human eye), otherwise specific circuitry and software are designed to process the signals from the transducer. The concentration of an analyte in a given sample can often be calculated by the level or rate of increase given by the signal. Examples are the time taken for an output to occur, higher or lower output signals or the shade of colour in optically based sensors. Biorecognition elements are typically adhered to the surface of inorganic materials, which are usually the transducers, by means of various immobilization techniques [5].

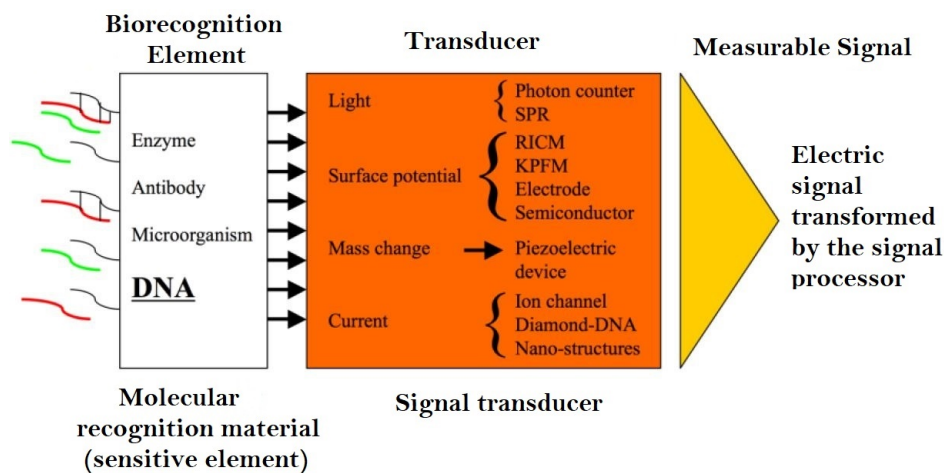


Figure 2.1: Typical biosensor model [6].

2.1.3 Biorecognition Elements

When the first biosensors were designed, biorecognition elements were extracted from living organisms. With recent technological advancements many recognition elements are synthesized in a laboratory and are not naturally occurring. Enzymes, antibodies and nucleic acid based biorecognition elements will be briefly discussed.

2.1.3.1 Enzymes

An enzyme is "A substance produced by body cells that helps bring about or speed up bodily chemical activities (as the digestion of food) without being destroyed in so doing" [7].

Enzymes are a popular biorecognition element choice due to the many different measurable reaction products created by the catalytic process. These products include protons, electrons, light and heat. An engineered enzyme biorecognition element has been used to successfully detect HIV antibodies in serum. The most widely used and successful enzyme based biosensor is the glucose biosensor in aid of diabetes patients [8].

2.1.3.2 Antibodies

The majority of rapid detection biosensors utilize antibodies as the chosen biorecognition element, because they are good for recognition, identification and quantification of target analytes. Advances in technology now allow for large quantities of antibodies to be produced. Antibodies as a biorecognition element produce high sensitivity and specificity due to their bimolecular antibody-antigen interaction. The biggest advantage of antibody based biosensors is that the target need not be purified. Antibody based biosensors have been used to detect and identify HIV, hepatitis B and C, simian immunodeficiency, Ebola, rabies, Epstein-Barr, and measles viruses [8].

2.1.3.3 Aptamers

Aptamers are nucleic acid ligands (RNA (Ribonucleic acid), ssDNA (single stranded DNA), modified ssDNA, modified RNA or peptide) that are isolated from libraries of oligonucleotides by an *in vitro* selection process called SELEX (Systematic Evolution of Ligands by EXponential enrichment). Aptamers bind with high affinity and specificity to a wide range of target molecules. Aptamers have been used successfully for both analytic and diagnostic applications. Due to the fact that aptamers are synthetically made in a laboratory environment, the potential range of applications for their use is virtually unlimited. Aptamers have been used to detect a wide range of targets, including small molecules, proteins and whole cells. Nucleic acids tend to be more flexible

than their protein counterparts. Once aptamers have successfully bound with their ligands, they fold into an architecture in which the ligand becomes an intrinsic part of the nucleic acid structure. Due to the high binding strength, easy storage and wide range of use, aptamer based biosensors are emerging as a great new technology in comparison to the more commonly used antibody based biosensors.

A key development of aptamer based biosensors is that of "signaling" or "molecular beacon" aptamers, which are able to act as the biorecognition element as well as the transducer. This means that they can signal directly after target binding. These beacons are able to act like a switch that is normally-closed or off. When the target has successfully bound to the DNA aptamer, the "switch" is turned on. This is done by use of a hairpin where, before binding, the aptamer is folded back on itself and prevents any readable signal (fluorescent, electrochemical, heat, etc.), but when the target binds, the hairpin is forced to open and create a readable signal [8].

2.1.3.4 Hybridization Probes

A hybridization probe or DNA probe is a fragment of DNA or RNA of variable length (usually 100-1000 bases long). DNA/RNA probes are used in DNA or RNA samples to detect specific nucleotide sequences that are complementary to the designed DNA sequences of the probe. The probes are single stranded nucleic acid (DNA or RNA) sequences. The target DNA is first denatured by heating, which forces double stranded DNA to split into two single stranded DNA strands. The target DNA is then allowed to hybridize to the probe DNA. When hybridization occurs the probe can act in a similar manner to the aptamer, in that a label or molecular marker can be added and therefore create some form of measurable signal (fluorescent, electrical or radioactive labels are commonly used). DNA probes can also make use of the hairpin structure, which is explained in detail in Section 4.3.1.

An aptamer and a DNA probe may seem similar, but there are some distinct differences. An aptamer is an oligonucleotide used for its 3D structure and ability to bind to a target and act like an antibody (binding is not based on base-pairing but overall 3D confirmation and interaction with other molecules). Aptamers are often used to bind to proteins (called antigens). In comparison a DNA/RNA probe is an oligonucleotide used to bind to, and recognize its complement through Watson and Crick complementary base-pairing (G (Guanine) binds C (Cytosine), A (Adenine) binds T (Thymine)).

The advantages of DNA probes are that DNA can be pre-amplified (for example by PCR (Polymerase Chain Reaction)). This means that target DNA

can be mass produced, which makes detection far more feasible when there is very low initial target. DNA probe production is much more scalable and the synthesizing process is faster and more affordable when compared to antibody production. DNA is also very versatile, for example, if a biosensor is designed for DNA detection, it can be used to detect virtually any DNA sequence just by changing the sequence of the DNA probe used without any changes in fabrication of the device. DNA probes can also be designed with additional modifications other than labels, such as tethers or linkers that enable different immobilization methods. An example would be that it is possible to add a biotin or thiol tether to the DNA probe, enabling either biotin-avidin or thiol-gold SAM (Self Assembled Monolayer) immobilization as described in Section 2.1.5.2 and Section 2.1.5.3.

2.1.4 Label vs Label-Free Biorecognition

Biorecognition elements can be classified in terms of labels as either label-based or label-free biosensors. Label-free implies that the detected signal is produced directly by the interaction of the analyzed material with the transducer [9]. Alternatively, label-based sensing requires the use of a label which is an added component onto the biorecognition element that is included as a preprocessing step. Labelled biosensors employ external methods of marking the analyte with either antibodies, electrical or fluorescent markers [5]. The use of labels complicates the system, making it more expensive and time consuming. The disadvantages of labeling include lack of sensitivity, interference, and cross-reactivity [10].

2.1.5 Immobilization Techniques

The chosen immobilization technique is one of the most critical steps in biosensor design, because various aspects (sensitivity, dynamic range, reproducibility and response time) are directly related to how well the original properties of the biorecognition element are kept after immobilization. The existing immobilization techniques available include biomolecule physisorption, entrapment and encapsulation into polymers or membranes, silanisation, and SAM formation coupled to biomolecule cross-binding or covalent bonding. The chosen immobilization technique needs to ensure biorecognition stability and the modified surface must be inert and biocompatible. A few of these immobilization techniques will be discussed [11].

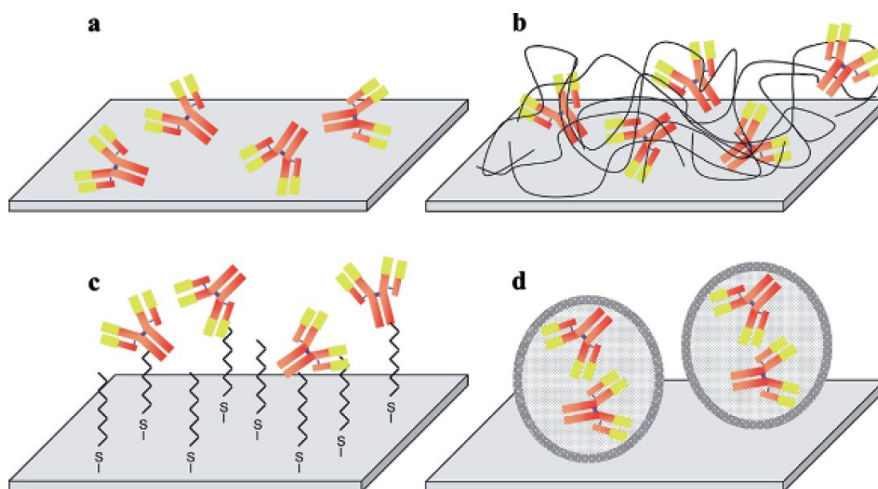


Figure 2.2: Different examples of biomolecule immobilization strategies. (a) Unspecific adsorption, (b) Entrapment, (c) Cross-linking to a pre-assembled SAM, and (d) Encapsulation [11].

2.1.5.1 Adsorption

The simplest method of immobilization onto a physical substrate is nonspecific adsorption, which consists of only depositing the target molecules (antibodies, antigen, etc.) on the surface and leaving them to interact in a completely random way [Figure 2.2(a)]. The driving forces may be initially hydrophobic (for hydrophobic surfaces such as polystyrene) or electrostatic (for more polar substrates such as silica), but protein adsorption will be further stabilized by a combination of hydrophobic interactions, hydrogen bonding, and/or Van Der Waals forces, resulting in a behaviour highly dependent on each individual protein-surface involved, which will result in very stable bonds. Proteins containing free SH_2 and/or S-S bonds have a very strong affinity to gold. One disadvantage of adsorption is that the proteins may partly denature and thus lose structure or function [11].

2.1.5.2 SAM (Self-assembled Monolayer)

SAMs are crystalline chemisorbed organic single layers formed by spontaneous organization of thiolated molecules, generally on metal surfaces [Figure 2.2(c)]. They enable the formation of organic surfaces whose composition, structure, and properties can be varied rationally. The most popular group of SAM research is based on the adsorption of n-alkanethiols on gold, silver, copper, palladium, platinum, and mercury. The formation of these well-defined organic surfaces, with useful and highly alterable chemical functionalities, is made pos-

sible by the high affinity of sulfur for noble and coinage metals (copper, silver, and gold). The typical thickness of a SAM layer is only a few nanometers, which gives SAMs the following advantages.:

- Ease of manufacturing and functionalization in basic laboratories.
- SAM can form on virtually any surface size.
- Allowing molecular level structures to link to macroscopic interfacial phenomena.

Gold is the industry chosen standard for SAM formation, because gold is easy to obtain, its use in photolithography is well defined and, most importantly, is biocompatible. It is possible for a SAM formation to occur in a matter of minutes. In order to maximize the molecular density and enable well ordered structures, a couple of hours may be required. The most important factors to consider during SAM formation are solvent, temperature, thiol concentration, purity of structure, substrate immersion time, concentration of oxygen and substrate cleanliness. SAM depositions are generally very stable, and considered permanent, but there are a few methods of SAM desorption, such as piranha treatment, exchange methods, photo oxidation (UV (Ultraviolet) irradiation), or electrochemical reactions. SAM formations can be used in conjunction with biorecognition elements during immobilization (antibodies, nucleic acids, aptamers, peptides, etc.) and it seems there are infinite possibilities due to the fact that functional groups can be individually tailored to specific requirements [11].

2.1.5.3 The Biotin-(Strept)Avidin System

This immobilization technique utilizes the natural strong binding affinity of avidin to a small molecule called biotin (or vitamin H). This is a very popular non-covalent conjunction method. The biospecificity of the interaction is similar to that of antibody-antigen recognition. Variations of buffer salts and pH (potential of hydrogen), extreme temperatures, or denaturants do not prevent the bonding interaction. Biotin groups can be added to proteins, nucleic acids or other molecules using known processes. Another similar protein called streptavidin is also often used due to the fact that avidin may be prone to non-specific bindings. The disadvantages of streptavidin are that it exhibits a peptide that presents a high affinity for integrins on cell surfaces resulting in high levels of bacteria unspecific adsorption. Another disadvantage of both avidin and streptavidin is that many proteins naturally possess covalently bound biotin which may lead to greater background signal [11].

2.1.5.4 Entrapment

Biomolecules can be immobilized within organic or inorganic polymer matrices by entrapment during the matrix polymerisation. Capturing biorecognition elements in small inert areas inside the entrapment material (possibly the transducer), allow stability by reducing unfolding and by shifting equilibrium in different configurations. An example would be enzymes entrapped within nanopores of silica beads. The disadvantages of entrapment are the need of high concentrations of both monomer and biomolecules, potential biomolecule loss of structure and/or function, certain individual biorecognition elements may be inaccessible (unable to bind) and the lack of reproducibility between sensing surfaces [11].

2.1.6 Blocking

Blocking is a technique used to prevent unspecific binding to a surface rather than the specific binding of a target analyte to the immobilized biorecognition element. An example would be an unspecific analyte naturally binding to a gold surface, where only the biorecognition element should be binding to the gold surface and thereafter the target analyte should bind only to the biorecognition element. In cases where it is possible for the target analyte or unspecific analytes to bond to an undesired surface, a blocking treatment may be required after the biorecognition element has been immobilized, and before introduction of the target. Blocking agents available include bovine serum albumin, casein, and skimmed milk [11].

2.1.7 Transducers

Biosensors can be classified into 5 basic groups depending on the transducer technology used. These 5 groups are [3, 12]:

1. Optical : Intensity, Wavelength, Phase, Polarization.
2. Mass/Mechanical : Position, Velocity, Acceleration, Force, Pressure.
3. Thermal : Temperature, Heat, Heat flow.
4. Magnetic : Field intensity, Flux, Magnetization.
5. Electrochemical : Voltage, Current, Charge.

The two most common and most rapidly developing groups of biosensors are the optical and electrochemical based biosensors. These two most popular technologies will be briefly discussed.

It should be noted that almost all biosensors can have a digital element incorporated. This means that although the transducer method may not provide an

electronic signal, an electronic sensor can be designed to measure and report the specific changes electronically.

2.1.7.1 Optical Biosensors

There are two main areas of development in optical biosensors. These involve the detection in changes in light adsorption between reactants and the products of a reaction, or measuring the light output by a luminescent process (colorimetric and photometric respectively) [13]. Optical biosensors enable the direct, real-time and label-free detection of many biological substances. Their advantages include high specificity, sensitivity, small size and cost-effectiveness [9].

Colorimetric Sensors: A typical example of a basic colorimetric based biosensor would be the simple strip pregnancy test (lateral flow immunochromatographic assay). This test works with the use of a lateral flow assay and causes a change in colour on a surface that is visible to the human eye. As mentioned, it is possible to digitize such a test and have an electronic sensor that can detect the colour change and report the results in an electronic binary fashion.

Fluorescence Sensors: Fluorescence based biosensors are commonly used in bio-Optrodes. Fluorescence occurs when molecules absorb light at one wavelength and then emit light at a longer wavelength. Since the excitation and emission occurs only at distinct energy levels, each fluorescent molecule has a unique fluorescence spectral fingerprint, which is very important for the optical biosensor application [14]. A fluorescent based biosensor will therefore present a fluorescent light wavelength in the presence of a target analyte. Figure 2.3 shows the typical fluorescent biosensor output when the target analyte is present.

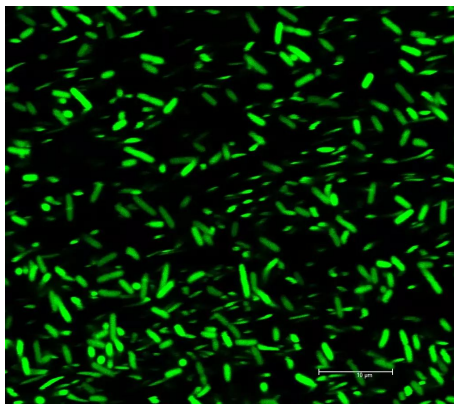


Figure 2.3: Typical fluorescent biosensor output when the target analyte is present. Images are typically taken under confocal or fluorescent microscopy [15].

Chemiluminescence/Bioluminescence Sensors: Chemiluminescence is similar to fluorescence except that chemiluminescence occurs by exciting molecules with a chemical reaction, thus chemiluminescence requires no external source of light. Bioluminescence is in fact chemiluminescence that occurs in living organisms. A typical example of high-efficiency bioluminescence is the fire fly. Luciferin from a fire fly can be adapted and used to detect a wide variety of bacteria. These luminescence based methods can even be used for DNA based detection [16]. Figure 2.4 depicts bioluminescence emitted from individual colonies of microbial cells containing the genes for bacterial luciferase [17].

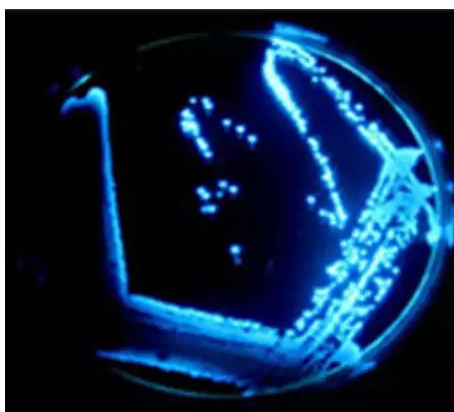


Figure 2.4: Bioluminescence emitted from individual colonies of microbial cells containing the genes for bacterial luciferase [17].

Other Optical Based Biosensors: There is a very wide variety of optical based biosensor types. Some are simple and visible to the human eye while others are more complex and need very sensitive sensors and mathematical algorithm software in order to determine the presence of a target analyte. A few optical based biosensor methods are listed below [9].

- Surface plasmon resonance (SPR).
- Localized surface plasmon resonance (LSPR).
- Evanescent wave fluorescence.
- Optical waveguide interferometric.
- Ellipsometric.
- Reflectometric interference spectroscopy (RIfS).
- Surface-enhanced Raman scattering (SERS).

2.1.7.2 Electrochemical Biosensors

Electrochemical biosensors have some advantages over the other transduction methods, such as the ability to operate in turbid media, comparable instrumental sensitivity, the capability of miniaturization and finally the equipment required for electrochemical analysis is generally simpler and cheaper in comparison to most other analytical techniques [3]. The ability to significantly miniaturize the biosensor system directly affects the cost of a specific test. A miniaturized system requires a vastly smaller volume of sample and costly reagents in order to manufacture the biosensor.

Typically in bioelectrochemistry, the reaction under investigation would either generate a measurable current (amperometric), a measurable potential or charge accumulation (potentiometric) or measurably alter the conductive properties of a medium (conductometric) between electrodes. Two other electrochemical based technologies that do not specifically fall under the first three technologies also include impedimetric, which measures impedance (both resistance and reactance), and field-effect, which uses transistor technology to measure current as a result of a potentiometric effect at a gate electrode [18].

Electrochemical Sensor Principle:

Electrochemical reactions take place at electrode-electrolyte interfaces and provide a switch for electricity to flow between two phases of different conductivity, i.e. the electrode (electrons or holes are the charge carriers) and solid or liquid electrolyte (ions are the main charge carriers) [12].

Due to the fact that most reactions are generally only detected in close proximity to an electrode surface, the electrodes themselves play a very important role in the performance of an electrochemical biosensor. The material, surface modification or dimensions of a specific electrode directly affect the detection ability and sensitivity of a biosensor.

Electrochemical Sensing

Electrochemical sensing usually requires a reference electrode, a counter or auxiliary electrode and a working electrode, also known as the sensing or redox electrode. The reference electrode, commonly made from Ag/AgCl, is kept at a distance from the reaction site in order to maintain a known and stable potential. The working electrode serves as the transduction element in the biochemical reaction, while the counter electrode establishes a connection to the electrolytic solution so that a current can be applied to the working electrode. These electrodes should be both conductive and chemically stable. Therefore, platinum, gold, carbon (e.g. graphite) and silicon compounds are commonly used, depending on the analyte [18].

Amperometry: Amperometry is based on the measurement of the current resulting from the electrochemical oxidation or reduction of an electroactive species. It is usually performed by maintaining a constant potential at a platinum, gold, carbon (e.g. graphite) or silicon compound working electrode with respect to a reference electrode [18]. The resulting current is directly correlated to the bulk concentration of the electroactive species or its production or consumption rate within the adjacent biocatalytic layer. Typically, the current is measured at a constant potential and this is referred to as amperometry. If a current is measured during controlled variations of the potential, this is referred to as Voltammetry [19, 18].

Potentiometry: Potentiometric devices measure the accumulation of a charge potential at the working electrode compared to the reference electrode in an electrochemical cell when little to no current flows. In other words, potentiometry provides information about the ion activity in an electrochemical reaction. Potentiometric sensors are very good for measuring low concentrations in tiny sample volumes, since they ideally offer the benefit of not chemically influencing a sample [18, 19].

Conductometry: Conductometric devices measure the ability of an analyte or a medium to conduct an electrical current between electrodes or reference nodes. In most cases conductometric devices have been strongly associated with enzymes, where the ionic strength, and thus the conductivity, of a solution

between two electrodes changes as a result of an enzymatic reaction. Another approach is to directly monitor the changes in conductance of an electrode as a result of the immobilization of e.g. enzymes, complementary antibody-antigen pairs, etc. onto the electrode surface [18, 19].

2.1.8 Electrochemical Detection Techniques

In Section 2.1.7.2, the three different electrochemical reactions were discussed (amperometric, potentiometric and conductometric). These three types of reaction describe how a signal is produced. This section will now discuss the different electrochemical techniques that use these reactions in order to detect the presence of a target analyte.

2.1.8.1 Voltammetry

Voltammetry is an electrochemical detection technique that uses varying potentials in order to measure a current response which in turn provides information about an analyte. Voltammetry is, therefore, an amperometric technique. There are many ways to vary potential, which implies that there are many forms of Voltammetry, such as polarography (DC (Direct Current) Voltage), linear sweep, differential staircase, normal pulse, reverse pulse, differential pulse and many more [18]. Figure 2.5 shows a few of the different Voltammetry based potential variance techniques.

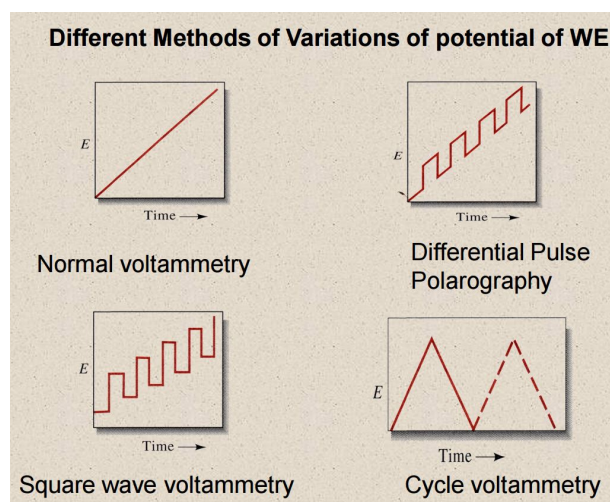


Figure 2.5: Different Voltammetry methods by varying the potential of the Working Electrode (W.E) [20].

Voltammetry has two physical setups, the first is a simpler method only requires two electrodes [Figure 2.6], and the second requiring three electrodes

[Figure 2.7]. The two electrode method measures the potential of the cell as well as the current through the circuit. The three electrode method measures the potential of the working electrode vs. the reference electrode and the current flowing through the working electrode to the counter electrode [20].

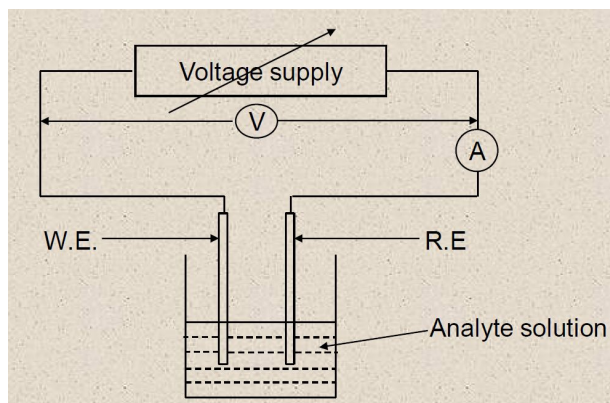


Figure 2.6: Representation of a simple Voltammetry setup with two electrode cell. W.E. - Working electrode, R.E. - Reference Electrode, V- Voltmeter, A- Ammeter [20].

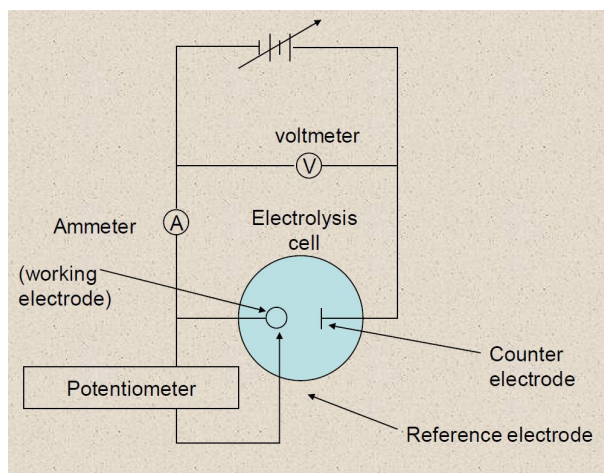


Figure 2.7: Representation of a modern voltammetric setup, with a three electrode cell with a potentiostat [20].

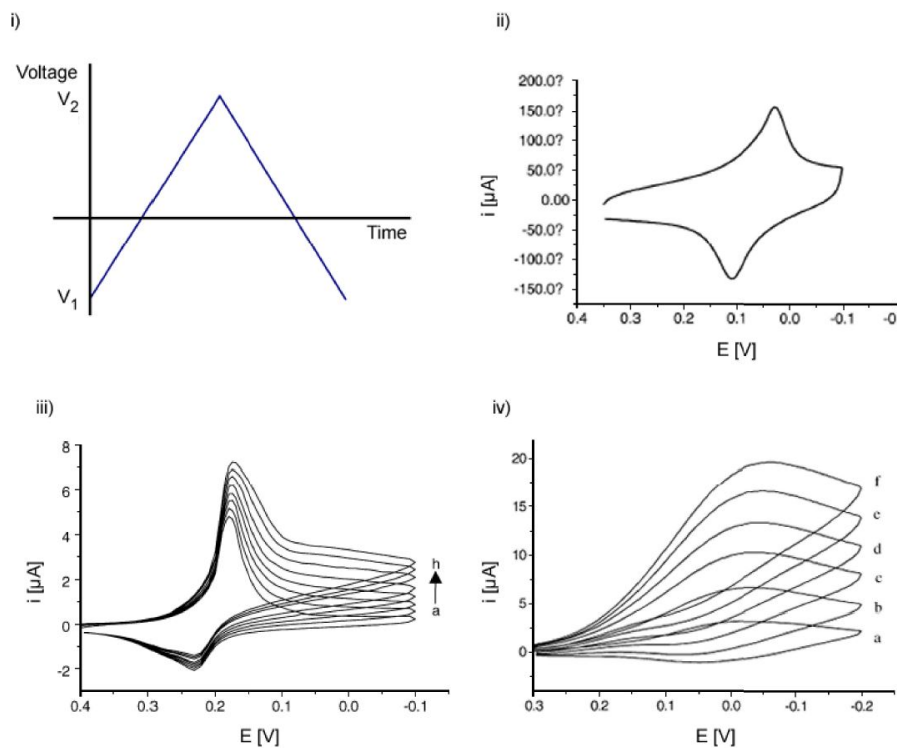


Figure 2.8: An overview of selected cyclic voltammograms: i) a single generic linear voltage sweep; ii) a cyclic voltammogram of the Prussian Blue-modified (PB) glassy carbon electrode was prepared in 0.1 M KCl + 0.1 M HCl at a scan rate 50 mV/s; iii) cyclic voltammograms of the PB sol-gel modified glassy carbon electrode and iv) the cholesterol/PB sol-gel modified glassy carbon electrode in a phosphate buffer (pH 6.8) at varying concentrations of the analytic solution: a) blank solution; b-f) blank solution + cholesterol 1×10^{-5} , 2×10^{-5} , 3×10^{-5} , 4×10^{-5} , 5×10^{-5} mol/L [20].

Figure 2.8(iv) shows a typical example of how a target analyte would be detected. Curve (a) depicts a blank or target free solution while curves (b-f) show increasing concentrations of target analyte in solution. Figure 2.8(ii) and Figure 2.8(iii) depict the voltammograms of the substrate at various manufacturing steps before the target analyte has been added.

2.1.8.2 EIS (Electrochemical Impedance Spectroscopy)

Impedance is defined by

$$Z_T = Z_R + Z_I \quad (2.1.1)$$

where Z_T , the total complex resistance (impedance), is equal to the sum of Z_R , the real part of impedance and Z_I , the imaginary part (reactance). This

is due to a circuit element (typically resistors, capacitors and inductors) being supplied with an AC (Alternating Current) signal. The electrical impedance can be related to voltage in the time domain by

$$V(t) = Z_T(t).I(t) \quad (2.1.2)$$

where $I(t)$ is the current and $Z_T(t)$ is the total impedance. The AC excitation signal (voltage) can be described in the time domain and related to frequency by

$$V(t) = V_a \sin(\omega t) \quad (2.1.3)$$

where ω is the excitation frequency and V_a is the excitation amplitude. A Fourier transform is then used to change a time based function to the frequency domain. This is defined by

$$\mathcal{F}\{f(t)\} = F(\omega) = \int_{-\infty}^{\infty} f(t)e^{-i\omega t} dt \quad (2.1.4)$$

where $F(t)$ is the time domain signal and ω is defined as

$$\omega = 2\pi f \quad (2.1.5)$$

where f is the frequency of excitation. These transforms provide harmonic spectra which can be evaluated [5].

EIS: Through the application of small sinusoidally varying potential, it is possible to measure the resulting current response of a target analyte. By varying the excitation frequency of the applied potential over a range of frequencies, the complex impedance can then be calculated as explained. EIS has the ability to study any intrinsic material property or specific processes that could influence the conductivity/resistivity or capacitance of an electrochemical system. For this reason EIS is an attractive tool in the development and analysis of materials for biosensor transduction. For example, by coating conductive electrodes with insulating polymers and then introducing this to an enzymatic reaction, the direct or indirect degradation of the polymer coating can be studied. If during the reaction, existing free ions are able to penetrate into the polymer, the insulating nature of the polymer would be compromised and result in modified impedance characteristics of the transducing element.

For electrochemical sensing, impedance techniques are useful to monitor changes in electrical properties arising from biorecognition events at the surfaces of modified electrodes. For example, changes in the conductance of the electrode can be measured as a result of protein immobilization and antibody-antigen reactions on the electrode surface [18].

2.1.8.3 Nanowires

Nanowires are part of a growing nano-technology group called nano-objects, which also include nanoparticles, nanorods, nanobelts, nanosprings, thin films and others. Nanowires are becoming increasingly more attractive as part of biosensor building blocks. Their use as high sensitivity electrodes is one example. Nanowires have diameters in the nanometer range. Thus, their diameters have a length scale comparable to the atoms of which they are comprised of and are sometimes referred to as quantum wires. Additionally, nanowires are referred to as one-dimensional structures, since their lengths are orders of magnitude larger than their diameters. The reason nanowires may be more useful or sensitive in comparison to larger wires is that, as a wire decreases in diameter to the nanometer regime, the ratio of surface atoms compared to interior atoms, i.e. the surface-to-volume ratio, drastically increases. Therefore, external influences by charged particles or biological species increasingly influence the conduction both on the wire surface and in the wire interior. The penetration into the wire interior is typically determined by the Debye screening length. Conductance in a nanowire is related to the sum of electron transport in the separate conduction channels of the nanowire defined by their quantization energy. The thinner the wire, the smaller the available unaffected volume, and hence the smaller the probability of uninterrupted conduction. Nanowires, therefore, represent very attractive bioelectrochemical transducer components, since their diameters are comparable to the size of the biochemical analytes under analysis and since their conductance is sensitive to surface perturbations [18].

2.1.9 Biosensor Testing and Standards

2.1.9.1 Types of Microbial Testing Performed

Biosensor tests are designed to detect and signal certain information about a biological element. Depending on the type of test, these sensors answer one or more of the following questions and hence can be classified accordingly [21]:

1. Is something there? **Qualitative Testing**
2. If there, how much is there? **Quantitative Testing**
3. If there, what is it? **Identification Testing**

Qualitative testing indicates whether a particular substance is present or not. It does not tell how much of the substance is present. An example of a qualitative test would be the pregnancy test as the test simply indicates that the user is pregnant and no more. Quantitative testing, on the other hand, gives a precise measure of how much target analyte is present or its concentration in a sample being analyzed. An example of a quantitative test would be a sensor

that indicates the amount of white blood cells in a sample when testing to see how advanced an HIV infection may be. Another example would be of a water sensor that can indicate the concentration of *E. coli* in a water sample. Finally, Identification testing has the ability to identify one of many analyte possibilities. An example of this would be a sensor that is designed to detect multiple target analytes, such as bacteria. This type of sensor would have different labels or markers (usually colorimetric in the form of fluorescence) attached to each of the different biorecognition elements and when either one or more of the target analytes are detected, each marker would give a unique and identifiable signal (i.e different colours of each marker.)

2.1.9.2 Biosensor "Gold" Standards

There are many different methods of detecting the presence of a target analyte, but not all the available tests are reliable or specific. Culturing methods continue to be the "gold" standard; followed by nucleic acid-based assays, ranked "silver", and the immunoassays, ranked "bronze". However, immunoassay is by far the most rapid compared to the other two methods. Culture methods require 24-48 hours or more in order to get the bacterial colonies on a petri dish. Some of the bacteria, like *M. tuberculosis*, takes 7-14 days to grow on the selected media. A nucleic acid based assay requires good technical expertise and a nucleic acid extraction step. Currently attempts are being made to automate the system for on-site application. In contrast, most of the antibody-based detection methods, such as lateral flow immunoassays, dipstick assays, and slide agglutination tests, can be done outside the convenience of a laboratory, with little technical knowledge, and the results can be obtained relatively quickly, in 10-15 minutes [22].

2.2 Human Immunodeficiency Virus (HIV)

HIV is a virus that attacks the immune system, specifically the white blood cells which are called CD4 (cluster of differentiation 4) cells (T-helper cells). The immune system and T-helper cells help fight off infections and diseases. HIV cannot grow or reproduce on its own. HIV makes copies of itself inside the T-helper cells. The process of T-helper cells multiplying in this manner is called the HIV life cycle [23, 24] as seen in Figure 2.10.

AIDS (Acquired Immunodeficiency Syndrome) is the final stage of HIV infection. Not all patients who have been infected with HIV are at the AIDS stage. This is the stage of infection that occurs when the immune system is so badly damaged that the number of CD4 cells is lower than 200 cells/cubic millimeter of blood (200 cells/mm³). At this stage of infection the body becomes vulnerable to opportunistic infections. The CD4 cell count of a healthy

uninfected adult ranges between 500 cells/mm³ and 1600 cells/mm³ [23].

The origin of HIV: Scientists have discovered a chimpanzee version of the immunodeficiency virus (called Simian Immunodeficiency Virus, or SIV) in Central Africa. They believe that SIV was transmitted and mutated into HIV in humans when chimpanzees were hunted for meat and the infected blood came into contact with humans [23].

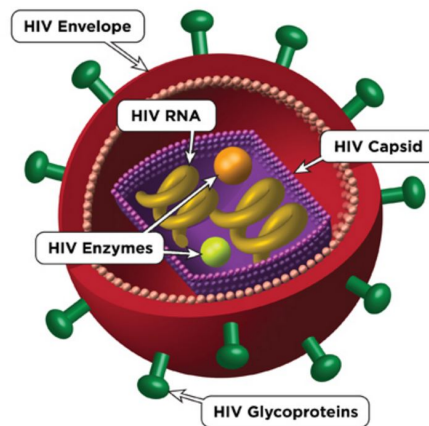


Figure 2.9: A representation of what HIV looks like [25].

Figure 2.9 shows what a typical HIV cell looks like. The key terms will be briefly explained [25]:

- HIV Envelope: The outer surface of HIV.
- HIV glycoproteins: Protein "spikes" embedded in the HIV envelope.
- HIV capsid: HIV's core that contains HIV RNA.
- HIV RNA: HIV's genetic material.
- HIV Enzymes: Proteins that carry out steps in the HIV life cycle.

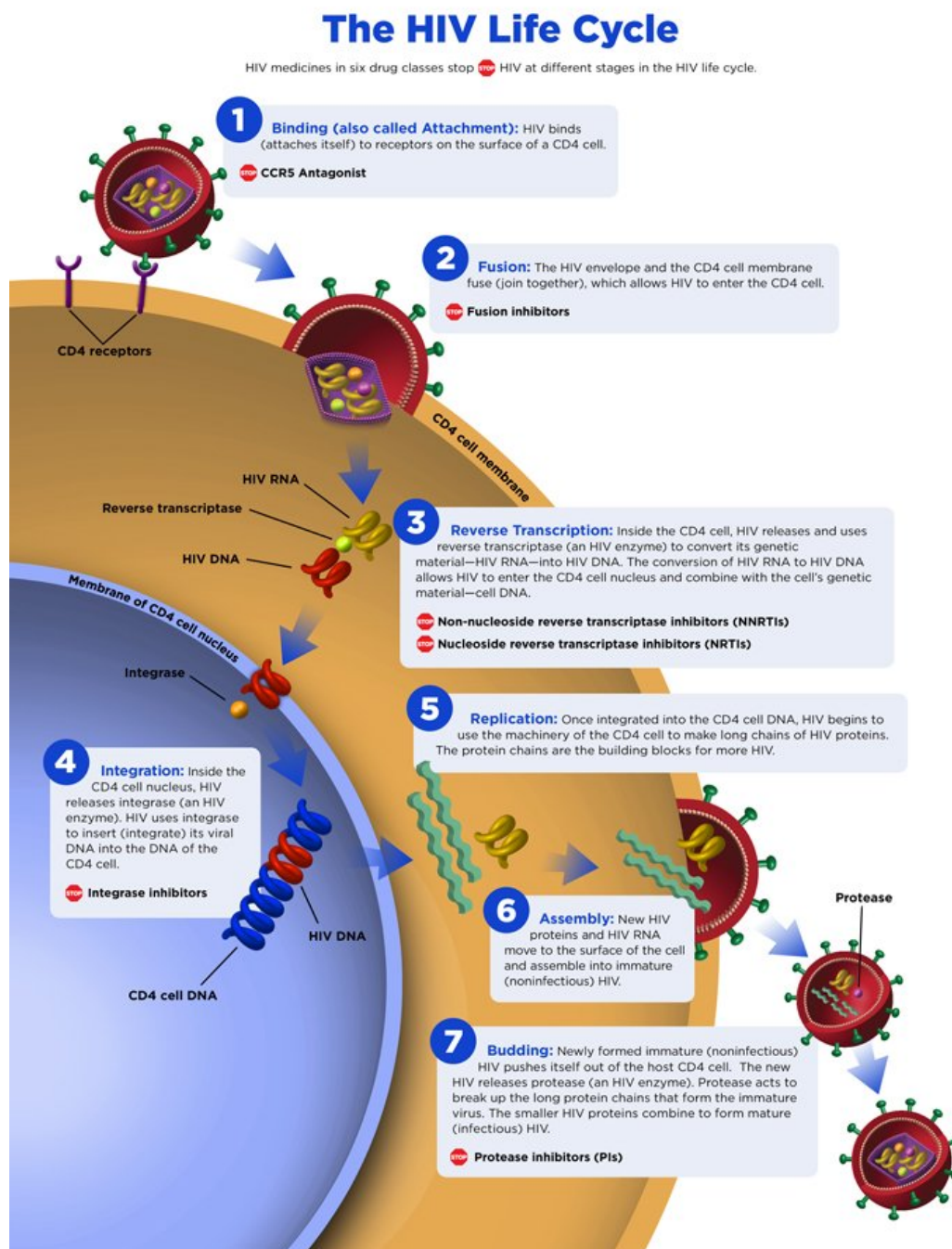


Figure 2.10: The HIV life cycle [25].

Figure 2.10 depicts the life cycle of HIV in 7 different stages. The seven stages are [25]:

1. Binding/Attachment

2. Fusion
3. Reverse Transcription
4. Integration
5. Replication
6. Assembly
7. Budding

2.2.1 HIV Diagnosis

If a patient does not know that they have come into contact with HIV, the first signs to cause a doctor to suspect HIV infection are when seemingly unrelated symptoms (fever, sore throat, headache, muscle ache, swollen glands or skin rash) last and no other cause can be found for these symptoms. If a patient has been infected with HIV, the immune system will begin producing antibodies to try destroy the virus. Urine, saliva or blood can be tested to find these antibodies. If a simple urine or saliva test shows positive for HIV, it is necessary to confirm with blood tests.

Most doctors use two blood tests to confirm HIV infection, ELISA (Enzyme-Linked Immunosorbent Assays) and the Western blot. HIV antibodies will usually only be detectable 2-3 weeks after infection and may take as long as 6 months to be detected [26], this is known as the window period.

2.2.1.1 HIV Screening Tests

As mentioned there are many ways to detect an HIV infection. A few of the commercially available HIV screening tests will be discussed.

ELISA:

Enzyme-Linked Immunosorbent Assays (ELISA) is the most commonly used test to screen for HIV infection. This method is relatively simple, has high sensitivity and is suitable for testing large numbers of samples. ELISA is a plate-based assay technique designed for detecting and quantifying substances such as peptides, proteins, antibodies and hormones [27, 28]. In the case of HIV testing, the most popular ELISA involves an indirect method in which HIV antigens are attached and antibodies in a sample which are allowed to react with the antigen coated solid support. The antibodies are left to react for 30 minutes at 37 °C - 40 °C. A wash step is then necessary to remove unbound serum components and a conjugate (an antihuman immunoglobulin with a bound enzyme) is bound to the specific antibody that is attached to the antigens on the solid phase. A second wash is then conducted and an

appropriate substrate is added that results in a colour development which is detected by a spectrophotometer. Optical density values are produced as the coloured solution transmits light which is proportional to the amount of antibodies bound. A mathematical calculation is conducted based on the optical density of the negative controls and multiplied by a factor which produces an optical density cut-off value. This optical density cutoff value is then compared to the sample optical density to determine the antibody status. Samples with optical density cutoff values > 1.0 are considered to be positive [28].

A more recent ELISA technology which is considered more powerful than the previous method, is called the sandwich assay. This type of capture assay is called a "sandwich" assay because the analyte to be measured is bound between two primary antibodies, the capture antibody and the detection antibody. This format tends to be more sensitive and robust. One disadvantage of this format is that it requires a relatively large sample volume. Figure 2.11 shows the common ELISA formats, namely the direct, indirect and sandwich assay formats.

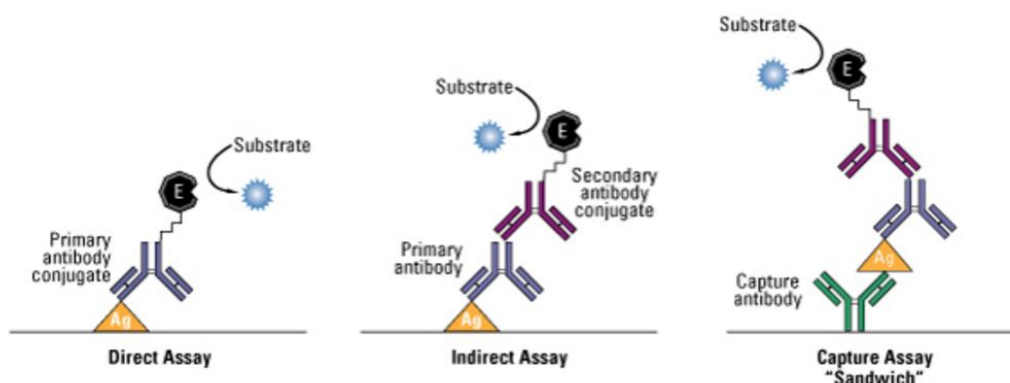


Figure 2.11: Common ELISA formats [27].

Western Blot:

The Western blot is the most common test used to confirm positive results from an ELISA or rapid HIV test. This is a test generally only used as a confirmatory test due to its complexity to perform and requires highly technical skills. The Western blot is considered the "Golden Standard" of HIV validation, because it is less likely to produce a false-positive result as it distinguishes the specific HIV antibody more effectively from other antibodies [28, 29]. The Western blot technique is based on an electrophoretic technique to separate HIV antigens derived from a lysate of virus grown in culture. The technique denatures the viral components and induces a negative charge to the antigens. It then separates the antigens primarily on the basis of their molecular weights.

The separation technique of antigens is similar to that of ELISA [28].

This test is conducted by splitting HIV into its various component proteins which are all different lengths and thus different weights (measured in kD - kilo Daltons). A sample of blood is then mixed with the proteins. If any HIV antibodies are present in the blood sample, they will attach to the proteins in a similar way to ELISA. These antibodies are then tagged using a marker. Each sample is then dipped into a special gel. An electric current is applied to the gel and the proteins begin to move down the gel. Heavier proteins will stop before the lighter ones. The more there are of each protein, the thicker and darker the layer of these proteins will be. The gel is then developed in a similar way to a non-digital photograph to show which proteins are present. If there are stripes where the HIV proteins should be, then the result is positive. If there are no stripes, the result is negative [28]. Figure 2.12 shows typical examples of Western blot reactions.

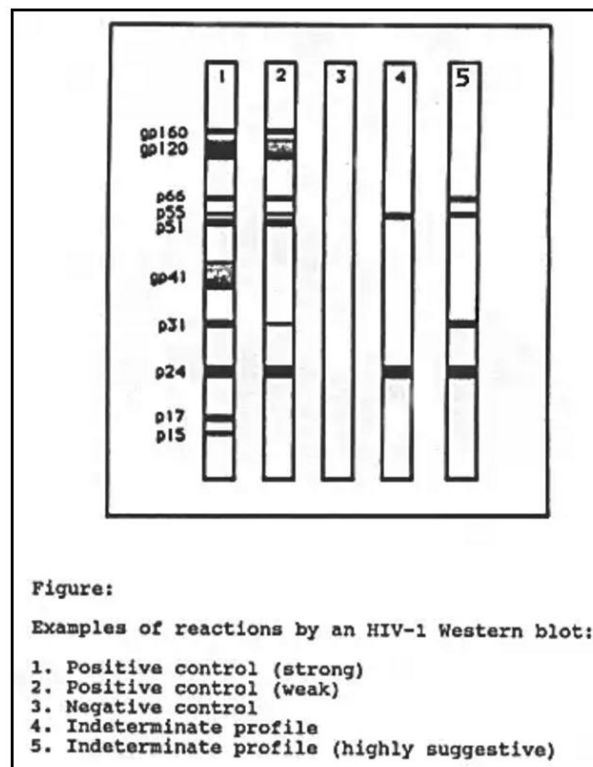


Figure 2.12: Typical examples of Western blot reactions [30].

Western blot is capable of identifying antibodies for lots of different HIV proteins or antigens at the same time, in comparison to ELISA which can only

detect one at a time. Western blot tests can, however, also yield inconclusive results in some samples [31].

Oral Fluid or Saliva:

A more convenient and less invasive test for HIV involves collection of saliva. Although the sample is generally referred to as saliva, the fluid is actually "crevicular fluid from capillaries beneath the tooth-gum margin, which is a transudate of blood and therefore similar to the samples used in serum-based tests." [28]. Antibody concentration in oral fluid is only about 1/400 of that in plasma, this implies that saliva based tests need to be extremely sensitive. Advantages of this test are ease of collection, group collection, collection from patients where blood is difficult to obtain (infants) and an increase in collection adherence. One FDA approved oral fluid test called the OraQuick Advance (OraSure Technologies; Bethlehem, PA) is a device that combines collection and testing. The device itself consists of an absorbent pad on a stick coupled to a lateral flow testing device. When testing, it is swabbed once around the gums, and then placed in a vial of buffer solution. The sample is then incubated for 20 minutes and the results are displayed in the same way other lateral flow rapid tests are displayed (pregnancy test with control line and reporting line). This test is reportedly equivalent in specificity and selectivity to ELISA. For this reason it is necessary to conduct a confirmation test via Western blot if the results are positive [28].

PCR tests: DNA and RNA (viral load)

Polymerase chain reaction (PCR) is a testing method that recognizes specific genetic material. This genetic material could be RNA (single strand) or DNA (double strand). RNA and DNA are both nucleic acids which can be used to specifically detect the genetic code of any living organism. During the PCR test a sample is amplified (to make many more identical copies of the DNA/RNA chain) multiple times to ensure there is a sufficient amount of RNA or DNA to be detected [31]. Once the amplification is complete, the amplified segments need to be compared to a known source (i.e a known HIV positive sample). The actual detection method is similar to that of the Western blot. An electrical current is supplied to a gel and various nucleotide sequences form bands or stripes according to their electrical charge and molecular size. This is termed gel electrophoresis. The bands that form from the unknown sample are then compared to bands that formed from the known sample [32].

The following reagents are needed to conduct PCR amplification [33]:

- A sample that contains a nucleotide sequence or DNA (blood, hair, skin etc.).

- DNA primers: Short single stranded DNA that attaches to nucleotide sequences which promotes synthesis of a complementary strand of nucleotides.
- DNA polymerase: an enzyme that, when the DNA has a primer bound, goes down the DNA segment attaching DNA building blocks to form complementary base pairs and thus synthesizes a complementary nucleotide strand of DNA (the introduction of a heat resistant DNA polymerase, Taq polymerase, derived from heat-resistant bacteria, markedly improved the ability to perform PCR).
- A large excess of DNA building blocks termed nucleotides (Adenine, Thymidine, Cytosine and Guanine, abbreviated as A, T, C and G, respectively) are present in the solution. When these blocks are linked together, they form a nucleotide sequence or a single strand of DNA. When these building blocks bind to their complementary building blocks, by weak hydrogen bonds (for example, A will only bond with T and G only with C), a complementary DNA nucleotide sequence is formed and bound to the original single stranded DNA. When the binding is completed, a complementary double strand DNA is formed in a specific sequence.

To begin the PCR procedure, a segment of the sample DNA is placed in a tube with the reagents listed above. The solution is then heated to 94 °C. The heat causes the hydrogen bonds in complimentary DNA strands to break and so creates single stranded DNA. This is termed denaturation of double stranded DNA. The sample is then cooled to about 54°C. At this temperature the DNA primers and DNA polymerase bind to individual single stranded DNA. Due to the fact that the DNA building blocks are in high quantity in solution, the polymerase uses them to make new complementary strands of DNA (termed extension of the DNA). Finally the end result is a new set of double stranded DNA molecules from each of the single strands of the original molecule. This process is completed in excess of 40 times using a machine called a thermal cycler. The thermal cycler automatically repeats each heating and cooling step. Due to the fact that the sample DNA doubles after every thermal cycle, it can be seen that the amplification is exponential. Where the original sample may have only contained a single short segment of DNA, after 40 cycles there could be over 100 billion new copies [33].

Rapid Tests:

Rapid tests are simplified versions of the ELISA tests. They detect HIV antibodies in samples [31]. Rapid tests are defined as tests that can produce results in <30 minutes. They are generally very accurate (95%-99%) and are comparable to the ELISA accuracy [28]. The most important advantage of rapid tests is that they are easy to perform and do not require higher training. This is particularly useful in developing countries where facilities may not

be optimal, there may be little to no stable electricity or unsuitable formal education programmes for laboratorians. The immunochromatographic assay type rapid test consists of a flat cartridge device, usually plastic or paper. The sample (blood, oral fluid or serum) is placed at the tip of the device and allowed to diffuse along the strip that is immobilized with reagents (usually protein A colloidal gold) that bind and permit visual detection of HIV antibodies, some use third-generation (antigen sandwich) technology. Most modern tests have built-in quality control test lines that indicate that the test was performed correctly [28].

Once a rapid test has been completed it is standard procedure to do a confirmatory test by either a separate rapid test manufactured by another company, ELISA, or Western blot which is said to be 100% accurate. It is also advised that, if any test is negative, a patient take another test after 3 weeks to ensure the window period has passed.

There are some disadvantages to the rapid test which are as follows [34]:

- **Poor staff training:** In some cases clinical staff or HIV counselors do not get the correct training in regards to specific rapid test use and interpretation. The lack of well-trained professionals available to administer testing not only affects the efficacy of the results, but also the quality of counseling that patients receive.
- **Ambiguous test results:** Results from rapid HIV tests are sometimes difficult to interpret. Tests that display faint lines may lead to a negative or positive interpretation, depending on a staff members opinion. Ambiguous results combined with poorly trained or inexperienced staff greatly increases the likelihood of inaccurate interpretations of results. It is advised that where results are inconclusive, the results and sample should be sent for laboratory testing. This then negates the fast and cheap advantages of rapid tests.
- **Ethical concerns:** There are some rapid tests which are available for home use. This leads to some major ethical concerns where counseling may not be readily available following a positive result. This may also lead to non-consensual testing or no protection of confidentiality of results. The World Health Organization's (WHO) Policy Statement regarding HIV testing strongly recommends that clinicians adhere to the three C's of screening: confidentiality of results, counseling before and after testing, and consent to be tested. The other concern is that where resources and training are limited, there is also little to no pre-test or post-test counseling. This is of great concern, as many patients may not understand the likelihood of a false-positive result or what to do in the case of a positive result that may completely alter their lives.

The HIV clinic at Stellenbosch University uses INTEC's "ADVANCED QUALITY™ RAPID ANTI-HIV (1&2) TEST CARD", as its primary rapid test. The user document, Appendix A.1, claims 100% sensitivity. The rapid test includes all relevant materials and instructions for use. The HIV clinic adheres to strict procedures and all HIV testing staff are trained to counsel the patients professionally. After a positive HIV result, the clinic staff run a second rapid test by a different manufacturer and if that result is also positive, they recommend an ELISA test to confirm.

2.3 DNA Introduction

2.3.1 DNA Definition

DNA or Deoxyribonucleic acid is a molecule that contains the building blocks and instructions living organisms need to develop, live and reproduce. These instructions are found in every living cell [35].

"A nucleic acid that carries the genetic information in cells and some viruses, consisting of two long chains of nucleotides twisted into a double helix and joined by hydrogen bonds between the complementary bases adenine and thymine or cytosine and guanine. DNA sequences are replicated by the cell prior to cell division and may include genes, intergenic spacers, and regions that bind to regulatory proteins"[36].

2.3.1.1 DNA Structure

"DNA is made up of molecules called nucleotides. Each nucleotide contains a phosphate group, a sugar group and a nitrogen base. The four types of nitrogen bases are adenine (A), thymine (T), guanine (G) and cytosine (C). The order of these bases is what determines DNA's instructions, or genetic code. Similar to the way the order of letters in the alphabet can be used to form a word, the order of nitrogen bases in a DNA sequence forms genes, which in the language of the cell, tells cells how to make proteins. Another type of nucleic acid, ribonucleic acid, or RNA, translates genetic information from DNA into proteins"[35].

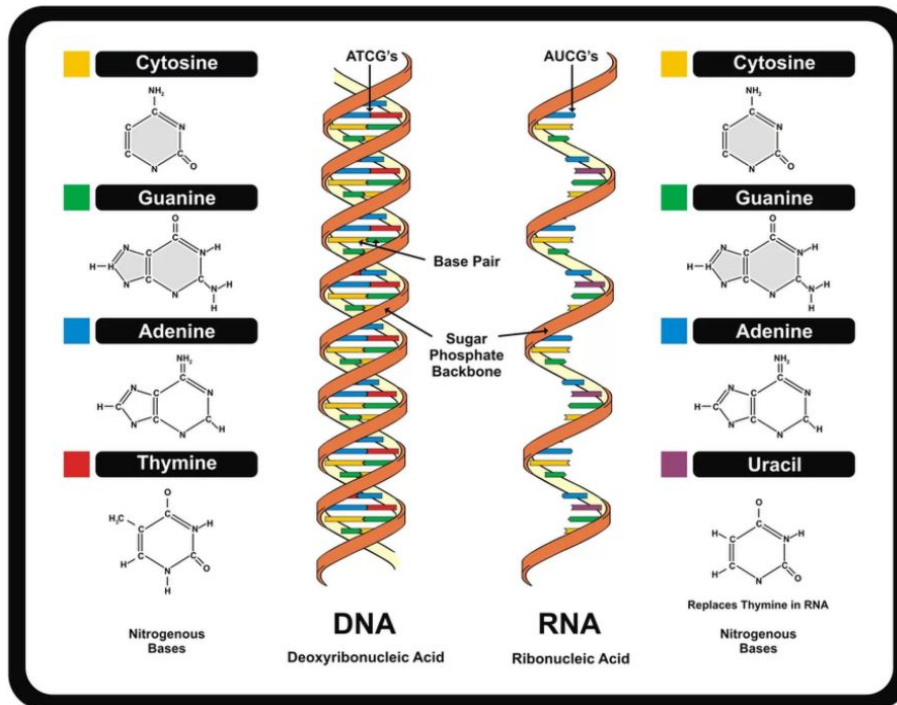


Figure 2.13: The structure of DNA and RNA. DNA is a double helix, while RNA is a single helix. Both have sets of nucleotides that contain genetic information [35].

Figure 2.13 is a representation of the structure of DNA and RNA. The nucleotides are attached together to form two long strands that spiral to create a structure called a double helix. The nitrogen bases on one strand bind with the nitrogen bases of the other. Adenine pairs with thymine and guanine pairs with cytosine.

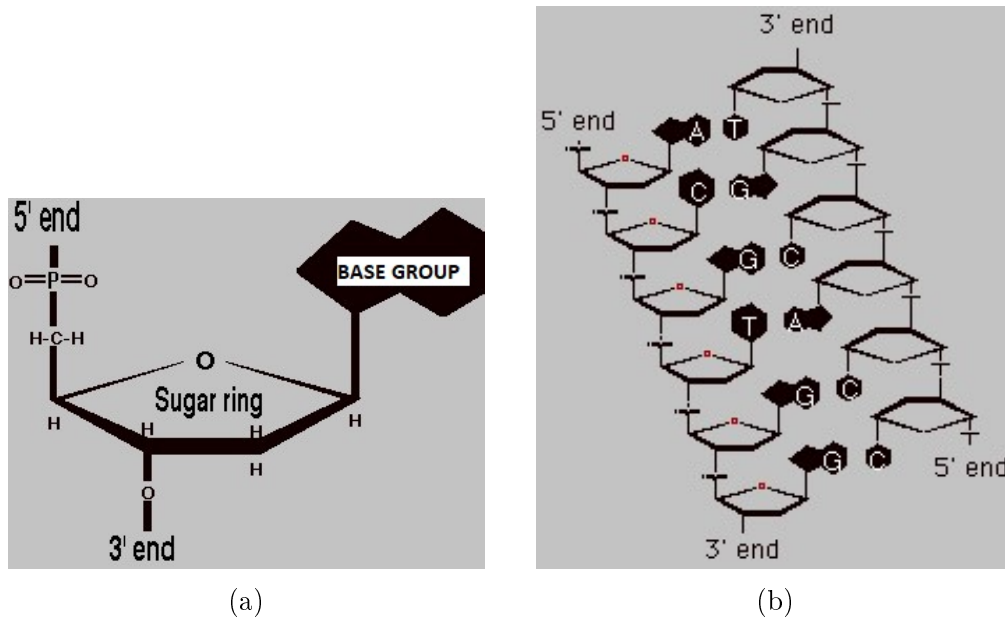


Figure 2.14: Representation of DNA nucleotides and their directionality [37].

2.3.1.2 DNA Directionality

The structure of a DNA strand has a direction. When a DNA strand is formed, it is constructed in a specific order. This is called directionality. DNA is always formed from the 5' (5 Prime) end towards the 3' (3 Prime) end. Figure 2.14(a) is a depiction of a single base nucleotide showing where the 5' and 3' ends are. The direction of the second strand of DNA in a double helix is always opposite to the first, also known as anti-parallel. This means that the 5' end of one strand will always bind to the 3' end of the other strand. Figure 2.14(b) shows an example of two strands of DNA and their end formation.

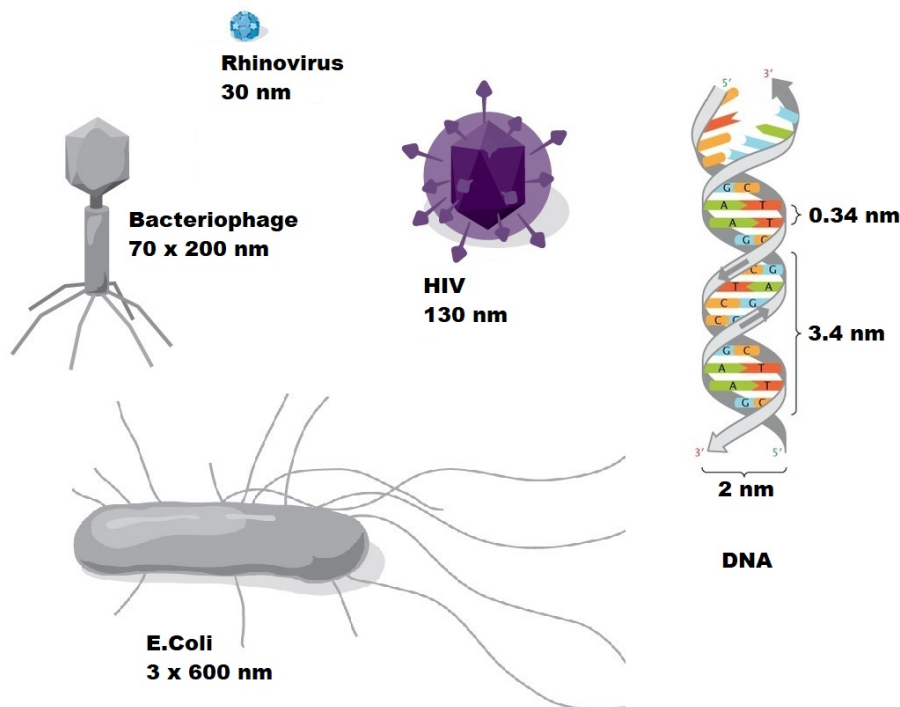


Figure 2.15: A size comparison of different biological elements. Images edited and compiled from [38, 39, 40].

2.3.1.3 DNA Size Comparison

Figure 2.15 depicts the size of DNA in comparison to other biological elements, such as the HIV virus and the *E. coli* bacteria. It can be seen that DNA is considerably smaller than most bacteria and antigens.

2.3.1.4 DNA Temperature of Melting (T_m)

When DNA is heated, double stranded DNA (dsDNA) is *denatured* into single stranded DNA (ssDNA) by breaking the hydrogen bonds between the bases. Denaturation can also be accomplished by a change in pH or salt concentration. The temperature of melting (T_m) is defined as "The temperature at which 50% of double stranded DNA is changed to single-stranded DNA. The higher the melting temperature the greater the guanine-cytosine content of the DNA" [41]. The T_m depends on two major factors. First the length or number of bases in a DNA sequence and second, the specific nucleotide sequence of the DNA (i.e more guanine-cytosine base pairs will form stronger bonds.). The guanine-cytosine pair is bound by three hydrogen bonds, while adenine-thymine pairs are bound by two hydrogen bonds. There are several methods of calculating the T_m of a DNA sequence, but the simplest is the method of

Wallace, which is suitable for short DNA sequences (14-20 base pairs). The Wallace method simply assigns 2°C to each A-T pair and 4°C to each G-C pair in a given sequence. The T_m is then calculated as the sum of all the individual pairs. The equation for calculating the T_m is seen in Equation (2.3.1). It can be seen that more base pairs in a DNA sequence, require higher temperatures and again higher temperatures with more G-C base pairs [42].

$$T_m = 2^\circ\text{C}(A + T) + 4^\circ\text{C}(G + C) = ^\circ\text{C } T_m \quad (2.3.1)$$

When ordering specific DNA oligonucleotides, the T_m can usually be calculated automatically on the manufacturing websites or other DNA analysis tools with more accurate methods. The T_m is also commonly listed on the specification sheets of DNA oligonucleotides upon delivery.

2.3.1.5 DNA Self Dimers

"DNA and RNA oligonucleotides can form adverse secondary structures. Self-dimers (also called homo-dimers) occur when some portion of an oligonucleotide is complementary to itself, resulting in an oligonucleotide molecule that can hybridize to another oligonucleotide molecule of the exact same sequence"[43].

The self dimers of a DNA oligonucleotide can also be automatically predicted on most manufacturing websites or other DNA analysis tools.

2.3.2 DNA Based Biosensors

Once one has an understanding of DNA and the structure of DNA it is not hard to imagine the biosensing possibilities. As previously mentioned in Section 2.1.3.3, if the DNA sequence or even a small portion of the sequence of a particular biological element is known, it is possible to synthesize a single stranded DNA complementary copy of this DNA. This synthesized DNA can then be used as the recognition element of a biosensor and is called Probe DNA. When in the presence of target DNA, the Probe DNA will be able to bind to the target DNA like a puzzle piece, because it has been designed to be complementary to that DNA and no other.

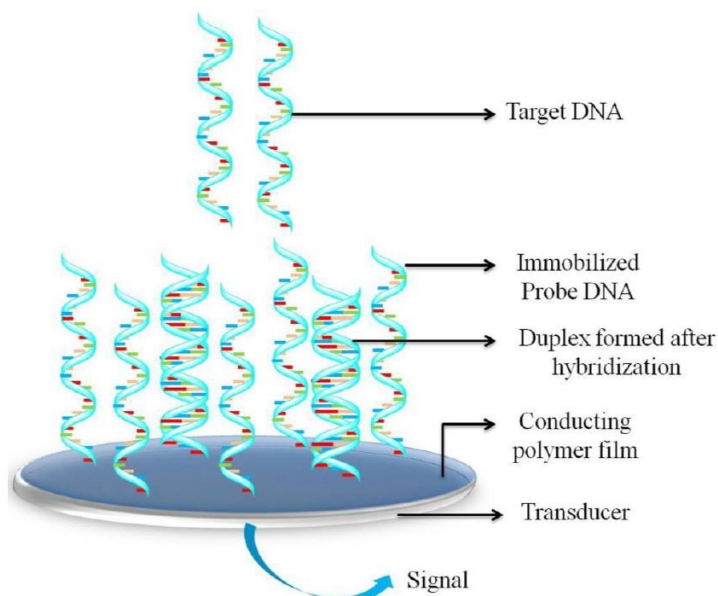


Figure 2.16: A basic example of a DNA based electrochemical biosensor [44].

Figure 2.16 shows a typical example of an electrochemical DNA biosensor. The DNA probe is immobilized to the transducer and when the target is hybridized with the probe, an electronic signal can be read.

2.4 HIV DNA Biosensor Research

Section 2.2.1.1 described the current industry standard methods of HIV detection. This section is a brief review of HIV DNA detection research articles. These articles give a good indication of the electrochemical properties of DNA, as well as the types of transducers and immobilization techniques that are more practical for research purposes. Three of the most relevant articles were chosen, but there are many more available that relate to either DNA detection, electrochemical biosensors, HIV detection or a mixed combination of all of the above.

2.4.1 A label-free electrochemical biosensor for detection of HIV related gene based on interaction between DNA and protein

Guo *et al.* [45] have described a novel label-free electrochemical based HIV biosensor.

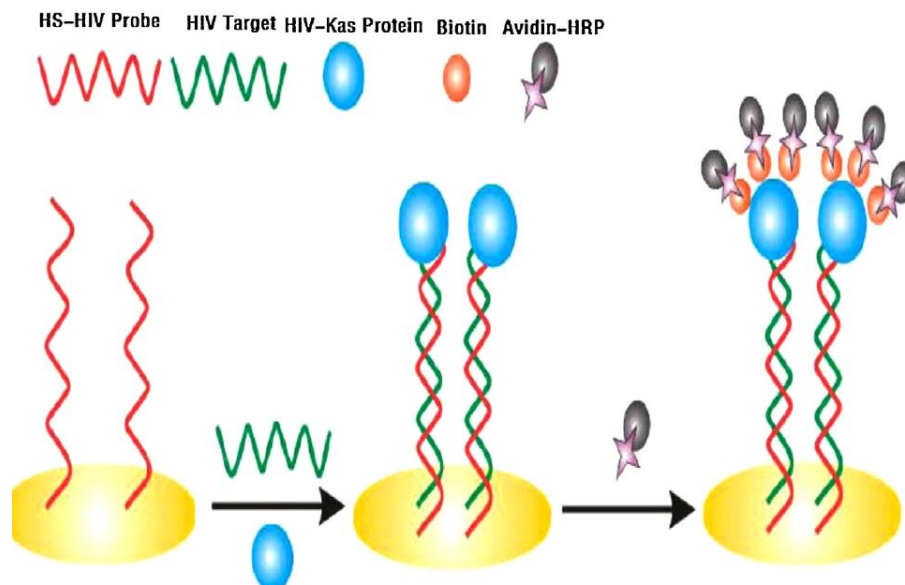


Figure 2.17: Schematic illustration of biosensor proposed by Guo *et al.*[45] .

Figure 2.17 depicts the schematic illustration of the proposed biosensor. An HIV DNA capture probe is immobilized on the surface of a screen printed electrode by means of Au-S bond, which form SAM. A target sequence is then introduced which then naturally hybridizes to the capture probe to form a double stranded hybrid. Once the double stranded hybrid is formed, a NF-kB protein uniquely binds to the probe. The NF-kB would have been previously marked with Biotin and as a result the streptavidin-HRP conjugate integrates to the biotin marked NF-kB protein via the strong biotin-avidin interaction. "HRP enzymes can efficiently catalyze the reduction of hydrogen peroxide with the help of an electroactive cosubstrate, TMB, which could be readily transduced to electrochemical current signals that quantitatively reflected the amount of DNA targets." [45]. The result is a biosensor that has a current signal that is proportional to the amount of reverse transcription DNA present. The results show high electrochemical sensitivity and selectivity with limit of detection (LOD) as low as 7.05pM.

2.4.2 Coupling of a Reagentless Electrochemical DNA Biosensor with Conducting Polymer Film and Nanocomposite as Matrices for the Detection of the HIV DNA Sequences

Fu *et al.* [46] conducted research on reagentless electrochemical DNA biosensing, to detect (HIV) sequences based on electrochemical impedance spec-

troscopy (EIS) and Cyclic Voltammetry (CV).

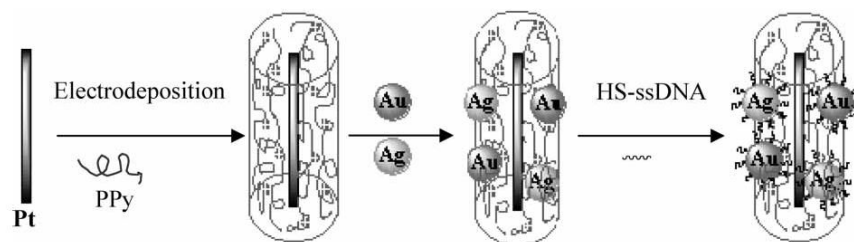


Figure 2.18: Schematic of stepwise fabrication process of biosensor proposed by Fu *et al.*[46].

Figure 2.18 depicts a schematic diagram of the modified electrode showing the stepwise fabrication process. The electrode in this biosensor is fabricated by depositing conductive Polypyrrole (PPy) on a platinum rod. Thereafter gold (Au) and silver (Ag) nanoparticles are bonded onto the PPy surface. Specific HIV sequenced Mercapto DNA probes (HS-ssDNA) were then allowed to bind to the gold and silver nanoparticles to complete the sensor. PPy was used because research shows that there may be conductivity changes in PPy film and nanocomposites in response to bio-activity. PPy has also received most attention due to its high conductivity, redox activity, good ion-exchange capacity, strong adsorptive capabilities, together with a fairly long-term thermal and mechanical stability. Once fabrication is complete, the sensor hybridized with target DNA to the probe for 3 minutes at a constant potential of 0.5V. EIS and CV were used to analyze the sensor for detection of the target DNA (HIV). Fu *et al.* report a detection limit of .5 nM.

2.4.3 Label-free DNA biosensor based on resistance change of platinum nanoparticles assemblies

Skotadis *et al.* [47] have designed an innovative nanoparticle based biosensor. Gold interdigitated electrodes (IDE) are deposited on a silicon wafer with a prior titanium layer for adhesion purposes. Differing gaps between interdigitated electrodes were tested (namely 30 μm , 10 μm and 5 μm). Figure 2.19 depicts the gold interdigitated electrodes on a silicon wafer substrate.

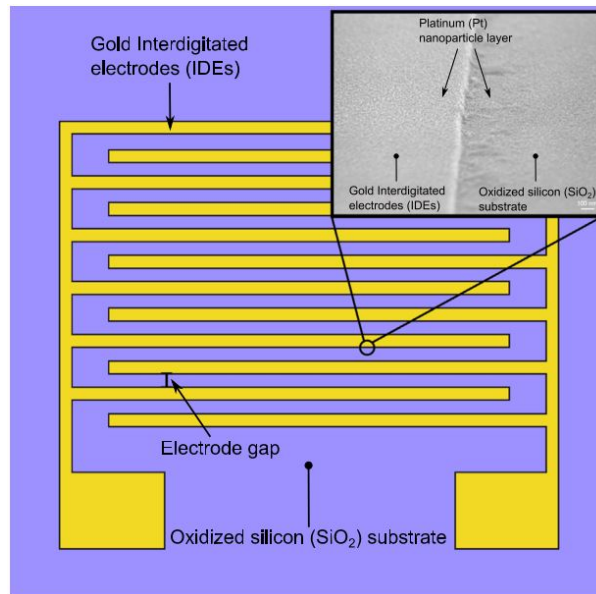


Figure 2.19: Gold interdigitated electrodes on silicon wafer substrate [47].

Platinum nanoparticles are then sputter coated onto the substrate at varying thicknesses to produce specific resistance values between the electrodes. Resistance values between $110\text{k}\Omega$ - $95\text{M}\Omega$, depending on electrode gaps and platinum deposition thickness, are reported. Thiol-modified ssDNA probes are used as the detection element. The thiol tether is capable of binding to both the gold electrodes and the platinum nanoparticles. The hybridization of target DNA to DNA probe create nanoparticle networks or conductive "bridges" between the nanoparticles and electrodes, which effectively decreases the overall resistance of the sensor. Figure 2.20 depicts a cross section of the sensing device and a representation of target-probe DNA hybridization "bridges" between nanoparticles.

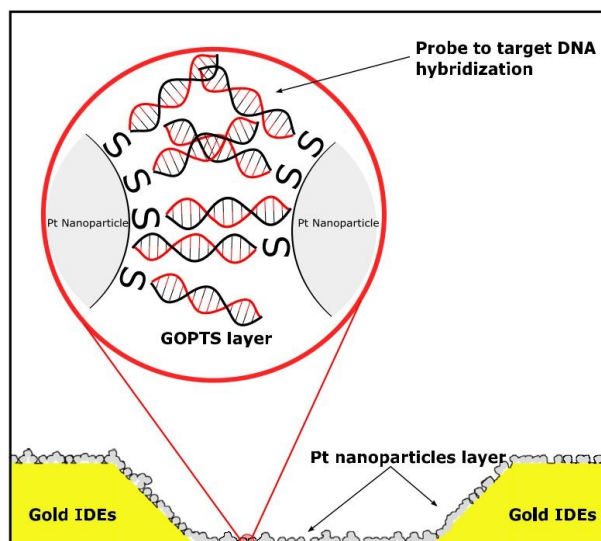


Figure 2.20: Cross section of the sensing device (schematic) after the target to probe DNA hybridization event [47].

A buffer solution ($2\mu\text{L}$) is added to the sensor, and resistance measurements are taken until the sensor reaches a steady state, and another $2\mu\text{L}$ buffer is added to ensure no further distortion. At this point a base resistance is noted and the target DNA is added to the sensor. The resulting resistance change is directly related to target DNA hybridization to the DNA probe and the change can be depicted as a function of $|\Delta R|/R_0$. A LOD of 1nM is reported and is able to differentiate between fully complementary DNA and a single base pair mismatched (1 base MM) probe to target DNA hybridization. It is also reported that there is no measurable change in response when comparing $1\mu\text{M}$ and $10\mu\text{M}$ concentration of probe DNA, indicating that the sensor surface is very quickly saturated with probe ssDNA.

2.5 Conclusion

Section 2.1 introduced basic biosensor definitions, models, concepts, and techniques. Section 2.1 also detailed differing transducer techniques with the main focus on optical and electrochemical based transducers. Although the main focus is electrochemical based biosensors, the other techniques have similar fabrication techniques and may provide more options that can be used within the electrochemical design, such as immobilization techniques, blocking and labeling. Section 2.2 gave an introduction to HIV and AIDS. The different screening techniques were reviewed and compared and some ethical concerns were mentioned. Section 2.3 gave a very basic definition of DNA and its structure. Finally, Section 2.4 reviewed the three most relevant Electrochemical

HIV DNA based biosensor articles found. These articles provide insight into the necessary components of DNA sensing, as well as the viability of electrochemical DNA detection.

Chapter 3

Research Background

3.1 Current Biosensor Research at Stellenbosch University

3.1.1 Superconductors Advanced materials and Nano Devices (SAND) Research group

In 1989 Prof. Willem Perold began a new research group called SAND (Superconductors Advanced materials and Nano Devices). For the first few years the team focused research on superconductors and processing of high temperature superconducting device structures. About 6 years ago, the team's primary focus shifted towards nanosensors and nano devices such as piezoelectric generators. Over the last 4 years however, the SAND team's efforts shifted yet again towards biosensing. The SAND team size is rapidly growing from an initial team size of about 4-6 postgraduate students per year to more recently about 15 members in the team. Due to the nature of the biosensing research field, the SAND team established collaborations with a few other Stellenbosch research departments such as Mechatronic Engineering, Microbiology, Physiology and Agricultural Sciences, to name a few. These collaborations form well rounded multidisciplinary research that accelerates and increases the quality of research.

3.1.2 Development of a Resistive Microfluidic Sensing Device for Pathogen Detection

In 2015, Christiaan Viviers joined the SAND team and conducted an undergraduate project titled "Development of a Resistive Microfluidic Sensing Device for Pathogen Detection"[48]. The focus of the project was to design a biosensor that measures the resistive change of a transducer due to positive antibody-antigen binding. A proof of concept study was established using lysozyme and an antibody specific to its antigen. Non-woven polypropylene mi-

crofibers coated with a conductive polypyrrole, co-polymerized with carboxylic acid functional 3-thiopheneacetic acid and treated with iron(III)chloride doped with 5-sulfosalicylic acid, rendering the fiber sheets conductive was used as the sensor transducer. Mr Viviers was able to positively detect the presence of the lysozyme antigen.

3.1.3 Low Cost and Portable *E. coli* Biosensor

Due to the positive findings of Mr Viviers' project, Prof. Willem Perold put together a small engineering team to develop a small low cost and portable *E. coli* biosensor funded by the Technology Innovation Agency (TIA). The team had a short 4 months from December 2015 to March 2016 to design and fabricate this device and run experiments. The engineering team consisted of: Michael Maas (project leader, electronic engineering Master's graduate), Christiaan Viviers (primary engineer, electronic engineering Master's student), Nicholas Lawrenson (myself, electronic engineering Master's student), Lowku Leeuwner (undergraduate electronic engineering student) and Ayan Booyens (undergraduate mechatronic engineering student).

The biosensor that was designed was a modified and optimized version of Mr Viviers' initial project design. *E. coli* specific antibodies were used as the recognition element and the same non-woven polypropylene microfibers (made to be conductive) were used as the transducer. A simple voltage divider circuit was designed by Mr Leeuwner as the sensing device. My role in the team was to assist Mr Viviers with the fabrication of the conductive fibers, binding of the antibodies to the transducer and the testing procedure. Other roles included circuit board design, routing and building as well as 3D printer availability and research for the housing of the device.

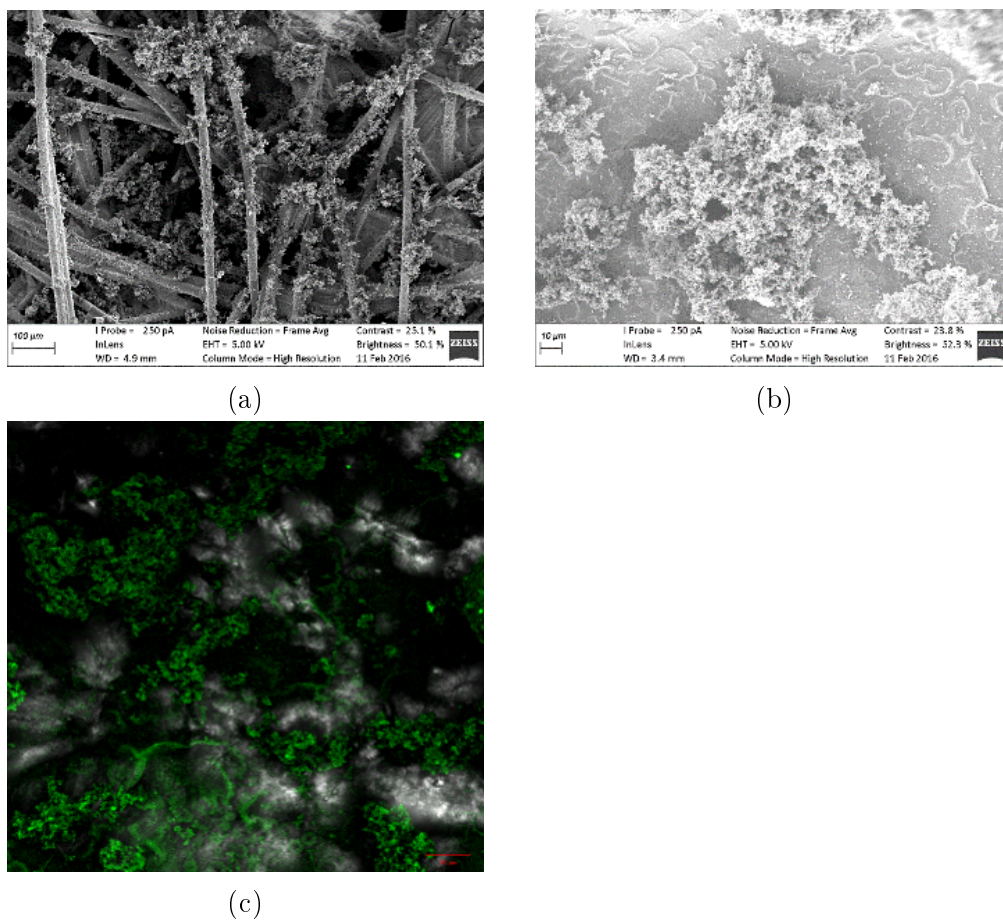


Figure 3.1: Imaging of microfiber at different steps of fabrication. (a) SEM (scanning electron microscope) imaging of conductive coated microfiber. (b) SEM imaging of glutaraldehyde added coating as cross linker. (c) Confocal image of antibody immobilization with fluorescent labeled secondary antibody to validate immobilization.

Figure 3.1 shows the results of the various fabrication steps. Figure 3.1(a) shows the individual microfibers with the conductive coatings, it can be seen that the coating is not uniform and covers sections of fibers rather than individual fibers. Figure 3.1(b) shows the glutaraldehyde cross linker added after the conductive coating is complete. Again this coating is not uniform and covers multiple layers. Figure 3.1(c) is a confocal image that validates that the antibody immobilization steps are correct and that binding of antibody immobilization is stable and long lasting following various wash steps. In order to complete confocal imaging, a secondary antibody with a fluorescent label was necessary. The final sensor did not incorporate this secondary antibody and therefore did not fluoresce. Figure 3.1(a) and Figure 3.1(b) were taken at the CAF EM (Central Analytical Facility Electron Microscopes) unit on the MERLIN FE SEM at the department of Geology, Stellenbosch University.

Figure 3.1(c) was taken at the CAF Fluorescence Microscopy Unit on the Zeiss LSM780 Confocal Microscope at the Department of Physiology, Stellenbosch University.

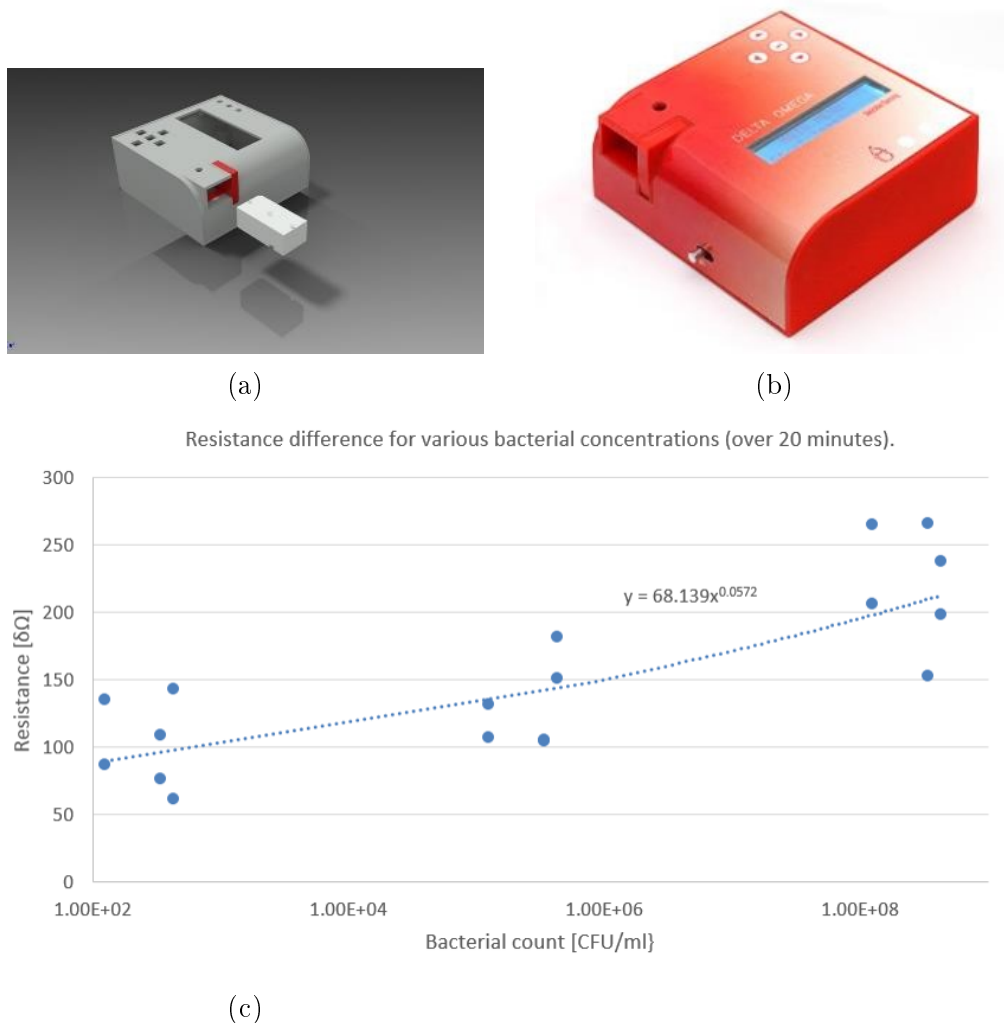


Figure 3.2: Project results. (a) A rendering of the proposed final biosensor. (b) The final *E. coli* biosensor. (c) In this results graph, the change in resistance across various prepared electrotexiles is compared. Every point represents a different fiber. It can be seen that the increase in resistance across a fiber with applied *E. coli* concentration of 100-1000 CFU/ml (Colony Forming Units/ml) is much lower than that where *E. coli*, in the range of 10^8 CFU/ml is applied.

Figure 3.2(a) shows the initial rendering of the proposed biosensor. The biosensor was designed with a small LCD screen to display the results, 5 buttons for menu functionality and a replaceable cartridge system that would allow the changing of the transducer after use. Figure 3.2(b) is the complete biosensor. The housing was 3D printed and covered in a laminated sheet. Figure 3.2(c)

is the positive test results of the biosensor. It can be seen that with higher concentrations of positive *E. coli* antigen, a higher response is measured.

3.2 Conclusion

Work on this project provided great personal insight into biosensing research. Resistive based biosensors are a relatively new concept and therefore there is little research in this field, but it seems to be an innovative and elegantly simple way to detect the presence of bacteria. The SAND team has begun experimenting with different methods and techniques of biosensing which utilize resistive based electronic sensing.

Chapter 4

Proposed Project Design

This chapter will focus on the design procedure as well as the design specific research completed. The overall design steps of each biosensor component will also be discussed. In the following chapters the full design specifications will be detailed with characterizations and thereafter, the results will be discussed.

Initially the research focus was very broad, with the basic objective being "Electrochemical Detection of Viruses". With this topic in mind, Prof. Willem Perold contacted Prof. Gert van Zyl from the Virology Department, Stellenbosch University. A collaboration was formed as Prof. van Zyl would be able to provide valuable information with regard to viruses. Due to this collaboration and as Prof. van Zyl's specialty is HIV, it was decided that the research topic be would refined to "Electrochemical Detection of HIV DNA". By detecting HIV DNA, instead of antibodies, it is possible that the three month window period may be significantly reduced. If the research results are positive, it is also possible that any DNA sequence may be detected with minimal changes to the overall design.

Chapter 2 gives a well defined description of the generic biosensor setup, sensing techniques used in biosensors and it reviews some relevant electrochemical DNA based biosensors. Chapter 2 also gives a brief introduction to DNA and HIV as well as the current methods and standards of screening for HIV. Chapter 3 gives a brief background on previous biosensor work done at Stellenbosch University as well as details on an *E. coli* biosensor designed by the SAND team.

Using the knowledge gained from Chapter 2 and Chapter 3, a proposed project design can be formulated. Referring back to the biosensing model in Chapter 2, Figure 2.1, it can be seen that, when designing a biosensor there are four main design decisions or components. Figure 4.1 shows a block diagram of these components.

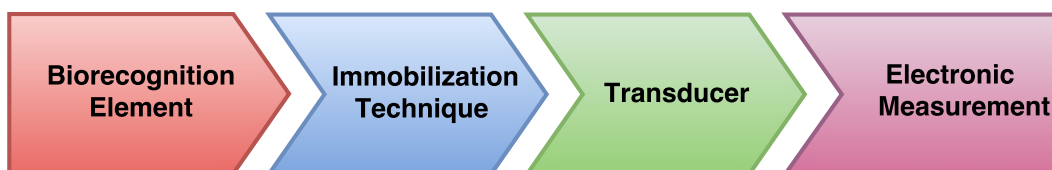


Figure 4.1: Biosensor design block diagram.

The four components of an electrochemical biosensor are the biorecognition element, immobilization technique, transducer and the electronic measurement device. Depending on the design of the particular biosensor, each component may or may not be mutually exclusive. So when making decisions, the characteristics of one component may affect the design needs of the next. For this reason, each design component needs to be carefully considered and the design process must be iterative. The next sections will follow the design decision procedure of each component.

4.1 Transducer

Due to the fact that the desired biosensor is electrochemical in nature, the transducer was the first component considered when design the began. The concept of nanowires was introduced in Section 2.1.8.3. It has been discussed that a good transducer has a relatively large surface area, which allows for more binding sites of the biorecognition elements. Nanowires exhibit much larger surface areas in comparison to planar surfaces. It was also noted that nanowires are a good choice due to their ratio of surface atoms to interior atoms (surface-to-volume ratio). This implies that the surface conductivity may have a bigger impact on the overall conductivity. Therefore, external influences by charged particles or biological species, increasingly influence the conduction both on the wire surface and in the wire interior [18].

As mentioned in Section 3.1.2 and Section 3.1.3, the SAND team have previously conducted research on a microfiber polymer mat with a conductive coating. While working with these microfiber mats, a few negative characteristics were found. It was found that the conductivity of the mats was very difficult to reproduce uniformly and in fact, it was near impossible. This was due to the fact that the conductive coating was somewhat random and uncontrolled. There was also a significant amount of unbound conductive composite on the mat which affected the overall conductivity of the mat. Mat conductivity was also drastically reduced when vigorously washed, which implied that the majority of the conductive properties of the mat was due to unbound conductive composite. For these reasons it was decided that an alternative solution be

found. An ideal solution to the problem would be an intrinsically conductive fiber to reduce fabrication steps and ensure uniformity.

4.1.1 Conductive Fibers

Research was done in order to determine the possibility of either manufacturing or ordering intrinsically conductive fibers that are ideally in the nanoscale range. The potential fiber must not only be conductive in nature, but also suitable for biosensor use. It was found that the conductive properties of a material can be altered by the pH level of a solution and thus the chosen fiber must be conductively stable at a pH between 6-8, because most biocatalyst and immunological reactions occur optimally at neutral pH [49].

Touhami [50] reports that one of the first new nanomaterials used in conjunction with amperometric biosensors was the carbon nanotube (CNT), which was doped into a number of different polymer formulations to improve current densities and overall performance of enzyme electrodes. Alocilja *et al.* [49] have reviewed Polyaniline (PANI) as a conductive polymer for specific use in biosensors. PANI is considered one of the best conductive polymers for biosensing due to its stability in liquid form, promising conductive properties and strong biomolecular interactions. Aussawasthien [51] conducted extensive research on conductive nanofibers which included materials such as Electrospun Poly (Ethylene Oxide), Electrospun Polyaniline, Carbon Nanofibers (CNFs), and other nanocomposites. Aussawasthien also described the basic electrospinning process and compared the various properties of the different materials used to electrospin conductive fibers. Finally Baker, *et al.* [52] used carbon nanofibers with biological molecules such as DNA. They reported that vertically aligned carbon nanofibers (VACNF) can be effectively functionalized with biomolecules such as DNA. The results showed that carbon nanofibers yield a high density of biomolecular binding sites that exhibit excellent selectivity with a high degree of accessibility. It was also reported that carbon nanofibers demonstrate good chemical stability.

These options were discussed with Prof. Peter Mallon from the Department of Polymer Science, Stellenbosch University. A number of suggestions were made which included electrospinning custom conductive nanofibers using CNTs and a polymer such as Polyaniline. It was decided, however, that the optimal solution would be to order a carbon fiber mat if possible. A carbon nanofiber or CNF Nano-mat was ordered from Pyrograf Products, Inc. [53, 54]. Matlock-Colangelo *et al.* [55] produced an article stating the many positive attributes of carbon based biosensors and referenced a number of articles that utilized carbon based materials in electrochemical biosensors.

4.2 Immobilization Technique

Once the carbon nanofiber mat was chosen as the transducer, the biorecognition element, as well as the immobilization technique, needed to be considered. A technique needed to be chosen that would allow DNA probes to bind to the carbon nanofiber. Section 2.1.5 discusses the various immobilization techniques available. Research on immobilization on carbon surfaces indicate that the two main techniques of interest are SAM, avidin-biotin binding (Section 2.1.5.2 and Section 2.1.5.3). In Section 2.1.3.4 it was discussed that DNA probes could be modified with an addition of a tether. It is possible to add a biotin tether to allow binding to avidin. It is also possible to add a thiol tether to allow binding to a number of materials, but most commonly gold. In order for either of these techniques to be utilized, it would be necessary to first deposit either gold or avidin onto the carbon nanofibers. It was discussed that the avidin-biotin bonds have a few disadvantages, such as unspecific adsorption and the possibility of greater background signal. For these reasons it was decided that gold-thiol SAM immobilization would be the best choice, because gold is readily available, stable and easy to deposit and the gold-thiol bond is relatively stable and well researched.

4.2.1 Deposition of Gold

There are a number of methods available for the deposition of gold, such as thermal evaporation, sputter coating and electroplating. Due to the fact that the gold deposition would be taking place on nanofibers, the deposition itself would need to be in the nanometer range. For this reason it was decided that sputter coating of gold would be the best choice, as sputter coated particles are in the single unit nanometer range. Sputter coaters are readily available and the sputter procedure is relatively easy and non-damaging. Thermal evaporation was also considered, but there are issues with non-uniform coverage and the nanofibers could also be potentially damaged. For similar reasons electroplating was also decided against, as nano-particle gold powder would be needed, which is not readily available and the procedure could also potentially damage the nanofibers.

4.3 Biorecognition Element

The biorecognition element is a vital part of any biosensor design. The decisions made directly affect the sensitivity, selectivity and reproducibility of a sensor. With the help of Prof. van Zyl it was decided that the best biorecognition element to detect HIV would be a DNA Hairpin Probe. Section 2.1.3 compares the different biorecognition elements and more specifically Section 2.1.3.4 details some key advantages of DNA probes. Aside from the overall benefits

of DNA biorecognition, there are some HIV specific advantages as well. Research shows that it is possible to detect HIV earlier using DNA/RNA over traditional methods. As previously stated, the window period of detection for HIV antibodies can range between 2-3 weeks to as long as 6 months. The detection of HIV DNA/RNA can reduce the window period to as little as 3 days [56].

With Prof. van Zyl's assistance, two DNA hairpin probes were designed. When designing a DNA probe, it is possible to add modifications to the DNA sequence to aid in certain functions. Additions include DNA tethers, labels, spacers, quenchers and many more [57]. It was decided that two DNA probes would be designed. The first probe design was used to verify that the DNA probe correctly bound to the transducer during the immobilization process and that the hairpin design operated correctly. The second probe design was the DNA probe used for electronic detection. First a generic hairpin probe is explained in Section 4.3.1 and then each DNA probe design is described in Section 6.2 and Section 6.3.

4.3.1 DNA Hairpin Probe

Figure 4.2 shows a typical representation of a hairpin probe, otherwise known as a molecular beacon. This particular example utilizes a fluorescent label (fluorophore) and a quencher. Fluorescence is briefly described in Section 2.1.7.1. The first and last 4 bases of the probe sequence are complementary (hairpin stem), which allows the probe to close in a loop or hairpin. When closed, the fluorophore and quencher are physically close together, this enables the quencher to absorb the fluorescence of the fluorophore (quenched by energy transfer). This makes the fluorescent signal more difficult to detect. In the presence of the target, the hairpin loop undergoes a conformational reorganization, because the loop hybridizes with the target which forces the loop to open. The hairpin stem is less stable than the binding between the loop and the target and so will not close again once the target has been hybridized. Once the loop has been opened, the quencher and fluorophore are physically separated, allowing the full fluorescent signal to be detected [58, 59].

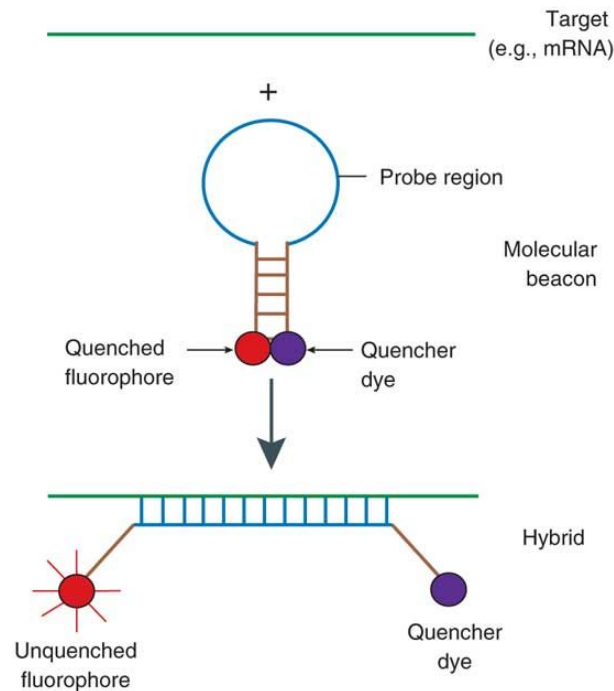


Figure 4.2: Hairpin probe representation. When target DNA (Green line) is introduced to hairpin probe/molecular beacon, the hairpin is opened and the fluorophore begins to fluoresce. [59].

4.4 Electronic Measurement Design

In this section, the basic theoretical electronic measurement design will be discussed and Chapter 7 will discuss the full practical design.

At this point in the design procedure, the chosen transducer, biorecognition element and immobilization technique can potentially be used in conjunction with any electrochemical measurement technique as described in Section 2.1.8. Due to the fact that resistive based biosensing is a relatively new concept, and that the SAND team has begun research in this area (Chapter 3), it was decided that the chosen electrochemical measurement technique should follow on with resistive detection. As discussed in Section 2.4.3, Skotadis *et al.* [47] conducted research on an innovative resistive based biosensor. Interdigitated electrodes with platinum nanoparticles sputter coated between them were used to create a relatively high resistance. DNA probes were immobilized on the platinum nanoparticles and upon hybridization of target DNA to the probe, a reduction in resistance was observed between the electrodes. The signal produced was due to the DNA probes creating direct electronic bridges between

nanoparticles, hence creating shorter electronic paths between the interdigitated electrodes.

In comparison, the biosensor being designed here is vastly different. The transducer will be directly connected between two electronic spring probes creating a direct path between them with a relatively low resistance due to carbon's high conductivity. Upon positive hybridization of the target to the probe DNA, there is a strong indication that the electrochemical characteristics of the carbon nano-fiber will be affected and so a readable signal can be measured. In Section 2.1.7.2 the electrochemical sensing principles are discussed. Since there is a direct current flow through the transducer and a change of electrochemical characteristics being measured across on the carbon nanofibers, this sensor falls under the conductometry group. It should be noted however that the chosen resistive technique is not like traditional biosensor research in that most designed biosensors utilize the electrolytic interface between the transducer and electronic sensor. The resistive technique chosen, as mentioned, utilizes a solid interface of the CNFs between the electronic sensing probes which may yield very different results.

4.4.1 Design Investigation

A number of methods can be use to measure resistance. Mr Viviers from the SAND team previously used the setup seen in Figure 4.3. Here a constant voltage source is used in series with a known resistance, and the transducer which has an unknown resistance. An oscilloscope was used to measure the voltage across the transducer before and after the target has been introduced. By using this setup, and simple voltage division equations, it is possible to calculate the current through the known resistance and hence the transducer. Using the calculated current, it is then simple to calculate the resistance of the transducer. Practically however, readings are more accurate if the known resistance is of a similar value to the unknown transducer resistance. This is the reason for using the auto-ranging function on most ohmmeters.

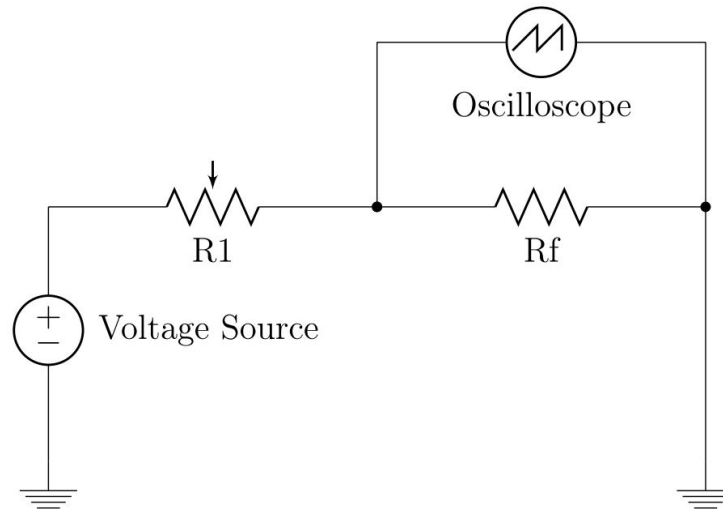


Figure 4.3: Voltage division circuit in order to calculate resistance [48].

The circuitry used in the *E. coli* project (Section 3.1.3) was an upgraded version of Mr Viviers'. The same basic principle was used, but the oscilloscope was replaced by a microcontroller with a 10-bit ADC (Analogue to Digital Converter).

Due to the fact that a new transducer material was chosen (CNF) with a possible unknown range of change in resistance, it was decided that a new circuit design was necessary. The new design should be able to accurately measure a variety of resistance ranges. This would allow for accurate readings if the electrochemical changes are sufficiently large and it also allows for possible changes in transducer materials for other experimentations. When designing circuitry for bio-recognition, a few variables must be taken into consideration such as pH level, voltage and current. If the voltage or current is too high, there is a possibility that the biological elements in the sample may be denatured or damaged. It was also found, in previous work, that the electronic spring probes that were used, get damaged over time due to oxidation and electrolysis because of the salt buffers used to stabilize pH and dilute biological solutions during experimentation.

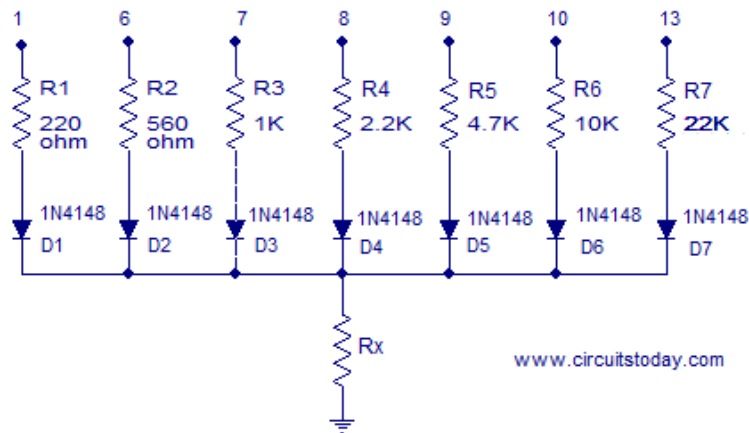


Figure 4.4: Auto ranging circuit using multiple inputs [60].

Initially an auto ranging design as seen in Figure 4.4 was considered. Here multiple inputs are used with diodes to prevent reverse current flow through the unused input channels. If input 1 above R1 is held high, at 5 V, and all the other inputs are held low then the voltage across Rx can be measured. If R1 and Rx are equal, then the voltage drop across Rx will be $(5 - 0.7)/2 = 2.15V$ where 0.7 is the diode drop. If the voltage across Rx is less than or equal to 2.15 V, we can assume that Rx is less than or equal to 220 ohms. If the voltage across Rx is higher than 2.15 V then the process will be done again by switching input 1 low and input 6 above R2 high and remeasuring the voltage across Rx. The process is continued until the voltage of Rx is lower than 2.15V, then it can be assumed that Rx is closest to the corresponding known resistance and the actual resistance can be calculated with the same voltage division calculations previously discussed [60]. The disadvantage of this design is the necessity for multiple input sources in order to switch to different channels. Another issue is that the ideal equations assume that all channel source voltages are equal, and the diode drops are also equal, whereas in a practical environment, this would not be the case, which would mean that every channel would need to be calibrated. For these reasons it was decided that a new method for measuring resistance would be necessary.

4.4.2 Proposed Electronic Design

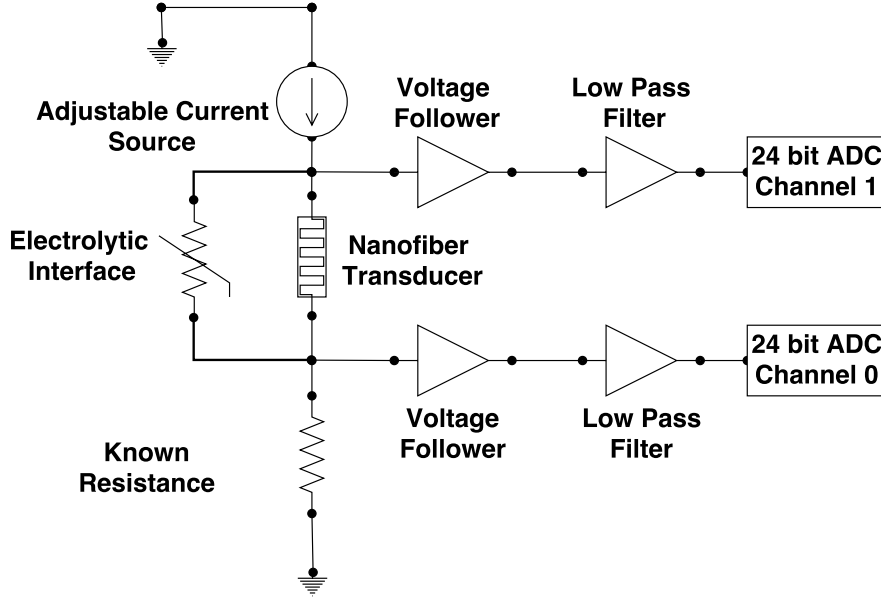


Figure 4.5: Proposed new electronic design.

Figure 4.5 shows the new proposed electronic design. It was decided that a constant current source would be used in place of a constant voltage source. This would allow for better control of the current and voltage through the transducer and hence the biological elements. A known resistor is used here, but is not necessary for the calculation of the transducer's resistance. The known resistor is used to increase the readable voltage by the ADC and can also be used to validate the instantaneous current to allow for more accurate resistance calculations. In order to measure the resistance of the transducer, first the voltage ($V_{R_{Known}}$) of the known resistor (R_{Known}) is measured and then the current ($I_{Constant}$) is calculated as seen in Equation (4.4.1). The calculated current should be very close to the designed constant current value. Using a calculated current value instead of a constant value negates any errors in resistance due to load and line regulation changes on the current source. Thereafter, the voltage of the transducer ($V_{Transducer}$) is measured and the transducer resistance ($R_{Transducer}$) is calculated by subtracting the voltage across the known resistor ($V_{R_{Known}}$) and dividing the result by the calculated current, as seen in Equation (4.4.2).

$$I_{Constant} = \frac{V_{R_{Known}}}{R_{Known}} \quad (4.4.1)$$

$$R_{Transducer} = \frac{(V_{Transducer} - V_{R_{Known}})}{I_{Constant}} \quad (4.4.2)$$

It was decided that a better ADC resolution of 24 bits would be necessary to ensure that even the smallest changes in resistance could be accurately measured. Simple voltage followers and low pass filters, with a desired gain, can also be used to filter out noise, amplify the signal and ensure stable ADC inputs. It is also noted that the added sample solution during biological testing will create an effective parallel electrolytic resistance as seen in Figure 4.5, but it is assumed that this will be a relatively high resistance and the low resistance of the transducer will almost negate the electrolytic effects.

4.5 Conclusion

In this chapter the theoretical background of design choices necessary to design an electrochemical biosensor were discussed as well as a brief overview of the final design decisions. It was discussed, that there were four main biosensor components that needed to be considered, these are the biorecognition element, the immobilization technique, the transducer and the electronic measuring method. Section 4.1 discussed the different transducer options in terms of conductive materials, and finally the decision was made to use a carbon nano-fiber as the chosen transducer. Section 4.2 discussed the different immobilization techniques, especially in terms of DNA probe immobilization and detailed the decision to utilize SAM by means of a gold-thiol bond. The biorecognition element decision to use hairpin DNA probes was noted in Section 4.3. The hairpin probe was generically explained in terms of operation. Finally Section 4.4 described past resistive measurement designs as well as other potential methods. It was discussed that a new measurement circuit would be designed that would use a constant current source in the place of a voltage source.

In conclusion, all the necessary design components and decisions needed to design a biosensor to detect the presence of HIV DNA were discussed in full. The next chapters will detail the specific designs of each component, the characteristics and final results.

Chapter 5

Carbon Nanofibers

Section 4.1.1 discussed the decision to purchase a conductive carbon nanofiber mat from Pyrograf Products, Inc. [53, 54]. This chapter will characterize the CNFs, detail the process of cutting the CNF mat to the correct size for biosensing and characterize the sputter coating of gold onto the CNFs in preparation of the immobilization process.

5.1 Nanofiber Characteristics

The PR-19 range of carbon nanofibers from Pyrograf Products, Inc. has an average diameter of about 150nm and has a chemically vapor deposited (CVD) layer of carbon on the surface of the CNF over a graphitic tubular core fiber (catalytic layer) as shown in Figure 5.1. CNFs are produced in a vapor phase, and as a result they generally become entangled during growth, producing a mesh-like configuration [54]. The paper form of the PR-19 range, also called the CNF Nano-mat, has a backing of non-woven carbon fabric on which the specific PR-19 product is formed.

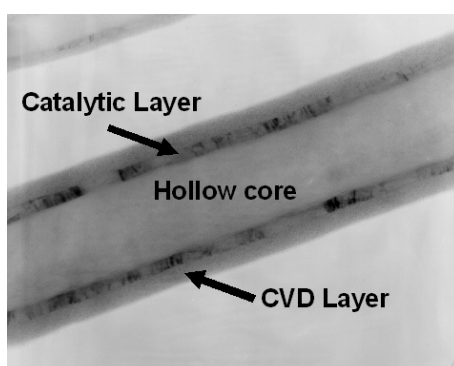


Figure 5.1: Transmission electron micrograph of the PR-19 product[54].

A key advantage, as can be seen in Figure 5.1, is a hollow core which reduces the overall volume of the CNF. As previously discussed, if the surface-to-volume ratio of a nanowire (or in this case nanofiber) is high, the influence of the biological species on the conduction of the surface and interior of the CNF is drastically increased (Section 2.1.8.3).

The specific product ordered from Pyrograf Products, Inc. is called PR-19-XT-LHT in paper form. The LHT grade is produced by heat treating to temperatures up to 1500°C, which allows for the highest conductivity in nanocomposites. The reported applications for this CNF type are both mechanical, and electrical [53, 54].

PR-19-XT-LHT Carbon nanofiber properties

- **Fiber diameter, nm (average):** 150
- **CVD carbon overcoat present on fiber:** no
- **Surface area, m²/gm:** 20-30
- **Dispersive surface energy, mJ/m²:** 120-140
- **Moisture, wt%:** <5
- **Iron, parts per million (ppm):** <14,000
- **Polyaromatic hydrocarbons, mg PAH/gm fiber:** <1

The size of the nano-mat ordered was 18" x 18" (45.72 cm x 45.72 cm). A small sample was taken to test the mechanical strength and stability of the CNF mat. It was found that the CNF mat can be cut with scissors and handled by hand, but are relatively brittle and would break down to a powder if mishandled. A sample was also put into a beaker with water and ultrasonically bathed. It was found that after a few seconds the sample was completely destroyed. These tests indicated that the CNFs are fragile and need to be handled with care during all experimental procedures.

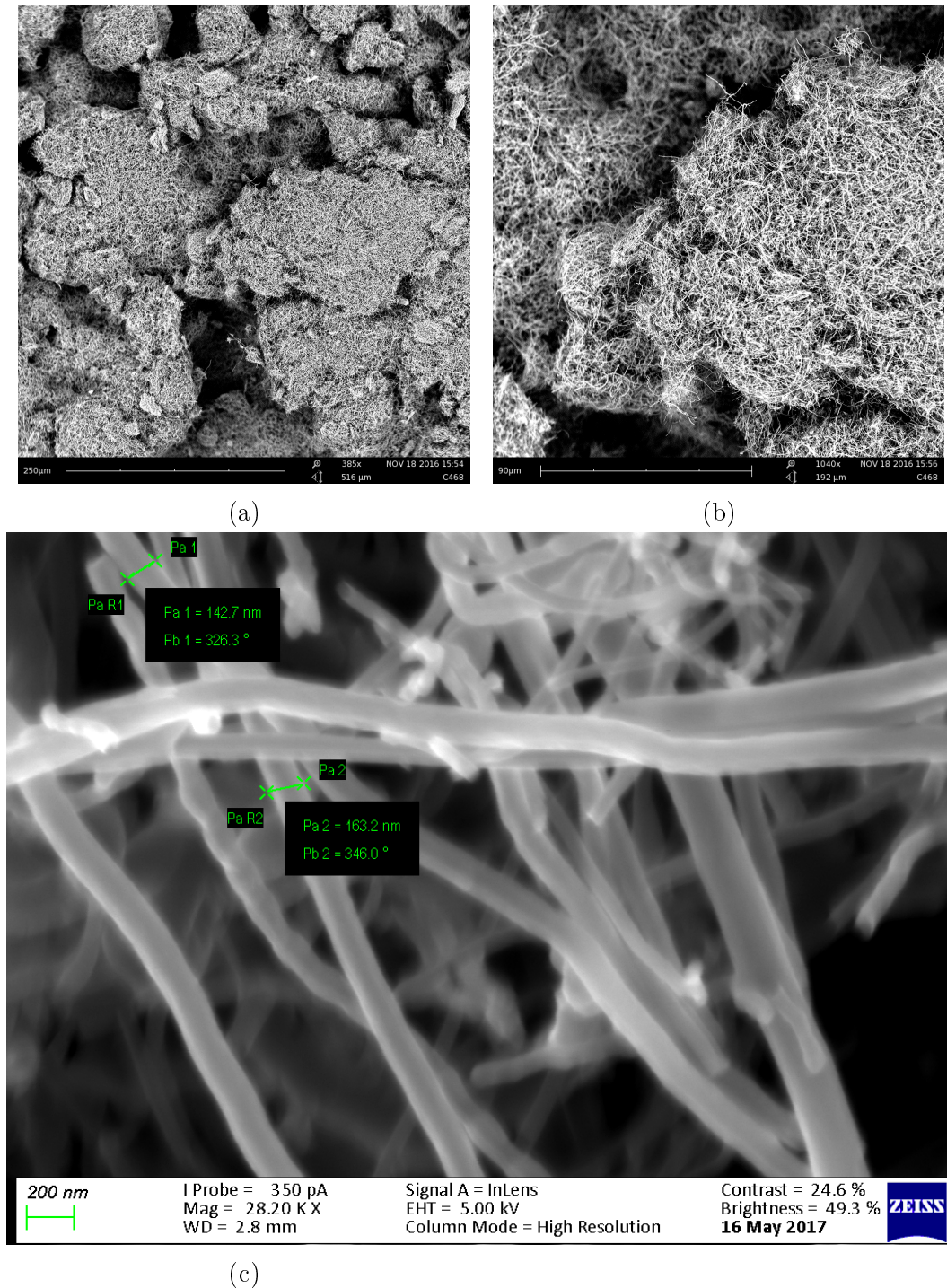


Figure 5.2: Carbon nanofiber imaging.

Figure 5.2(a) and Figure 5.2(b) are SEM images of the CNF mat taken on a Phenom SEM and show the overall surface arrangement of the samples. The fibers form many randomly clumped groups. Figure 5.2(c) is an image

taken on the Merlin SEM from the CAF Unit in the Geology Department of Stellenbosch University. The specifications stated that the average diameter of the CNFs is 150nm, Figure 5.2(c) validates that the specifications, are on average, correct.

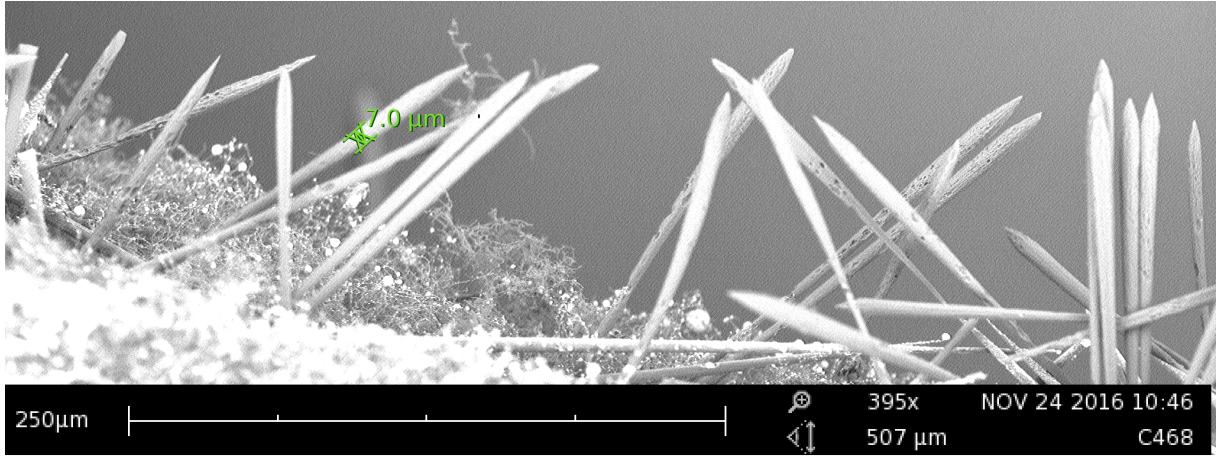


Figure 5.3: Non-woven carbon backing.

Figure 5.3 shows the non-woven carbon backing support structure of the nanofibers taken on the Phenom SEM. It can be seen that one fiber was measured at 7 μm. The backing is considerably larger in diameter than the PR-19-XT-LHT nanofibers with an average diameter around 10 μm.

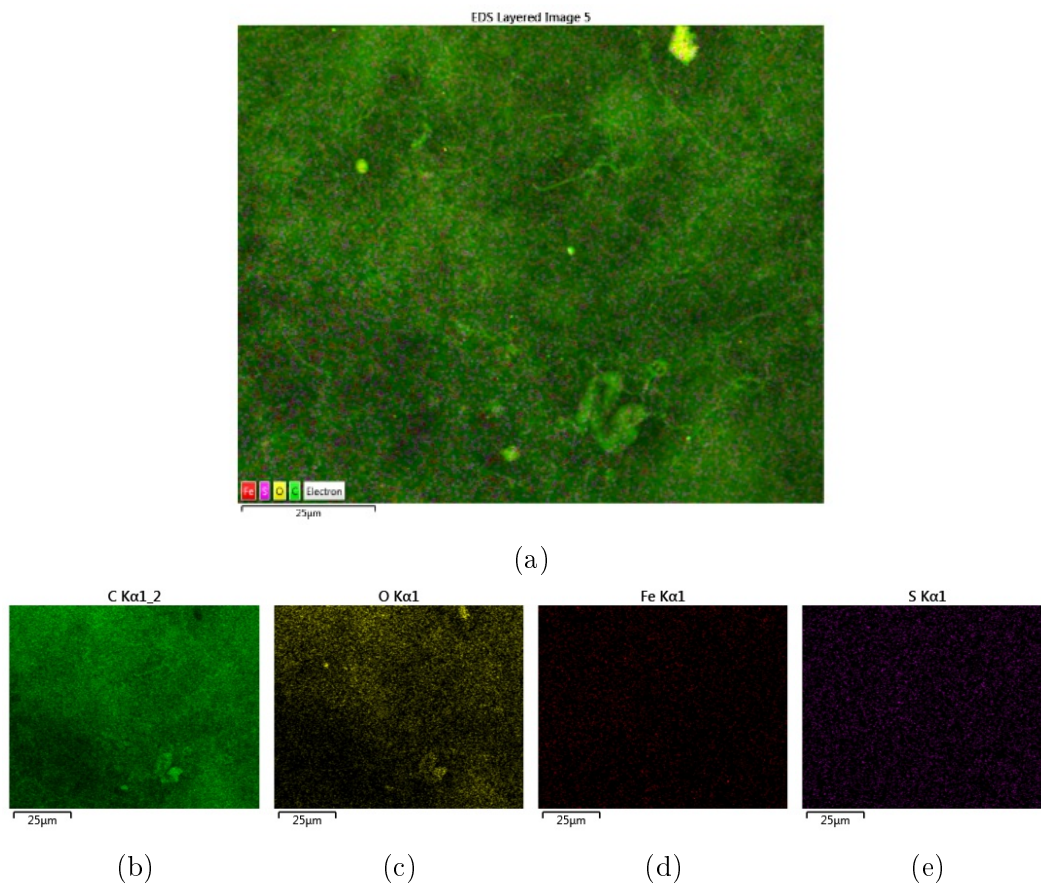


Figure 5.4: Carbon nanofiber EDX elemental map.

Using the SEM images obtained on the Merlin, an Energy Dispersive X-Ray Spectroscopy (EDX) analysis was performed in order to visualize the elemental properties of the CNF mat. The elemental map figures depicted in Figure 5.4, show that the majority of the fibers are made up of carbon, but trace amounts of oxygen, iron and sulfur were registered. Figure 5.5 shows the exact weight percentage of the elements registered. It can be seen that 89.2% of the fiber is made up of carbon, with 9.9% being oxygen, and iron and sulfur being a negligible weight percentage. The system also registered a possibility of copper, but the signal is not certain, which is why Cu is in red text.

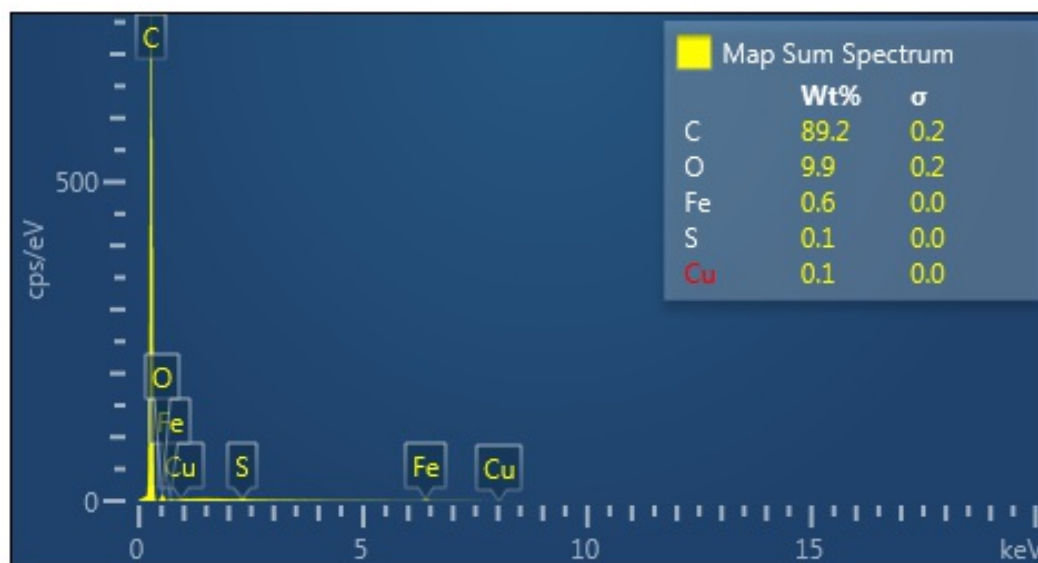


Figure 5.5: Energy Dispersive X-Ray Spectroscopy (EDX) analysis of Carbon Nanofibers.

5.2 Cutting of Nanofibers

As mentioned, the CNF mats were delivered as 45.72 cm x 45.72 cm sheets. The desired size of the transducer is less than 1 cm x 1 cm and so it was quickly determined that cutting the mat by hand with scissors or a guillotine would not be a suitable method due to the fibers brittle nature, difficulty to produce uniform samples and the possible contamination of the fibers. A number of options were investigated, which included the manufacture of a die cutter (similar to a "cookie cutter" or punch that would make multiple transducer sized samples at a time.). It was found that a die cutter would not be suitable as manufacturing such small cutting areas would be expensive and there is a possibility of iron contamination from the die cutter blades. The final decision was that laser cutting would be the best method to cut the CNF mat as it allows uniformity and little to no contamination or damage. Laser cutting provides accurate, consistent and detailed cuts and because it vaporizes the materials it cuts, no external contamination is left on the material.

5.2.1 Laser Cutting Nanofibers

This section details the investigation into laser cutting of the CNF mat. A number of different laser cutters were tested that were found either at Stellenbosch University or local businesses within the Western Cape.

The two most common laser cutter types are the Yag and CO₂ types. Most laser cutters come in different power ratings which influence the depth and precision of a cut, depending on the material.

5.2.1.1 Blue Laser Diode Cutting

The first laser cutter tested was a low cost 3 Watt blue laser diode type cutter owned by the Physics Department of Stellenbosch University. This type of laser diode is generally used for engraving purposes and can engrave many materials, including wood, plastic and paper.

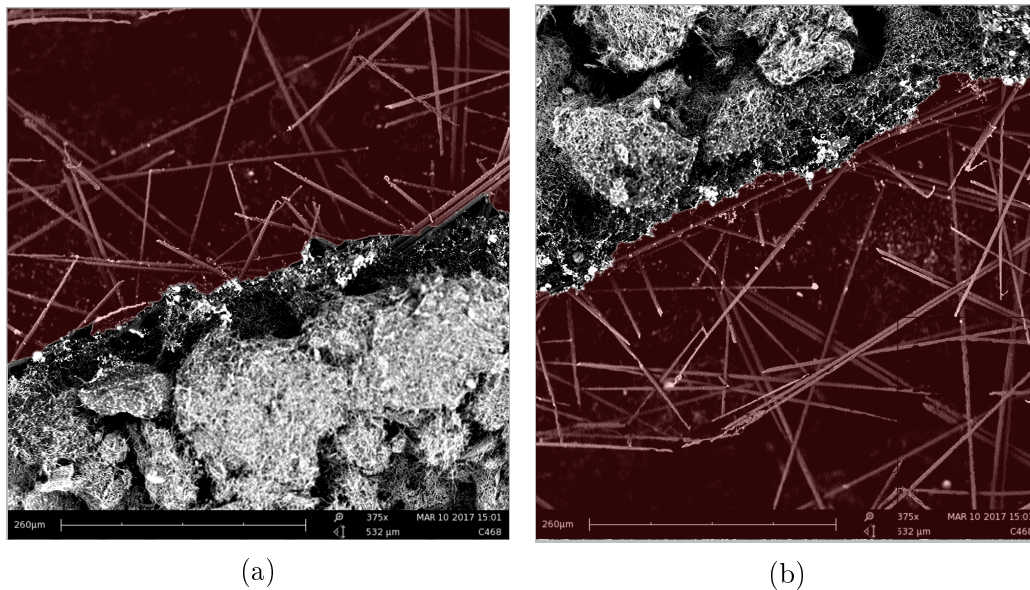


Figure 5.6: Blue laser diode results. In the red shaded area, it can be seen that the nanofibers were removed but the carbon microfiber backbone was not.

In Figure 5.6(a) and Figure 5.6(b) it can clearly be seen that the blue laser diode was able to cut through the CNFs, but did not cut the thicker non-woven carbon backing. The laser cutter was not able to cut completely through the CNF and the laser cut width was relatively large (shaded red), implying that the laser focal point was not optimal. Figure 5.6(a) and Figure 5.6(b) were captured on the Phenom SEM.

5.2.1.2 Yag Laser Cutting

The second laser cutter tested was a 3 Watt 1064 nm wavelength YAG laser cutter. This device belonged to David Powers.

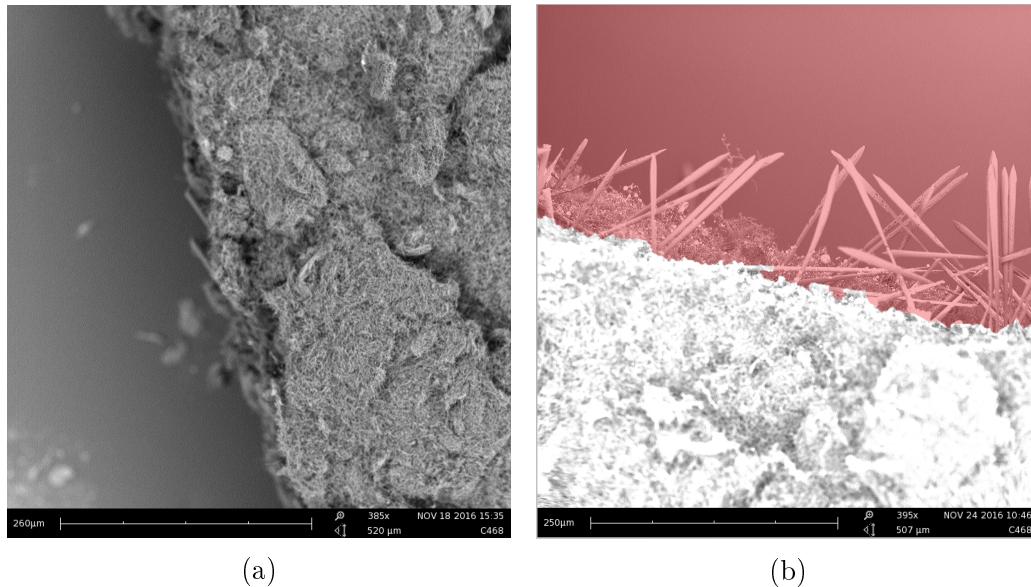


Figure 5.7: Yag laser cutter results.

It can be seen in Figure 5.7(a) and Figure 5.7(b) that the yag laser results are better than those in the previous test. The laser was able to cut through the nanofibers and the backing. However, it can be seen that there was a wide focal area causing the surrounding nanofibers to absorb energy and vaporize, but the energy was not sufficient to vaporize the thicker carbon backing (shaded red). It was also noted that the laser cutter was not in an enclosed environment and the work area was in an office, not in a laboratory setup, which may have lead to contamination of the nanofibers.

5.2.1.3 Gebrateq CO₂ Laser Cutting

The third laser cutter tested was the 80 W Beyond CNC CO₂ laser cutter. This laser cutter is owned by Gebrateq Advanced Engineering [61]. The laser cutter allowed for different power and speed settings. 20% and 12% power settings and a speed setting of 20 mm/s were tested. It was noted that the laser cutter was used in an industrial factory setting for the manufacture of mechanical parts which means that contamination of the fibers may occur.

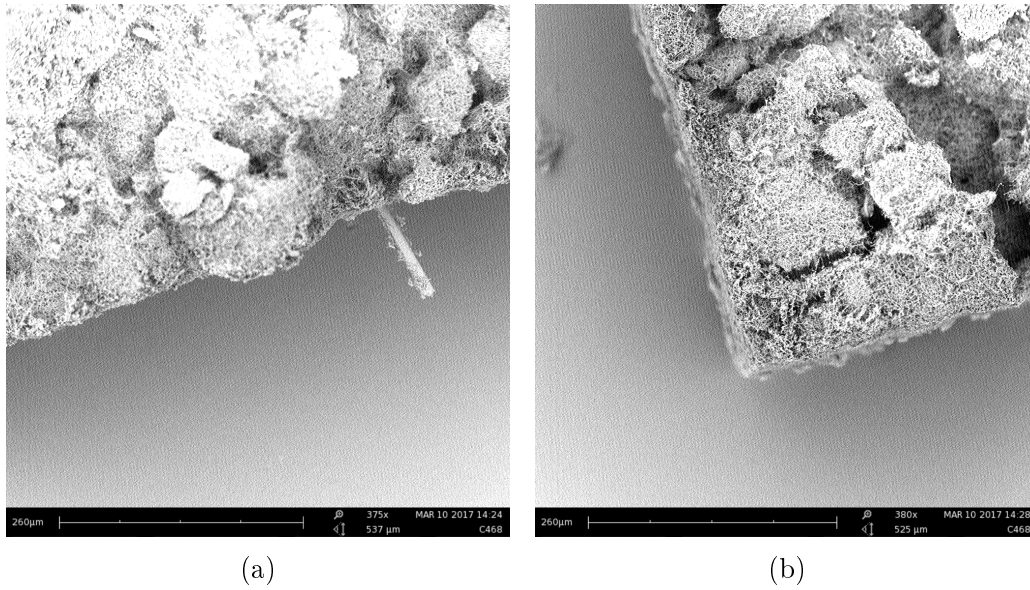


Figure 5.8: Beyond CNC CO₂ laser cutter: 12% power rating results.

Figure 5.8(a) and Figure 5.8(b) show a marked improvement in the laser cutting of the nanofibers with an almost straight cut through the entire fiber barring a few backing fibers. Figure 5.9(a) and Figure 5.9(b) show that the fiber is completely and cleanly cut through, thus implying that a higher power rating will vaporize and cut the fibers more efficiently.

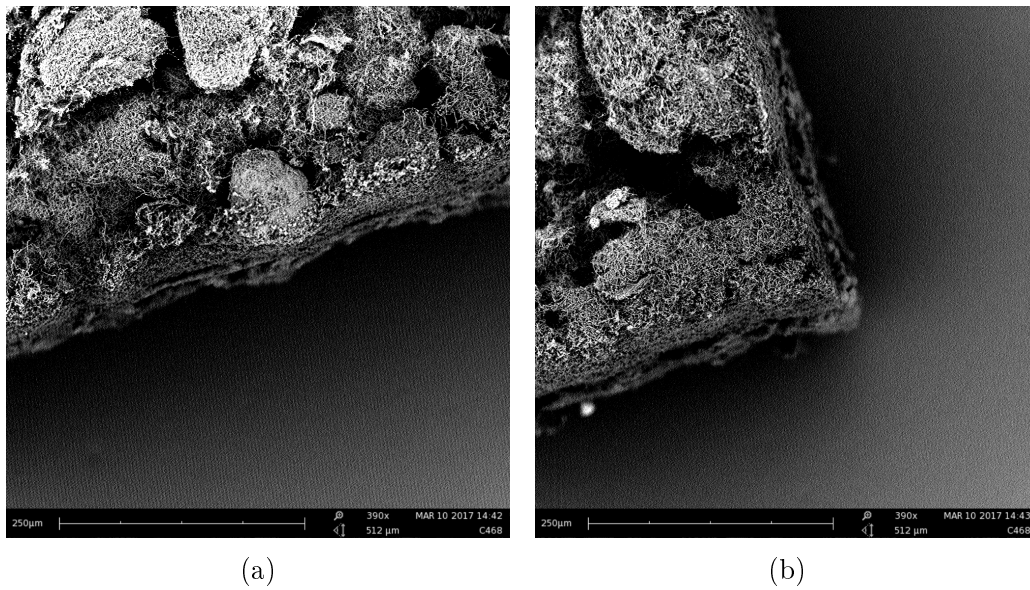


Figure 5.9: Beyond CNC CO₂ laser cutter: 20% power rating results.

5.2.1.4 Boyd and Ogier CO₂ Laser Cutting

The final laser cutter tested was a 60 Watt Speedy 300 Trotec CO₂ laser cutter belonging to Boyd and Ogier, an architectural model making company.

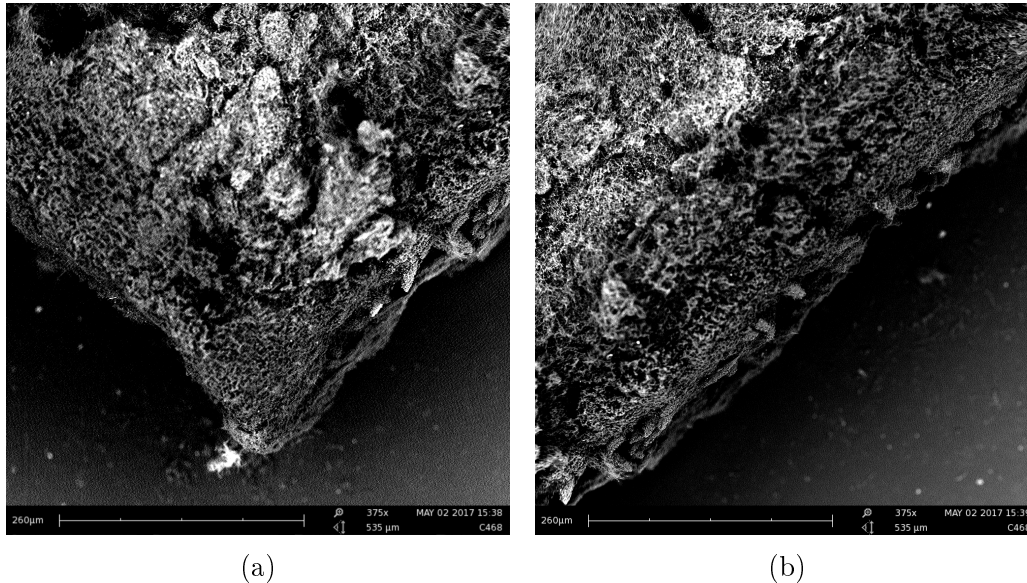


Figure 5.10: Speedy 300 Trotec CO₂ laser cutter: 15% power rating results.

Figure 5.10(a) and Figure 5.10(b) show that the 60 Watt laser had much the same results as the previous 80 Watt laser. The fibers were cleanly cut straight through with a well defined focal point. Boyd and Ogier have previously worked with the laser cutting of nanofibers and thus have some experience with controlling the environment while cutting, but the area is still a factory setting which is not contamination free. All samples used for biosensing were cut using this laser cutter. It was necessary to investigate a good backing material to avoid contamination which is explained in the next section.

5.2.1.5 Backing for Materials during Laser Cutting

During laser cutter testing, a few different backing materials were tested. The backing material is a substrate used underneath the sample being cut by the laser cutter. Usually this backing is a steel honeycomb grid, as it has very little exposed surface area that may reflect or absorb the laser energy. Unfortunately the honeycomb grid was not optimal, as the small fiber sample sizes would fall through the honeycomb holes and there is a high likelihood of contamination from the original laser cutter honeycomb grid.

A common household ceramic tile was suggested as it was thought that there would be little reflection and the ceramic tile would absorb the laser energy

without being cut. Unfortunately this was not the case as can be seen in Figure 5.11. Figure 5.11(a), Figure 5.11(b) and Figure 5.11(c) which show a visible contamination on the fibers in the form of small beads that have been deposited onto the fibers. The EDX analysis in Figure 5.11(d) shows that there is a significant weight percentage of contamination elements, namely 4.3% Si, 1.3% Ca, 1% Zn, 0.9% Na, 0.8% Al, 0.5% K and 0.3% Mg.

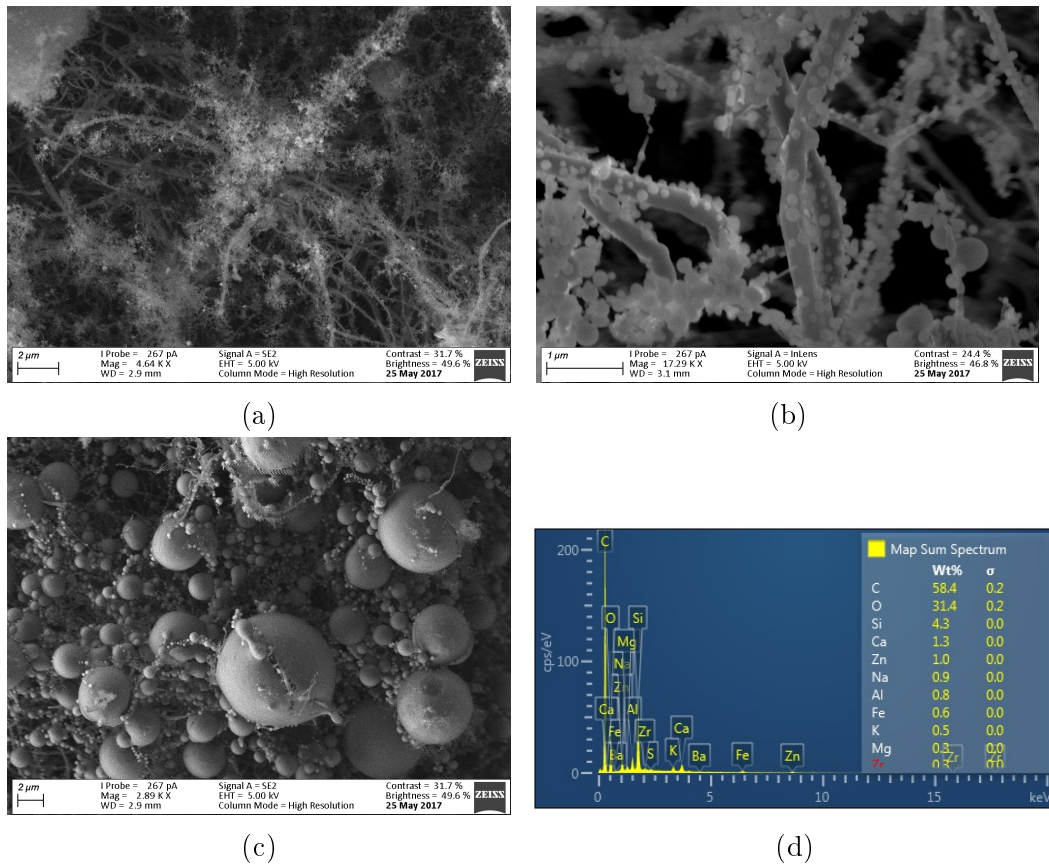


Figure 5.11: Laser cutting on ceramic backing.

A stainless steel sheet that was orbital sanded to reduce reflection was also tested. The laser cuts seemed to be clean and contamination free as seen in Figure 5.12. The EDX analysis yielded much the same results as the original fiber analysis. It was seen that there was some fiber debris and scorching of the steel after laser cutting, indicating that there was some reflection of the laser energy underneath the CNF, but this did not seem to affect the samples noticeably.

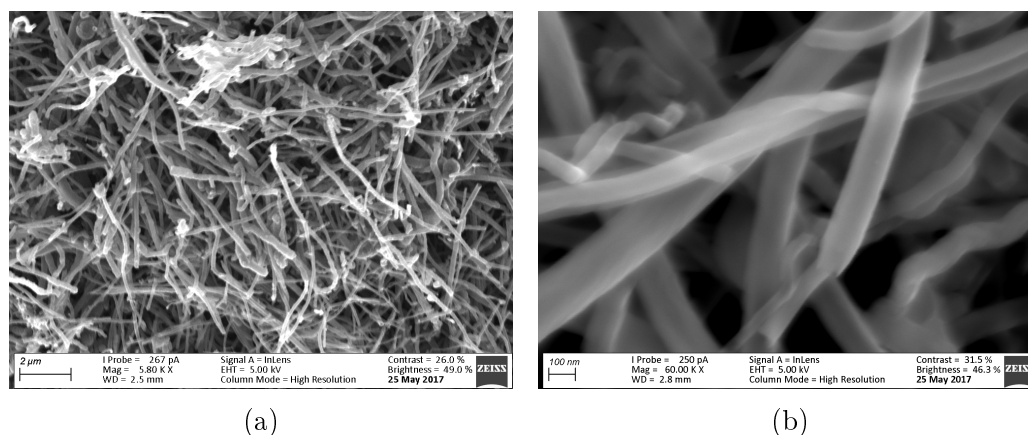


Figure 5.12: Laser cutting on stainless steel backing.

5.3 Gold Sputter Coating

A gold deposit is needed on the CNF mat to enable immobilization of the DNA probes via gold-thiol bonding. In order to deposit gold onto the mat, a Quorum Q150T ES sputter coater from the Physics Department of the University of Western Cape was used. The sputter coater has a rotating substrate holder to allow for more uniform coatings. The sputter coater has a quartz crystal microbalance (QCM) sensor that can accurately control the thickness of the deposited material. It was decided that different thicknesses of gold would be tested ranging from 5, 10, 15, 20 and 25 nm.

The figures in Figure 5.13 were taken on the Merlin SEM from the CAF unit at the Geology Department of Stellenbosch University at 60k magnification. It can be seen that a 5nm deposit (Figure 5.13(b)) covers the majority of the top surface of the fibers' but there are small cracks in the gold, most likely due to golds natural affinity to itself creating small SAMs across the surface. As the gold thickness increases, these cracks are reduced almost completely. The rotating substrate holder of the sputter coater allowed for a uniform deposit across the fibers' top surfaces and it also allowed some deposit of gold on the sides of the fiber as well, which decreased the chance of the gold from coming off.

The figures in Figure 5.14 were taken on the Merlin SEM from the CAF unit at the Geology Department of Stellenbosch University at 15k magnification. Here a bigger picture of the fiber is seen. The gold deposit forms around each individual fiber with little to no pooling of gold between multiple fibers.

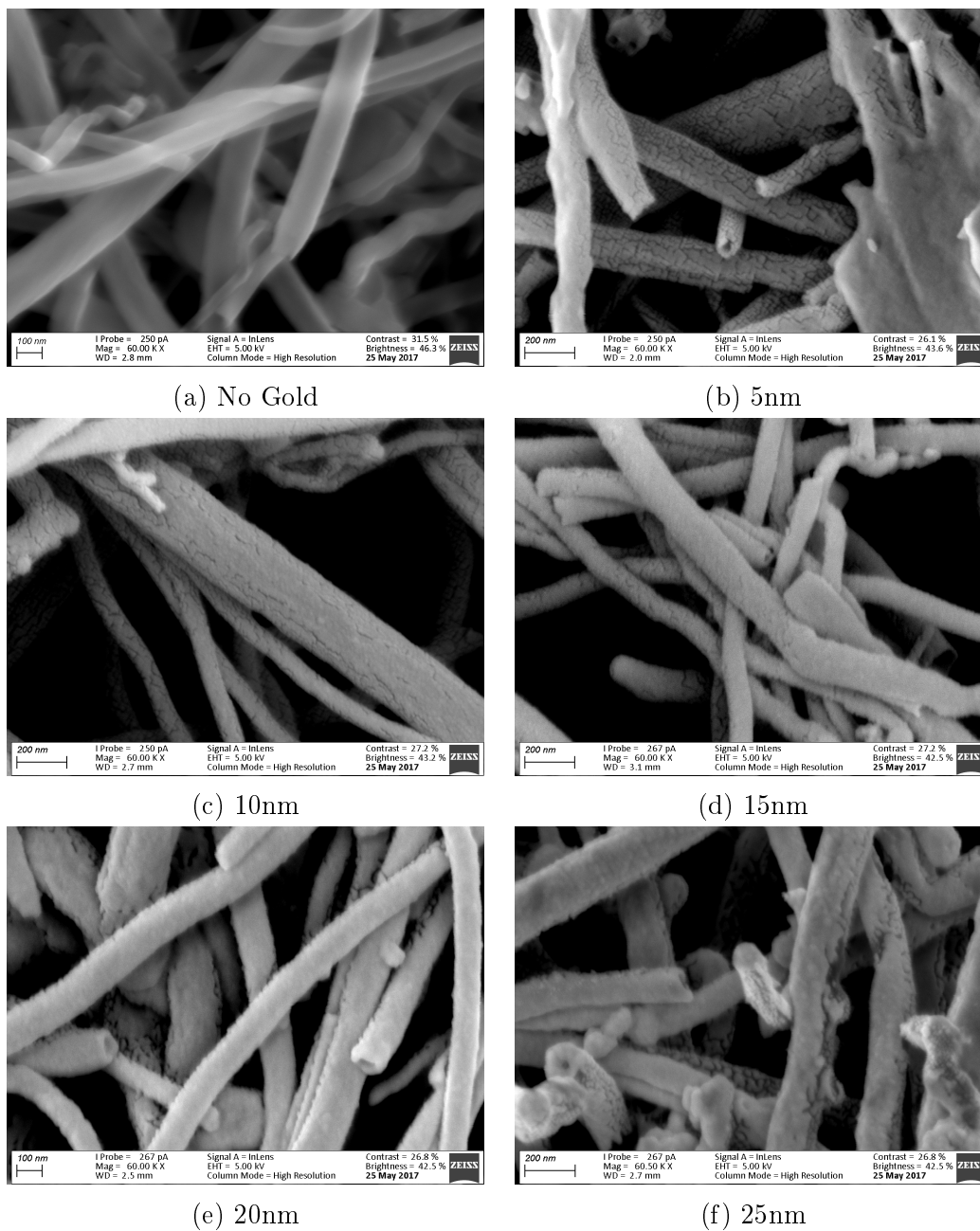


Figure 5.13: 60k times magnification SEM of gold deposited on nanofibers

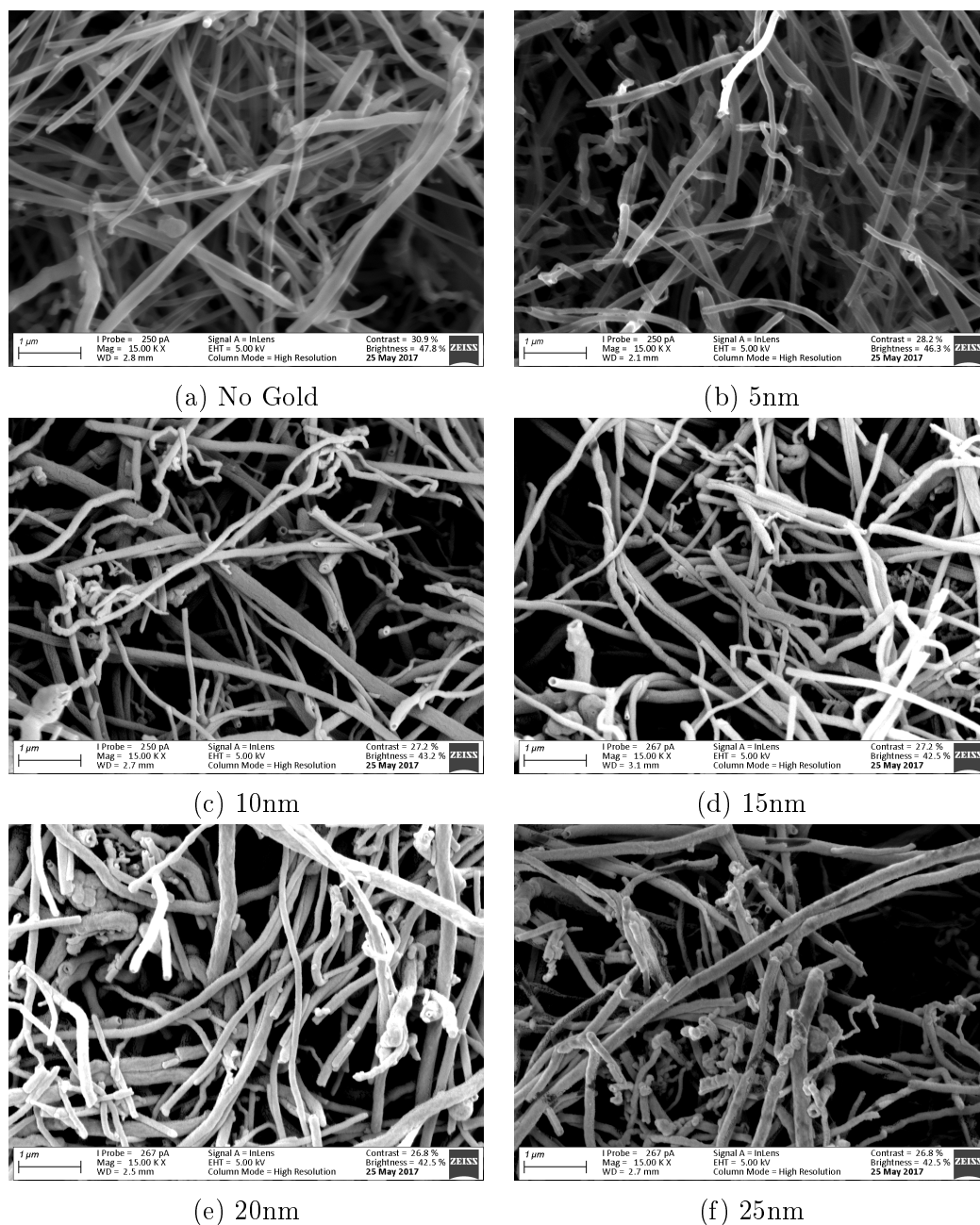


Figure 5.14: 15k times magnification SEM of gold deposited on nanofibers

Finally, the results depicted in Table 5.1 and Table 5.2 show the elemental composition of the samples as either a weight% or oxide%. Table 5.1 gives a good indication of the dominating elements in terms of weight/density, but here oxygen is considered an independent entity which is highly unlikely due to the high vacuum environment during analysis. Therefore, the elemental composition is also analyzed as oxides, in order to better quantify the identified elements, excluding oxygen. It can be seen in Table 5.1 that when the gold

| Result Type | Weight % | | | | | | |
|----------------|----------|-------|------|------|------|-------|-------|
| Spectrum Label | C | O | S | Ca | Fe | Au | Total |
| No Au 1 | 87.71 | 11.36 | 0.17 | 0.09 | 0.67 | 0 | 100 |
| No Au 2 | 89.77 | 9.47 | 0.13 | 0.02 | 0.61 | 0 | 100 |
| 5 nm 1 | 87.34 | 11.37 | 0.16 | 0 | 0.97 | 0.16 | 100 |
| 5 nm 2 | 91 | 6.77 | 0.22 | 0 | 0.84 | 1.16 | 100 |
| 5 nm 3 | 89.43 | 5.66 | 0.16 | 0 | 0.8 | 3.95 | 100 |
| 10 nm 1 | 83.57 | 6.1 | 0.15 | 0 | 0.6 | 9.58 | 100 |
| 10 nm 3 | 85.3 | 3.94 | 0.13 | 0.03 | 1 | 9.61 | 100 |
| 15 nm 1 | 75.38 | 2.75 | 0.15 | 0 | 0.57 | 21.16 | 100 |
| 15 nm 2 | 77.14 | 2.26 | 0.11 | 0 | 0.55 | 19.94 | 100 |
| 20 nm 1 | 66.02 | 2 | 0.3 | 0 | 0.78 | 30.9 | 100 |
| 20 nm 2 | 71.31 | 1.89 | 0.16 | 0.07 | 0.56 | 26.01 | 100 |
| 25 nm 1 | 65.66 | 2.36 | 0.2 | 0 | 0.52 | 31.25 | 100 |
| 25 nm 2 | 57.49 | 0.97 | 0.18 | 0.05 | 0.77 | 40.53 | 100 |

Table 5.1: EDX weight % analysis tabular form

| Result Type | Oxide % | | | | | | |
|----------------|---------|---|------|------|------|-------|-------|
| Spectrum Label | C | O | S | Ca | Fe | Au | Total |
| No Au 1 | 99.75 | | 0.08 | 0.02 | 0.15 | 0 | 100 |
| No Au 2 | 99.81 | | 0.06 | 0.01 | 0.12 | 0 | 100 |
| 5 nm 1 | 99.68 | | 0.08 | 0 | 0.22 | 0.03 | 100 |
| 5 nm 2 | 99.49 | | 0.1 | 0 | 0.18 | 0.23 | 100 |
| 5 nm 3 | 98.88 | | 0.08 | 0 | 0.18 | 0.86 | 100 |
| 10 nm 1 | 97.19 | | 0.08 | 0 | 0.17 | 2.56 | 100 |
| 10 nm 3 | 97.16 | | 0.07 | 0.01 | 0.27 | 2.49 | 100 |
| 15 nm 1 | 92.43 | | 0.09 | 0 | 0.21 | 7.27 | 100 |
| 15 nm 2 | 93.14 | | 0.07 | 0 | 0.19 | 6.59 | 100 |
| 20 nm 1 | 86.61 | | 0.23 | 0 | 0.35 | 12.81 | 100 |
| 20 nm 2 | 89.87 | | 0.11 | 0.03 | 0.22 | 9.77 | 100 |
| 25 nm 1 | 86.61 | | 0.15 | 0 | 0.24 | 13 | 100 |
| 25 nm 2 | 80.34 | | 0.15 | 0.02 | 0.4 | 19.08 | 100 |

Table 5.2: EDX oxide % analysis tabular form.

thickness reaches 25 nm, the weight percentage reaches up to 40% due to gold's high density. Table 5.2 shows that carbon is in the majority as an oxide %. In both tables the other elements make up very little of the overall composition and never exceed 1% of either the weight or oxide %.

5.4 Conclusion

In this chapter the carbon nanofiber was investigated, and the unique properties of the fiber were detailed and characterized. A suitable method for cutting the CNF mats was investigated that would allow for small, uniform and uncontaminated samples. This was done by means of a laser cutter. Various laser cutters were tested and the most optimal chosen, as well as a suitable backing material. Finally the results of the sputter coating of gold onto the fibers was shown, which yielded very positive results. Different thicknesses of 5, 10, 15, 20, 25 nm of gold were tested, with most resulting in complete and uniform covering of gold on individual fibers.

Chapter 6

DNA Hairpin Probe Design

In Section 4.3.1, the generic hairpin DNA probe was explained. This chapter fully details the design and operation of the two DNA probes that are to be used in experimentation. The first DNA probe is used to validate the positive immobilization of the DNA probe to the transducer, as well as the correct operation of the hairpin loop. This is done by the use of a fluorescent label that can be visually captured by confocal microscopy. The second probe was designed for the final electronic experiments. This probe utilizes a ferrocene label in order to increase the possibility of electrochemical signals.

6.1 Target DNA Sequence

In order to uniquely detect HIV, it was necessary to design the probe DNA sequence so that it matched as a complementary to a small portion of the actual single stranded HIV DNA sequence, also known as the target DNA. Prof. van Zyl provided a commonly used HIV target sequence. This DNA sequence was then synthesized and ordered from Inqaba Biotec [62] to be used as the final target DNA in experimentation. The designed target DNA length is 33 bases long with no modifications. The complete target DNA sequence is given by:

AGT GCA GGG GAA AGA ATA ATA GAC ATA ATA GCA

(6.1.1)

The target DNA datasheet can be found in Appendix A.2.

6.1.1 Hybridized Target T_m

Using the online OligoAnalyzer 3.1 tool from IDT [63], the melting temperature of the Target DNA when hybridized to the exact complimentary sequence, can be calculated. The analyzer reported a T_m of 59°C. The T_m is described in Section 2.3.1.4.

6.1.2 Target Self-Dimer

Using the OligoAnalyzer 3.1 tool, the self-dimers of the target can also be estimated. There are many possible combinations and so only the most probable self dimer is shown in Figure 6.1. The concept of self-dimers is briefly explained in Section 2.3.1.5.

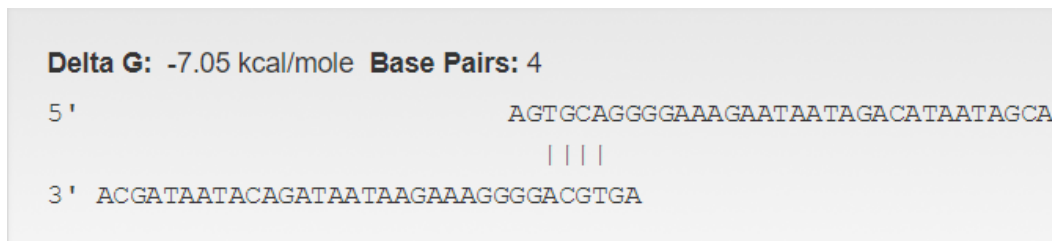


Figure 6.1: The most likely self dimer formed by two ssDNA target sequences. [63].

It can be seen that the most likely secondary structure of the target sequence, will form at most 4 hydrogen bonds (denoted |) which will require very little energy (heat) to break these bonds.

6.2 Fluorescent Labeled Probe Design

This section will describe the first DNA hairpin probe design. The probe was designed in a similar manner to the example Figure 4.2. Fluorescence is used to visually validate the immobilization and target hybridization procedures. Fluorescence is briefly described in Section 2.1.7.1. If fluorescence is detected then this validates that the DNA probe correctly bound to the transducer and that the target DNA forced the hairpin probe to open and allow the fluorescent signal to be detected. The probe was ordered from Integrated DNA Technologies [64]. From this point forward the fluorescent hairpin probe DNA will be referred to as FL probes.

6.2.1 Fluorescent Probe DNA Sequence

The designed FL probe sequence as seen is given by:

```
5'-/5DTPA//iSpC3//iCy3/CAG GGG TGC TAT TAT GTC TAT TAT TCT
TTC CCC TG/3IAbRQSp/-3'
```

(6.2.1)

and has 35 bases and a number of modifications which will be explained in the following sections. The specification sheet of the FL probe as well as advice for resuspension is found in Appendix A.3.

6.2.1.1 5DTPA

DTPA or Dithiol linker is a versatile linking reagent with each insertion providing two thiol (SH) functional groups. This thiol modification is used to couple DNA probes to ligands or surfaces, such as gold. The long term stability of the monothiol-gold bond is a major issue for chemical sensors based on thiol-capped gold surfaces. However, it has been demonstrated that functionalizing gold with polythiol anchoring results in an unrivaled stability of the derivatized gold surface [65]. DTPA can be inserted at any position in an oligo which in this case is on the 5' end, hence the name 5DTPA. Figure 6.2 depicts the chemical structure of the DTPA and the functional groups that bind to gold.

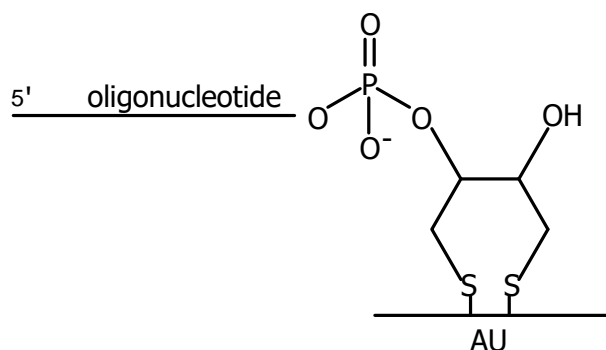


Figure 6.2: Dithiol (DTPA) linker providing two thiol (SH) functional groups that bind to gold. Image edited from [65].

6.2.1.2 iCy3

Int Cy3TM or Internal Cy3 is a red fluorescent dye modification that is added to the DNA probe with a maximum emission wavelength of 564 nm [66].

6.2.1.3 iSpC3

Int C3 Spacer is a DNA modification that provides space between other components in the DNA sequence or the substrate surface. Spacers impart a number of desirable characteristics, such as stability to enzymatic degradation. The spacer in this case also provides some distance from the nanofiber surface to allow freedom for the hairpin to form without surface interference.

6.2.1.4 3IAbRQSp

3' Iowa Black®RQ-Sp is a part of a new family of dark quenchers developed by IDT. They have excellent properties for use in fluorescence quenched probes. These compounds are stable over a wide range of conditions, including pH and heat. The quencher has a broad absorbance spectra ranging from 420 nm to 620 nm, with peak absorbance at 531 nm [67]. This indicates that when near the Int Cy3 fluorescent dye, the quencher will efficiently adsorb the emitted fluorescence.

6.2.2 Fluorescent Hairpin Probe Operation

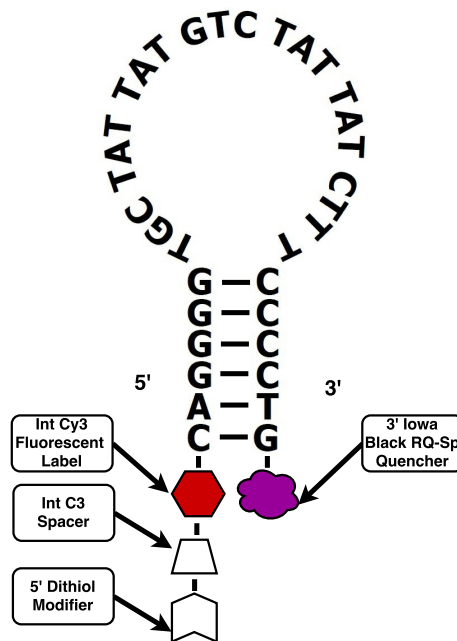


Figure 6.3: FL probe design when closed.

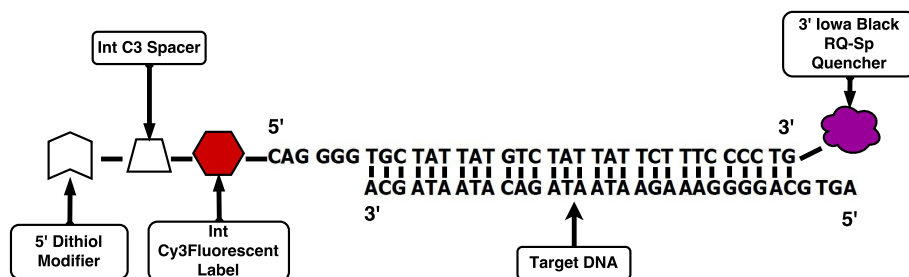


Figure 6.4: FL probe design when open and hybridized to target DNA.

Figure 6.3 and Figure 6.4 show the operation of the designed FL probe. When the hairpin is closed it can be seen that the first 6 bases on the 5' of the DNA sequence bind to the complementary last 6 bases on the 3' end of the sequence. This configuration forces the fluorescent dye next to the quencher and thus reduces the fluorescent signal visible. The spacer is between the thiol linker and fluorescent dye to enable the dye to emit efficiently without interference from the substrate surface. The spacer also provides room for the FL probe to open and close. Figure 6.4 shows what happens when the FL probe is opened and the target DNA is introduced. Only 29 bases of the 33 based target will bind to the FL probe. The fluorescent dye will no longer be quenched and the signal will be fully visible. It can be seen that the first 6 bases on the 5' end of the FL probe do not bind to the target DNA. These first 6 bases are added as a complementary to the last 6 bases on the 3' end of the FL probe to form the hairpin stem. It can be seen that the last 6 bases of the FL probe do however bind to the target DNA.

6.2.3 Hairpin Structure T_m

Using the OligoAnalyzer 3.1 tool, the FL probe structure can be simulated and the T_m calculated. The analyzer reports a melting temperature of 51.3°C for the FL probe.

6.2.4 Self Dimers

Using the OligoAnalyzer 3.1 tool, the secondary structure of the FL probe can be estimated. Here again only the most probable self dimer is shown in Figure 6.5.

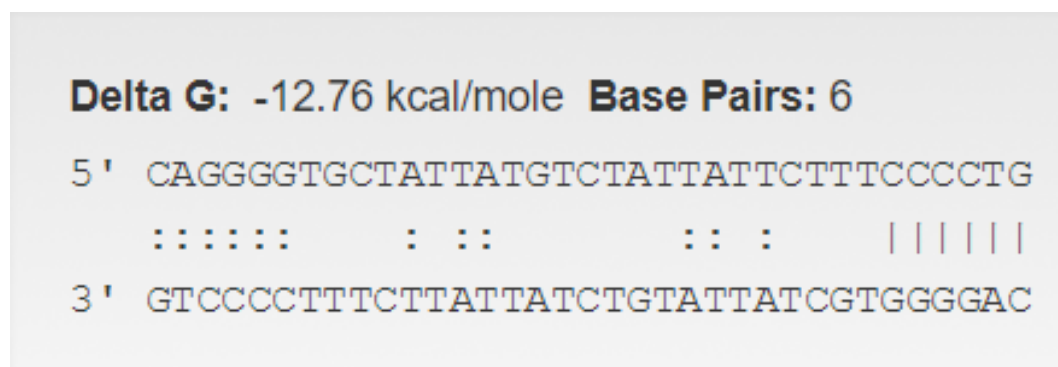


Figure 6.5: The most likely self dimer formed by the FL probe. [63].

Figure 6.5 shows that the most likely secondary structure of the FL probe will form 6 hydrogen bonds (denoted |) exactly where the stem of the hairpin

was designed and there will also likely be much weaker van der Waals bonds (denoted :) at 12 other base pairs. This should not greatly effect the overall operation of the hairpin.

6.3 Ferrocene Labeled Probe Design

Once the immobilization technique as well as the hairpin probe operation has been validated, the electrochemical experimentation can begin. Fluorescent modifications are no longer necessary for the electrochemical experimentation and so a new modification can be chosen that will aid in the production of an electronic signal.

Sarma [68] reported that several research groups have studied DNA modifications of covalently attached redox-active molecules such as ferrocene. It is seen that upon hybridization with a complementary sequence, there is a change in the electrochemical response of the attached ferrocene moiety. It has been reported that there have been studies utilizing a hairpin loop DNA probe with a ferrocene modification and upon hybridization of the target sequence, a large decrease in redox currents was observed [68]. The explanation to these results is that when the hairpin loop is closed, the ferrocene modification is held physically close to the conductive substrate surface allowing rapid electron transfer and efficient redox of the ferrocene modification. Once the target is present and the hairpin loop has been opened, the ferrocene modification is separated from the electrode surface and hence there is a decrease in the redox signal.

For these reasons it was decided that the fluorescent modification be replaced with a ferrocene modification with the expectation that the electrochemical response will be improved. Once again Prof. van Zyl provided the full ferrocene probe design and the DNA probe was ordered from Trilink Biotechnologies [69]. From this point forward the ferrocene hairpin probe DNA will be referred to as FE probe.

6.3.1 Ferrocene Probe DNA Sequence

The designed FE probe is given by:

$$\begin{aligned} &5'(\text{dT-Ferrocene})\text{CAG GGG TGC TAT TAT GTC TAT TAT TCT TTC CCC} \\ &\text{TGC AC (C6 Spacer)(DTPA)(DTPA)}3' \end{aligned}$$

(6.3.1)

and is essentially the same as the previously designed FL probe, except that there are 3 additional bases. This is because the ends of the FL probe needed to be parallel to allow the quencher to quench the fluorophore. There is also an

additional dithiol (DTPA) linker, which means there are now four thiol (SH) functional groups for binding to gold, which is said to be almost equivalent to a covalent bond. The DPTA and spacer modifications were also moved from the 5' end to the 3' end for manufacturing reasons. The modifications which are the same as the FL probe were explained in Section 6.2. There are no longer fluorescent or quencher modifications and the ferrocene modification is added, which will be briefly explained. The certificate of analysis for the FE probe is included in Appendix A.4.

6.3.1.1 dT-Ferrocene

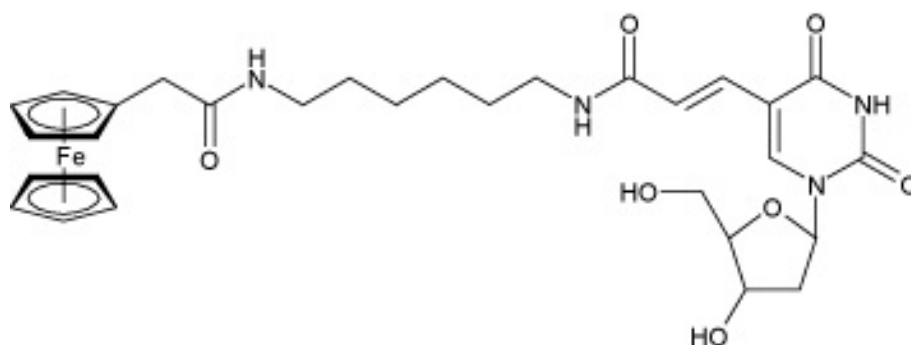


Figure 6.6: Ferrocene modification [69].

Figure 6.6 depicts the ferrocene modification structure. Ferrocene is comprised of two cyclopentadienyl rings bound by a central iron atom. Modification of the 5-position of thymidine with ferrocene does not disrupt regular Watson-Crick base pairing and allows multiple incorporations into a single oligonucleotide probe. Ferrocene modifications can be used in various sensing techniques including detection via electrochemical signal through a gold substrate, electrochemical based aptamer sensors for specific biomolecule detection and as an alternative to fluorescent-based probes in DNA microarray systems [69].

6.3.2 Ferrocene Hairpin Probe Operation

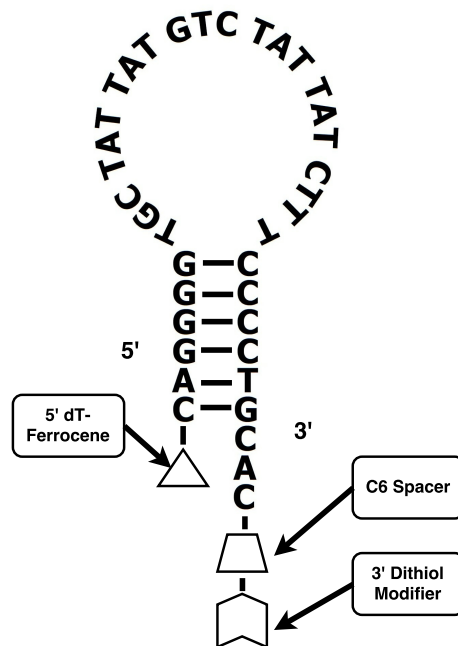


Figure 6.7: FE probe design when closed.

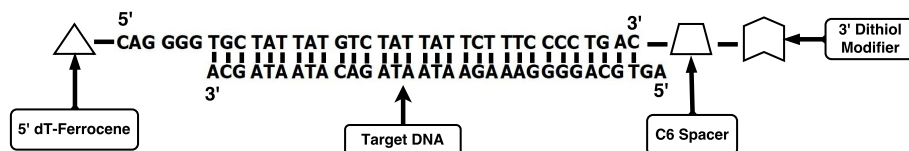


Figure 6.8: FE probe design when open and hybridized to target DNA.

Figure 6.7 and Figure 6.8 show the operation of the FE probe. The FE probe operates in much the same way as the previous FL probe with some minor changes. It can be seen that the dithiol and spacer modifications are now on the 3' end instead of the 5' end. There are 3 nucleotide bases on the 3' end that are not part of the hairpin stem, but this is not an issue as there is no longer a need for the stem to be parallel for the quencher and fluorophore. When the hairpin is closed, the ferrocene modification is physically close to the nanofiber substrate and when the hairpin has been opened the ferrocene is moved further away from the nanofibers. Figure 6.8 shows that there is more base pair matching with the target in comparison to the FL probe with 31 base pair matches.

6.3.3 Hairpin Structure T_m

Using the OligoAnalyzer 3.1 tool, the FE probe structure can be simulated and the T_m calculated. The analyzer reports a melting temperature of 51.6°C for the FE probe.

6.3.4 Self Dimers

Using the OligoAnalyzer 3.1 tool, the secondary structure of the FE probe can be estimated. Here again, only the most probable self dimer is shown in Figure 6.9.

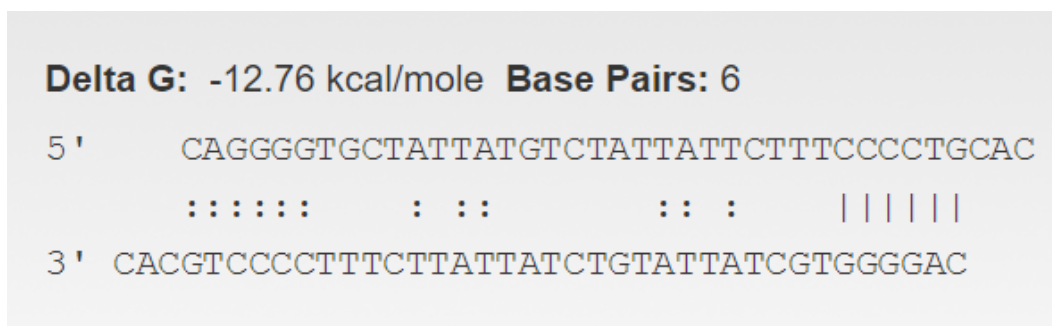


Figure 6.9: The most likely self dimer formed by the FL probe [63].

Figure 6.9 shows that the most likely secondary structure of the FE probe will form 6 hydrogen bonds (denoted |) exactly where the stem of the hairpin was designed and there will also likely be much weaker van der Waals bonds (denoted :) at 12 other base pairs. The secondary structure of the FE probe is very similar to the FL probe, although there are three free bases on the 3' end.

6.4 Conclusion

In this chapter two HIV DNA probes were designed and explained. The first incorporated a fluorescent label, as well as a quencher that would allow for the validation of immobilization and hairpin operation. The second probe was modified specifically for electronic detection, using a ferrocene modifier. The target DNA was also detailed and the probe-target hybridization was explained for both probes. The T_m and most the likely self-dimers (secondary structures) were also estimated using the IDT OligoAnalyzer 3.1 for both probes.

Chapter 7

Electronic Sensor Design

Section 4.4 discussed the decision to use resistive measurement as the chosen electrochemical signal from the biosensor. Figure 4.5 depicts the theoretical design of the resistive measuring circuit. In this chapter the complete measurement circuit, including hardware and user software will be described. The circuitry is designed in such a way that it is easily configurable for different applications and signal ranges. Specifically, the hardware communication was programmed in a simple manner that would allow various serial communication devices to receive the measured signals. The hardware was designed to allow for a change in constant current, gain of signal amplification, low pass filter frequency, voltage reference of the ADC and the option to use an external power supply for the circuitry or the standard 5 V supply from most serial devices.

Figure 7.1 depicts the block diagram of the electronic measurement design. A microprocessor is used to interface between the serial device, hardware and ADC. An Arduino Leonardo is used for these functions. The chosen serial device is a Windows personal computer, using a Python programmed GUI (graphic user interface) to interface via USB (Universal Serial Bus) serial communication. However, a different serial device such as a cellphone or any other handheld device can be chosen without any changes to hardware or microprocessor software needed. The power supply can either be sourced from the 5 V output of the USB port or an external source such as battery/PSU (Power Supply Unit). External power supply regulation was designed because certain laptops USB supplies are not stable and the Arduino's voltage line and load regulation is not optimal. The complete circuit schematic can be seen in Figure 7.2. In the next sections the design procedure will be described in a modular fashion and will describe the choice of hardware and all corresponding calculations.

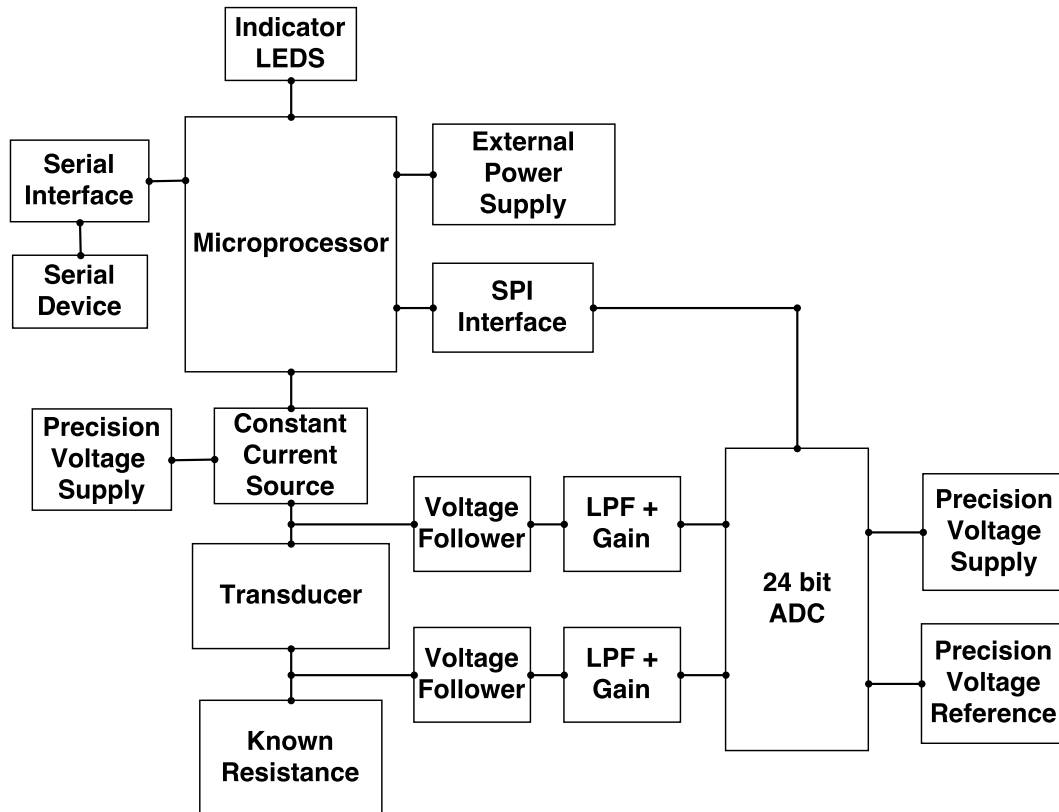


Figure 7.1: Electronic measurement block diagram.

7.1 Design Considerations

During the design process, a number of prototype circuits were built and tested to ensure stable and accurate readings. A number of design considerations were already known but the initial prototype circuits also provided valuable information for the final circuit design. The design considerations of the final circuit are briefly explained.

7.1.1 Constant Current Value

It was explained that a constant current source would be used in order to calculate the resistance of the transducer of the biosensor. When using organic materials, the electrochemical limitations of the bio-materials must be taken into account to prevent damage. A number of electrochemical biosensors articles that specifically used DNA were compared to identify the current and voltage limitations of DNA. Skotadis *et al.* [47] did not specifically detail the current limitations of the biosensor but noted a Keithley 2400 Multimeter was

used for resistive measurements. The Keithley 2400 Multimeter has a configurable voltage or current source when measuring resistance with the current source output ranging from 50 pA to 1.05 A [47]. The majority of DNA specific electrochemical biosensor research found was based on voltammetric technology. This method analyzes the bio-sample in an electrolytic solution which may not result in current flow directly through the organic materials. The voltage and current used in these articles were, however, still limited to relatively low levels. The current value ranges observed were widely spread from a considerably low range of 150 nA [70], to an average of around 5 μ A - 20 μ A [71, 52, 18] and a relatively high current of about 400 μ A [46]. From these articles it can be deduced that the constant current source should be designed to output as low a current as possible.

7.1.2 ADC Resolution

In order to get accurate resistance measurements, as well as the ability to register a very small change in the resistance of the transducer, the resolution of the ADC used, is vitally important. With a relatively low current supply, this becomes even more important, as will be discussed. The lowest voltage an ADC can measure ($V_{Resolution}$) is calculated by its own voltage reference divided by the ADC bit resolution.

$$V_{Resolution} = \frac{V_{reference}}{2^{bit\ resolution}}. \quad (7.1.1)$$

Using the circuitry described in Figure 4.5, it is then possible to calculate the lowest resistance measurement achievable. Assuming no signal amplification or known resistor ($R_{Known} = 0 \Omega$), the resistance resolution of the circuit can be calculated by dividing the voltage resolution by the designed constant current.

$$R_{Resolution} = \frac{V_{Resolution}}{I_{Constant}}. \quad (7.1.2)$$

The Arduino Leonardo has a 10-bit ADC resolution with either a 5 V or 1.1 V voltage reference. As an example, if the chosen constant current was 5 μ A, the lowest possible resistance resolution, using a 1.1 V reference voltage, would be 214 Ω . By using a 24-bit external ADC and if the voltage reference and current is kept the same as the previous example, the lowest possible resistance measurement would then be 13.11 m Ω . For these reasons an external ADC is the best choice, because the ADC resolution as well as the ADC voltage reference can be chosen.

7.1.3 Signal Amplification and Filtering

Due to the fact that the constant current is designed at a relatively low value (μ A range), the voltage signal to the ADC will also be relatively low with a

high possibility of signal and resistive noise. For these reasons signal amplification and low pass filtering may be necessary. Applying amplification to the signal will reduce the effective range the ADC can measure, because the ADC reference voltage is effectively divided by the amplification unit. By reducing the ADC range, the maximum resistance that can be calculated is reduced. Due to the fact that the signal to the ADC is a DC voltage, almost all noise can be filtered out by the use of a low pass filter (LPF), but the filter response may be slow if the LPF is not designed correctly. It is noted that resistive noise will not be completely removed, due to the fact that the LPFs and amplifiers will introduce their own inherent resistive noise.

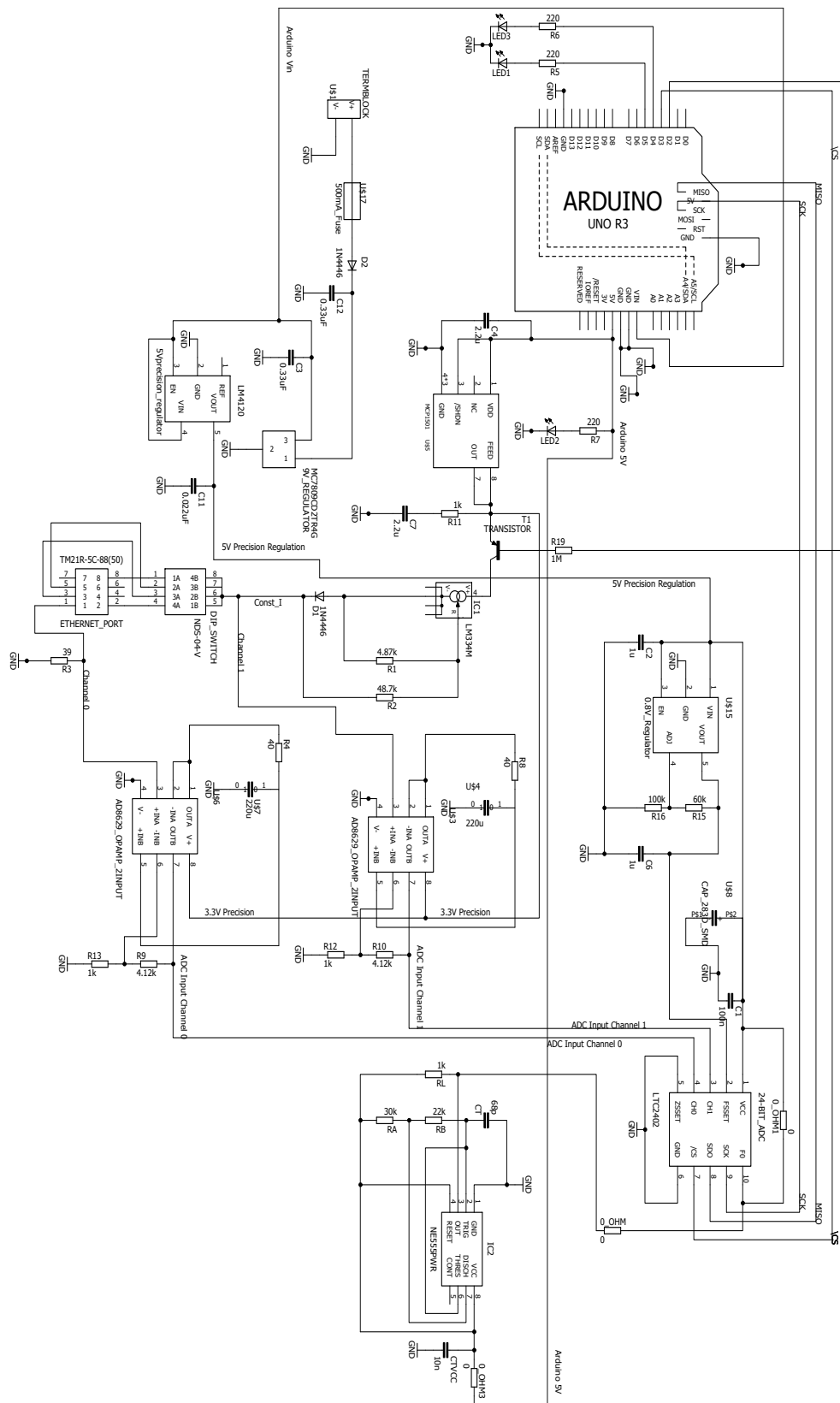


Figure 7.2: Electronic measurement schematic.

7.2 Spice Simulations

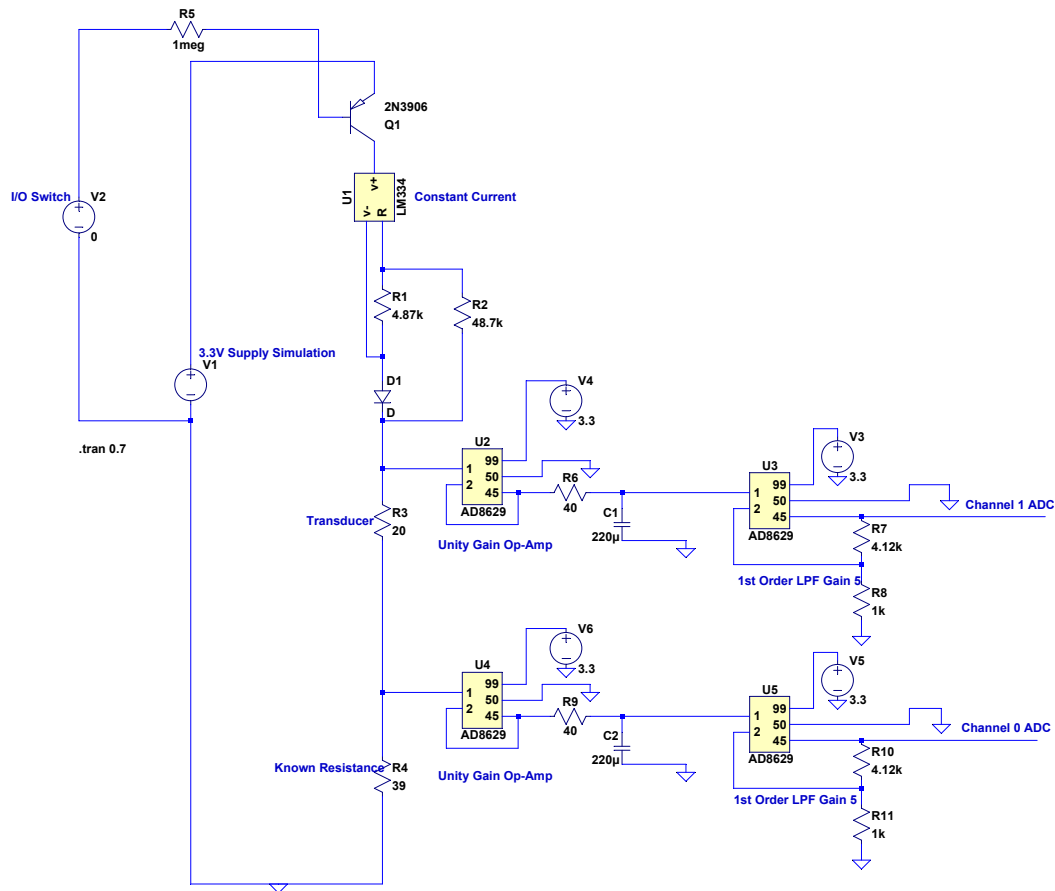
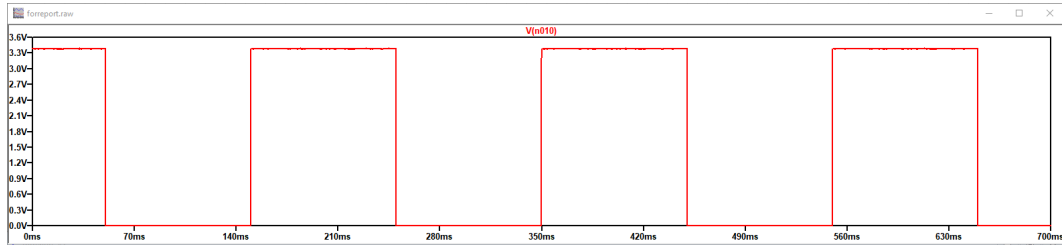


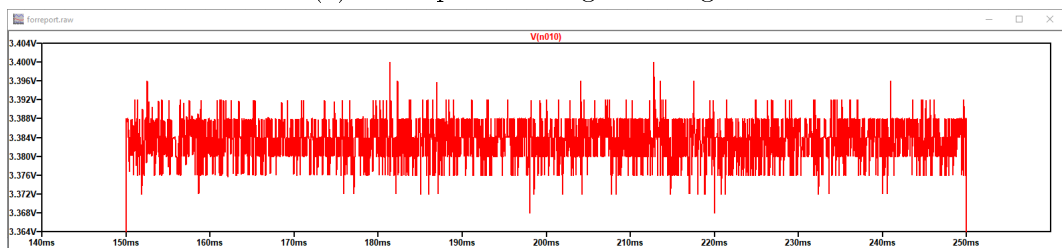
Figure 7.3: 3.3 V Supply LtSpice simulation with real time noise.

The analogue portion of the circuit design was simulated using LTSpice XVII. As mentioned, a number of prototype circuits were built which meant it was possible to record real data output and use these values for the next iteration of the Spice simulations. Selected voltage supplies, as well as the voltage inputs to the ADC channels were recorded on an oscilloscope (Tektronix TDS 1002B) and saved to a .csv file, to be used by LTSpice as simulated voltage sources. Figure 7.3 shows the Spice model used to simulate the 3.3 V supply which provides power to the constant current source. Using real time values for the 3.3 V supply, provides valuable information regarding the noise rejection and filtering as well as voltage rise times. Figure 7.4(a) shows a switching 3.3 V supply. Figure 7.4(b) shows the same 3.3 V supply but zoomed in, to see the real time noise. Figure 7.4(c) shows the voltage at the output of the constant current source (voltage above the transducer and input to the ADC channel 1). Figure 7.5(a) depicts the same signal zoomed in, as can be seen there is

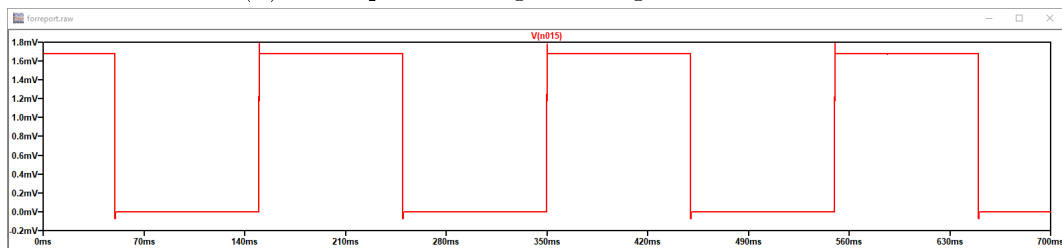
some noise still present on the signal. Finally Figure 7.5(b) depicts the signal after the unity gain opamp (operational amplifier) and LPF filter (red) as well as the signal after amplification (blue), which is the input to the ADC channel 1. Here no noise is seen, but in practice this is highly unlikely.



(a) 3.3 V precision regulator signal.

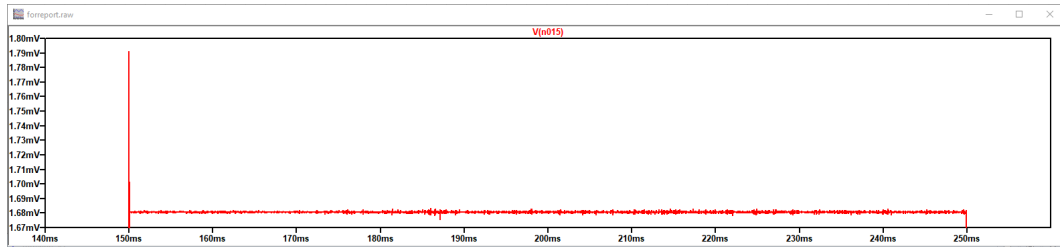


(b) 3.3 V precision regulator signal zoomed in.

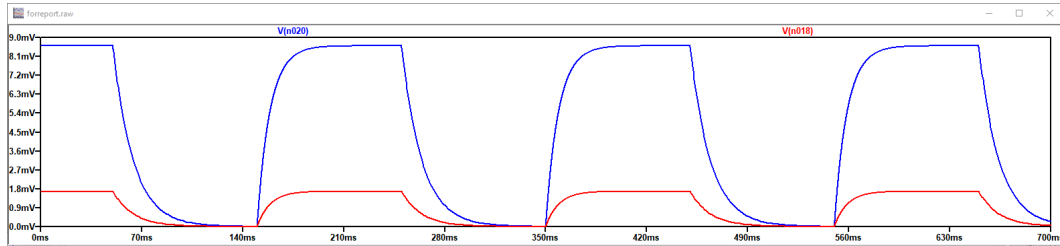


(c) Constant current voltage output.

Figure 7.4: Spice Simulation Results



(a) Constant current voltage output zoomed in.



(b) Unity gain in red. Filtering and amplification in blue.

Figure 7.5: Spice Simulation Results

The transducer voltage was also recorded on an oscilloscope and used to simulate the unity gain opamp, as well as the 1st order active LPF with gain to ensure the input to the ADC channels would be as stable as possible. Figure 7.6 shows the model used to verify this.

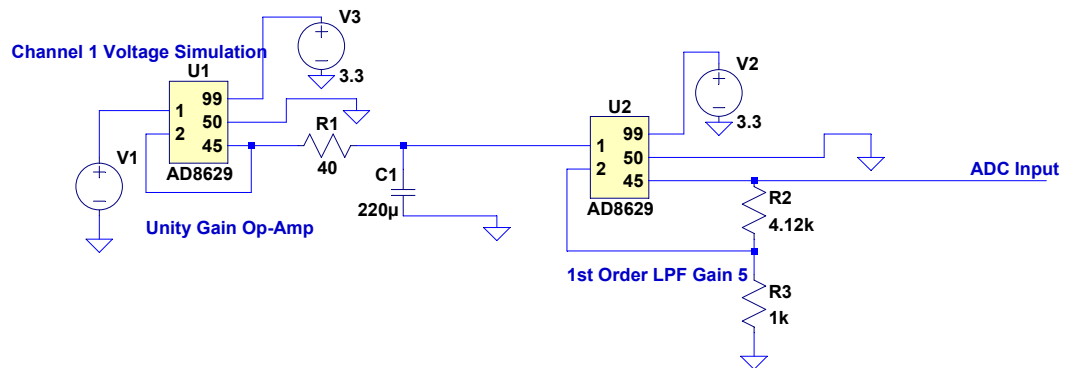
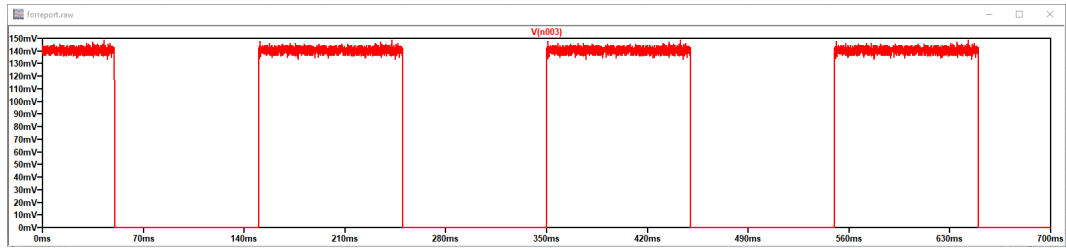
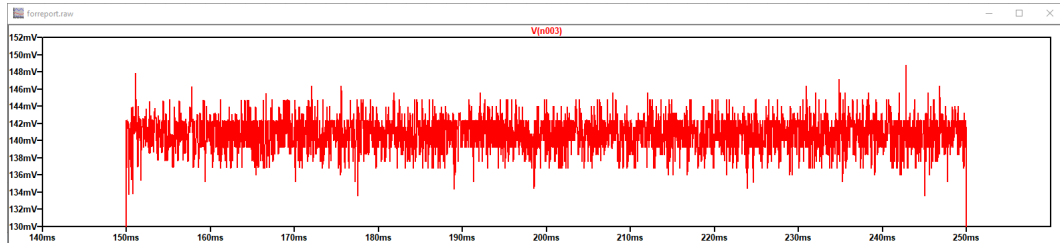


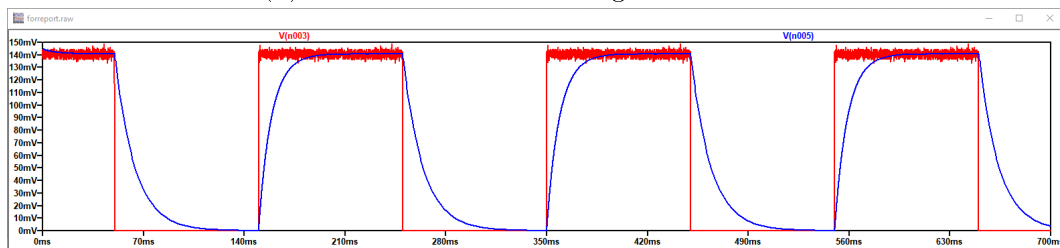
Figure 7.6: Transducer voltage LtSpice with real time noise.



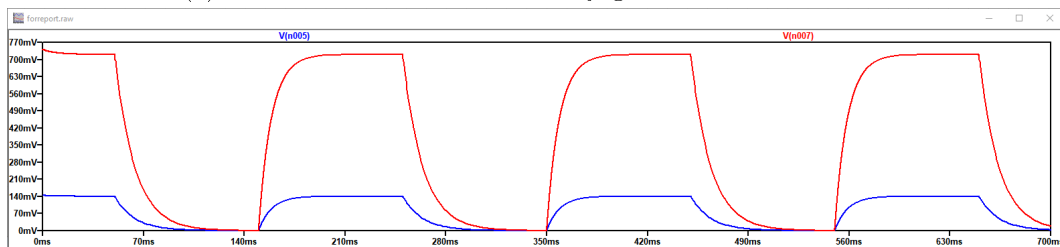
(a) Channel 1 Transducer Signal.



(b) Channel 1 transducer signal zoomed in.



(c) Channel 1 in red. After unity gain and LPF in blue.



(d) LPF and unity gain in blue. Active LPF and gain in red.

Figure 7.7: Spice simulation results.

Figure 7.7(a) depicts the simulated signal of real time oscilloscope recordings of the voltage above the transducer. Figure 7.7(b) is a zoomed in image of the same signal. Figure 7.7(c) shows the signal after unity gain and filtering superimposed onto the original signal. It can be seen that the majority of the noise is filtered, and it takes approximately 50 ms for the signal to reach steady state. Finally Figure 7.7(d) depicts the signal after amplification. It can be seen that the signal input to the ADC should be relatively stable, although in practice the results will not be as ideal.

7.3 Circuit Design

7.3.1 Arduino Leonardo Microprocessor

An Arduino Leonardo was chosen as the microprocessor, because there are many Arduino Leonardos readily available and they are easy to use and therefore suited for rapid prototyping. Most basic Arduino products provide serial UART (Universal Asynchronous Receiver-Transmitter) as well as SPI (Serial Peripheral Interface) communication. There are multiple digital and analogue ports available and there is a vast amount of online resources specifically for the Arduino Leonardo.

The microprocessor was chosen predominantly for its simple interfacing, communication and digital functionality. External circuitry was designed for the analogue functionality as well as necessary power supplies and references. The Leonardo was used to interface with the chosen Windows serial device via serial UART communication. An external 24-bit ADC was used instead of the Leonardo's internal 10-bit ADC and SPI communication was used between the devices. The Leonardo digital I/O (Input/Output) ports were used to switch the current source and the external ADC's enable pins. Additional I/O pins were also used to switch LEDs (Light Emitting Diode) to indicate communication and ADC conversion. As mentioned, Arduinos do not have efficient line and load regulation, therefore an external power supply was also made available. The Arduino can be powered by either the USB 5 V supply or by an external source connected to the V_{in} of the microprocessor. When the USB 5 V is used as the supply, V_{in} will act as an output, therefore circuitry was designed that allowed for either of the power options to be used.

7.3.2 External Power Supply Regulation

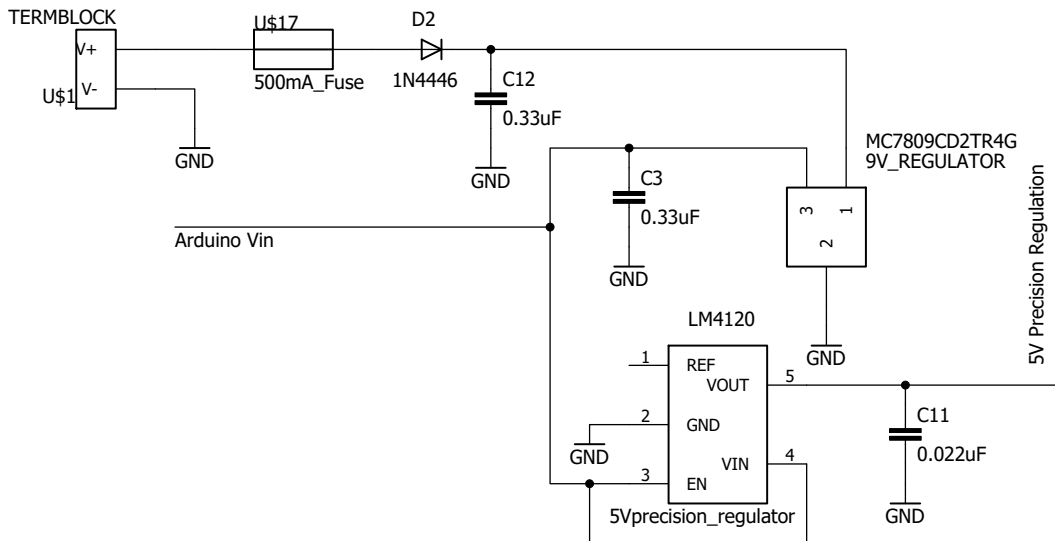


Figure 7.8: External voltage supply regulation.

Figure 7.8 depicts the external voltage supply regulation circuitry. The external supply (9 V-24 V) is connected to the terminal block. Most USB 1.0/2.0 devices are rated at 500 mA, therefore a 500 mA non-resettable surface mount fuse is used to prevent any surge current from the external source that may damage the USB ports of the serial device. In addition, a simple 1N4446 diode is also implemented to prevent any reverse currents that may also damage the USB ports. A 9 V, 2.2 A Linear Voltage Regulator (ON Semiconductor MC7809CD2TR4G- Appendix B.1) is used to supply power to the Arduino as well as a 5 V precision regulator. The 9 V output is connected to the Arduino Vin. When an external supply is applied to the Arduino, that is greater than 7 V, Vin acts as a voltage input and the Arduino will automatically source power from the external supply rather than the USB 5 V. When no external power is supplied, Vin acts as a voltage output and therefore supply power to the 5 V precision regulator. The capacitors' values used in conjunction with the 9 V regulator were obtained from the typical use diagram from the datasheet.

7.3.2.1 5 V Precision Regulator

Line regulation is the ability of a power source to maintain a stable set output with varying changes to the input. Due to the relatively small currents of the constant current needed, any small changes in either voltage or current will result in considerable measurement errors. In order to reduce any line regulation errors, high precision voltage regulators/references are used wherever

the measured signal may be affected. The drawback of using high precision references is that they do not commonly source a large amount of current. The Texas Instruments LM4120 Precision Voltage Reference (Appendix B.2) is used to supply power to the external ADC as well as the ADC variable voltage reference source (ADP123). The 9 V generic voltage regulator has a line regulation of typically 5 mV while the 5 V precision reference has a line regulation of typically 0.0007 %/V. Unfortunately the line and load regulation unit standards differ from datasheet to datasheet and can be typically quantified either by a set voltage (mV), as a ratio of percent to voltage (%/V) or as a parts per million (ppm) value. Essentially, the line regulation can be represented as a change in output voltage as a result of a change in input voltage ($\Delta V_{OUT}/\Delta V_{IN}$). The maximum current draw of the ADC supply rail, as well as the ADC reference pin, are both 300 μ A and the maximum current the 5 V precision regulator can supply is 5 mA, which is more than sufficient.

7.3.3 Constant Current

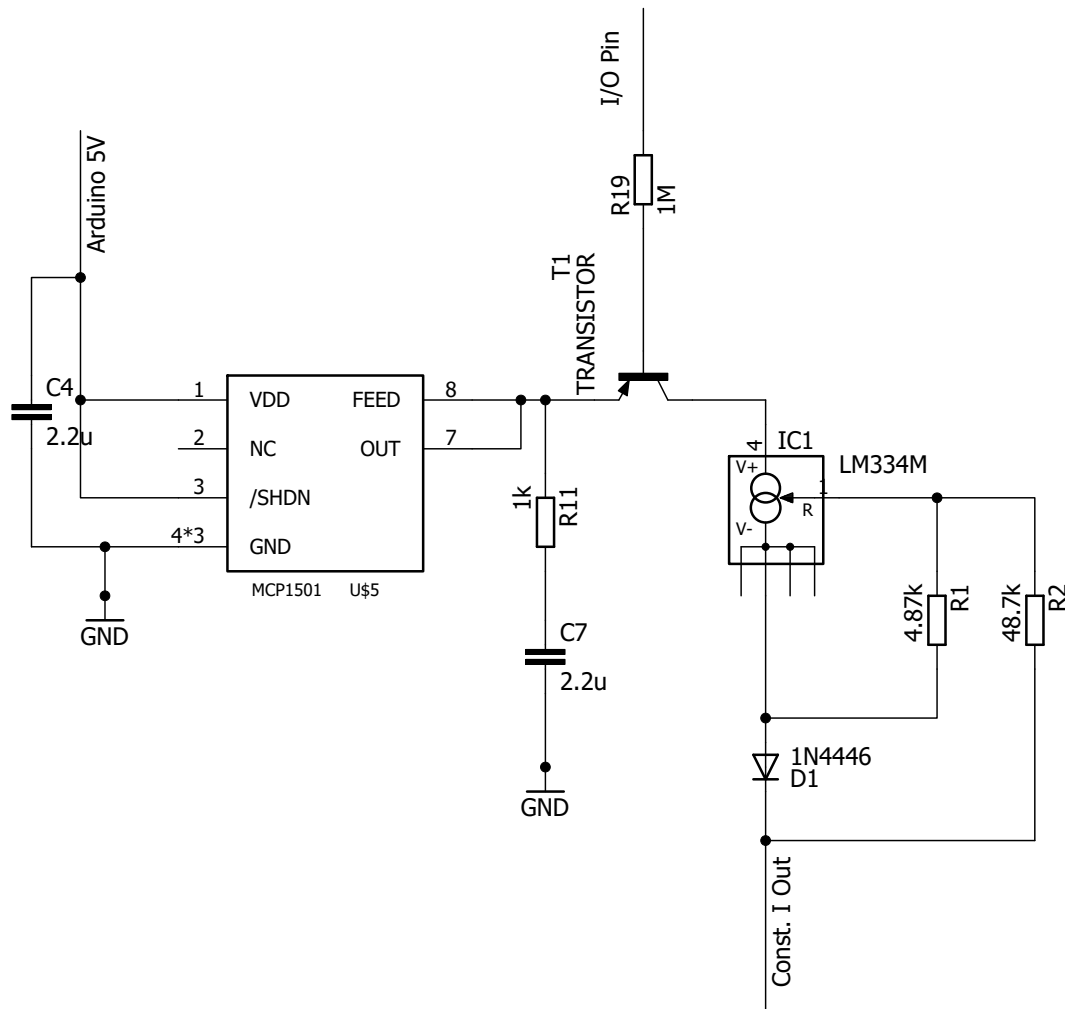


Figure 7.9: Constant current design.

Figure 7.9 depicts the constant current circuit design. It was found that the I/O pins of an Arduino are not truly 0 V when set low and so a BJT transistor (Bipolar Junction Transistor) switch was implemented to ensure the current was either fully off or fully on when needed. A PNP type transistor switch was used, which means that when the I/O pin is high (5 V), the transistor switch is open/off and when the I/O pin is low (0 V) the transistor switch is closed/on. A 3.3 V precision voltage source (Microchip MCP1501-33E/SN, Fixed Series Voltage Reference, Appendix B.3) is used at the collector of the transistor switch. When the transistor switch is closed the constant current chip is switched on and receives power from the 3.3 V source minus V_{ce} . The

3.3 V source is fixed and the capacitor and resistor values were taken from the typical application of the datasheet.

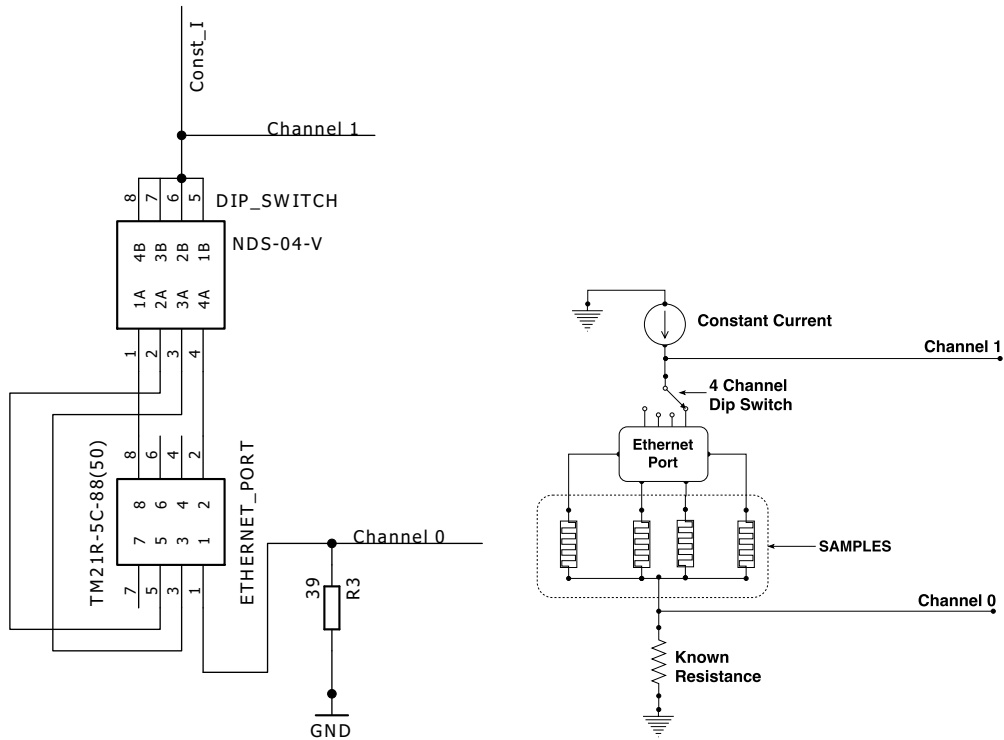
7.3.3.1 Setting Constant Current Value

The Texas Instruments LM334M/NOPB Programmable Current Source (Appendix B.4) was chosen to provide the current for the biosensor, because it was the lowest output current source available and the desired current can be set anywhere between 1 μA to 10 mA. The ability to change the constant current value gives a wider range of use for the biosensor and allows for better testing and optimization. Figure 15 from the datasheet in Appendix B.4 shows a typical application as a zero temperature coefficient current source. A diode and resistor are added to the typical generic application to cancel the temperature-dependent characteristic of the LM334. The datasheet suggested a 1N457 diode, which was not available, so the closest matching diode was chosen, that being the 1N4446. In order to determine the values of the resistors needed (R_1 and R_2 in Figure 7.9), an equation from the datasheet is used:

$$I_{SET} = \frac{0.134V}{R_1} \quad (7.3.1)$$

Therefore R_1 can be calculated and R_2 is $10 \times R_1$. It was decided that the constant current should be close to 25 μA and so by setting $R_1 = 5.87 \text{ k}\Omega$ and $R_2 = 48.7 \text{ k}\Omega$, the constant current was calculated as 27.52 μA . The constant current is set at 27.52 μA , because it was found that lower currents had greater signal-to-noise ratios and thus the resistance calculation error would be greatly affected.

7.3.4 Sample Switch and Connection



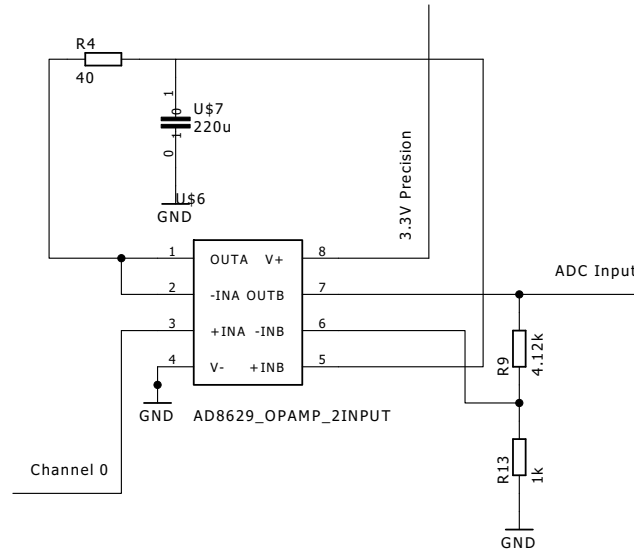
(a) Dip switch connecting to one of four samples via Ethernet cable (cat5). (b) Graphical representation of dip switch circuit.

Figure 7.10: Sample switch and connection.

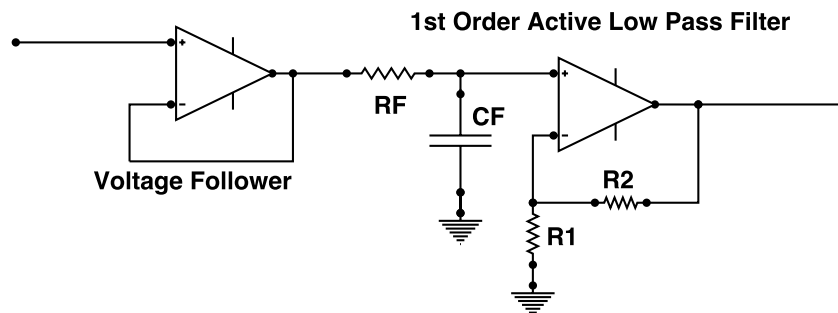
Figure 7.10(a) shows the circuit schematic of a four channel dip switch that connects to an Ethernet port. A dip switch was added to enable quick and easy switching of sample fibers, which allows for up to four tests to be run one after the other without having to unload and re-prepare samples for every test. The dip switch has a low internal resistance of 50 mΩ, which is ignored during calculations as it is relatively low and has a constant independent value. It was decided that the sample holder and CNFs would connect to the measurement circuit via Ethernet cable (cat5) as this is an easy method to connect and disconnect the sample holder from the circuit. Figure 7.10(b) shows a graphical representation of how the samples are connected over Ethernet to the measurement circuitry. The selected sample channel is chosen via the dip switch before the test. The constant current is then directed through the selected channel, the Ethernet port and cable, carbon nanofiber and finally the known resistor and ground. The known resistance was chosen a 39 Ω to match the impedance as close as possible to the carbon nanofiber. Channel 0 and Chan-

nel 1 represent the two points that are measured by the ADC to calculate the resistance.

7.3.5 Voltage Follower and Low Pass Filtering



(a) Active first order low pass filter circuit.



(b) Graphical representation of active first order low pass filter circuit.

Figure 7.11: Voltage Follower and Low Pass Filtering

Figure 7.11(b) shows the graphical representation of the voltage follower and filtering stages of the circuitry before the signal is input to the ADC. First a unity gain voltage follower is used to isolate the transducer from the ADC input. A simple first order active low pass filter is then used to reduce any signal noise. The cutoff frequency was designed at 18 Hz and can be easily altered by recalculating the values of R_F and C_F , as seen in Figure 7.11(b) (R_4 and $U\$7$ in Figure 7.11(a)). The cutoff frequency is calculated as:

$$f_{\text{cutoff}} = \frac{1}{2\pi R_F C_F} \tag{7.3.2}$$

An amplification stage is applied in conjunction with the filter, which can also be, altered as needed, by recalculating R_1 and R_2 as seen in Figure 7.11(b) (R_{13} and R_9 in Figure 7.11(a)). The chosen gain was set to 5.12. The gain can be calculated as:

$$A_V = 1 + \frac{R_2}{R_1}. \quad (7.3.3)$$

As can be seen in Figure 7.11(a), both operational amplifiers are located on a single IC which makes circuit design smaller and easier to route. The AD8629 operational amplifier (Appendix B.5) was chosen as it requires only a single 5 V supply rail and a full rail-to-rail input voltage range, which is important because the input voltage is relatively low and most operational amplifiers would not operate at such low levels.

7.3.6 Analogue to Digital Converter

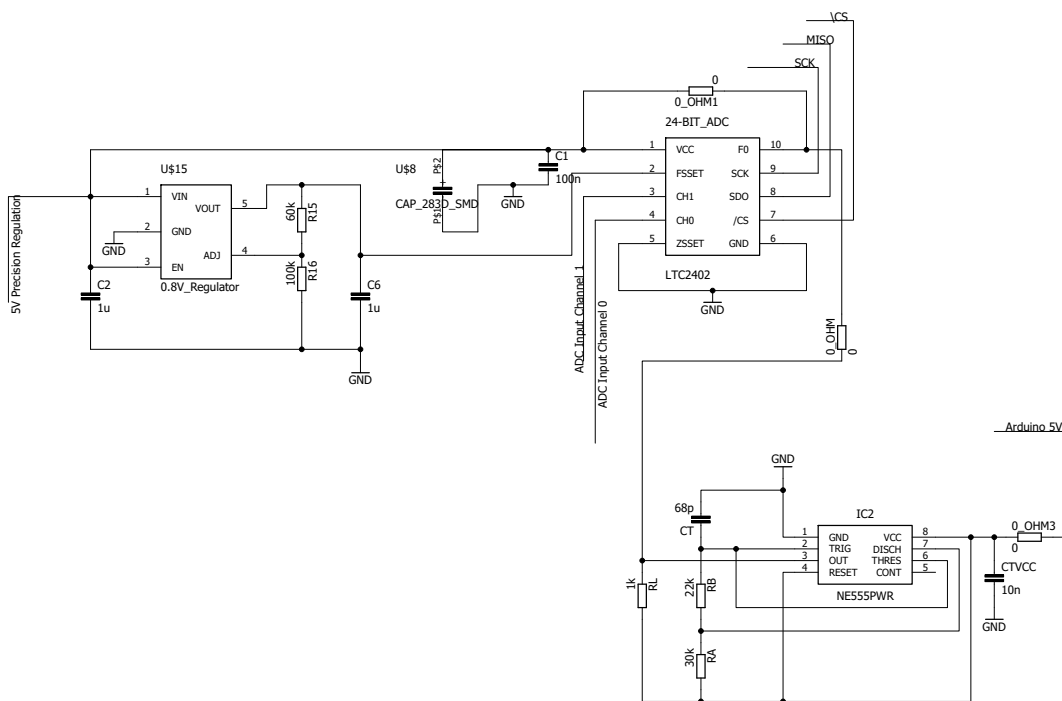


Figure 7.12: ADC design.

The final stage of circuitry design is the Analogue to Digital Converter (ADC). This includes the reference voltage, supply, clock frequencies and the communication methods used by the ADC. The Linear Technology LTC2402 24-bit ADC chip (Appendix B.6) was chosen, because it has two input channels, it allows for an upper and lower input reference and a supply range from 2.7 V - 5.5 V. It also has a 2 or 3 wire SPI communication interface and allows for

either 50 Hz or 60 Hz internal oscillation clock or an optional external oscillation clock for conversions. The LTC2402 has many serial interface timing mode options, so only the selected option will be discussed.

7.3.6.1 External Serial Clock, Single Cycle Operation

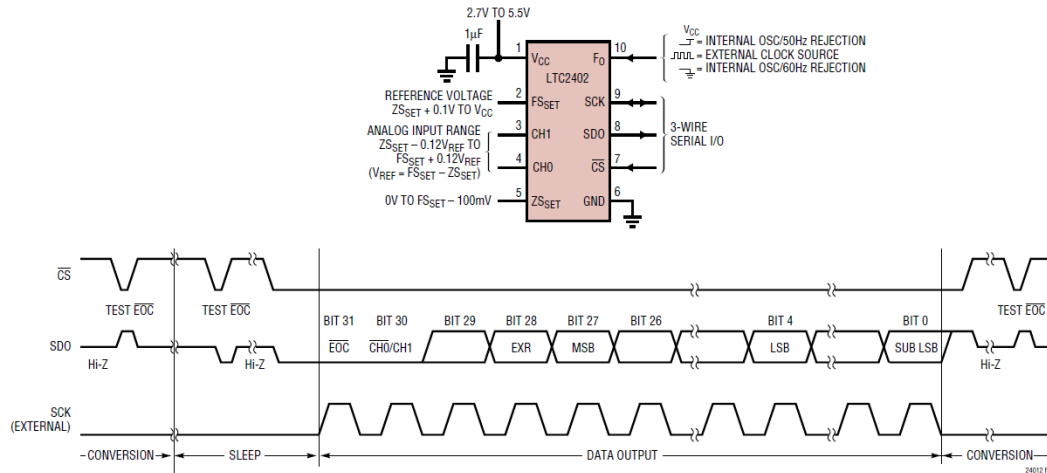


Figure 7.13: External serial clock, single cycle operation (Appendix B.6).

The chosen serial interface timing mode from the datasheet (Appendix B.6) was the external serial clock, single cycle operation mode. Using this mode, the SPI clock frequency is determined by an external source, in this case the clock frequency of the Arduino Leonardo's SPI SCK pin which is 16 MHz. The other determining factor of this mode is that the chip select pin (\overline{CS}) is connected to an I/O pin of the Arduino Leonardo (Active Low chip select). This makes the SPI a 3 wire interface. The datasheet states that in this mode the data output time is as long as \overline{CS} is low but no longer than $32/f_{SCK}$ ms.

7.3.6.2 ADC Supply

The datasheet suggests the use of a 10 μF tantalum capacitor in parallel with a 0.1 μF ceramic capacitor, placed as close to the chip as possible in order to properly decouple the source from the chip. As discussed in Section 7.3.2.1, a 5 V precision regulator is used to supply the ADC supply, as well as the ADC voltage reference chip.

7.3.6.3 Voltage Reference Input

The LTC2402 has two reference inputs, FS_{SET} (Upper limit) and ZS_{SET} (Lower limit). The ZS_{SET} is set to 0 V and so is connected straight to ground.

Therefore, with an ADC value of 00000_H , the voltage is calculated at 0 V. The FS_{SET} is set by an external voltage supply (ADP123 programmable CMOS linear regulator- Appendix B.7). The ADP123 adjustable output voltage range is 0.8 V - 5.0 V. The resistance of the carbon fiber is relatively low, with a single 1cm x 1cm piece no more than 30 Ω . For this reason the FS_{SET} is adjusted to 800 mV as this is the lowest possible value the ADP123 can output. If the constant current is set to 27.52 μA and the known resistance is 39 Ω , the ADC resistance resolution can be calculated as:

$$\begin{aligned}
 V_{Resolution} &= \frac{V_{Ref}}{2^{bit\ resolution}} \\
 &= \frac{800\text{ mV}}{2^{24}} \\
 &= 47.68372\text{ nV} \\
 R_{Resolution} &= \frac{V_{Resolution}}{I_{Constant}} \\
 R_{Resolution} &= \frac{47.68372\text{ nV}}{27.52\ \mu\text{A}} \\
 &= 1.733\text{ m}\Omega
 \end{aligned} \tag{7.3.4}$$

Assuming no amplification of the signal, the maximum resistance measurement can also be calculated as:

$$\begin{aligned}
 R_{max} &= \frac{V_{Ref}}{I_{Constant}} - R_{Known} \\
 &= \frac{800\text{ mV}}{27.52\ \mu\text{A}} - 39\ \Omega \\
 &= 29\text{ k}\Omega
 \end{aligned} \tag{7.3.5}$$

A gain of 5.12 was designed which therefore means that the maximum resistance measurable is $29\text{ k}\Omega/5.12 = 5.66\text{ k}\Omega$.

7.3.6.4 Adjustable Voltage Reference ADP123

As mentioned the ADP123 programmable CMOS linear regulator (Appendix B.7) was selected as the ADC upper limit voltage reference input. V_{in} of the regulator is supplied by the 5 V precision regulator, as well as the enable pin, which means that the reference voltage is always on. The ADP123 datasheet suggests 1 μF capacitors at both the input and output as decoupling capacitors. The output voltage is adjusted by setting the R15 and R16 resistors from Figure 7.12 as:

$$\begin{aligned}
 V_{Ref} &= 0.5\left(1 + \frac{R15}{R16}\right) \\
 &= 0.5\left(1 + \frac{60\text{ k}\Omega}{100\text{ k}\Omega}\right) \\
 &= 800\text{ mV}
 \end{aligned} \tag{7.3.6}$$

The voltage reference can easily be re-adjusted for other applications by changing the R15 and R16 resistors.

7.3.6.5 Conversion Clock Oscillator

The LTC2402 allows for the use of either a 50 Hz or 60 Hz rejection internal oscillator or an external oscillator frequency with a maximum value of 307.2 kHz for the conversion of the analogue values. The initial prototype circuitry was tested using the internal 50 Hz oscillator by connecting the F_o pin to V_{CC} (5 V precision regulator), which results in a conversion time of around 160 ms per channel. When the final circuit board design was ordered, it was decided that an external timer would be tested in order to speed up the conversion time. The fastest conversion time from the datasheet can be calculated as $20510/307.2 \text{ kHz} = 68.4 \text{ ms}$. As seen in Figure 7.12, the NE555PWR timer (Appendix B.8) is included but, there are a number of 0Ω resistors (0_OHM, 0_OHM1 and 0_OHM3) placed on the circuit. These resistors are used to enable the switching from either internal 50 Hz oscillator or external oscillator, due to the external oscillator being untested. By placing only resistor 0_OHM1, the internal oscillator is used and by placing only 0_OHM and 0_OHM3, the external oscillator is used. The NE555PWR timer was designed to output 286 kHz but unfortunately it was later determined that the maximum output frequency provided by the NE555PWR timer is only 100 kHz and therefore would not speed up conversion time ($20510/100 \text{ kHz} = 205.1 \text{ ms}$) and thus the internal 50 Hz oscillator is used instead.

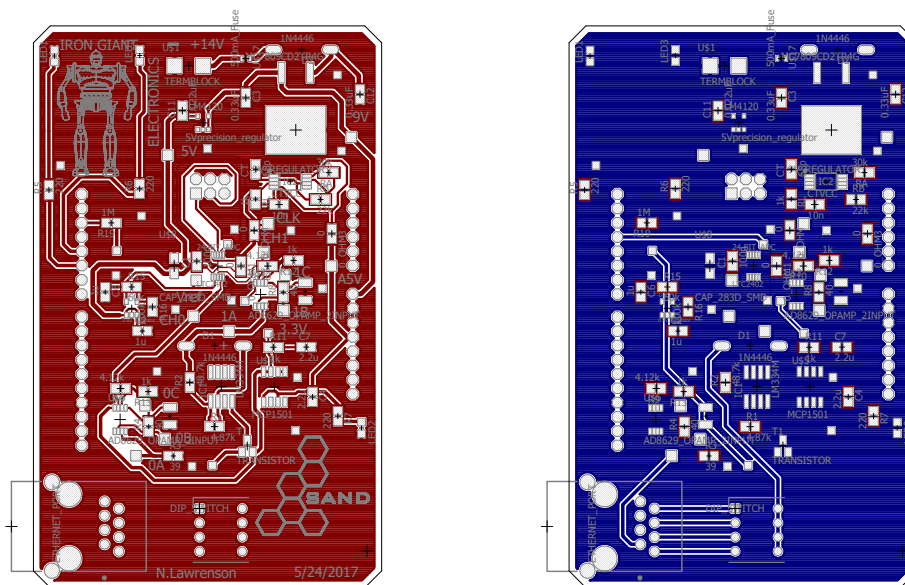
7.3.6.6 Serial Peripheral Interface (SPI)

As mentioned, three wire SPI is used to transfer the measured values from the external ADC to the Arduino Leonardo. On the ADC chip there are three pins that are used for SPI communication, SCK-Transfer clock, SDO- Three State Digital Output and /CS- Active low chip select. The ADC acts as the SPI slave, while the Leonardo acts as the SPI Master. The SCKs of the ADC and Leonardo are connected. The SDO of the ADC is connected to the MISO (Master In Slave Out) of the Leonardo and the /CS is connected to a free I/O pin. The MOSI (Master Out Slave In) of the Leonardo is left unconnected, because the ADC does not accept input commands, but rather relies on the /CS pin to begin the ADC conversions and the Leonardo must monitor the SDO pin in order to determine when data is ready and can begin being read from the ADC, as seen in the waveform diagram of Figure 7.13. The ADC outputs 32 data bits in the form of 4 bytes, which are fully detailed in the datasheet. In order to calculate the measured voltage, some bit manipulation needs to be performed in order to determine which channel is being used, if an error has occurred and the sign of the value and thereafter the bits that are not used to calculate the value are discarded. Once channel 0 and 1 have

been read and the necessary bit manipulation has been performed, the data is transferred via serial communication from the Leonardo to the serial device (Windows PC) and thereafter the voltage is calculated.

7.4 PCB Routing and Manufacture

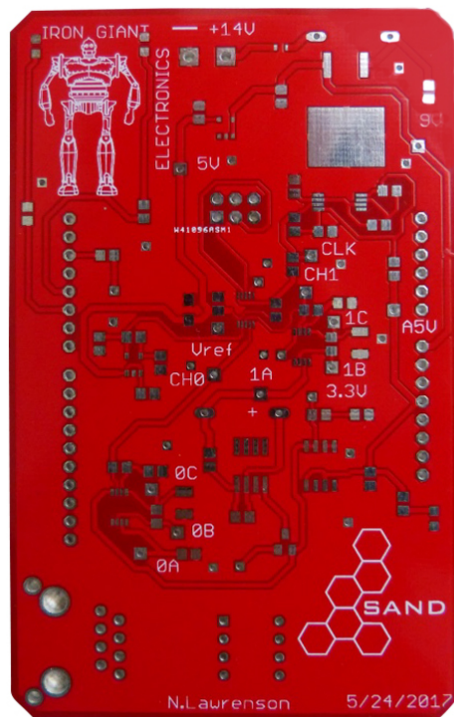
The final stage of the circuit design is the printed circuit board (PCB) component placement, routing and manufacture. All PCB designs were implemented using Cadsoft Eagle 7.3.0. The initial prototype circuits were manufactured on a LPKF ProtoMat S62 PCB Plotter within the Electrical and Electronics Engineering Department of Stellenbosch University. The final PCB designs were manufactured by PCBWay and shipped from China. The circuit schematic is seen in Figure 7.2. Wherever possible, surface mount devices (SMD) were chosen and 0.01% tolerance resistors were used. All decoupling capacitors were placed as close to the corresponding devices as possible. All supply and regulator track widths were set to 32 mil, all analogue track widths at 24 mil and all digital track widths at 16 mil. The regulator and analogue tracks were designed as thick as possible and all analogue tracks were ground shielded, wherever possible, to reduce noise. Figure 7.14 depicts the top and bottom layer board layout. A silk screen was added to the top layer to label relevant points (voltage terminals, as well relevant tests points). The SAND team logo, as well as a personal brand, was also added to the silkscreen. Figure 7.15 shows the results of the PCB manufacturing from PCBWay.



(a) PCB top layer board design.

(b) PCB bottom layer board design.

Figure 7.14: PCB board layout.



(a) PCBWay top layer.

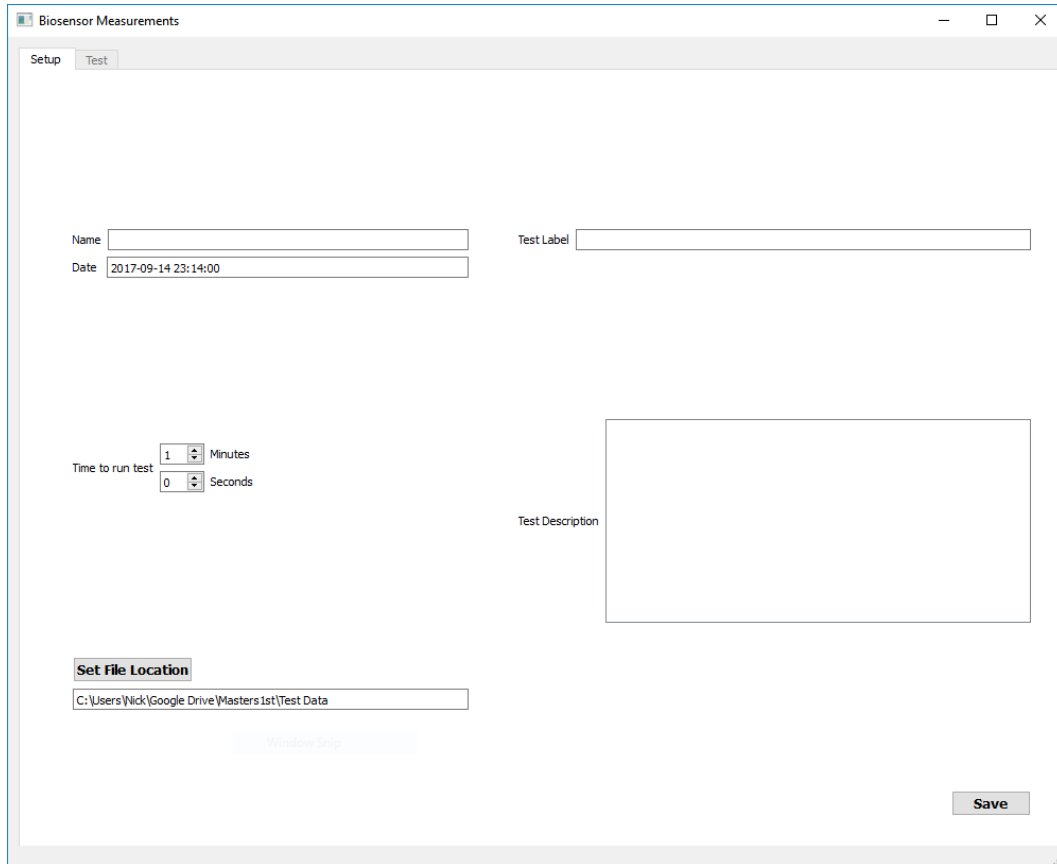


(b) PCBWay bottom layer.

Figure 7.15: PCBWay results.

7.5 User Interface Software

A Windows PC was chosen to receive, analyze and output the measured signals from the Leonardo. Python 3.6 and PySerial 3.3 were used to interface between the Leonardo and Windows PC. A Python class was written to automatically connect to the Leonardo, receive the measured values via serial UART communication and thereafter calculate the resistance of the transducer. A second Python class was written to provide a graphic user interface (GUI) during testing. The GUI was implemented using PyQt4 and designed using the Qt Designer tool. Matplotlib was used to display the calculated resistance values in real time. In order to use the designed software on multiple Windows systems, an executable (.exe) file was compiled using `cx_freeze`. The GUI will be briefly explained as follows:



The screenshot shows a software window titled "Biosensor Measurements" with two tabs: "Setup" and "Test". The "Setup" tab is active and contains the following fields and controls:

- Name:** A text input field.
- Date:** A text input field containing the value "2017-09-14 23:14:00".
- Test Label:** A text input field.
- Time to run test:** Two spinners. The first is labeled "Minutes" and has the value "1". The second is labeled "Seconds" and has the value "0".
- Test Description:** A large, empty text area.
- Set File Location:** A button with a dropdown menu showing the path "C:\Users\Nick\Google Drive\Masters 1st\Test Data".
- Save:** A button at the bottom right.

Figure 7.16: Test detail form.

The Biosensor GUI consists of two tabs, the Setup tab (Figure 7.16) and the Test tab (Figure 7.17). Before a test can begin, the user is prompted to input the specific details of the current test within the Setup tab. This is to ensure that all tests are properly recorded and later understood. The user must input Name (Tester), Test label, Time to run test (minutes and seconds), Test description (all valid details or changes to test environment) and the File location to save all recorded data. The date form block is automatically filled in and the time to run test, as well as file location, have initial default values. The file location is selected by opening an external Windows File Explorer window, thereafter the user can choose or create a directory with the traditional Windows methods. Without filling in the relevant data, the test will not continue to the Test tab. When the user is ready, the save button is clicked and all the relevant data is saved to a .txt file and the Test tab of the GUI is displayed. The Setup tab is disabled and cannot be accessed again.

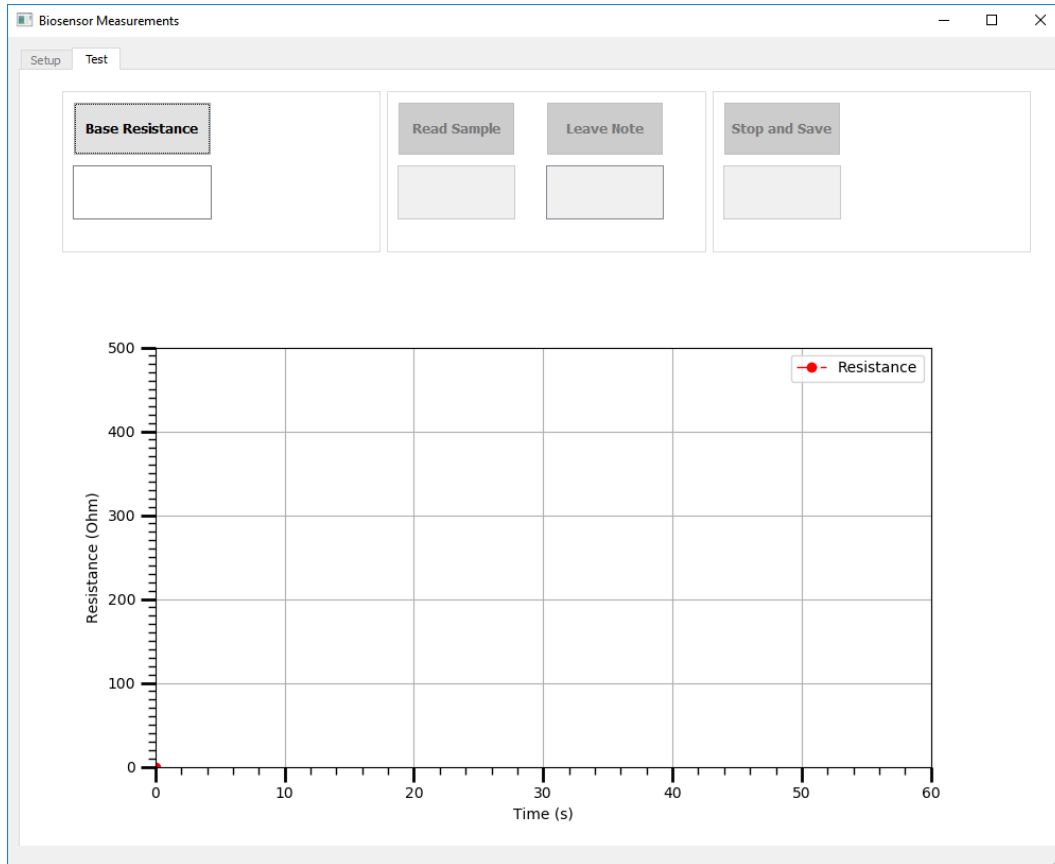


Figure 7.17: GUI plotting tab.

Once directed to the Test tab, only the Base Resistance button is enabled. The Base Resistance button is clicked once the test sample has been prepared and the test can begin. The Base Resistance button runs a function that performs five measurements which are averaged and the resistance is calculated and displayed in the box below the Base Resistance button. Once the base resistance is calculated, the Base Resistance button is disabled and the Read Sample and Leave Note buttons are enabled. The user will then click the Read Sample button to begin real time measurements of the sample, which will be displayed on the matplotlib graph below. The Stop and Save button will then be enabled. The test will run for as long as the user selected time or until the Stop and Save button is clicked. Once the Read Sample button is selected and the resistance values are being displayed, the user can begin the reaction testing phase by adding sample solutions (HIV target or other controls) and the resulting changes to the transducer resistance will be displayed. The resistance results recorded are averages from three individual readings to reduce deviances as a result of noise. At any time during this phase, the user may type a note below the Leave Note button. The note that is typed by the user may include

additional test data not included in the test description or some test anomalies or errors during this phase. These notes will be appended to the .txt file created with a time stamp. Once the time has completed or the Stop and Save button is clicked, the test will end and the matplotlib graph will be saved as a .png, the total change in resistance in comparison to the base resistance will be recorded to the .txt file and displayed in the box below the Stop and Save Button. Finally all the measured values and their times during the test are written to a .csv file to allow for post-processing or alternative graphing of the data. If the Stop and Save button is selected, a note will also be appended to the .txt file indicating that the test was halted as well as the time that this occurred.

7.6 Conclusion

The full electronic and software system was described in this chapter. Figure 7.1 depicts the system block diagram. The analogue portion of the design was simulated with LtSpice, using real time data recorded on previous versions of the circuit design. The full circuit design was described and each component choice was detailed. The PCB component placement, routing and manufacture was briefly discussed and the final product shown. Finally the full GUI software system was detailed. The software was designed to fully record and detail each test and allow for real-time monitoring of the signal. An executable (.exe) was compiled to allow the software to be used on any Windows system.

Chapter 8

Mechanical Design

The final design processes needed to complete the biosensor system are the mechanical designs. First a test bath was designed to contain the transducer and sample solutions as well as provide an electronic connection to the sensing circuitry. Then a test mount was designed to mount the test bath and circuitry on a single platform. Finally, an immobilization bath was designed to be used during the preparation processes of the transducer.

8.1 Test Bath

The test bath design consists of two parts, the base and lid. Both the base and lid were machined from Acetal - Polyoxymethylene (POM), because it is commonly used in biomedical devices, has low moisture adsorption, good thermal and electrical stability, as well as very good chemical resistance. The test bath was designed with the help of Mr Viviers and Mr Croukamp (Chief Electronician E&E Department, Stellenbosch University). Mr Viviers provided the CAD (Computer Aided Design) sketches of the test bath to be machined. The lid and base are clasped together using a simple toggle latch and stainless steel guiding rods. The test bath was designed to reduce the use of costly materials as much as possible. The transducer size and test bath volume were designed as small as possible to reduce the use of the DNA hairpin probes, target DNA and CNFs. It was determined that the size limitations of the biosensor were defined by machining capabilities, as well as the size of the electronic connection method to the carbon fibers from the sensing circuitry.

8.1.1 Test Bath Lid

In order to connect the carbon nanofibers to the sensing circuitry, gold plated spring test probes were chosen. It was determined that a concave radius head provided more stability than a convex head. Figure 8.1 depicts the dimensions of the chosen spring test probes.

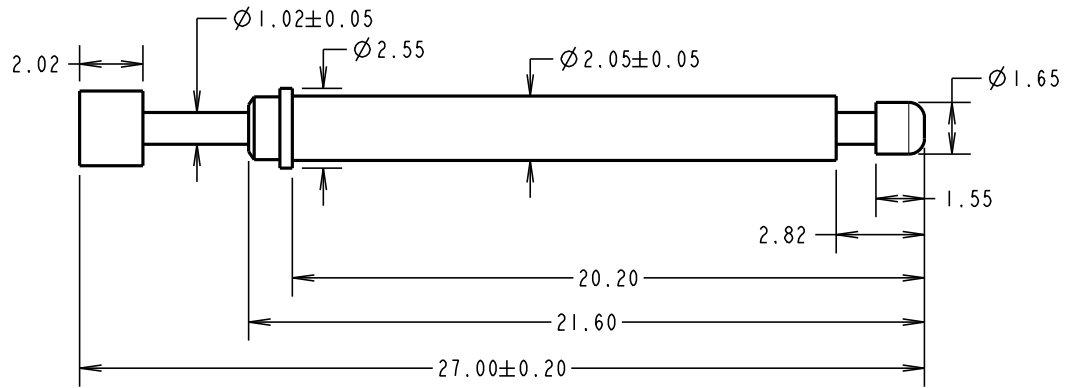
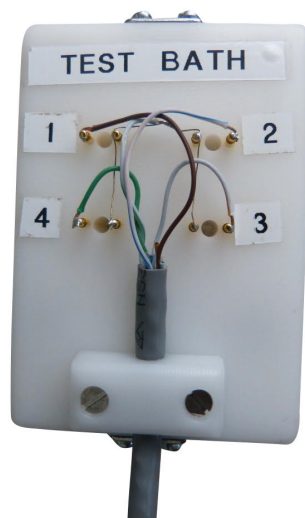


Figure 8.1: Spring test probe (Appendix B.9).

Two spring test probes are used to measure the resistance of a single carbon nanofiber. The lid of the test bath can be seen in Figure 8.2 and the dimensions and isometric view can be seen in Figure 8.3. The two spring test probes are spaced 7mm apart, with a single 3.5mm hole in between. The 3.5mm hole is the access point to apply sample solutions during testing. Four testing points are designed on a single test bath as explained in Section 7.3.4. The four test points are connected to the sensing circuitry via an Ethernet cable to a dip switch. A sealing channel is machined around the four test points to allow for the placement of a rubber seal. As can be seen in Figure 8.2, four guiding rods are placed in the guide rod holes, which allows for precise placement onto the test bath base.



(a) Test bath lid top.



(b) Test bath lid bottom.

Figure 8.2: Test bath lid.

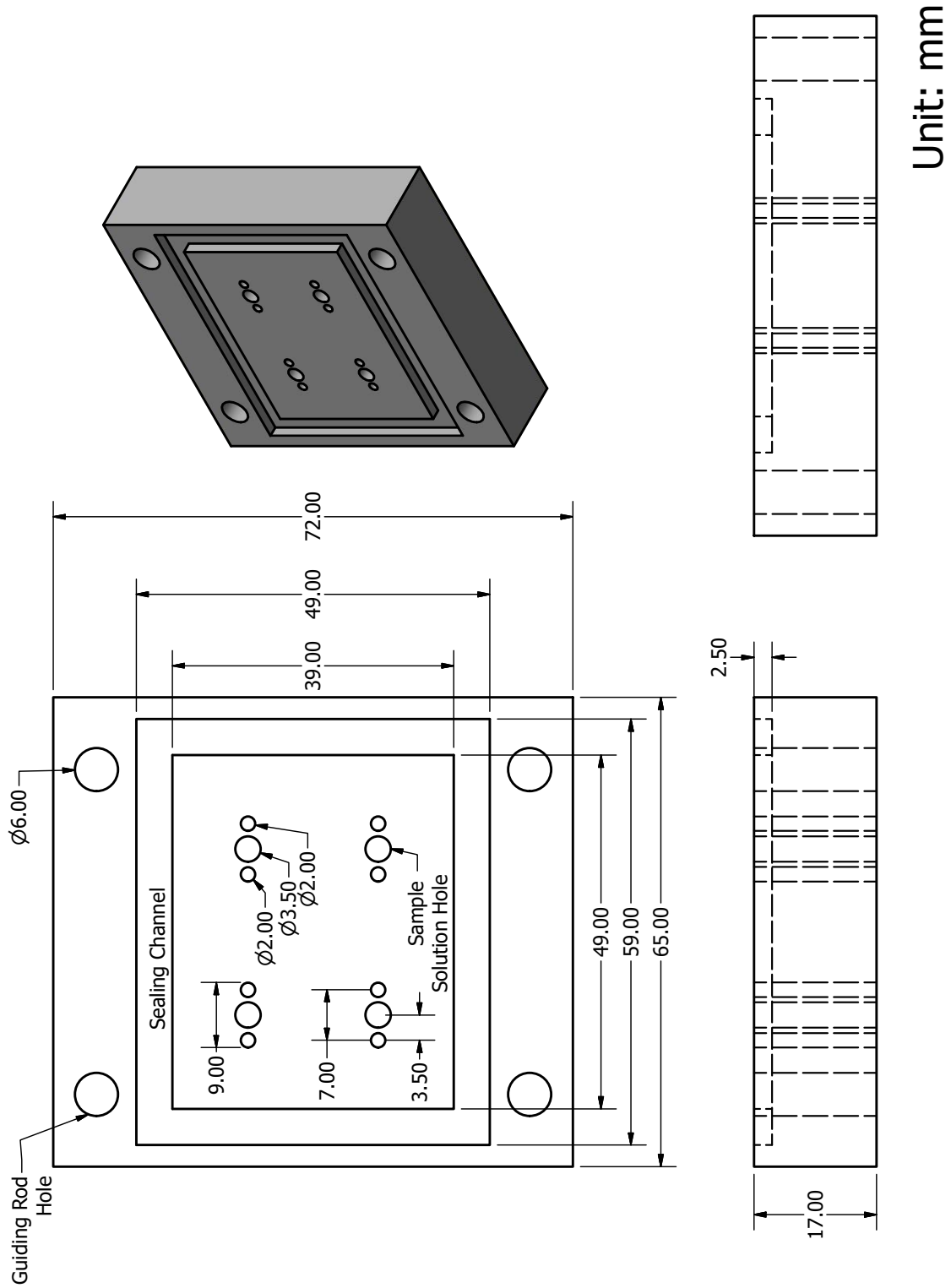
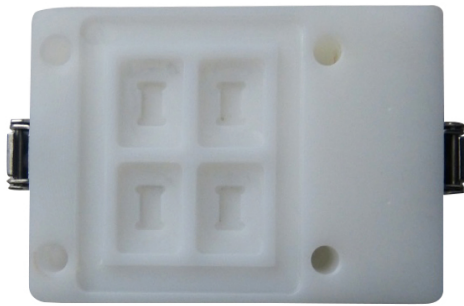


Figure 8.3: Test bath lid design.

8.1.2 Test Bath Base

The test bath base was designed to align with the four test points of the test bath lid. The transducer size must be greater than 9mm and therefore the chosen size to laser cut the carbon nanofibers was 10 mm x 5 mm. The test bath base is shown in Figure 8.4 and the dimensions and isometric view is seen in Figure 8.5. The test holes were designed with the same dimensions as the laser cut fibers and small half circle holes were placed at the corners to easily place and remove transducer samples with tweezers. The depth of the sample holes is 2 mm. It was found that the test baths are sufficiently filled with 120 μL and only 40 - 60 μL when a fiber has been placed in the test hole. A sealing channel and guide rod holes were machined as with the test bath lid.



(a) Test bath base, top view.



(b) Test bath base.

Figure 8.4: Test bath base, side view with clamp.

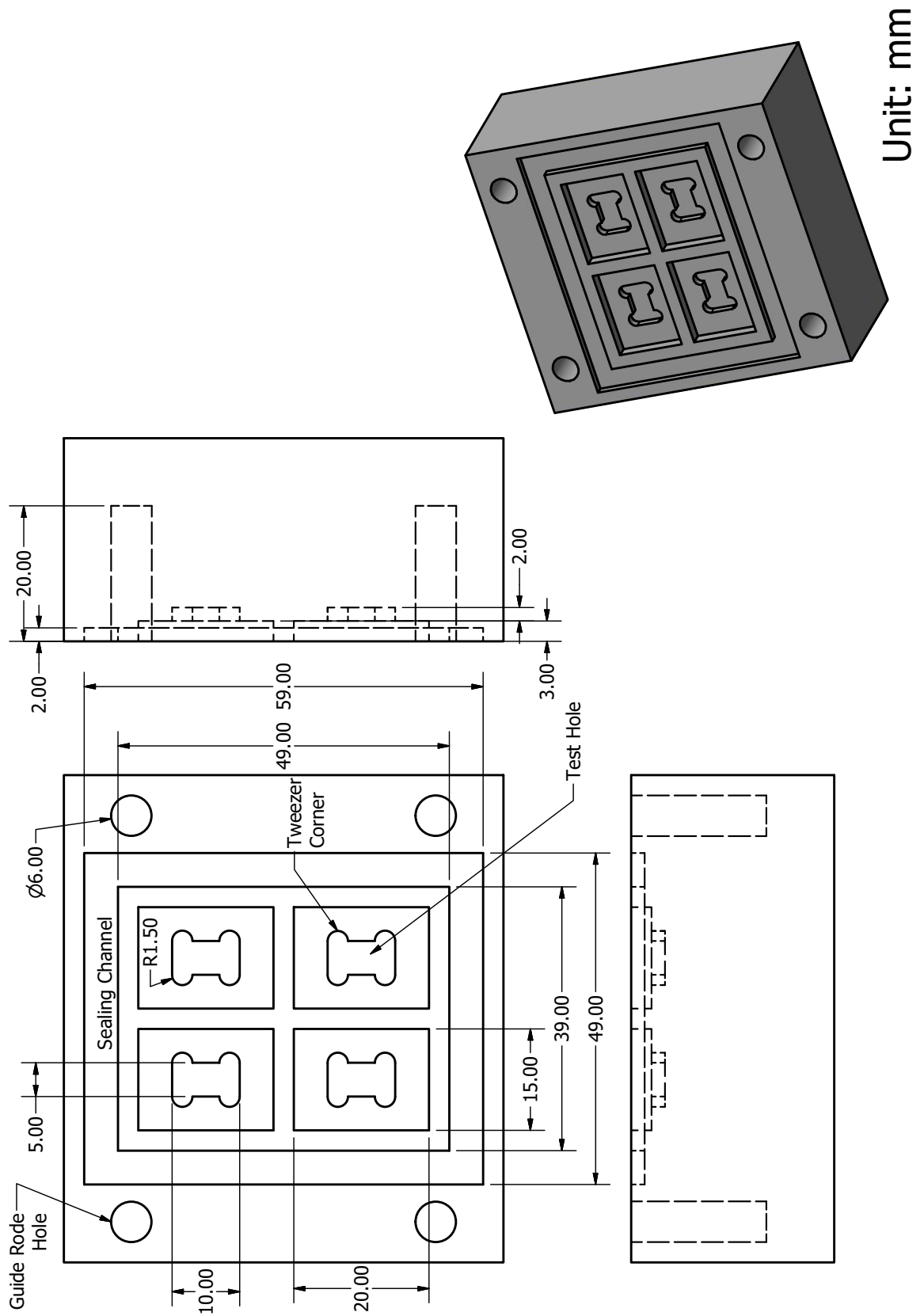


Figure 8.5: Test bath base design.

8.2 Biosensor Mount

A full system mount was designed and 3D printed with a PLA filament on a MakerBot Replicator Z18. Figure 8.6 depicts the mount with the circuitry and test bath in place. Figure 8.7 shows the dimensions and isometric view of the mount. The mount consists of a basic 4mm base and 4mm walls that hold the test bath and circuitry. Four mount boots were designed to align with the Arduino Leonardo mounting holes to attach the circuitry to the mount. Sufficient space was provided to allow ease of access to the Ethernet cable and toggle latch. The size of the full mount is 11cm x 22.5cm.

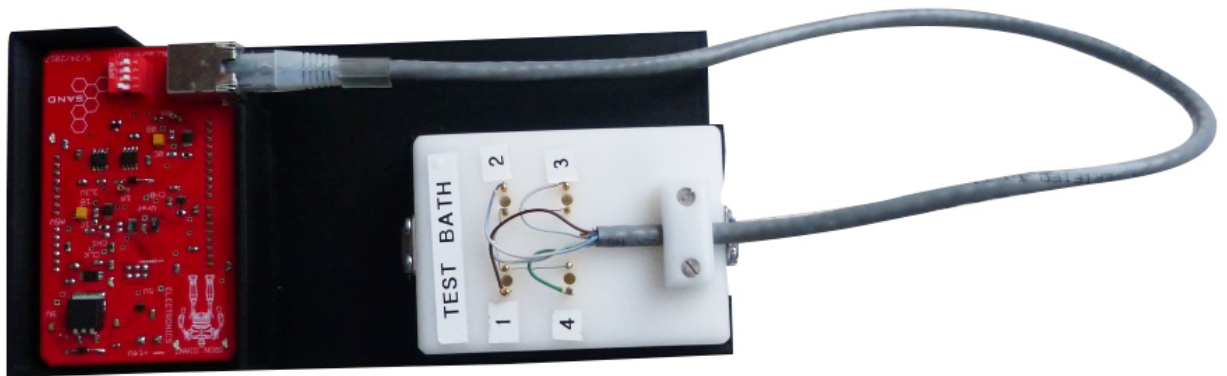


Figure 8.6: Full system on mount.

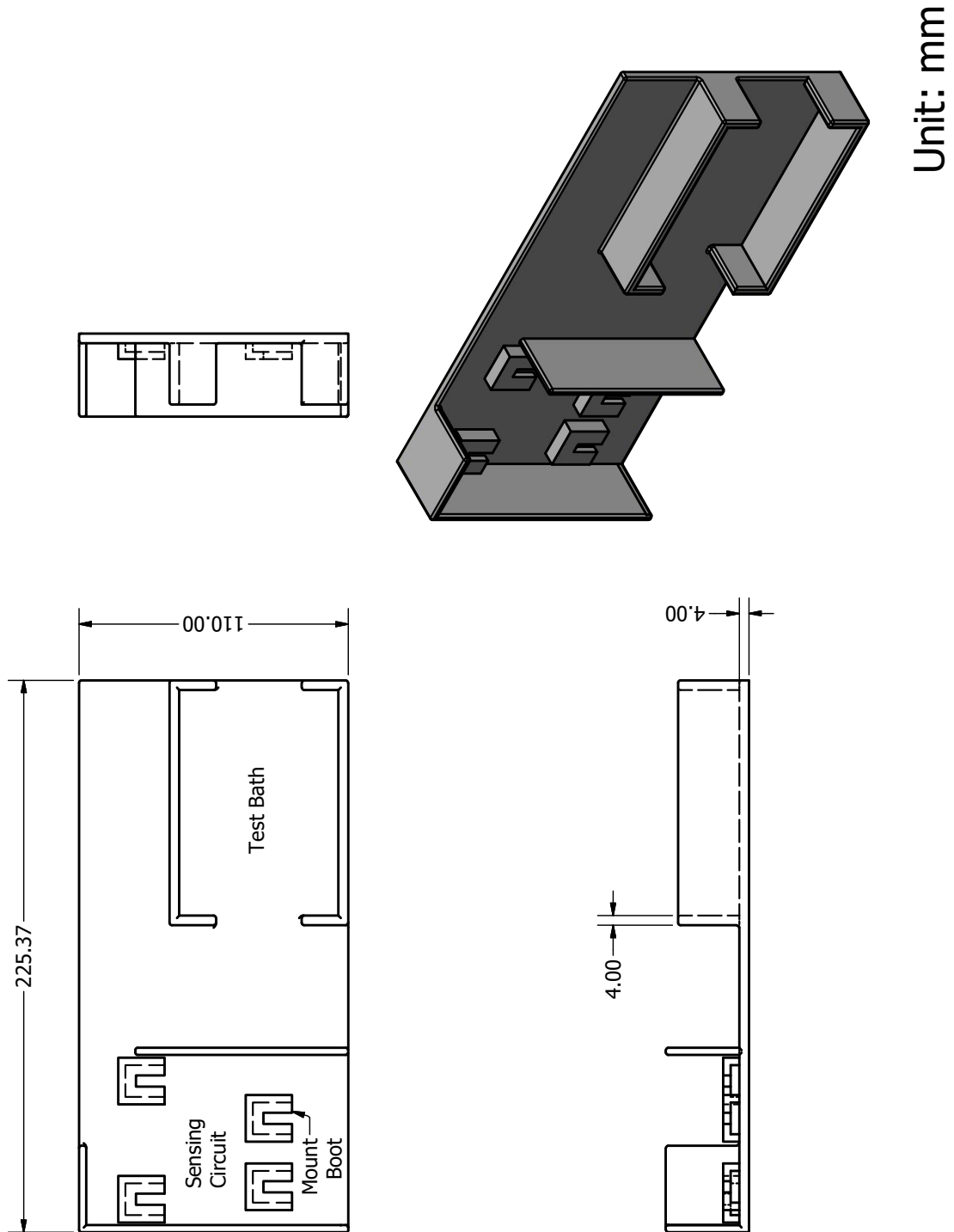
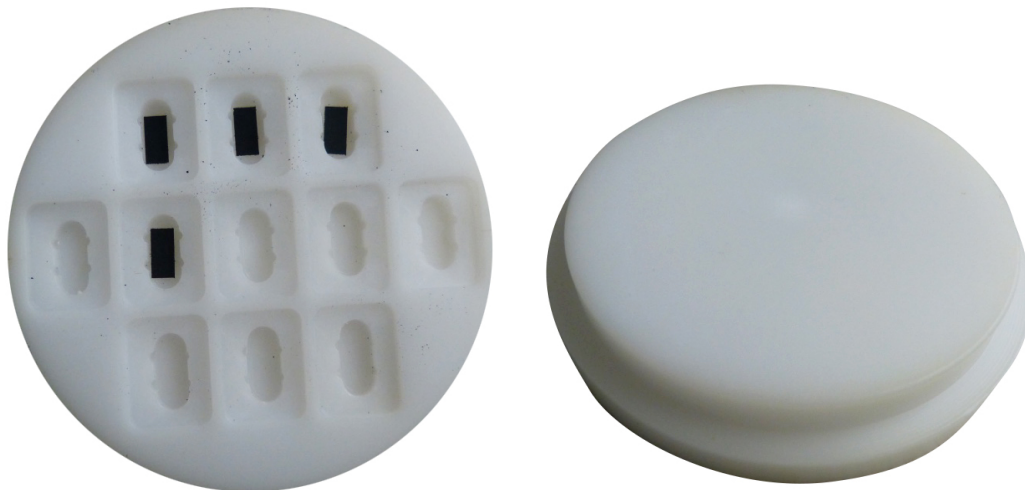


Figure 8.7: System mount CAD sketch.

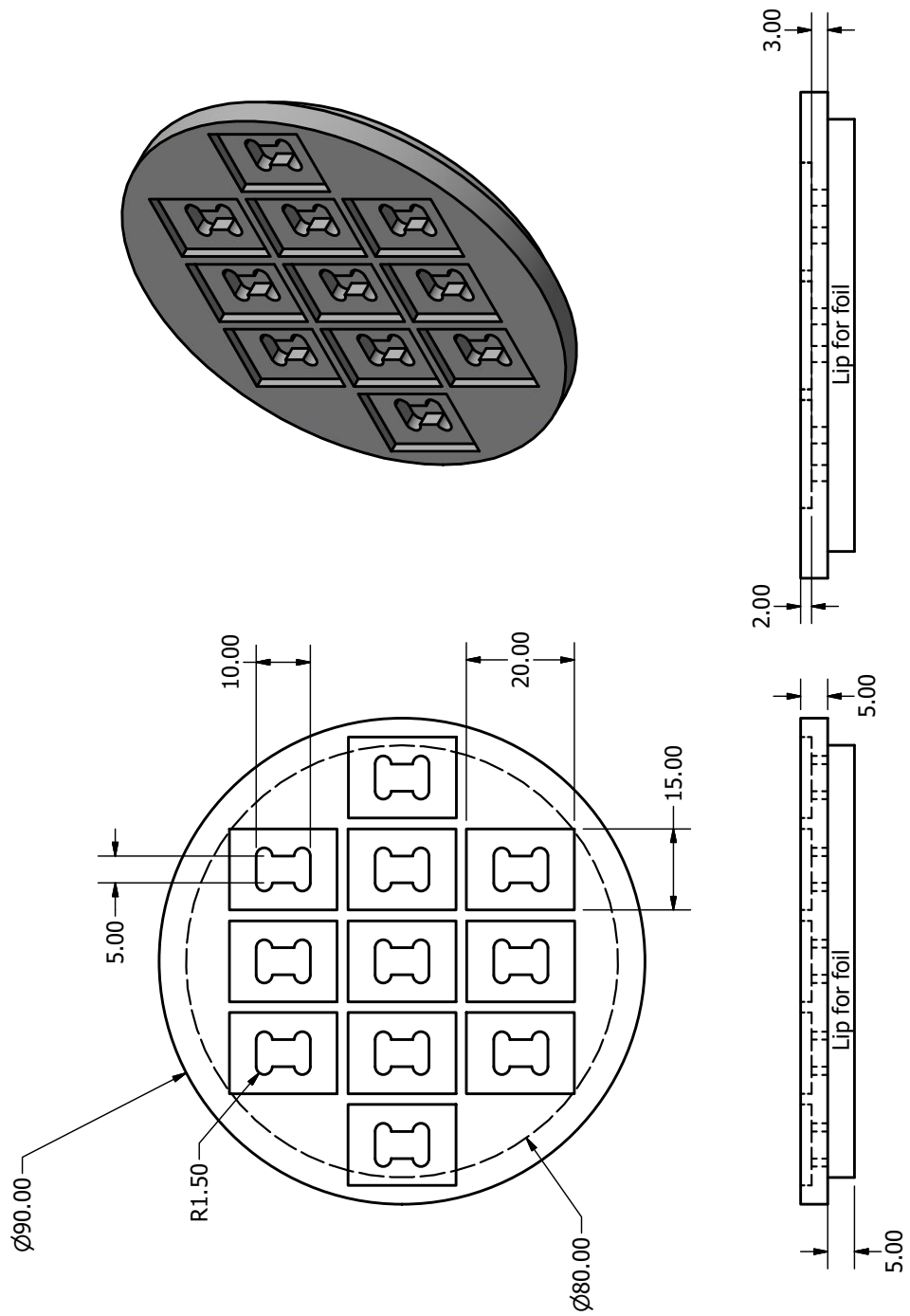
8.3 Immobilization Bath

Finally, immobilization process baths were designed. Initially, petri dishes were used, but it was determined that immobilization solution containing the DNA hairpin probe may not stay on the gold coated fibers, which may result in little to no DNA hairpin probe immobilization. Four immobilization baths were machined from Acetal. Figure 8.8 depicts the immobilization bath and Figure 8.9 shows the dimensions and isometric view. The immobilization baths were designed with the same test holes as the test bath to ensure that the immobilization solution stays in place. The immobilization baths were designed with the same circular dimensions of a petri dish to allow the setup to fit into an oxidation chamber. 11 test holes could be fitted on the petri dish sized surface. A small lip was added to the immobilization bath to allow for foil to be folded around the setup. The immobilization bath is used during the DNA hairpin probe immobilization to the carbon fibers, as well as the hybridization process of the FL probe tests.



(a) Immobilization bath top view with carbon fibers placed. (b) Immobilization bath bottom view.

Figure 8.8: Immobilization bath.



Unit: mm

Figure 8.9: Immobilization bath CAD sketch.

8.4 Conclusion

In this chapter, the physical designs of the biosensor are described. It is shown how the CNF samples are physically connected to the electronic circuitry and the test baths they reside in during testing. A full mounting bath was designed to hold the test bath and circuitry on a single platform. Finally, an immobilization bath was also designed to be used when immobilizing the hairpin probe DNA to the gold coated CNFs, as well as the hybridization incubation steps during the FL probe testing.

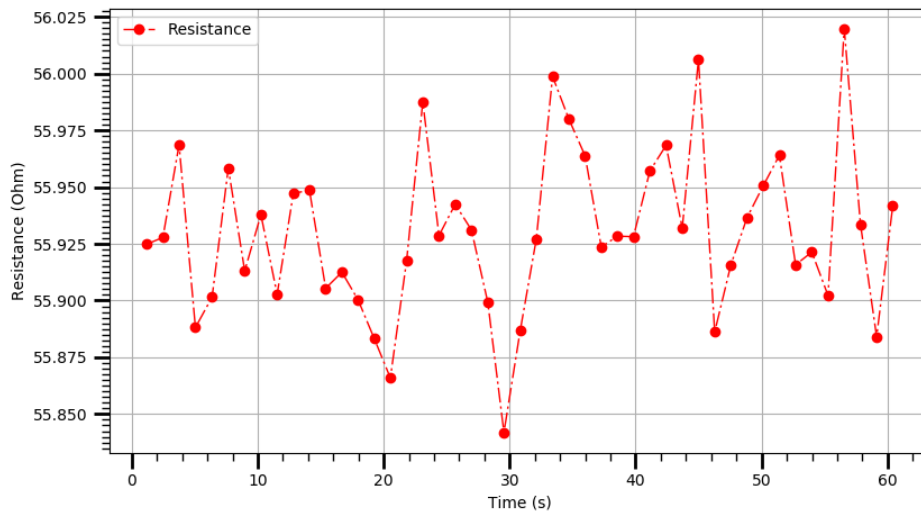
Chapter 9

System Validation and Testing

In Chapter 7 and Chapter 8 the electronic, software and mechanical designs of the biosensor were fully detailed. In this chapter, the full system will be validated and characterized to determine that the GUI software works without errors, to characterize the circuitry precision and accuracy and to characterize the system under different working conditions.

9.1 Software Testing and Validation

Software testing and validation is a continuous process. The software is tested after each significant change on both the Arduino and Python PC code. This section will briefly describe the final working results of the entire software package. The next section will detail the accuracy and precision of the results. To test that the software works in conjunction with the circuitry, a known resistor is used in place of a carbon nanofiber transducer. In this example a 56Ω resistor is used. Figure 9.1 shows the results of a 60 second test. Figure 9.1(a) shows that the resistance of a sample can be read in real time and even the smallest of changes is registered. Figure 9.1(b) shows that the details of the test detail form (Figure 7.16) are saved to a .txt file and the base resistance and maximum deviance values are appended to the .txt after the test is complete. A .csv was also created which can be used for post processing and graphing when necessary.



(a) Matplotlib graph saved as .png image.

```
RB2_55.txt - Notepad
File Edit Format View Help
Name of Tester: Nick
Date: 2017-06-07 18:14:00
Test Code: RB2_55
Test Time: 1 Minutes 0
Description:
Known Resistance Test_55 Ohm
No External Power
No External Clock for ADC
Csource switching
LEDs switching
Loop2 used- i.e averaging of 3 readings per datapoint
Base Resistance: 55.90
Max deviance :
0.18 Ohm
```

(b) .txt file created by Python software.

Figure 9.1: GUI output.

Auto scaling is used during the plotting of the data points on the matplotlib graph, which makes the changes in signal look much greater than their relative scale. It was thus decided that a dummy point be added to the matplotlib graph to negate this effect. The first dummy point is set to 90% of the base resistance that is read before plotting. An example of this is shown in Figure 9.2.

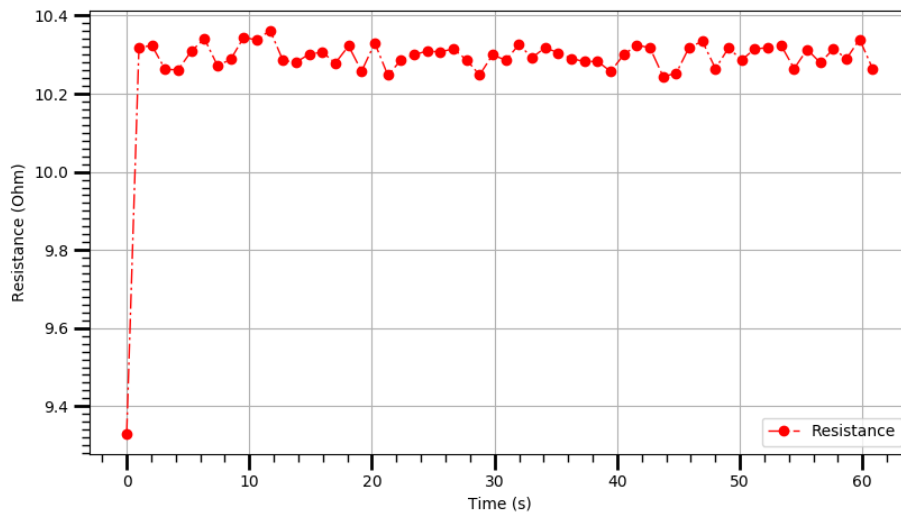


Figure 9.2: Dummy point added to reduce scaling effect.

9.2 Circuit Accuracy and Precision

The accuracy and precision of the biosensor was characterized in full by replacing the transducer with various known resistors (56 Ω , 100 Ω , 1 k Ω and 4.6 k Ω respectively). The deviance error was compared and improved by testing using software averaging. Finally, USB vs. external power was tested and compared. The first set of tests included testing of USB powered sensing with either no software averaging or software averaging of three values per data point. The same set of tests was then repeated using the same resistors, but an external power source was used instead of USB power to ensure stability of the circuitry.

9.2.1 USB Powered, Averaging Data vs. No Averaging

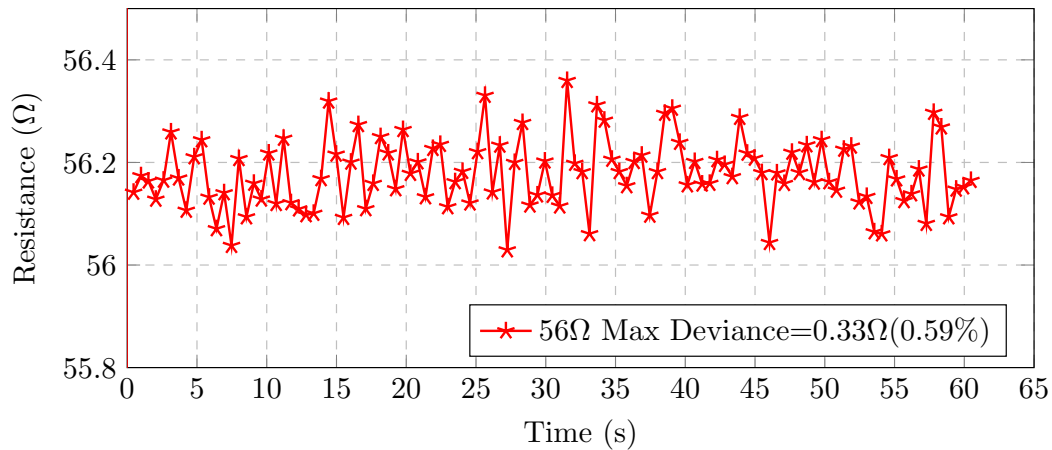


Figure 9.3: Typical 56 Ω resistance test. USB powered, no averaging.

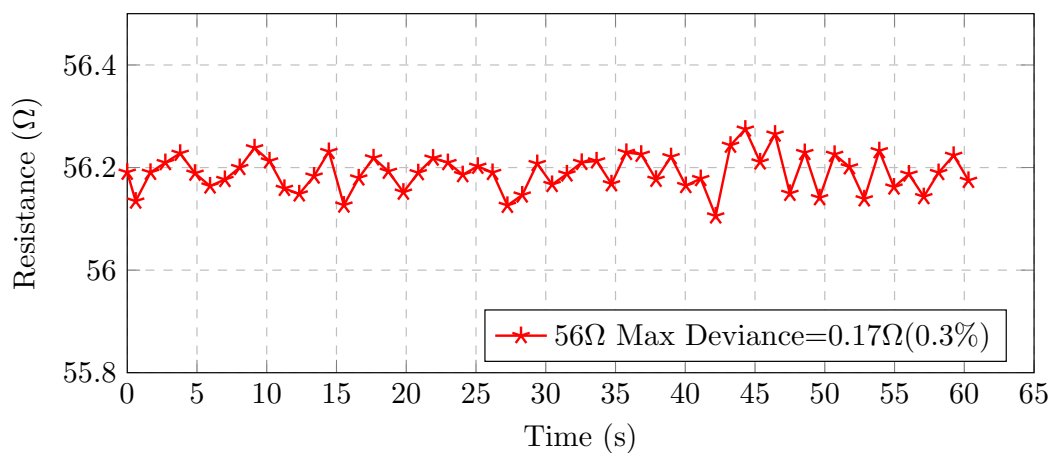


Figure 9.4: Typical 56 Ω resistance test. USB powered, with averaging.

Figure 9.3 shows a typical example of a single USB powered, 56 Ω resistance test with no averaging. The base resistance was measured at 56.23 Ω and the max deviance (maximum - minimum value) was 0.33 Ω which is only a 0.59% error deviance from the original base measurement. Figure 9.4 shows a similar example using averaging. It can be seen that there are fewer data points but the max deviance is also reduced.

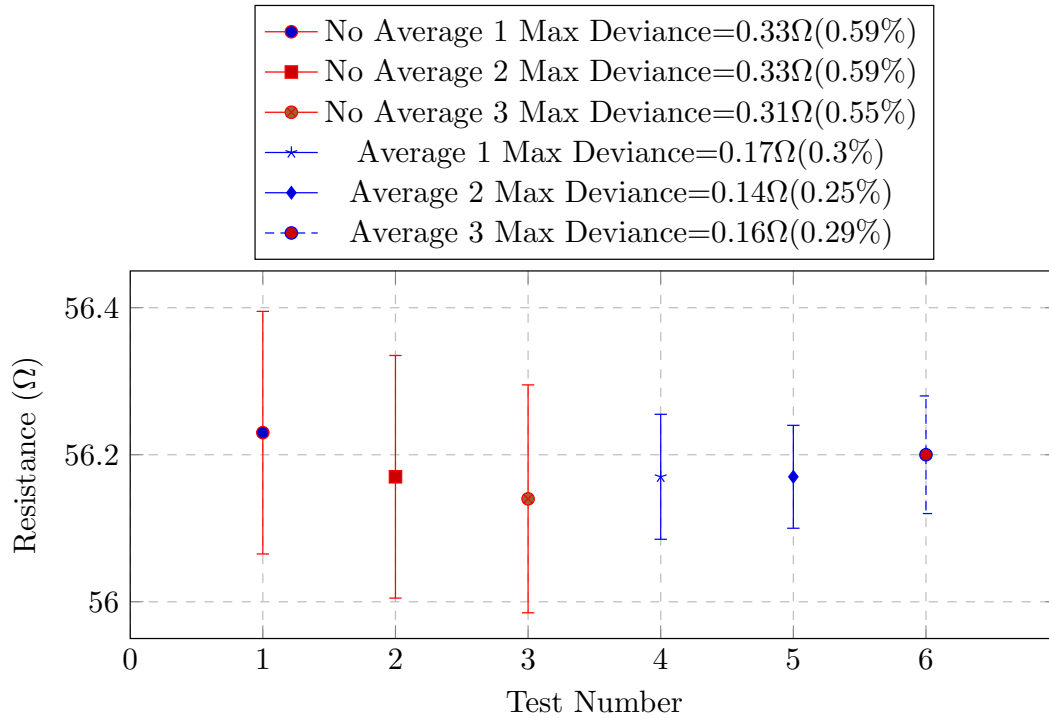


Figure 9.5: 56 Ω resistor, USB powered, max deviance comparison of software averaging (3 values) vs no averaging.

Figure 9.5 depicts the 56 Ω resistor, the USB powered test results that compare the base resistance values calculated, maximum deviance of error and how software averaging improves these measurements. It should be noted that only three values were used to generate a single averaged data point. Section 7.3.6.5 explained that each reading from the ADC takes approximately 160ms per channel, resulting in $3 * 2 * 0.160 = 0.96s$ in order to measure both channels three times. 3 averaged values results in approximately 1 data point per second. It can be seen that with software averaging the % error deviance is reduced to around 0.3% of the base value. Figure 9.6, Figure 9.7 and Figure 9.8 all show similar results for their respective resistor values. It was decided that a rolling average would not be used as this would delay the response of any resistance changes that might occur during biological testing.

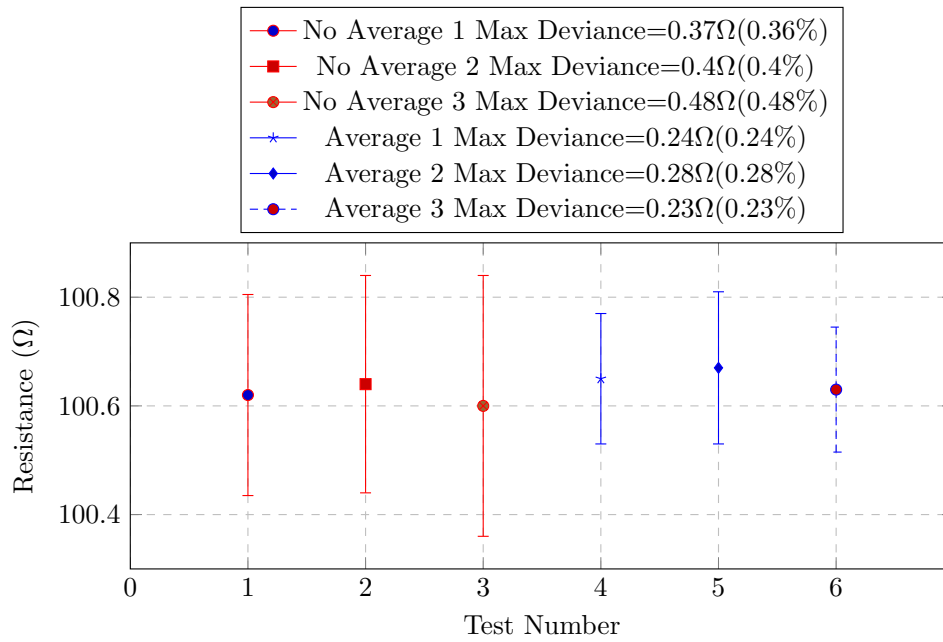


Figure 9.6: 100 Ω resistor, USB powered, max deviation comparison of software averaging (3 values) vs no averaging.

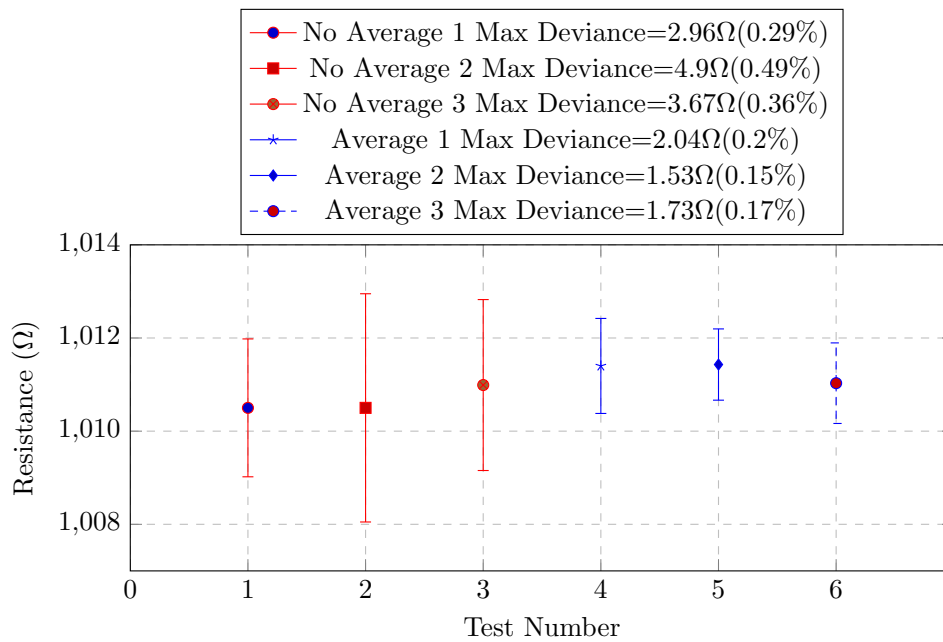


Figure 9.7: 1 k Ω resistor, USB powered, max deviation comparison of software averaging (3 values) vs no averaging.

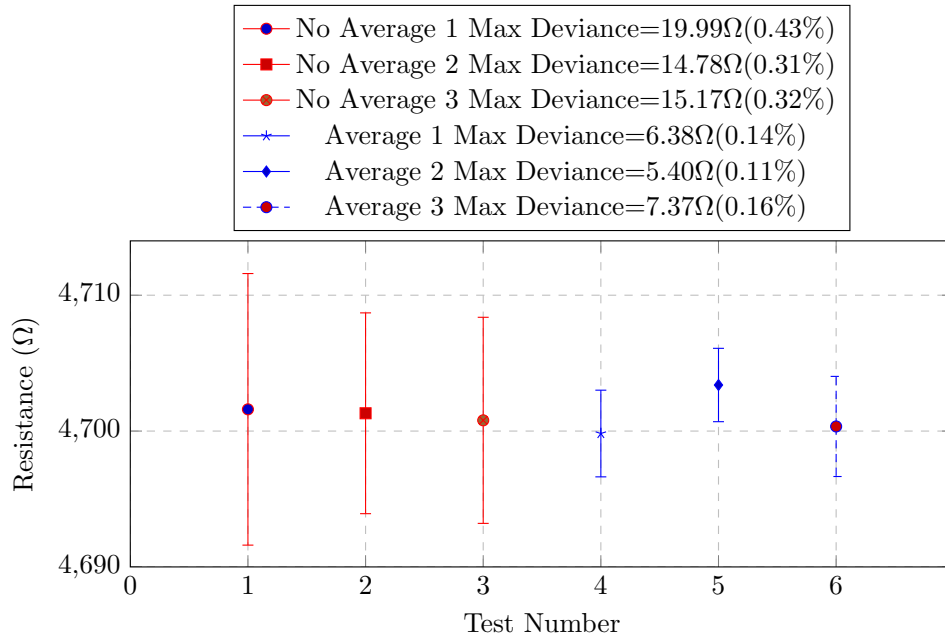


Figure 9.8: 4.6 k Ω resistor, USB powered, max deviance comparison of software averaging (3 values) vs no averaging.

It can be seen that with an increase in transducer resistance, the resistance deviance error also increases, but as a percentage of the original base value, it remains relatively small. This provides very relevant data when biological testing begins, because it can be seen that a change in resistance that is $<1\%$ of the base resistance, is most likely due to resistive noise and not the presence of complementary DNA.

9.2.2 External PSU Powered, Averaging Data vs. No Averaging

An external power supply was used to repeat the tests done in the previous section. Only the 56 Ω and 4.6 k Ω resistors test results are shown in Figure 9.9 and Figure 9.10. It can be seen that the external supply results are comparable to the USB supply results, although the error deviance is slightly higher. This is most likely due to an older PSU being used, which has poorer power regulation than a USB supply.

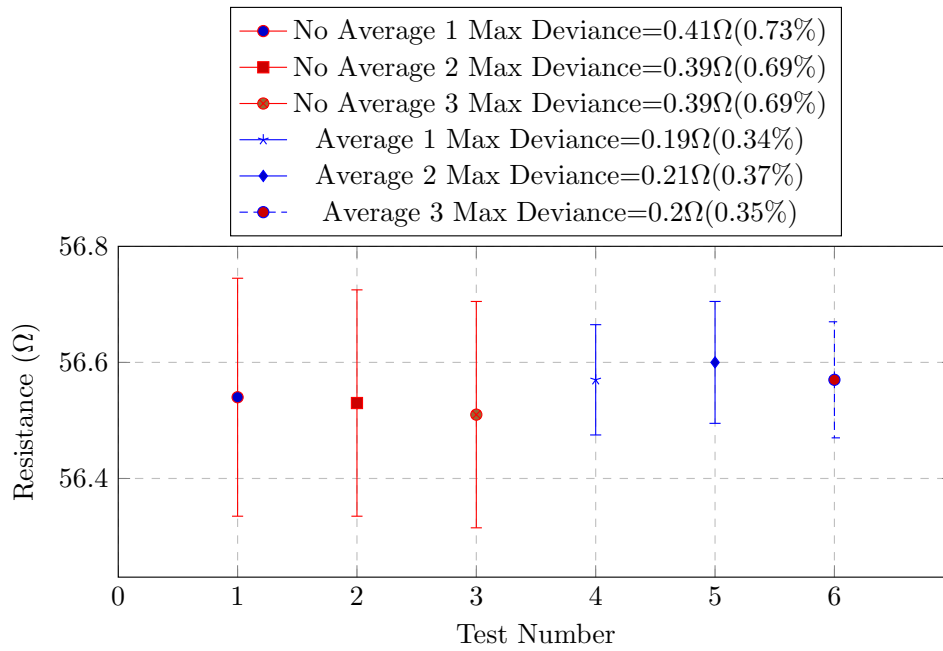


Figure 9.9: 100 Ω resistor, external PSU power, max deviance comparison of software averaging (3 values) vs no averaging.

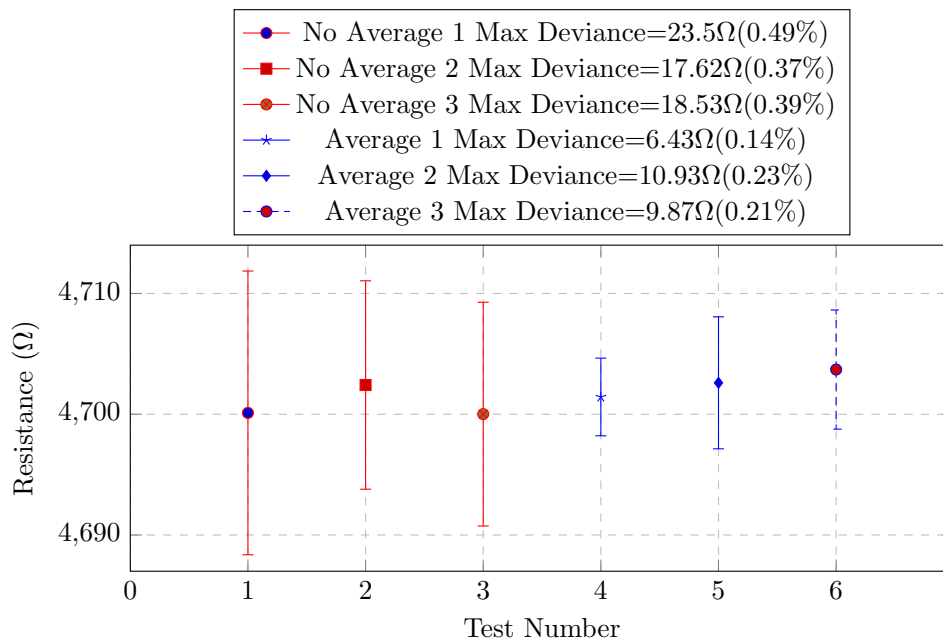


Figure 9.10: 1 k Ω resistor, external PSU power, max deviance comparison of software averaging (3 values) vs no averaging.

9.3 Carbon Nanofiber Resistance

Once the sensing circuitry's precision and accuracy were within acceptable limits, the resistance of the carbon nanofibers is characterized. Three tests of 30 minutes and three tests of 60 minutes were conducted on individual carbon nanofiber samples using software averaging to reduce the maximum deviance.

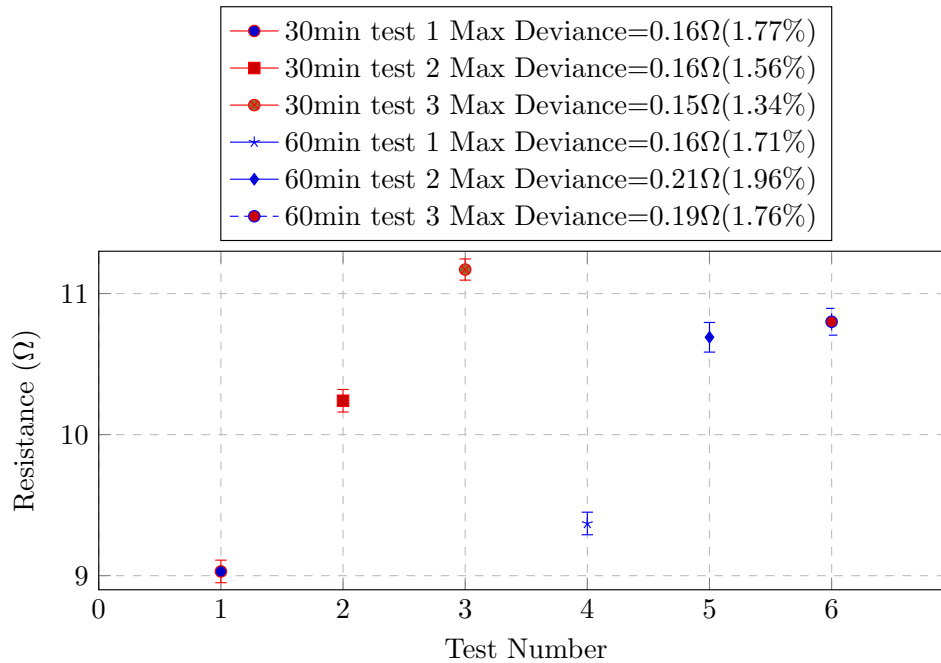


Figure 9.11: Carbon fiber resistance tests (averaging used).

It can be seen in Figure 9.11 that the initial base resistance of a carbon fiber sample ranges between 9 Ω and 12 Ω and that the maximum deviance is no larger than 2% of the initial base resistance.

9.4 Gold Coating Effect on Resistance

The next set of tests was to determine if the sputter coating of gold onto the carbon nanofibers would affect the initial base resistance of the fibers. Two 60 minute tests were conducted per gold deposit thickness.

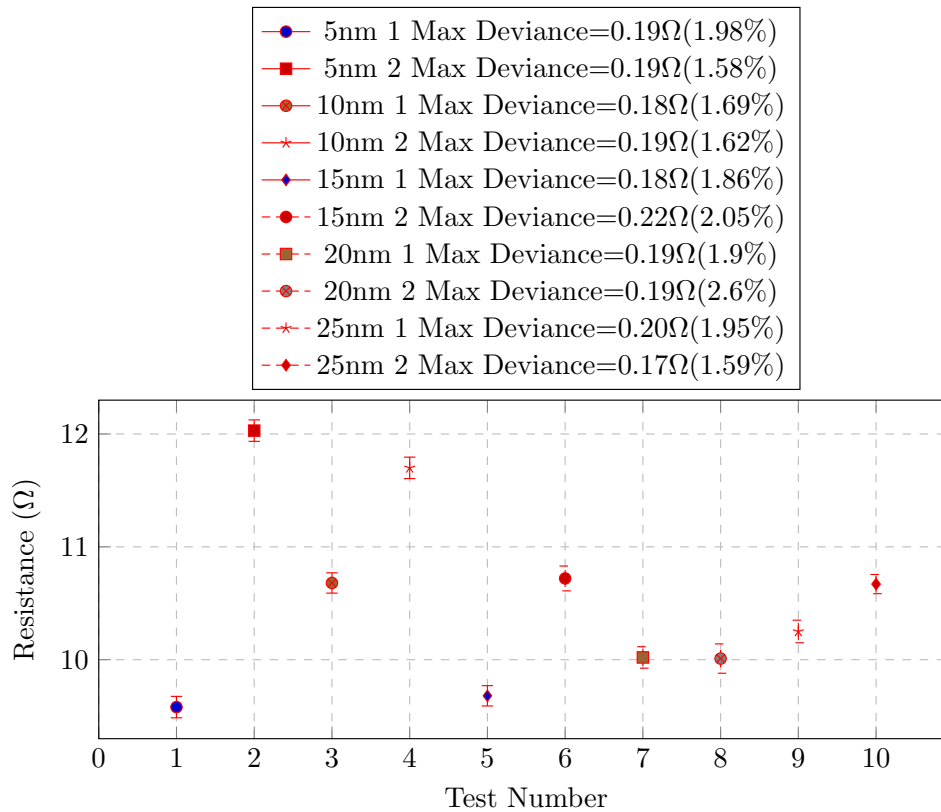
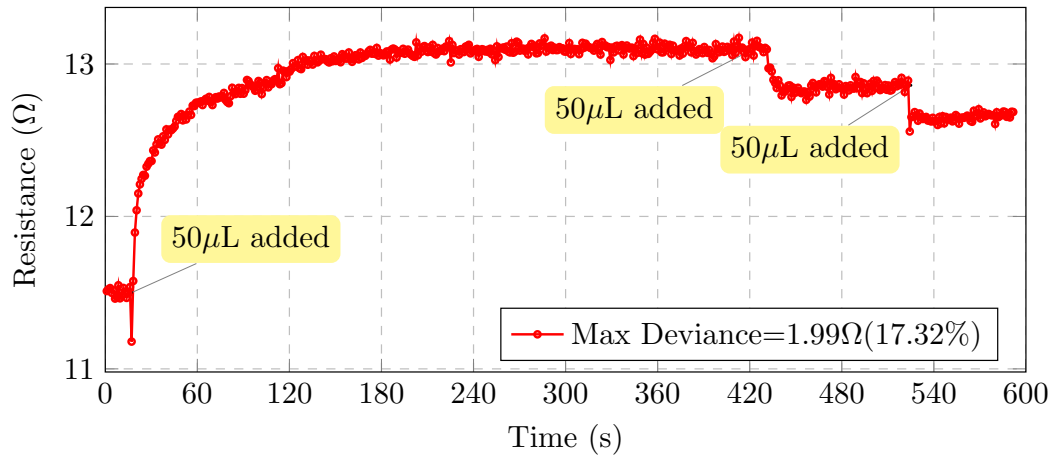


Figure 9.12: Gold coated carbon fiber resistance tests (averaging used). Gold deposit thicknesses of 5, 10, 15, 20 and 25nm.

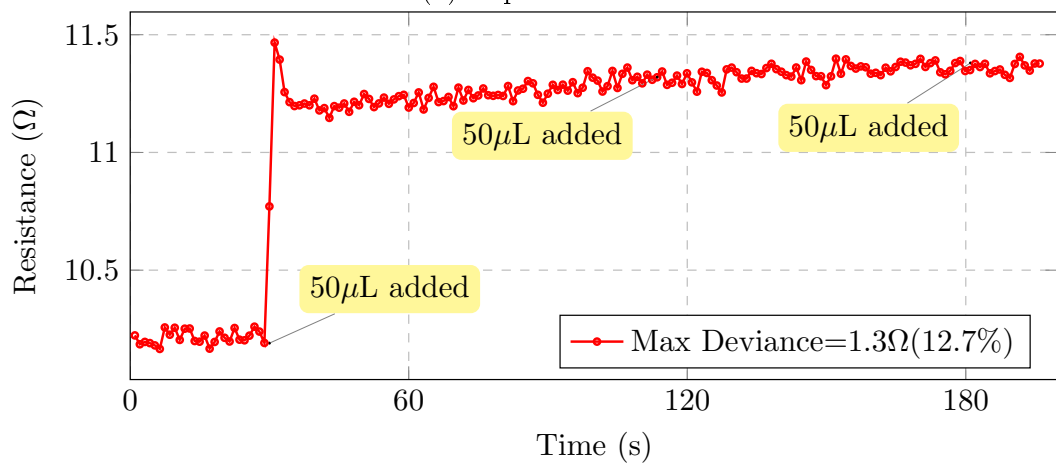
Figure 9.12 shows that the gold coating does not have any noticeable effect on the resistance of the carbon nanofiber and that the maximum deviance may be greater than 2%.

9.4.1 Addition of Liquid to Fibers

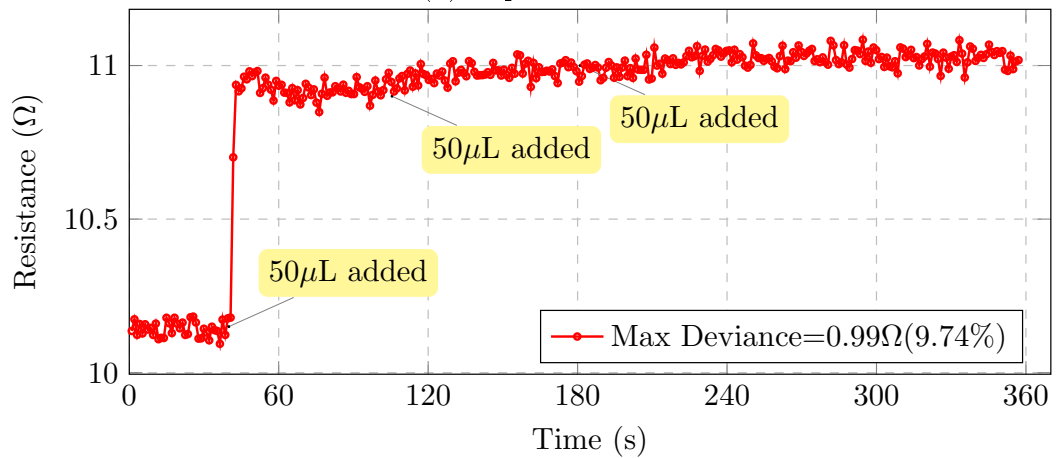
During final testing, the target DNA will be added in a TE buffer solution. A number of tests were conducted in order to negate any resistance changes due to the TE buffer. First 50 μL of TE buffer was pipetted onto dry fibers in stages. Figure 9.13 shows that when TE buffer is added to dry fibers, there is an initial spike in measured resistance. It can also be seen that the response is varied and dependent on how the liquid is adsorbed by the CNFs. Figure 9.13(b) and Figure 9.13(c) show, however, that the resistance can reach an equilibrium once the CNFs are completely wet. The maximum deviance of the measured resistance reached as high as 17%.



(a) Experiment 1



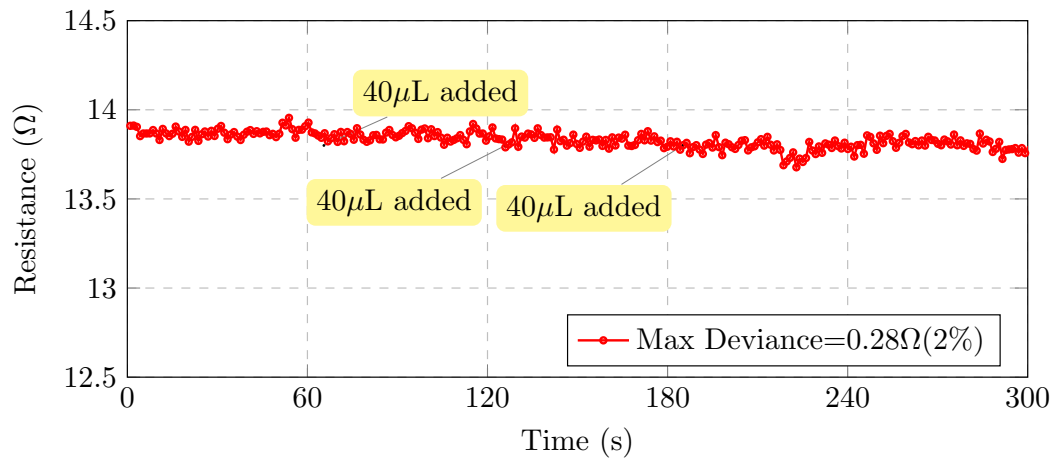
(b) Experiment 2



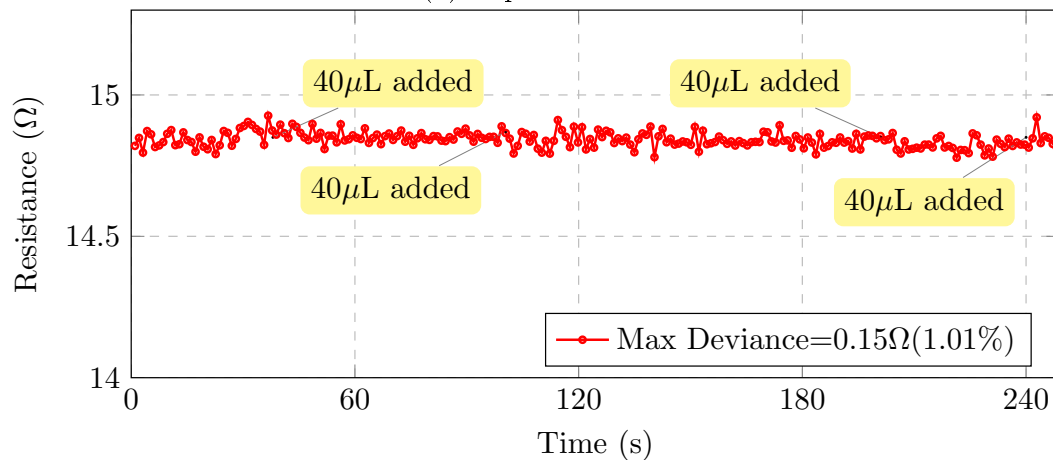
(c) Experiment 3

Figure 9.13: Dry fibers, results when 50 μ L TE buffer added to the fibers at different stages.

In an attempt to reduce the changes to base resistance, it was decided that the fibers should first be wet by TE buffer before measurements began. Tests were conducted by dipping the carbon fibers in TE buffer before placing them in the test baths for measurements. The figures in Figure 9.14 show that wetting fibers before measurements prevents any additional changes when adding 40 μL of TE buffer during testing. The maximum deviance is comparable to the initial results of resistance tests and was thus it is not caused by the TE solution.

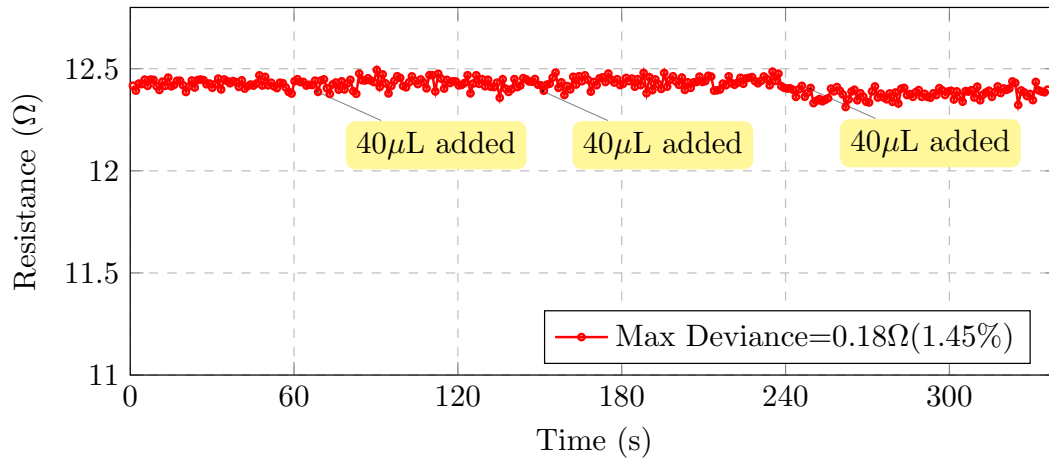


(a) Experiment 1



(b) Experiment 2

Figure 9.14: Previously wet fibers, results when 40 μL TE buffer added to the fibers at different stages.



(c) Experiment 3

Figure 9.14: Previously wet fibers, results when 40 μL TE buffer added to the fibers at different stages.

9.4.2 Temperature Testing

The final set of validation tests of the system was in a higher temperature environment. Due to the fact that the target hybridization incubation period may need to be in a higher temperature environment, the circuitry was tested in a 37°C controlled room. The tests included resistance tests of both dry and wet carbon fibers for 15 minutes each. Figure 9.15 shows the results of the 37°C tests. It can be seen that the maximum deviance is still comparable to previous tests, with the results no larger than 5% of the initial base resistance.

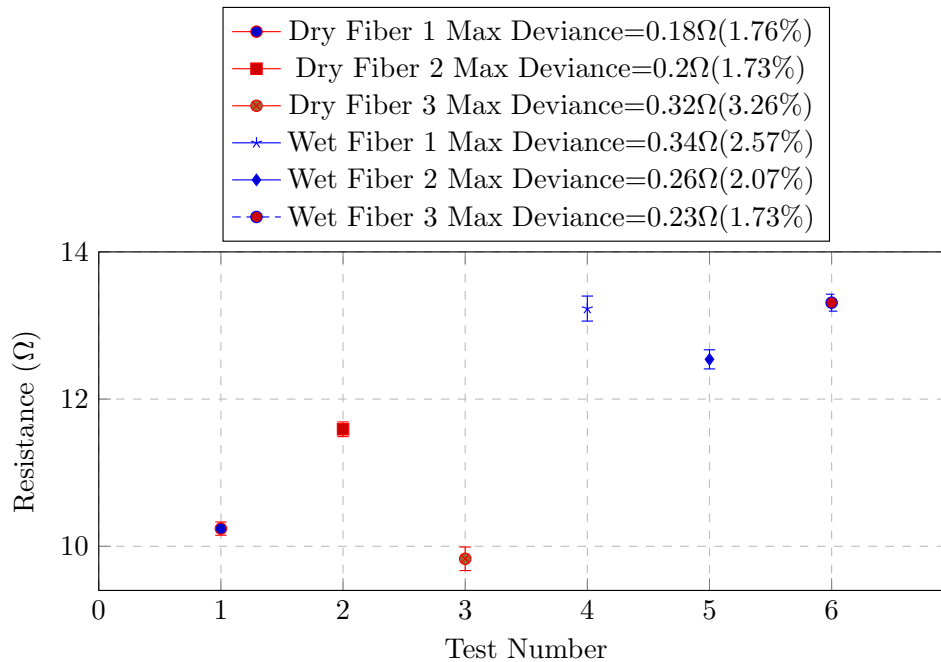


Figure 9.15: Results of temperature tests in 37°C environment. Both dry and wet fibers were tested.

9.5 Conclusion

In this chapter, the full software and hardware design was validated and tested. The GUI and PC readings were fully tested and confirmed to be working in a stable and reliable manner. Software averaging was compared to single readings and it was determined that the precision was improved. It was also shown that external and USB power sources both work and that USB power is sufficient for future testing with the current PC used. It can be seen that as a traditional ohmmeter, the system provides, errors of $< 1\%$, and that the accuracy is within normal limits. The CNFs resistances were also fully characterized, both dry and wet, and with gold coatings. Finally, the system was tested in a heated environment. It can be seen, that at most, the error deviance of the system is $< 5\%$. This means that during biological tests, if a change greater than 5% is measured, it can be determined to be due to hybridization of the target DNA to the hairpin probe DNA. Skotadis *et.al.* [47] report a resistive change of up to 51% of the base resistance and so it is hoped that the current sensor design will yield similar results.

Chapter 10

Hairpin Probe Validation

In order to validate that the hairpin probes operated as expected, it was necessary to use fluorescent techniques to visually confirm that the hairpin probes reacted as theoretically expected. Hairpin validation is conducted by varying the temperature and validating that the fluorescent probe reacts appropriately both with and without target DNA.

During the initial confocal microscopy experimentation of the FL probe, immobilized on the CNF samples, results were very unstable and unexpected. The first experiment went as theoretically expected, but all following tests yielded an undesired response. Appendix C details the failed experiments and discusses what went wrong and what was done to resolve the issues. During the investigation into the failed experiments, it was decided that the FL probes should be tested in solution before immobilization onto the CNFs, to ensure the operation of the probes without external factors that may be the cause of contamination and degradation.

In Section 2.2.1.1, the basic PCR amplification method is described. Another commonly used PCR method is real-time polymerase chain reaction (Real-Time PCR), or quantitative polymerase chain reaction (qPCR). qPCR monitors the amplification of targeted DNA molecules during the PCR in real-time. Two methods are used to detect the amplification of PCR products. The first, is the use of non-specific fluorescent dyes that intercalate with any dsDNA (double stranded DNA) and the second, is sequence-specific DNA probes consisting of oligonucleotides that are labelled with a fluorescent marker which permits detection only after hybridization of the probe with its complementary sequence. The FL probe described in Section 6.2 is a perfect example of the second method.

Using a qPCR measurement device, it is possible to detect the fluorescent signal of DNA without actually amplifying the product. qPCR measurements typically require low sample volumes (10-30 μL), which save on costly reagents. PCR reactions require thermal cycling as described in Section 2.2.1.1. Most

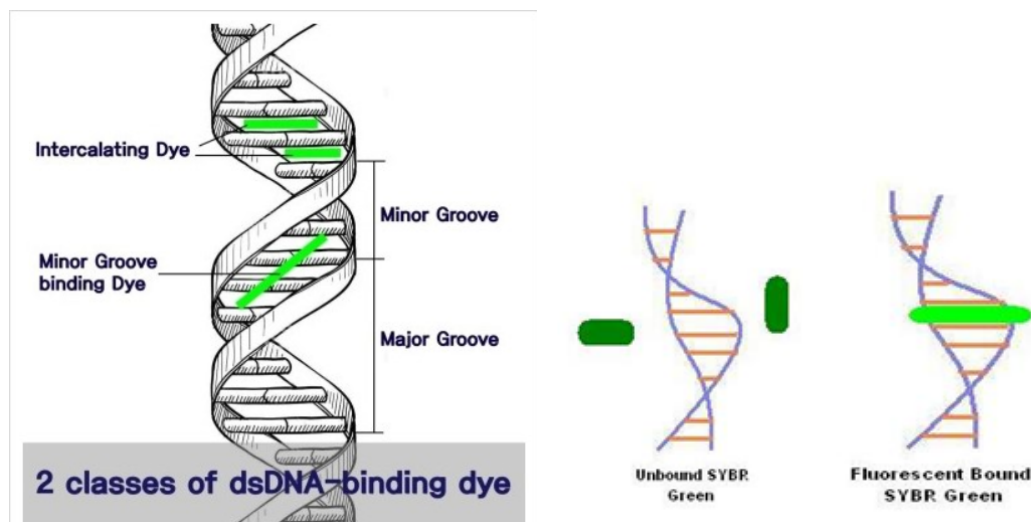
qPCR devices allow for custom thermal cycling profiles to be programmed at any user defined temperatures and for as long as required.

The operation of the FL probes, as described in Section 6.2, can be detected directly by qPCR fluorescent measurements. The operation of the FE probes as described in Section 6.3, however, cannot be measured directly. It was necessary to use non-specific fluorescent dye, in order to visually quantify the operation of the FE probes.

10.1 SYBR Green

"SYBR Green is a dsDNA binding dye, which can be used to quantify amplicon amount during the course of the PCR, by tracking overall fluorescence emission. The dye binds into the minor groove of dsDNA, and does not bind to ssDNA. When bound, it increases its fluorescence by up to 100 fold. During PCR, as the target sequence is amplified, SYBR Green I binds to each new copy of dsDNA during the extension step." [72].

Figure 10.1 depicts how the SYBR Green dye binds to dsDNA. SYBR Green is not a typical intercalating dye, in that it also binds in the minor grooves of dsDNA. It can be seen that when unbound, SYBR Green gives a low fluorescent signal but upon binding to dsDNA, the fluorescence increases 100 fold as mentioned.



(a) The two classes of dsDNA binding dye [73].

(b) Operation of SYBR Green with dsDNA [74].

Figure 10.1: SYBR Green.

10.2 qPCR Measurements

The Virology Department of Stellenbosch uses the Bio-Rad "CFX Connect Real-Time PCR Detection System", for all qPCR procedures. In order to conduct fluorescent measurements, the system needed to be programmed to detect the exact fluorophore that is to be detected (i.e the fluorophores' excitation and emission spectra).

To validate the operation of both the FL and FE probes, it was necessary to detect the Cy3 label (fluorescent marker) as well as SYBR Green, which was added to all experiments. The Bio-Rad CFX is not calibrated by default to detect Cy3. Therefore, it was decided to choose to detect another fluorescent dye that had similar excitation and emission spectra that the system was calibrated for. Using the Chroma Spectra Viewer from chroma.com [75], it was decided that Cal Orange and Cy3 had similar enough excitation and emission spectra to detect Cy3 by using a Cal Orange filter. Cy3 has peak excitation at a wavelength of 553nm, while Cal Orange has a peak at 539nm. Cy3 has a peak emission wavelength at 569nm, while Cal Orange has a peak at 559nm.

10.2.1 qPCR Experiment Setup

Figure 10.2 shows the thermal cycling that was programmed for the qPCR experiments. First the samples are rapidly heated to 95°C for three minutes, during which time, no measurements are taken. This first step completely *melts* or denatures all dsDNA and then cools to allow them to form their most optimal primary structures as well as allow the SYBR Green to bind during hybridization into dsDNA. The second step, called the "melt curve", gradually increases the temperature from 13°C to 93°C in 2°C increments and waits at each temperature for 5s. The melt curve is used to monitor the fluorescence at specific temperatures to show at which temperature the dsDNA begins to melt to ssDNA. The final step is an inverted melt curve or cool curve. This step gradually decreases the temperature from 93°C back to 13°C in 2°C decrements and again waits 5s per decrement. The cool curve is used to monitor the fluorescence at specific temperatures where ssDNA begins to hybridize and forms dsDNA again. This step is used to validate the stability of the samples to ensure they reform into their primary structures. The following sections will discuss the results of the experiments. All experiments were conducted simultaneously in triplicate (three separate sample solutions prepared in the same way). SYBR Green was added to all experiments in order to compare the FL probe operation to the FE probe. The FL and FE probes were tested in 1 μ M concentrations while the target DNA was tested with 3 μ M concentrations, to ensure saturation of target to hairpin probe hybridization. The full qPCR experiment protocol is described in Appendix D.9.

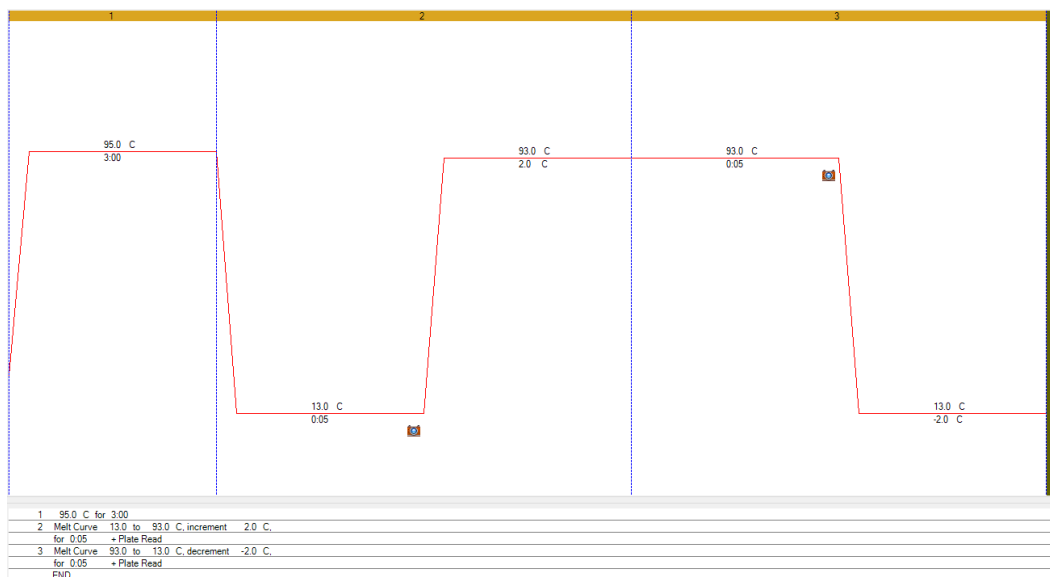
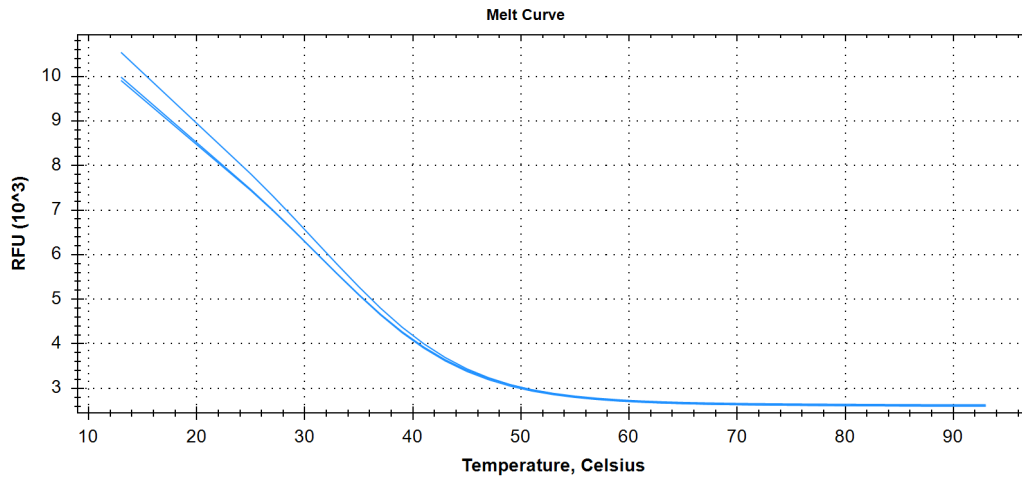


Figure 10.2: Melt Curve Setup

10.2.2 Target DNA qPCR Measurements

SYBR Green measurements of the target DNA are analyzed first to visualize the melt temperatures of the self-dimers. The target DNA, in its primary structure is ssDNA, so it is expected that the initial fluorescent signal should have a relatively low signal, but as temperature increases, the fluorescence should decrease even further as the secondary structures break down and there should no longer be any dsDNA. Figure 10.3(a) shows exactly the expected results where as temperature increases the fluorescent signal begins to decrease as the target secondary structure begins to melt. Figure 10.3(b) shows that the secondary structure has a T_m of 30°C. The cool curve yielded very similar results.



(a) Relative Fluorescent Unit (RFU) measurements vs. temperature

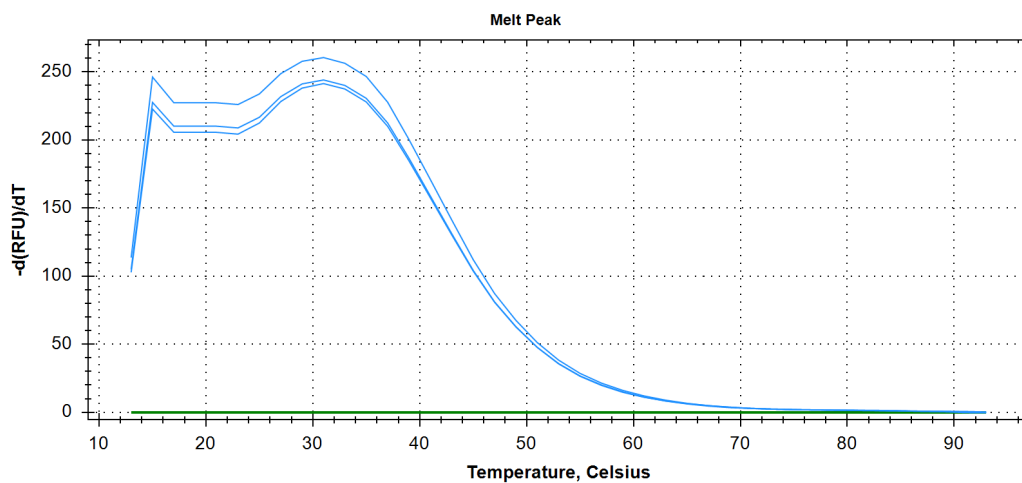
(b) Derivative curve $-d(\text{RFU})/dT$

Figure 10.3: Melt curve 13°C to 93°C of target DNA (3 μM), SYBR Green measurements.

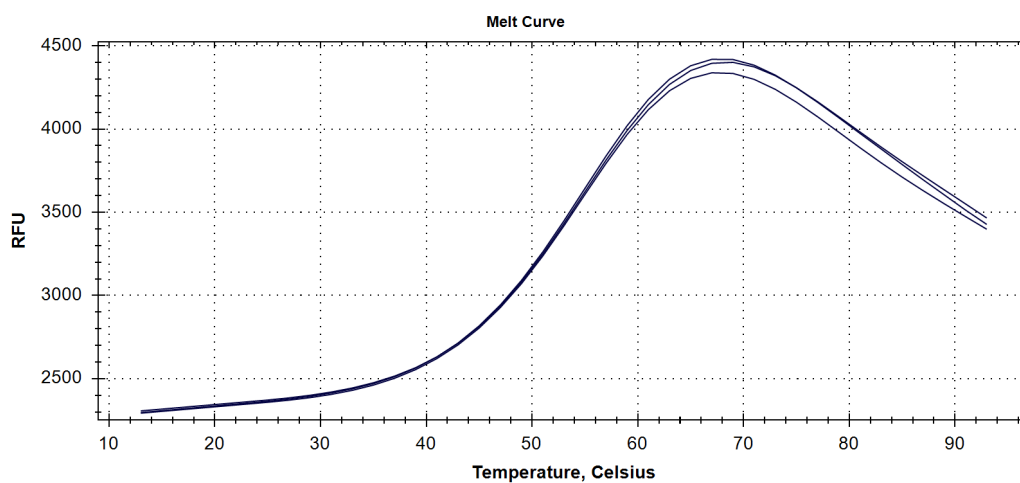
10.2.3 Fluorescent Hairpin DNA qPCR Measurements

10.2.3.1 Fluorescent Hairpin Probe Measurements Alone

Cal Orange measurements of the FL probes alone (i.e no target DNA added) are analyzed. It is expected that as measurements begin, the fluorescent signal should be relatively low because the hairpin structure should be closed and so the signal should be fully quenched by the quencher. As temperature increases, the fluorescent signal should begin to increase as the hairpins begin to open until the signal is saturated. A negative derivative curve ($-d(\text{RFU})/dT$) is also generated to show the peak temperatures at which the fluorescent signals begin to change. A negative peak on a $-d(\text{RFU})/dT$ curve, indicates an

increasing gradient in fluorescence and a positive peak, a decreasing gradient in fluorescence.

Figure 10.4(a) shows that as temperature increases, the fluorescent signal also increases and reaches a maximum fluorescence at around 65°C, indicating that all the hairpins are open at this temperature. Figure 10.4(b) shows a maximum change of increasing fluorescence (negative peak) at 53°C. Section 6.2.3 show that the estimated melting temperature was 51.3°C, which is fairly accurate. It can be seen that, above 65°C the signal begins to decrease. Upon further investigation, it was found that the Cy3's quantum yield (Fluorescence quantum yield is a measure of the efficiency with which a fluorophore is able to convert absorbed light to emitted light) shows a decrease of almost 70% of its quantum yield at 65°C, when compared to room temperature [76, p. 13][77]. The cool curve of the FL probe had almost identical results, implying that the primary structure is very stable.



(a) Relative Fluorescent Unit (RFU) measurements vs. temperature

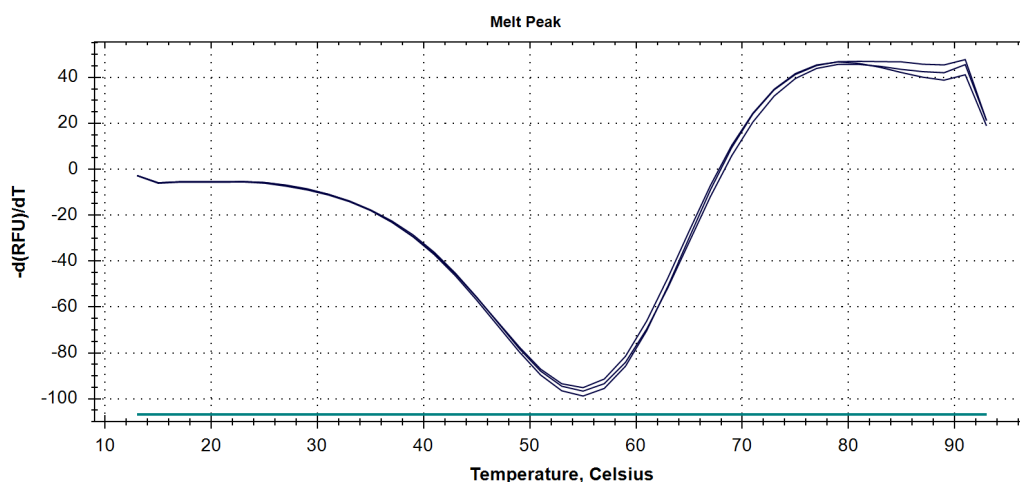
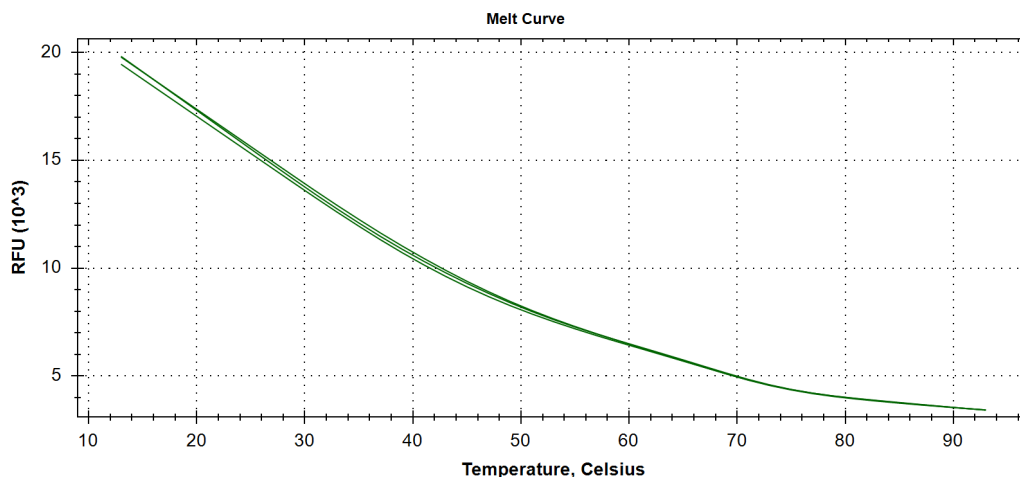
(b) Derivative curve $-(d(\text{RFU})/dT)$

Figure 10.4: Melt curve 13°C to 93°C of FL probe (1 μM), Cal Orange measurements.

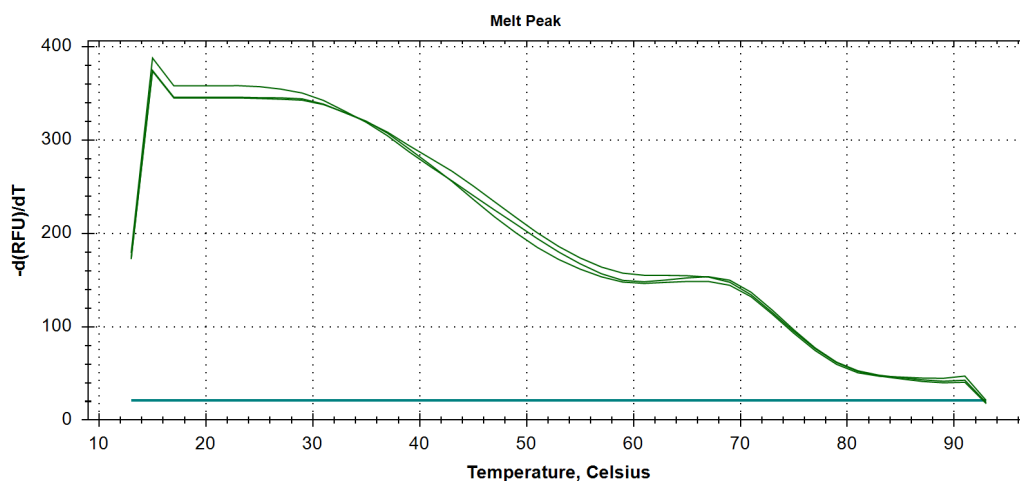
10.2.3.2 Fluorescent Probe and Target DNA Measurements

Cal Orange measurements of the FL probe with target DNA are analyzed. Here it is expected that, because the target DNA is present, the majority of the hairpins should be open and therefore the fluorescence should be much greater than that of a measurement containing only the FL probe (Figure 10.4(a)) at the starting temperature of 13°C. It can be seen in Figure 10.5(b) that there is a negative peak at 60°C, which is the melting temperature of the FL probe where the remaining closed hairpins begin to open. Finally there is a positive peak at 67°C, where the quantum yield of Cy3 decays more rapidly, although the quantum yield begins to decay as soon as the temperature increases. The

cool curve had very similar results.



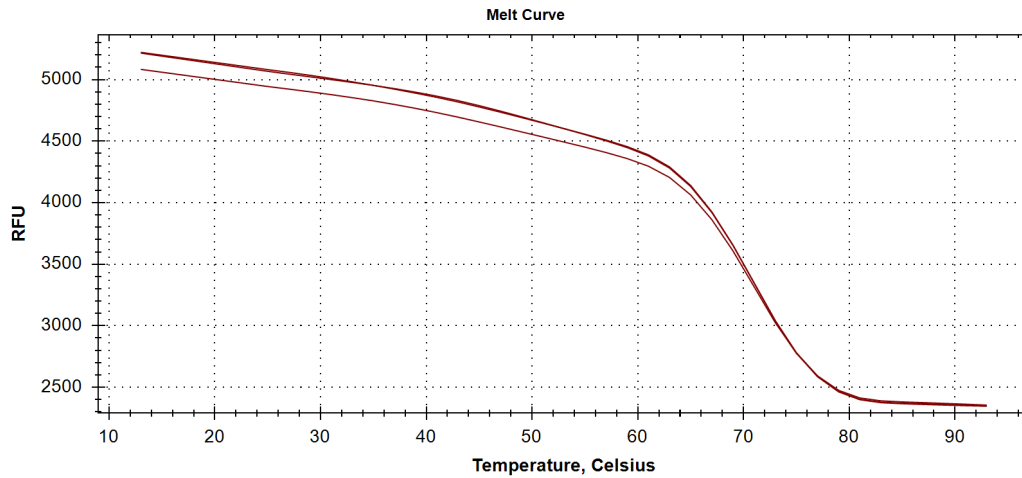
(a) Relative Fluorescent Unit (RFU) measurements vs. temperature



(b) Derivative curve $-(d(\text{RFU})/dT)$

Figure 10.5: Melt curve 13°C to 93°C of FL probe (1 μM) with target DNA (3 μM), Cal Orange measurements.

SYBR Green measurements of the FL probe and target DNA were conducted, which could then be compared to the FE probe with target DNA melt curves. Figure 10.6(a) shows an initial fluorescent signal due to hybridized FL probe to target dsDNA. The fluorescent signal remains relatively stable as temperature increases, until a melting temperature of 70°C is reached (Figure 10.6(b)). The estimated T_m of fully hybridized target dsDNA was 59°C, but concentration of oligonucleotides and various other factors can effect the T_m . The cool curve yet again yielded almost identical results.



(a) Relative Fluorescent Unit (RFU) measurements vs. temperature

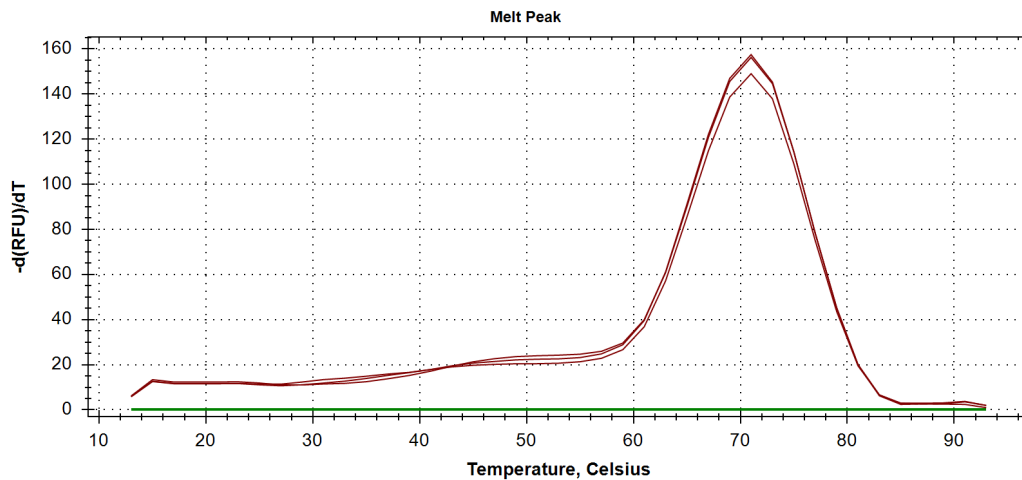
(b) Derivative curve $-(d(\text{RFU})/dT)$

Figure 10.6: Melt curve 13°C to 93°C of FL probe (1 μM) with target DNA (3 μM), SYBR Green measurements.

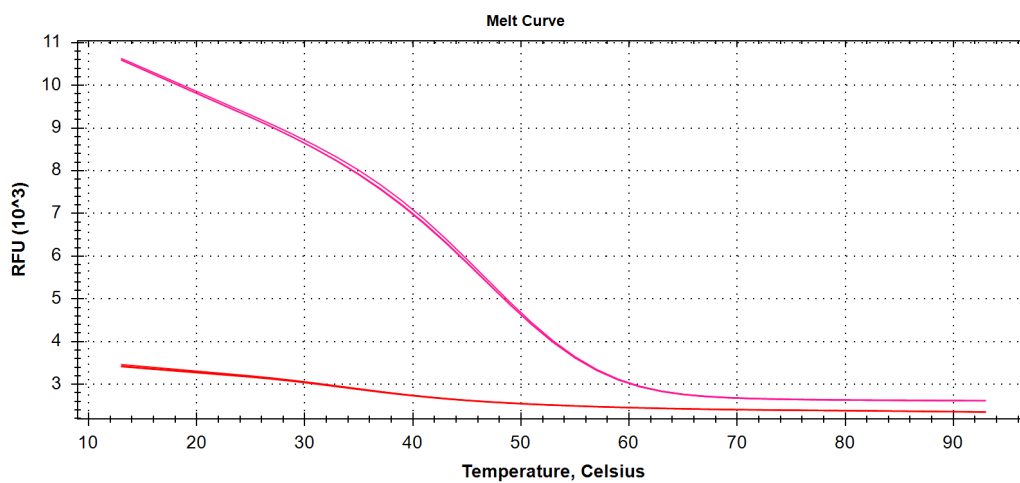
10.2.4 Ferrocene vs Fluorescent Hairpin DNA qPCR Measurements

In the previous section, the operation of the FL probes was detailed by qPCR measurements of both Cal Orange (Cy3) and SYBR Green. It was seen that the FL probes reacted as theoretically expected under different temperatures and with the addition of target DNA. It was found, however, that the FL probes were not stable, as they degraded over time and it was assumed that this was caused by contaminated TE buffer during resuspension. The FE probes were resuspended using specifically nuclease free DI water and a 5mM Tris buffer instead of the initial TE buffer, to ensure that the FE probes did

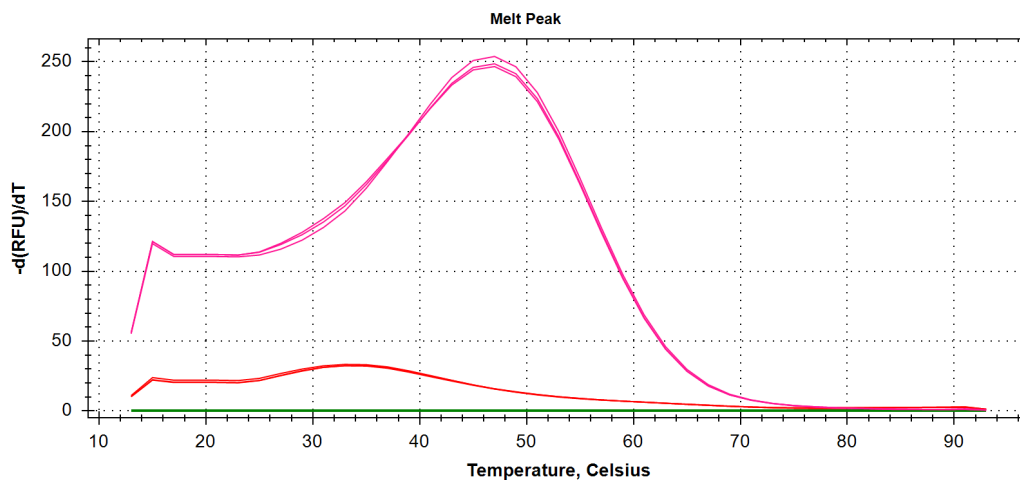
not also degrade. It was then possible to validate the operation of the FE probes by comparing the SYBR Green measurements of the two probes.

10.2.4.1 Ferrocene vs Fluorescent Hairpin DNA, no Target DNA

Figure 10.7(a) depicts the SYBR Green melt curves of both the FL and FE probes with no target present. It can be seen that both curves are similar but the FE probe (pink) has a higher RFU due to the degradation of the FL probes. Figure 10.7(b) shows a melt peak of 46°C where the stem of the hairpins starts to melt. The FE probe has a much clearer melt peak which indicates higher stability. It was seen that the cool curve yielded very similar results.



(a) Relative Fluorescent Unit (RFU) measurements vs. temperature

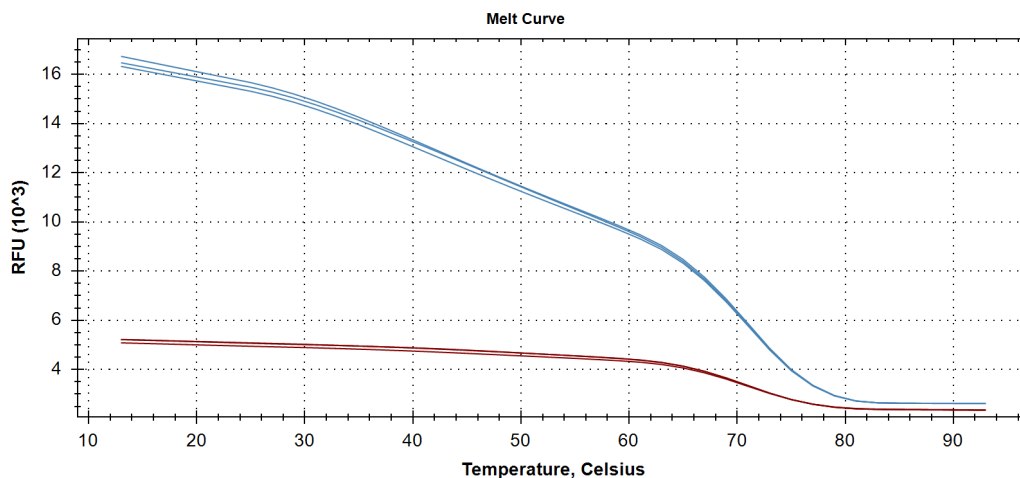


(b) Derivative curve $-(d(\text{RFU})/dT)$

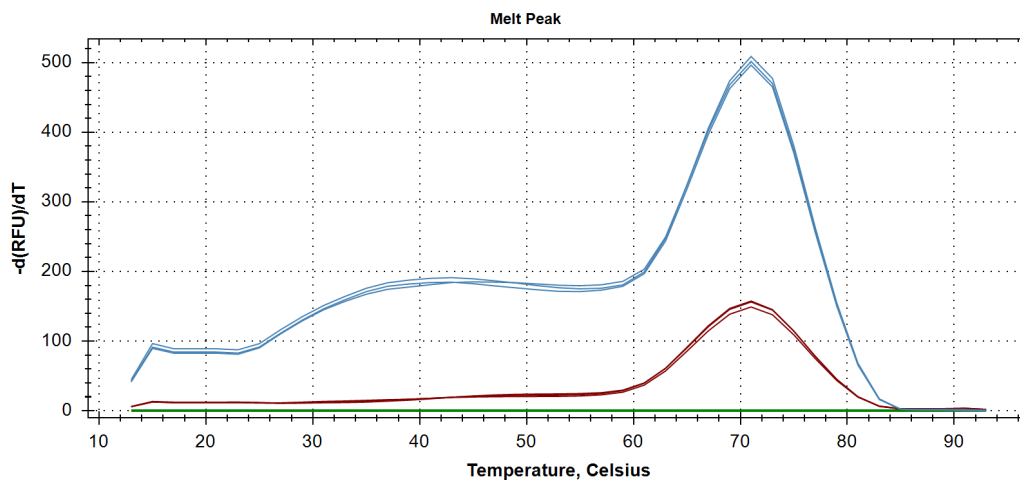
Figure 10.7: Melt curve 13°C to 93°C of 1 μM FL probe (red) and 1 μM FE probe (pink), SYBR Green measurements.

10.2.4.2 Ferrocene vs Fluorescent Hairpin DNA with Target DNA

The final qPCR results to be analyzed are both hairpin probes with target DNA. Figure 10.8(a) again shows that the FE probe (blue) has a much higher RFU, but with similar melting curves. Figure 10.8(b) shows that both hairpin probes have a similar melt peak of around 72°C. The cool curves were very similar, indicating the high stability of the hairpin probes.



(a) Relative Fluorescent Unit (RFU) measurements vs. temperature



(b) Derivative curve $-(d(\text{RFU})/dT)$

Figure 10.8: Melt curve 13°C to 93°C of 1 μM FL probe (red) and 1 μM FE probe (blue) with 3 μM target DNA, SYBR Green measurements.

10.3 Conclusion

In this chapter, the operation of both the FL and FE probes was fully characterized using qPCR measurements. The melting temperatures of all variations were discussed, and the operation of the hairpins was compared, both with and without target DNA. It was found that, unfortunately, the FL probes had been contaminated and as such, would begin to degrade over time, causing unstable results. It was seen that the FE probes yielded very stable and clear results. The hairpin probes' operation were fully validated and therefore, in the next sections, the immobilization of the hairpin probes can be validated and thereafter electronic testing could begin. By referring to Figure 10.4(a) and Figure 10.5(a), it can be seen that there is a very clear difference in fluorescence at 30°C, which is also the temperature at which the targets secondary structures begin to melt. Therefore 30°C would be an optimal temperature at which to conduct electronic experiments. Higher temperatures may result in more background signal as the hairpin probes may begin to open without the presence of target DNA. Lower temperatures would also yield good results, but the time for target DNA to hybridize to the hairpins may greatly increased, as the hairpin probes are less likely to open and the target DNA may be in their secondary structure.

Chapter 11

Hairpin Probe Immobilization Validation

In Section 6.2 the FL probe was described and it was explained that it would be used to validate the immobilization of hairpin probes to the carbon nanofibers via gold-Thiol bonding. In the previous Chapter 10, both the FL and FE probes were validated in solution. In this chapter the immobilization onto CNFs will be validated for both FL and FE probes.

Before the immobilization could begin, the carbon nanofibers were laser cut to the chosen size (10mm x 5mm) and gold was deposited at varying thicknesses as described in Section 5.3. The full immobilization protocol, as well as all reagent preparation, including resuspension and dilution, is detailed in Appendix D. The wash protocol for the immobilization and test baths are also described in Appendix D. It was determined that the carbon fiber samples were relatively hydrophobic and so the samples were dipped in Tris buffer three times at 30 seconds each, with gentle movements.

11.1 Confocal Microscopy

In this section confocal microscopy is used to validate the immobilization of FL and FE probes onto CNF samples. The Zeiss LSM780 confocal microscopy system, belonging to the CAF unit of Stellenbosch University, was used for all confocal imaging. In Chapter 10 it was discussed that a problem was found with the FL probes during initial testing. It was during these confocal imaging tests that the error was discovered and it was decided that the hairpin operation should be validated first by qPCR.

11.1.1 Fluorescent Hairpin Probe Confocal Imaging

As mentioned, the FL probes did not perform as expected during confocal imaging (seen in Appendix C). Although the results in Appendix C showed failed hairpin operation, they did however confirm the positive immobilization of the probes via gold-thiol bonding. The first confocal experiment, however, did yield expected results, which is most likely due to the fact that the FL probes had not yet degraded. The expected results are a low fluorescent signal on CNFs with FL probe only and no target DNA. It is then expected that CNFs with Fl probe and target DNA should fully open the hairpins and the fluorescent signal should greatly increase.

A FL probe concentration of $5\mu\text{M}$ was immobilized on the CNFs. The Target DNA concentration used was also $5\mu\text{M}$. Two control samples were imaged, the first with FL probe only, and the second with target DNA only. Figure 11.1 depicts the results of the first confocal experiment. This experiment was conducted before the immobilization bath was manufactured, so it can be seen in Figure 11.1(d), that the FL probe did not properly immobilize to the CNF. It can be seen, however, that with a gold deposit greater than 5nm, the fluorescent signal is greater in comparison to the control sample with FL probe only (Figure 11.1(f)). The results seen in Figure 11.1 validate the immobilization technique, as well as the operation of the FL probe on a solid substrate. From these results, it was decided that a gold coating thickness of 15nm would be used in all future experiments.

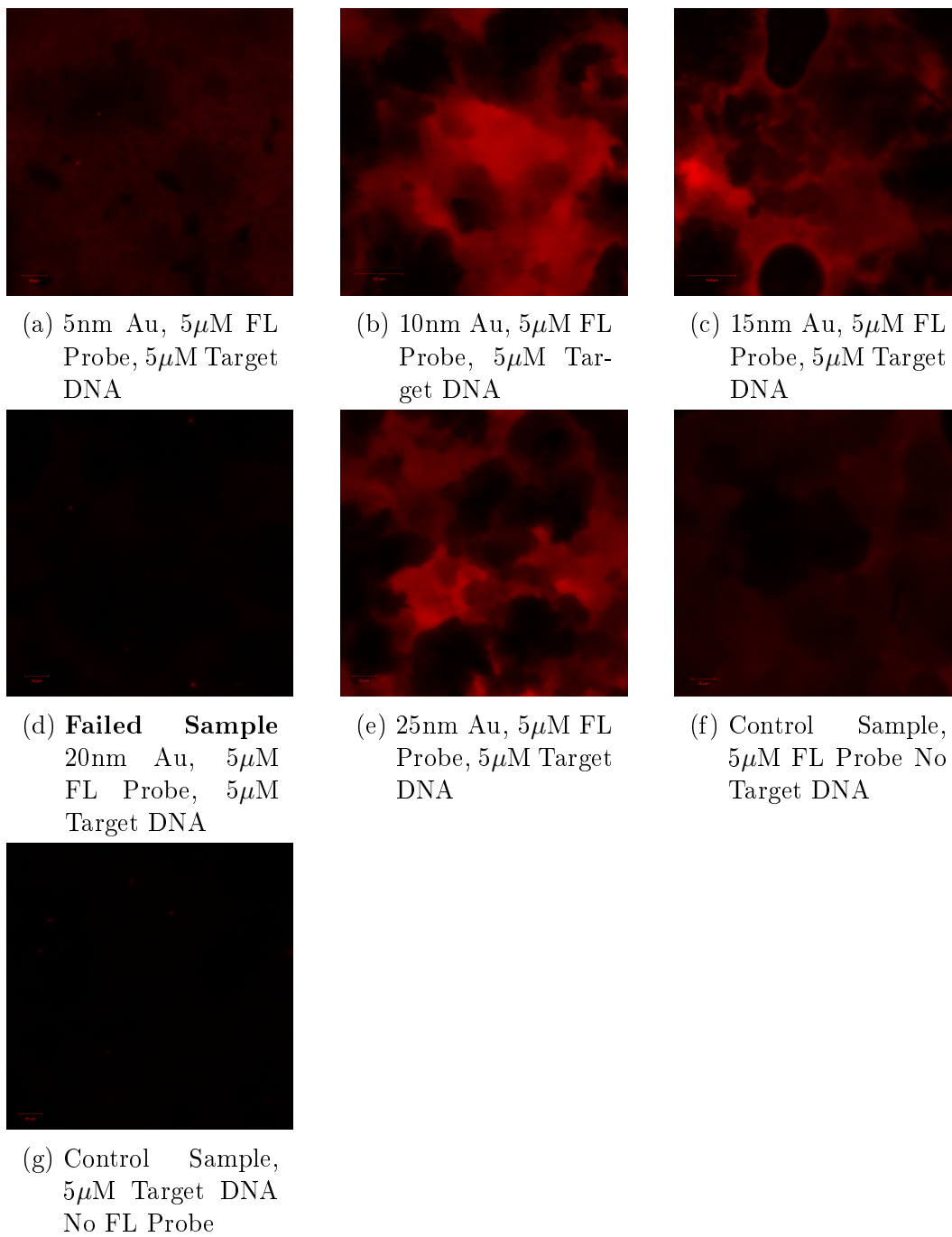
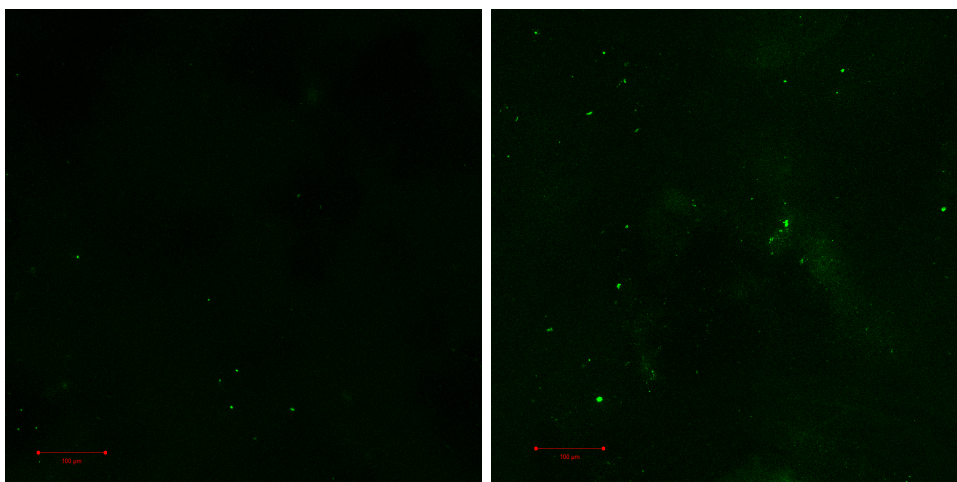


Figure 11.1: Confocal imaging of FI probe on various thicknesses of gold coated CNFs. Imaging taken at room temperature (20k magnification).

11.1.2 Ferrocene Hairpin Probe Confocal Imaging with SYBR Green

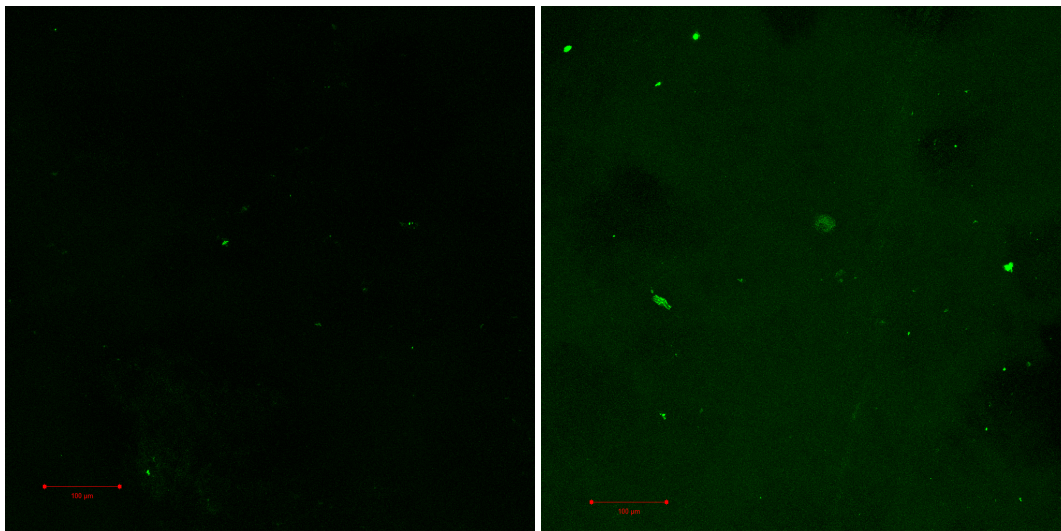
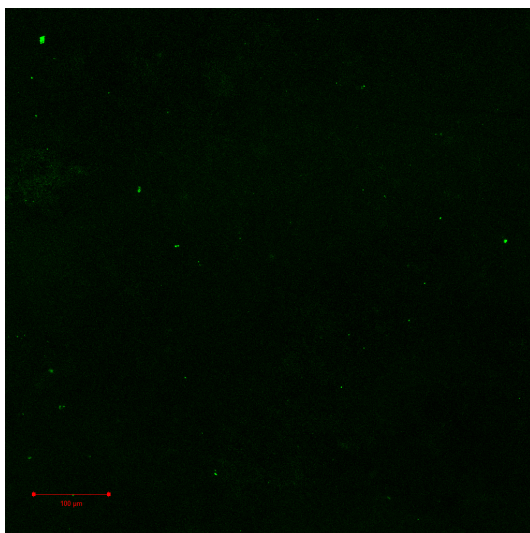
For additional validation, it was decided to conduct confocal imaging of the FE probes with SYBR Green. FE probe concentrations of $5\mu\text{M}$ and $1\mu\text{M}$ were tested. Images were taken of CNF fibers with FE probe only as well as FE probe and target DNA. The target DNA concentration was three times higher than that of the FE probe tests ($15\mu\text{M}$ and $5\mu\text{M}$ respectively). Due to the fact that SYBR Green binds to any dsDNA, it is expected that there should be a low fluorescent signal when only FE probe is present and a higher fluorescent signal should be observed when target DNA is also present. Figure 11.2 shows that the expected results are seen. Figure 11.2(b) shows slightly higher fluorescence than Figure 11.2(a) ($1\mu\text{M}$ FE probe). Figure 11.2(d) shows a much greater fluorescence than Figure 11.2(c) ($5\mu\text{M}$ FE probe). Figure 11.2(e) is a control sample of SYBR Green only, no FE probe or target DNA is present.



(a) $1\mu\text{M}$ FE probe, no target DNA.

(b) $1\mu\text{M}$ FE probe, $3\mu\text{M}$ target DNA.

Figure 11.2: FE probe validation, SYBR Green confocal imaging

(c) $5\mu\text{M}$ FE probe, no target DNA.(d) $1\mu\text{M}$ FE probe, $15\mu\text{M}$ target DNA.

(e) SYBR Green only, no FE probe, no target DNA.

Figure 11.2: FE probe validation, SYBR Green confocal imaging

11.2 Conclusion

Both the FL and FE probes immobilization and operation were validated by confocal microscopy on the Zeiss LSM780 confocal microscopy system. It was seen that the hairpin probes were sufficiently and evenly immobilized across the CNF surfaces and that the operation of the probes was not affected. All preliminary tests have been completed and the hairpin probe operation fully characterized. In the next section the electronic testing can begin.

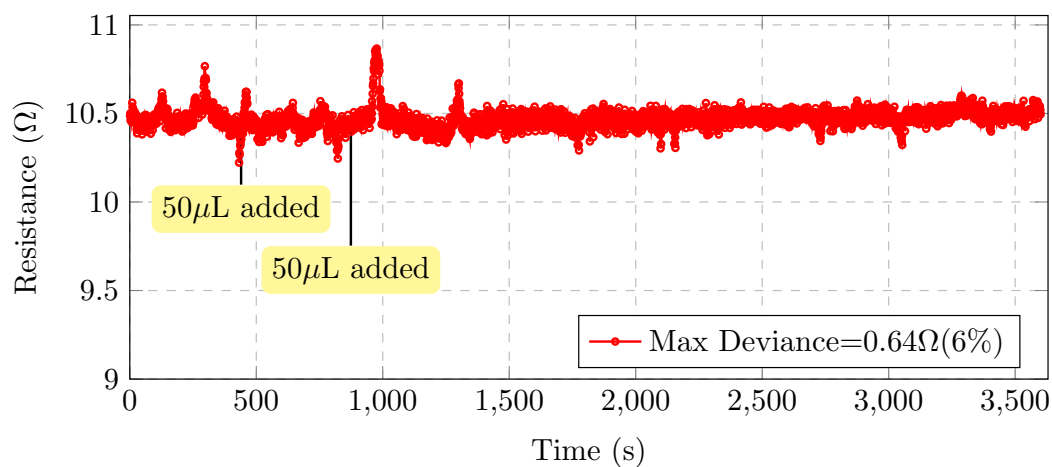
Chapter 12

Biosensor Results

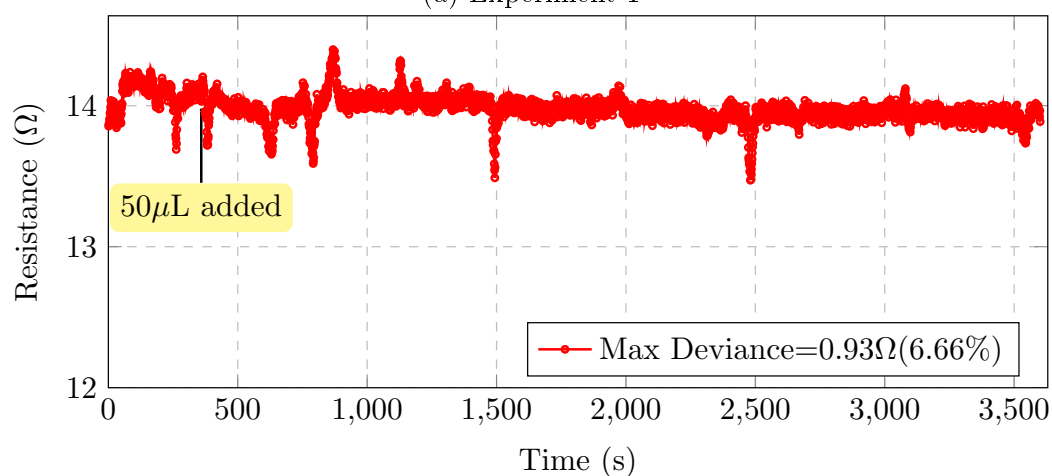
In Chapter 9 the electronic measurement system was fully validated and it was found that an addition of TE buffer did not significantly change the resistive measurements of the CNFs with a maximum deviance of around 2% of the base resistance. As previously mentioned, Skotadis *et.al.* [47] report a resistive change of up to 51% of the base resistance and so it is hoped that the current sensor design will yield similar results. In this chapter the biosensor will be tested by comparing measurements with addition of Tris buffer with measurements of the target DNA. The full test protocol can be found in Appendix D.8. All electronic experiments were conducted in a 30°C environment.

12.1 Tris Resistive Measurements

Figure 12.1 depicts the resistive measurements of a CNF with only Tris buffer added. It can be seen that there is no significant change even after multiple additions of Tris. It is also noted that there is some significant noise throughout the measurements that contributes to the majority of the calculated maximum deviance.



(a) Experiment 1



(b) Experiment 2

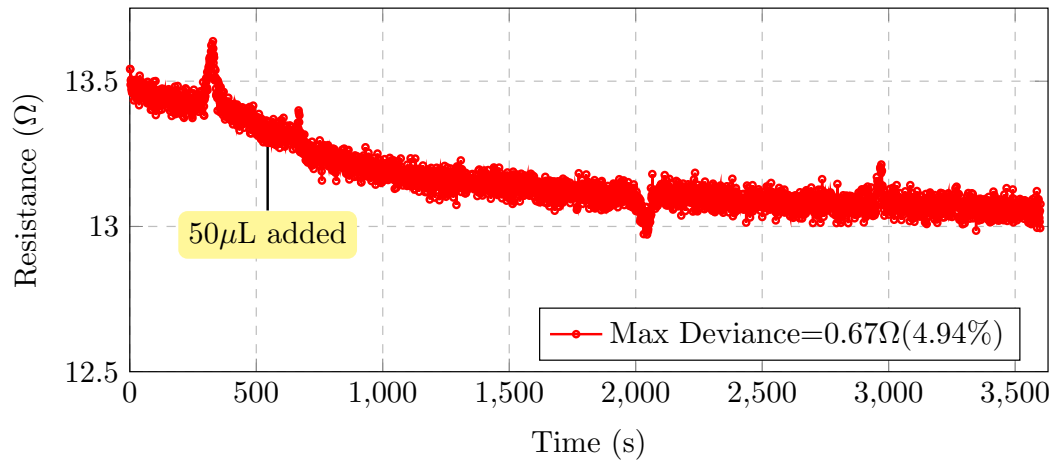
Figure 12.1: Resistive measurements of CNF during addition of 50 μL Tris buffer.

12.2 10 μM FE Probe and 10 μM Target DNA Resistive Measurements

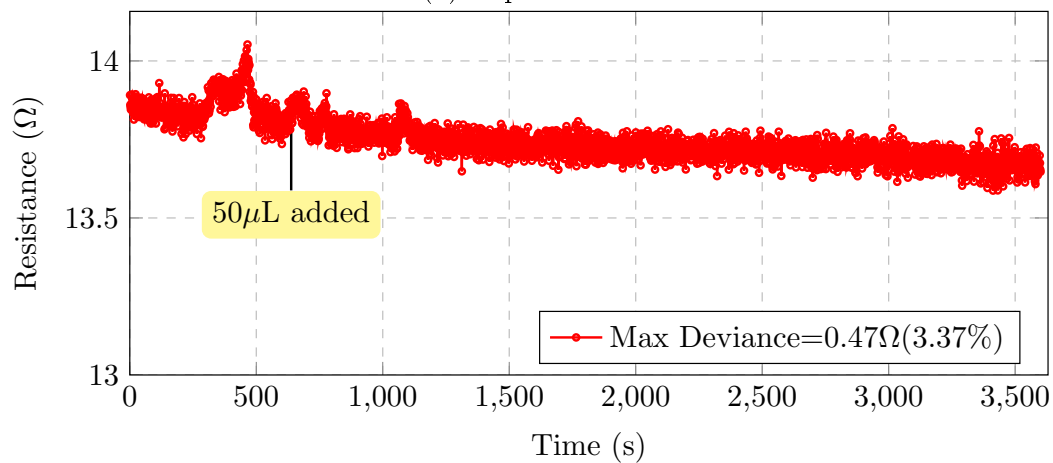
The first positive control biosensor tests are seen in Figure 12.2. CNFs were prepared with 10 μM FE probe the day before testing, following the protocol seen in Appendix D.1. It was found during testing that if measurements began as soon as the CNFs were placed in the test baths, there would be a slow decrease in resistance for the first few minutes, which is most likely due to the physical pressure exerted on the CNFs by the electronic spring test probes or the electrolytic interface of the electronic spring test probes and the Tris buffer solution. It was therefore decided after these tests, that the CNFs would be left

for 10 minutes before measurements began. Following these tests the electronic test protocol found in Appendix D.8 was redefined to ensure stability of testing.

Figure 12.2 shows that, unfortunately, with the addition of target DNA with a concentration of $10 \mu\text{M}$, there is no significant change in resistance measurements. It can also be seen that there are random peaks due to noise, which contribute to the majority of the calculated maximum deviance.

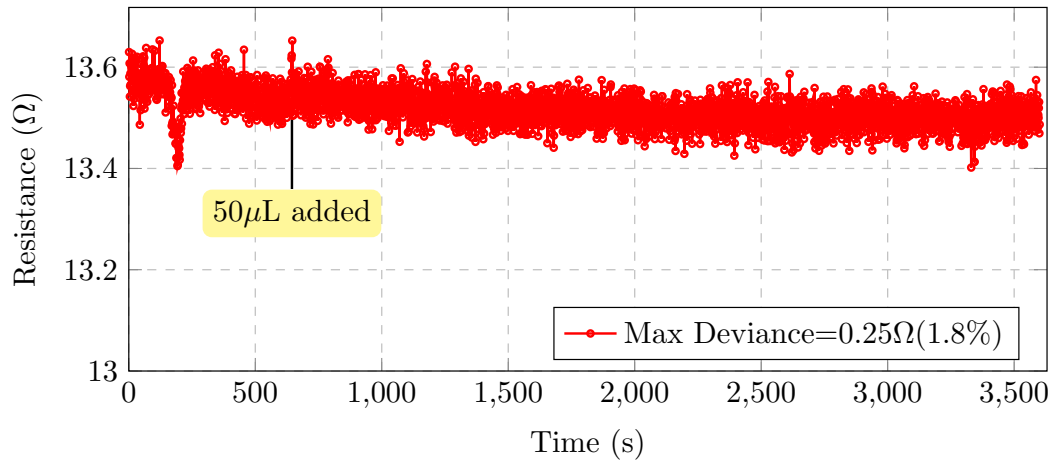


(a) Experiment 1



(b) Experiment 2

Figure 12.2: Resistive measurements of CNF during addition of $50 \mu\text{L}$ of $10 \mu\text{M}$ target DNA with $10 \mu\text{M}$ immobilized FE probe with $10 \mu\text{M}$ immobilized FE probe.



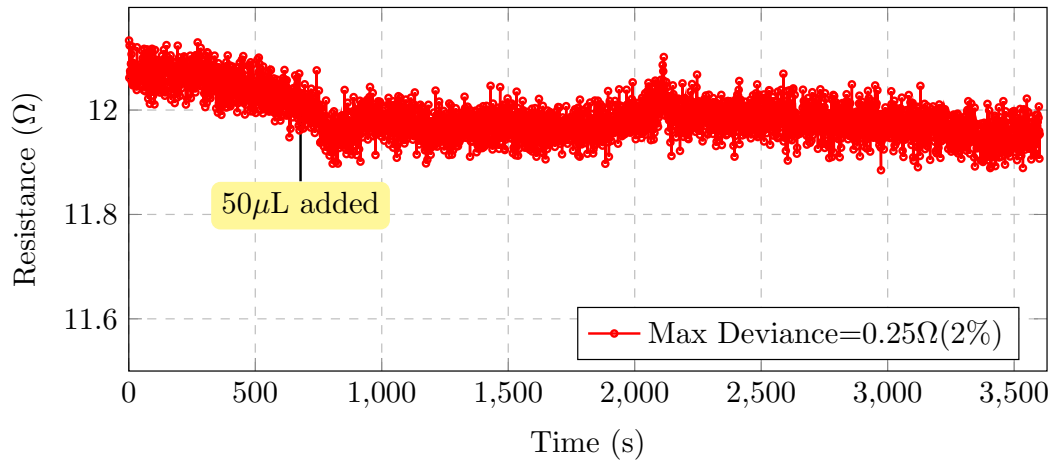
(c) Experiment 3

Figure 12.2: Resistive measurements of CNF during addition of 50 μL of 10 μM target DNA with 10 μM immobilized FE probe.

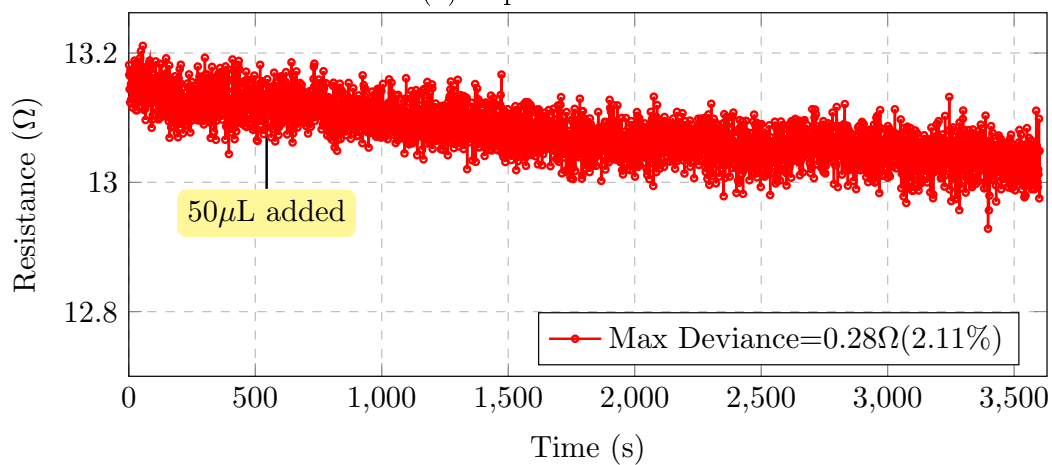
12.3 20 μM FE Probe and 10 μM Target DNA Resistive Measurements

The second set of tests completed are seen in Figure 12.3. It was decided to increase the concentration of the FE probe from 10 μM to 20 μM to ensure maximum saturation of immobilized probes. Although the concentration of the FE probe was known before immobilization, it is uncertain what percentage of the probes actually immobilize before the wash step. The results shown in Chapter 11 do however indicate that the immobilization efficiency is good.

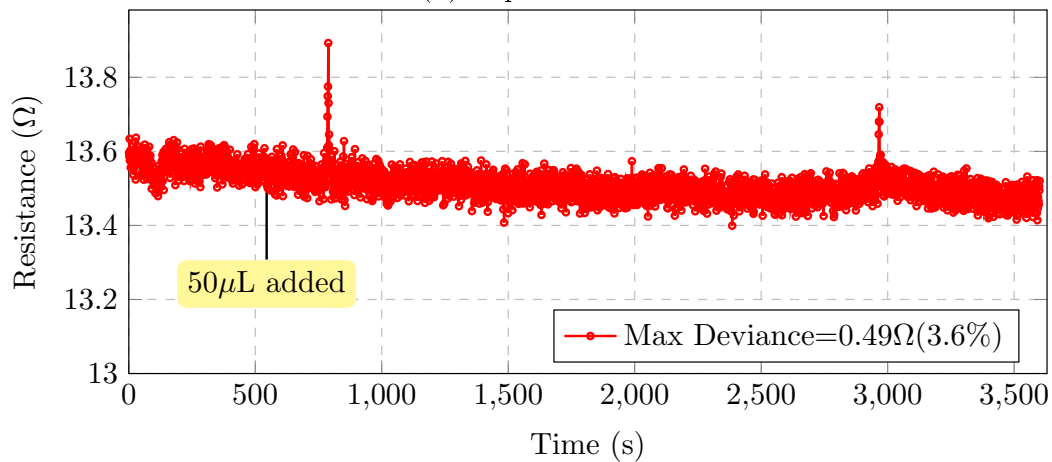
Figure 12.3 shows similar results to the previous tests in Section 12.2. Unfortunately there is no marked change in resistance after target DNA (10 μM) is introduced. Figure 12.3(a) shows a slight decrease just after target DNA is added, which indicates that there may be a very small underlying signal change, but noise is also a possibility.



(a) Experiment 1



(b) Experiment 2



(c) Experiment 3

Figure 12.3: Resistive measurements of CNF during addition of 50 μ L of 10 μ M target DNA with 20 μ M immobilized FE probe.

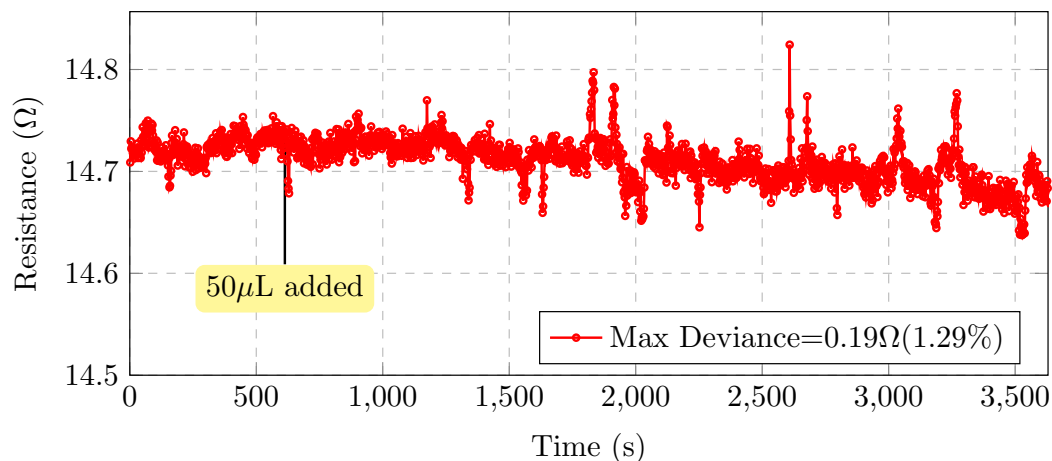
12.4 Circuit Adjustments

Due to the fact that the previous tests showed no positive results, it was decided to adjust the electronic circuitry to reduce noise as much as possible. The LPF cut-off was adjusted to 0.3 Hz (initially 18 Hz). By lowering the LPF cut-off, rapid signal changes will be dampened, but the response of the signal will also be slowed (3 seconds). This was done, in the hope that it would reduce noise spikes and if the introduction of target DNA produced any resistive change, this might still be measurable. It was also decided to increase the constant current to 100 μA .

The Tris based tests, as well as the FE probe and Target DNA tests were repeated with the new circuit adjustments and will be briefly discussed. It was noticed here that, even after a 10 minute waiting period before measurements began, there was still a slight decrease in resistance over time, which can be attributed to the electrolytic interface of the electronic spring test probes and the Tris buffer solution.

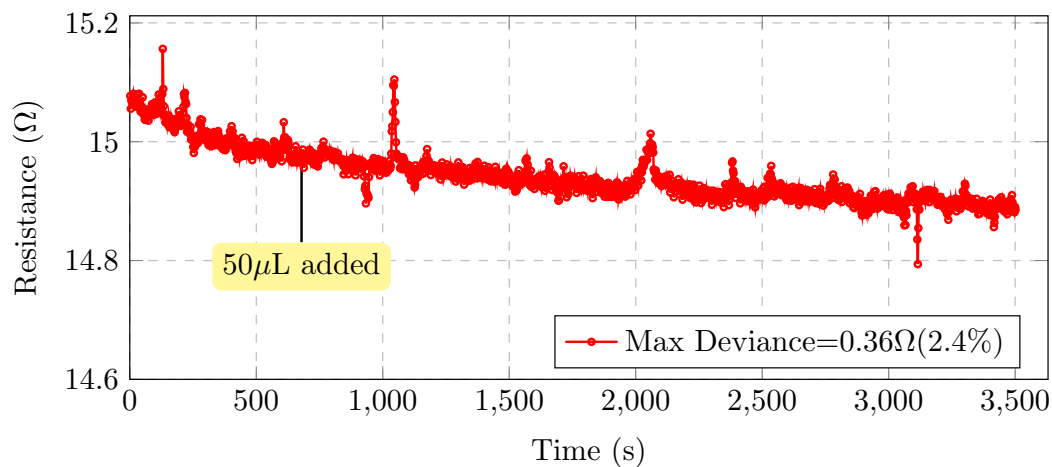
12.4.1 Tris Resistive Measurements

Figure 12.4 depicts the resistive measurements when Tris buffer is added with adjusted LPF cut-off and increased current. It can be seen that the noise has been reduced significantly with the maximum deviance almost a third of the initial Tris based tests.

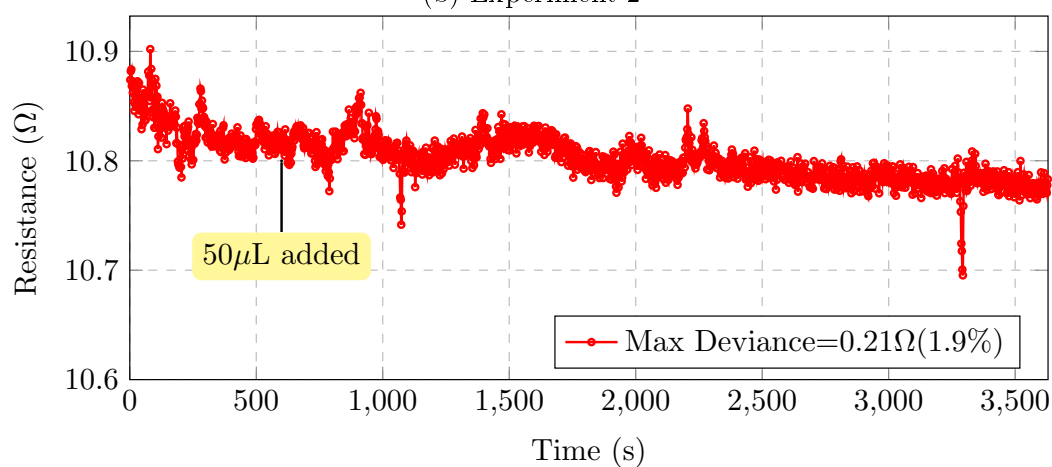


(a) Experiment 1

Figure 12.4: Resistive measurements of CNF during addition of 50 μL of Tris buffer.



(b) Experiment 2



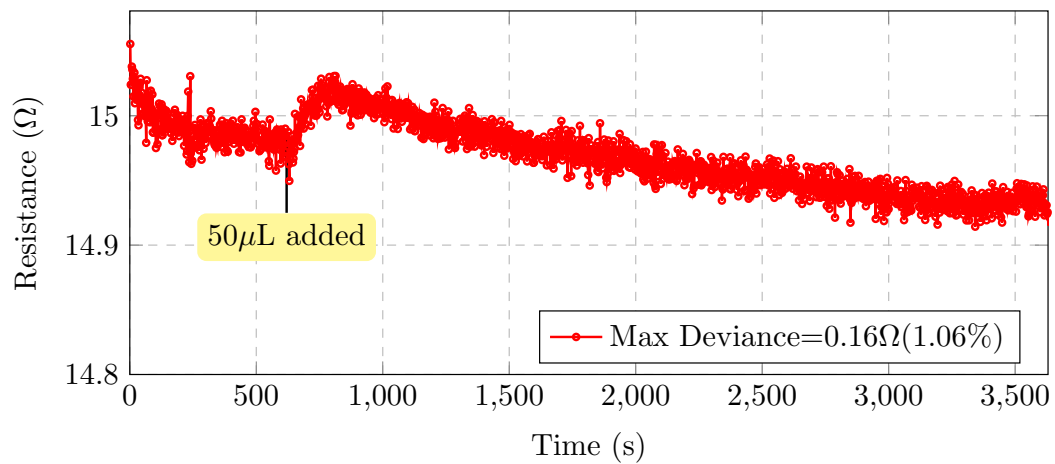
(c) Experiment 3

Figure 12.4: Resistive measurements of CNF during addition of Tris buffer.

12.4.2 20 μM Fe Probe and 10 μM Target DNA Resistive Measurements

Figure 12.5 shows the results of CNFs with 20 μM immobilized FE probe with an addition of 10 μM target DNA. It can be seen that the signals are far more stable and that there is a definite decreasing gradient over time (most likely due to electrolytic interface). Unfortunately there is still no clear indication of a positive signal arising from the addition of target DNA. It can be seen in some measurements that there is a slight disturbance just after a sample has been added, most notably in Figure 12.5(a), but this is most likely due to movement during the addition of the samples and not necessarily target DNA. These results indicate that if there is a signal being produced by the hybridization of target DNA to the FE probes, it is difficult to directly detect

the changes by resistive measurements alone. It was decided that the data obtained would be post-processed in order to determine if a positive result could be obtained.



(a) Experiment 1

Figure 12.5: Resistive measurements of CNF during addition of 50 μ L of 10 μ M target DNA with 20 μ M immobilized FE probe.

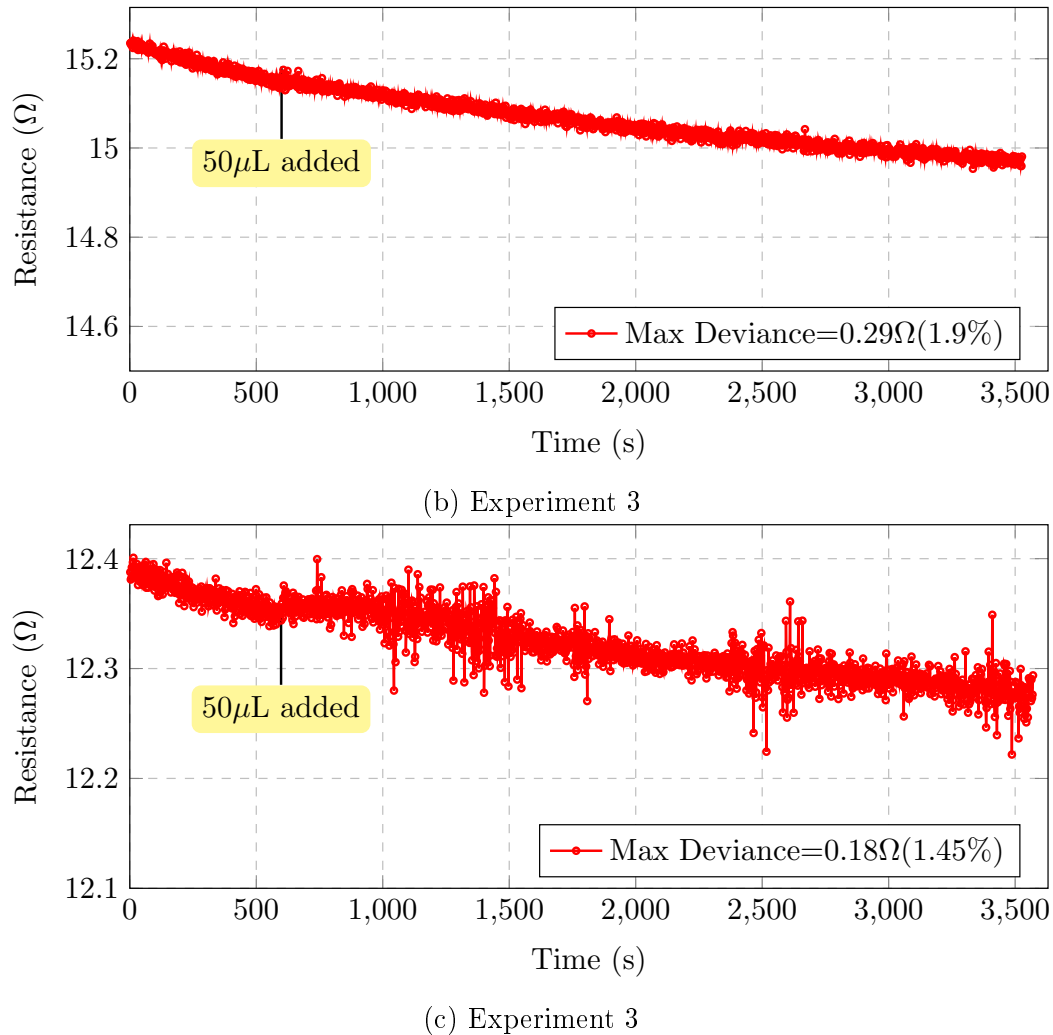


Figure 12.5: Resistive measurements of CNF during addition of 50 μL of 10 μM target DNA with 20 μM immobilized FE probe.

12.5 Data Processing

Due to the fact that the measurements obtained did not yield any directly positive results, it was decided that the data already obtained would be post-processed and averaged in order to validate if there were any noticeable trends. The post processing will be briefly discussed.

12.5.1 Trend Line Fitting

Using Microsoft Excel 2013 a 6th order polynomial trend line was fit to the data. The trend lines were fit to three minutes before and 15 minutes after the samples were added. Figure 12.6 shows an example of a 6th order polynomial

trend line fit from an experiment where Tris buffer was added. The generated equation and R^2 value is seen in Equation (12.5.1).

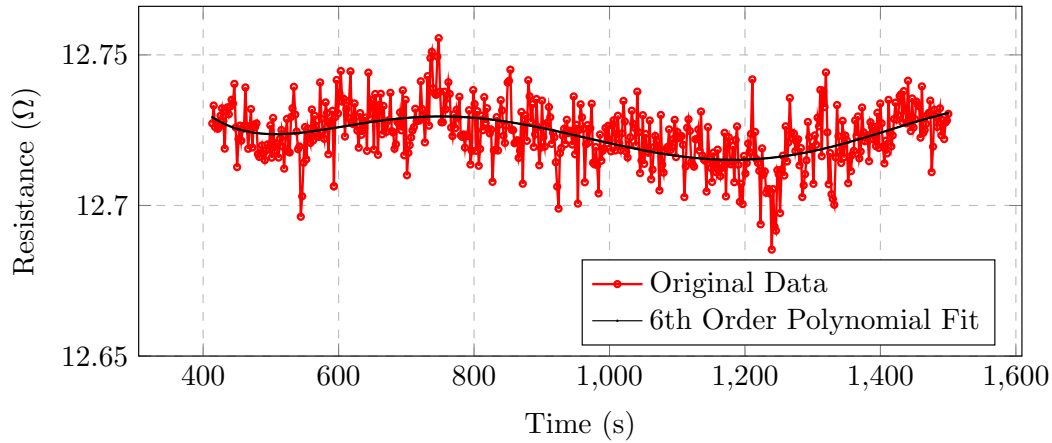


Figure 12.6: 6th order polynomial trend line fit.

$$\begin{aligned}
 y &= 3.106115642094990 \times 10^{-19}x^6 - 2.659535563395330 \times 10^{-15}x^5 \\
 &+ 8.49582452517598010 \times 10^{-12}x^4 - 1.317097214308310 \times 10^{-08}x^3 \\
 &+ 1.051638577088160 \times 10^{-05}x^2 - 4.119724028977490 \times 10^{-03}x \\
 &+ 1.334809746700230 \times 10^{+01} \\
 R^2 &= 2.543338092892830 \times 10^{-01}
 \end{aligned}
 \tag{12.5.1}$$

12.5.2 Derivative Curve

A derivative curve was generated from the newly obtained trend line data. A derivative point was generated by calculating the gradient between two data points, one hundred places apart ($\frac{R_{n+100}-R_n}{t_{n+100}-t_n}$). It was decided to calculate the gradient between one hundred points to reduce error and produce smoother results. Figure 12.7 shows the derivative curve of added Tris buffer. The Tris buffer was added close to 600s (10 minutes), minus one hundred seconds for the derivative gradient. A clear peak can be seen around 500s, indicating that an addition of solution is measurable.

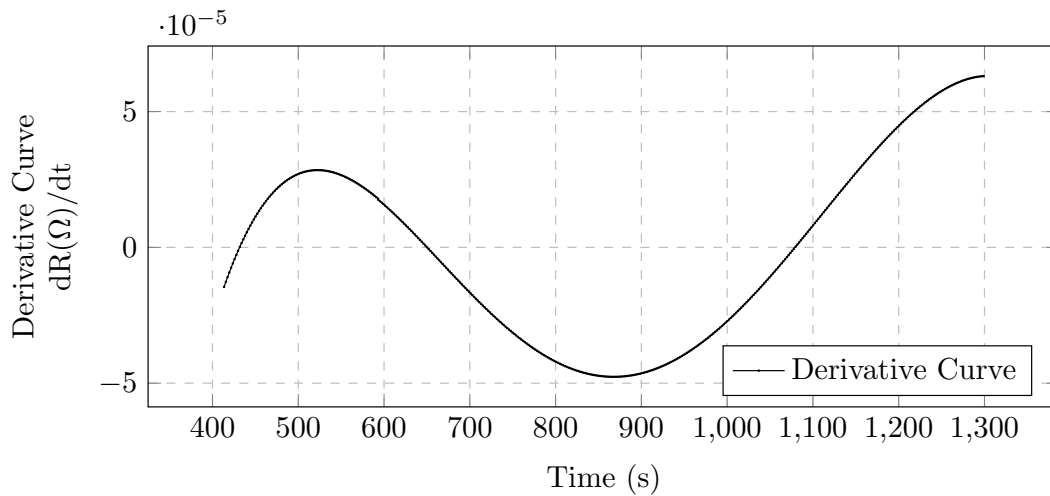
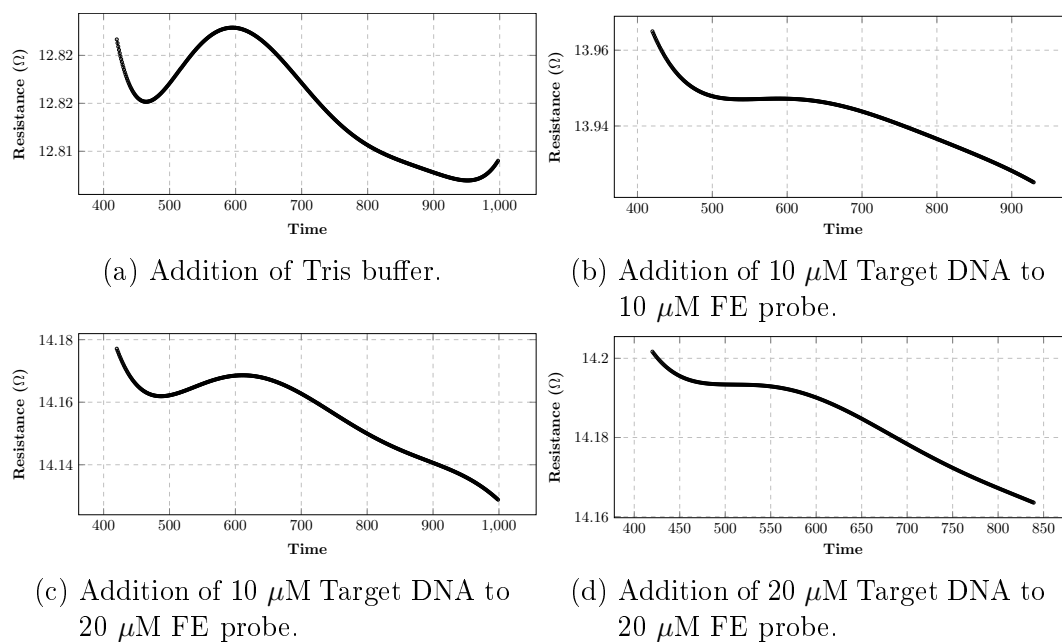


Figure 12.7: Derivative Curve

12.5.3 Averaging of Polynomial Fit Curves

Each individual experiment was processed in the same way as described in the previous section and thereafter the results of each respective test were averaged. Each experiment was completed four times and thus the results of each experiments' 6th order polynomial trend line fit average is seen in Figure 12.8. It can be seen in all curves that there is always a slight peak at 600s as this is the point at which the sample solution was added.

Figure 12.8: 6th order polynomial averages of 4 experiments each.

12.5.4 Averaging of Derivative Fit Curves

Finally the derivative curves of each experiment were also averaged and the results are seen in Figure 12.9. It can be seen that the results are almost identical for all tests and a clear peak can be seen at 500s, indicating that the circuitry is able to detect an addition of any solution, but that the FE probe response when introduced to complimentary target DNA, does not generate a measurable signal.

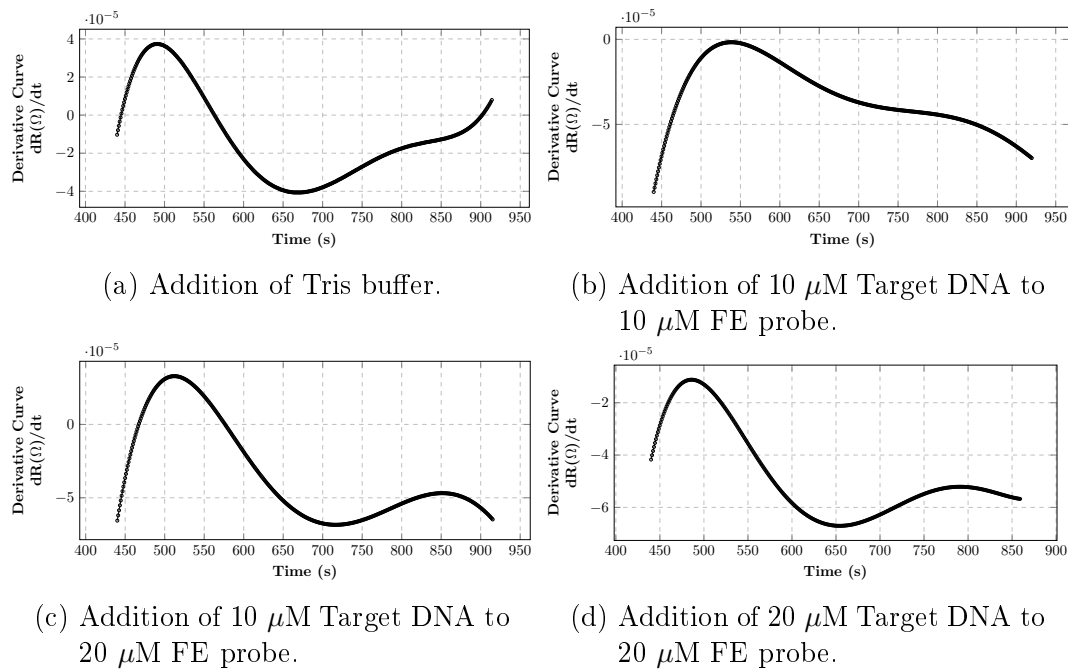


Figure 12.9: Derivative curve averages of 4 experiments each.

12.6 Conclusion

The full biosensor system was tested in this chapter in order to determine whether the introduction of complimentary target DNA to immobilized FE probes on CNFs would generate a measurable signal. Probe and target DNA concentrations of 10 μM and 20 μM were tested in different variations and compared to tests with only Tris buffer added. The electronic circuitry was adjusted to increase the constant current and decrease the LPF cut-off. The obtained data was then post-processed using polynomial trend lines and derivative curves, and it was found that the circuitry was able to detect the addition of solution, but the addition of target DNA was not able to be detected. In conclusion, it was not possible to detect the presence of target DNA using the current system. Chapter 13 will discuss the various optimizations or alternat-

ive solutions recommended in order to possibly increase the chances of being able to detect complimentary target DNA.

Chapter 13

Optimizations and Alternative Solutions

It was found in Chapter 12, that the electronic biosensor was not able to positively detect the presence of the Target DNA. It is strongly believed that, with certain optimizations or alternative design decisions, target DNA can be detected using resistive techniques. In this chapter a few optimizations and alternative solutions will be briefly discussed.

13.1 Optimizations

13.1.1 Biosensor Miniaturization

13.1.1.1 Sensor Miniaturization

The size of the biosensor can easily be miniaturized to reduce materials and especially costly reagents used during biosensing. In a practical system, only one test bath would be needed, which would vastly decrease the size of the test bath. The main size limitation of the CNFs was the machining capabilities of the test bath. With industrial machinery and more efficient test bath designs, it is possible to reduce the volume of the test bath and hence the size of the CNFs. By reducing the test bath volume and CNFs, lower volumes of hairpin probes and target DNA would be required. A smaller transducer may also lead to a more sensitive and stable sensor. The most challenging problem is the method of connecting the CNFs to the electronic measurement device. If a more elegant method can be designed, instead of the electronic spring test probes, the sensor can most definitely be miniaturized.

13.1.1.2 Electronic Miniaturization

In order to further miniaturize of the biosensor, it is also possible to reduce the size of the electronics used. The most simple solution, with very few changes

to the electronic design or programming, would be the use of an Arduino Nano [78]. The Arduino Nano is a compact board similar to the Arduino UNO or Leonardo, with a PCB size of 18 x 45 mm in comparison to the Leonardo's PCB size of 53.3 x 68.6 mm. It is possible to reduce the electronic PCB still further by redesigning a custom microcontroller, as there are many components and unused pins on the Arduino Leonardo.

13.1.2 On-Chip Technology

13.1.2.1 On-Chip Heating

In order to make the biosensor more portable, it is necessary to include on-chip heating of the CNFs and sample solutions. By using on-chip heating to bring the CNFs and solutions to a single defined temperature, the biosensor would not need to be used in an incubated environment. An even more useful function of on-chip heating would be the ability to vary the temperature at defined rates to defined temperatures. This would allow the full characterization of electronic signal variations at differing temperatures, much like the fluorescent measurements of a qPCR. By using temperature profiles, it would be possible to validate the electronic response of a hairpin probe (i.e ferrocene modification), without the addition of target DNA.

13.1.2.2 On-Chip PCR Amplification

If an on-chip heating device were to be included, it would be possible to conduct PCR amplification. PCR amplification will be very useful in conjunction with biosensors when the initial target DNA concentration is very low, and possibly too low to obtain a measurable signal. PCR tests are briefly described in Section 2.2.1.1.

13.1.3 Electronic Filtering

It may be possible to increase the sensitivity or precision of the designed electronics measurements by introducing better filtering techniques. By utilizing a more efficient and stable low pass filter, it may be possible to reduce resistive and signal noise at the ADC input, which in turn would increase the sensitivity and precision of the biosensor. It may be beneficial to utilize an IC based low pass filter instead of manually designing one. An example of such a chip is the Maxim MAX7400ESA+, 8th-Order, Lowpass, Elliptic, Switched-Capacitor Filters [79].

13.1.4 Fluorescent Label

In Section 10.2.3 it was found that the operation of the Cy3 fluorescent modification was not temperature independent. As temperature increases the quantum

yield of the Cy3 fluorophore decreases and can decrease more than 70% at temperatures $> 65^{\circ}\text{C}$. It is suggested that a more stable fluorescent label be used such as TET, HET, ROX or Texas Red. It has been reported that these fluorophores do not show any significant change in quantum yield with an increase in temperature [76, p. 13][77].

13.1.5 Post-Processing Algorithms

If the alternative solutions described in Section 13.2, do not yield any directly detectable resistive measurements, it may be necessary to improve the post-processing techniques. In Section 12.5, the data was post-processed using polynomial trend lines and derivative curves. It may be possible to generate positive results by using more efficient data processing. After sufficient data has been collected, it may be possible to remove the effect of solution addition and thereafter normalize the data, negating the changes effected by generic solution addition and possibly being able to detect the target-probe DNA hybridization. Other options may include more complex solutions, such as machine learning.

13.2 Alternative Solutions

13.2.1 Nanofibers

When the biosensor design began, it was assumed that the conductive substrate should be highly conductive due to the fact that most fiber based biosensors used some form of carbon [55]. It was believed that a highly conductive substrate would be more significantly affected by a biological reaction than a less conductive substrate. Due to the results found in Chapter 12, it is now assumed that the opposite may be true. It is now believed that, because the CNFs are directly connected between the electronic spring test probes, electrons will flow with more probability through the center of the CNFs and not the surface where DNA binding takes place.

It is possible that a more significant measurable signal may be obtained with the current design, by using less conductive nanofibers. It is suggested that an alternative conductive nanofiber be investigated, such as Polyaniline (PANI), doped with a conductive substance (carbon nanotubes, gold, etc.). By doping a non-conductive polymer with a conductive nano-material, it will be possible to control the conductivity of the nanofibers created.

With reference to research by Skotadis *et al.* [47], it is suggested that a conductive nanofiber be electro spun with a relatively low conductivity (higher resistance). Skotadis *et al.* [47] designed an IDE based biosensor that meas-

ures resistive change. Here, resistances before biological reactions were tested in the range of 600 k Ω to 1-10 M Ω . It was found that a base resistance of 700 k Ω , produced the greatest resistive change during a hybridization event. It should be noted that with an increase in resistance, a considerable increase in resistive noise is expected and thus a change in sensor design may be required, and an optimal base resistance would need to be investigated.

13.2.2 Electrolytic Interfaced Experiments

The biosensor designed, utilized a solid interface of the CNFs between the electronic spring test probes. An alternative solution would be to disconnect the solid interface between the CNFs and electronic spring test probes. By doing this the CNFs will no longer be the majority charge carrier and the experimentation would become electrolytic in nature, as the salt solution (Tris buffer) would complete the circuit by introducing a series resistance between the CNFs and the electronic spring test probe. The difficulty with this solution would be that the overall resistance, and hence resistive noise, will greatly increase. In order to obtain a stable system, the distance between the CNFs and the electronic spring test probe would need to be as small as possible without physically touching. The electronic biosensor model of this proposed solution is seen in Figure 13.1. This solution would align much closer to traditional electrochemical biosensing methods such as EIS or Voltammetry.

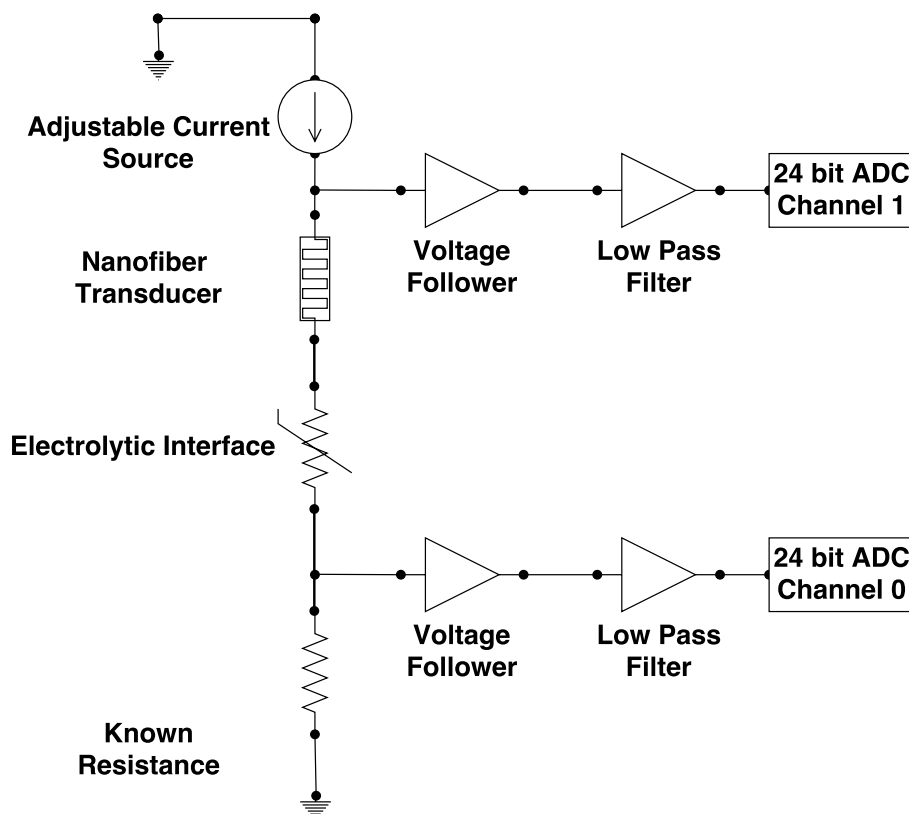


Figure 13.1: Electrolytic Interface Electronic Model.

13.2.2.1 Screen-Printed Electrodes

In order to simplify the manufacture of the above proposed alternative solution, it is possible to order pre-fabricated screen-printed carbon electrodes. Examples of such electrodes can be found at dropsens.com [80]. These types of electrodes are commonly used in Voltammetric based techniques but can still be used for resistive based measurements by ignoring one of the three electrodes. It is also possible to order modified screen-printed carbon electrodes, such as gold nanoparticles modified screen-printed carbon electrodes [81], which may aid in the immobilization of thiol modified DNA probes. If the gold modification is not sufficient, gold can still be deposited via sputter coating using masking techniques to allow deposition only where necessary. The screen printed carbon electrodes can be seen in Figure 13.2.

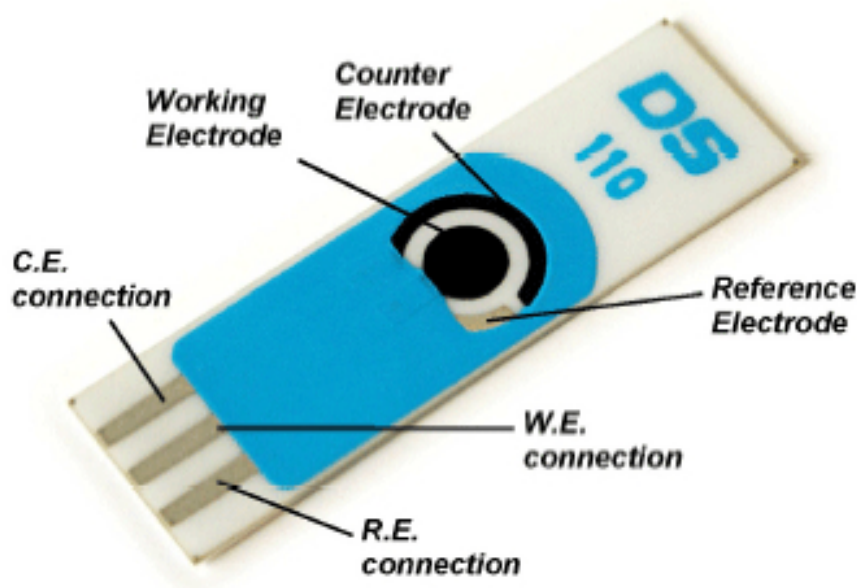


Figure 13.2: Screen printed carbon electrodes [82].

13.2.2.2 Interdigitated Electrodes

In a similar design solution described by Skotadis *et al.* [47], IDEs may be used to produce an electrolytic interfaced based design. Here CNFs would not be used and IDEs would be used instead. By depositing gold in the gaps of the IDEs, the resistance can be controlled to an acceptable value. The major difference between the design by Skotadis *et al.* and this proposed solution, is the use of ferrocene modified hairpin probes with a thiol linker. The FE probes would bind to the deposited gold and it is possible that the use of FE modified hairpin probes may result in a more sensitive biosensor.

13.3 Conclusion

It is strongly believed that a resistive based biosensor can be used to detect the presence of HIV DNA. The methods used unfortunately did not produce positive results but this may be made possible by optimizing the current solution or slightly altering the design with alternative solutions. This chapter described various optimization options of the biosensor by miniaturization, the use of on-chip technology (specifically on-chip heating), electronic filtering, and finally more complex post-processing techniques. Two alternative solutions were discussed that are believed may greatly improve the operation of the biosensor.

The first, the use of alternative nanofibers that are less conductive in comparison to CNFs, and the second, are electronic measurements over an electrolytic solution, rather than a solid interface, by use of either screen-printed carbon electrodes or IDEs. It is believed that an electrolytic interface may provide a much larger electrochemical change during a hybridization event than that of a solid interface.

Chapter 14

Conclusion

The aim of this study was to assess whether a biosensor could be designed using electrochemical techniques and hairpin probe DNA to detect the presence of HIV ssDNA. It was decided that a resistive based electrochemical technique would be used to electronically detect the presence of HIV DNA.

The concept of biosensors and the biosensor model was investigated, and it was determined that there were four main design decisions to be made when designing a biosensor. Due to the fact that the desired sensing technique was electrochemical in nature, the first design decision was to use CNF mats as the transducer. It was then decided that hairpin probe DNA would be used as the biorecognition element, as hairpin probes have been shown to be highly sensitive and with added modifiers, may produce greater electrochemical signals. The third design decision was how the biological element would be attached to the CNF mats. It was decided that a thiol modifier be added to the DNA hairpin probes to allow gold-thiol bonding. Differing thicknesses of gold sputter coating were investigated and it was found that a gold layer >10 nm was highly effective for immobilization of DNA on CNFs.

The fourth design decision was the electronic sensing system. A high precision, very low current ohmmeter was designed to measure a change in resistance of the biosensor. It was decided that a constant current be used with a high resolution ADC in order to measure very small changes in voltage across the transducer when a biological reaction occurs in order to calculate the change in resistance. It was found that the designed circuitry was very precise, with $< 1\%$ error in precision when measuring traditional resistors. It was found that precision error increased slightly when wet transducer fibers were tested, and that could be attributed to the electrolytic interface between the electronic spring test probes.

A graphic user interface was designed to communicate with the electronic circuitry in order to conduct, log and view current biosensing tests. The GUI

program proved to be very stable and displayed and recorded all data for post processing at a later stage.

A number of mechanical designs were produced, which included the physical biosensor testing setup and mount. The biosensor mechanical designs were used as a prototype and it was mentioned that these can easily be optimized and miniaturized. An immobilization bath was also designed in order to assist with the different preparation steps prior to testing.

A fluorescent label was initially used as a modification on the designed DNA hairpin probes in order to validate immobilization and hairpin operation. The immobilization validation proved to be highly successful and stable and was validated by confocal microscopy. It was initially found that there were some complications with the hairpin probe operation validation, as unexpected results were observed. qPCR was used to validate the hairpin probe operation in solution and it was found that the TE buffer was degrading the fluorescent hairpin probe DNA. A Tris buffer was used instead and the hairpin operation was fully validated and successful. A ferrocene label was used as the second hairpin probe DNA design, to be used in electronic testing. The ferrocene hairpin probe DNA was also fully validated via qPCR using a SYBR Green dye.

The electronic tests did not yield positive results, it was found that no measurable change in resistance was found with the addition of target DNA to the hairpin probe DNA. Adjustments were made to the circuitry to reduce noise, but no change in results was found. Finally, the data obtained was post-processed to determine whether trend lines may be used to detect a change in resistance when target DNA was introduced. It was found that by using 6th order polynomial trend line fit curves and derivative curves, an addition of any sample could be detected, but it was not possible to differentiate between a positive control test and a negative control test.

Due to the fact that the designed biosensor was unable to detect the presence of HIV DNA, a number of optimizations and alternative solutions were given. It was suggested that miniaturization of the biosensor would reduce the use of costly reagents and possibly provide a more sensitive system. On-chip heating was also discussed, as that would provide very useful tools in the characterization of the electronic operation of the designed hairpin probes. It was also suggested that a different fluorescent label be used for the validation of the hairpin probes, as it was found that Cy3 is not temperature stable.

It is strongly believed that is possible to design a biosensor that can detect a change in resistance due to a DNA hybridization event. It was suggested that, with some alternative solutions to the current biosensor design, the desired

results may be possible. It was discussed that if the current biosensor design remains relatively unchanged, by using a less conductive alternative material for the nanofibers, there may be a greater electrochemical change to be measured. It was also discussed that with slight alterations to the current design, the system could be changed from a solid interface to an electrolytic interface. It is believed that an electrolytic interface has a much higher probability of generating the results needed to be measured by the biosensor. It was suggested that screen-printed electrodes or interdigitated electrodes be pre-ordered to simplify design and provide a more stable system.

In conclusion, although the desired results were not obtained, it is believed that with a few minor changes to the current design, a resistive based biosensor that can detect the presence of HIV ssDNA may be possible.

Appendices

Appendix A

Datasheets

A.1 Rapid Anti-HIV test

CAT. NO. ITP02002 REV.51215

ADVANCED QUALITY™ Rapid Anti-HIV(1&2) Test

(Whole blood / Serum / Plasma)

FOR IN VITRO DIAGNOSTIC USE

INTENDED USE

THE ADVANCED QUALITY™ RAPID ANTI-HIV(1&2) TEST IS A COLLOIDAL GOLD ENHANCED, RAPID IMMUNOCHROMATOGRAPHIC ASSAY FOR THE QUALITATIVE DETECTION OF ANTIBODIES TO HUMAN IMMUNODEFICIENCY VIRUS (HIV) IN HUMAN WHOLE BLOOD, SERUM OR PLASMA. THIS TEST IS A SCREENING TEST, AND ALL POSITIVES MUST BE CONFIRMED USING AN ALTERNATE TEST SUCH AS WESTERN BLOT. THE TEST IS INTENDED FOR HEALTHCARE PROFESSIONAL USE ONLY.

SUMMARY

The human immunodeficiency virus (HIV) is the causative agent of acquired immune deficiency syndrome (AIDS). The general method of detecting infection with HIV is to observe the presence of antibodies to the virus by an EIA method followed by confirmation with Western Blot. The Advanced Quality Rapid Anti-HIV(1&2) Test is a simple, visual qualitative test that detects antibodies in human whole blood serum or plasma. The test is based on immunochromatography and can give a result within 15 minutes.

PRINCIPLE OF THE PROCEDURE

The assay starts with a sample applied to the sample well and add provided sample diluent immediately. The HIV antigen-colloidal gold conjugate embedded in the sample pad reacts with the HIV antibody present in serum or plasma sample forming conjugate/HIV antibody complex. As the mixture is allowed to migrate along the test strip, the conjugate/HIV antibody complex is captured by a second antibody immobilized on the membrane forming a colored test band in the test region. A negative sample does not produce a test band due to the absence of conjugate/HIV antibody complex. The antigens used in the conjugate test are recombinant proteins that correspond to highly immunoreactive regions of HIV1 and HIV2. A colored control band in the control region appears at the end of test procedure regardless of test result. The control band indicates that the colloidal gold conjugate is functional.

REAGENTS AND MATERIALS SUPPLIED

- Test cards individually foil pouched with a desiccant.
- Plastic dropper
- Sample Diluent
- Safety lancet
- Alcohol swab
- Package Insert

MATERIALS REQUIRED BUT NOT PROVIDED

- Positive and negative controls

STORAGE AND STABILITY

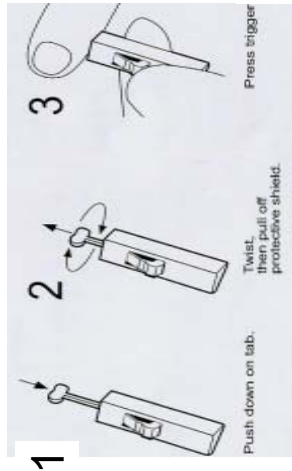
- The kit must be stored at 2 - 30°C.

WARNINGS AND PRECAUTIONS

1. ALL positive results must be confirmed by an alternative method.
2. Treat all specimens as though potentially infectious. Wear gloves and protective clothing when handling specimens.
3. Devices used for testing should be autoclaved before disposal.
4. Do not use kit materials beyond their expiration dates.
5. Do not interchange reagents from different lot of kit.

BEFORE TESTING

1. Bring the HIV test device, sample diluent, alcohol swab, safety lancet, plastic tube.
2. Remove test card from the sealed pouch.
3. Read the instruction for safety lancet.

**SPECIMEN COLLECTION**

1. Clean the area to be lanced with an alcohol swab.
2. Squeeze the end of the fingertip and pierce with the safety lancet as instructions below.

3. *Invalid:* There should always be a purplish red control band in the control region regardless of test result. If control band is not seen, the test is considered invalid. Repeat the test using a new test device.
- Note: It is normal to have a slightly lightened control band with very strong positive samples as long as it is distinctly visible.*

PERFORMANCE CHARACTERISTICS

1. Specificity

Clinical studies were done to evaluate the performance of Advanced Quality Rapid Anti-HIV(1&2) Test In USA and Canada. In both studies, 119 confirmed negative serum samples (USA: 63 samples and Canada: 56 samples) were tested by Advanced Quality Rapid HIV Test using EIA and Western Blot as reference tests. Both studies gave 100% specificity for the test.

2. Sensitivity

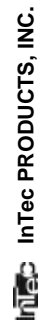
In both the studies mentioned above, Advanced Quality Rapid Anti-HIV(1&2) Test was evaluated with 64 confirmed positive serum samples (32 samples each in USA and Canada). The sensitivity of Advanced Quality Rapid Anti-HIV(1&2) Test was found to be 100% relative to consensus with EIA results, supported by Western Blot assay.

LIMITATIONS

1. Only samples that are clear and with good fluidity can be used in this test.
2. Fresh samples are best but frozen samples can be used. If a sample has been frozen, it should be allowed to thaw in a vertical position. Do not agitate the sample. Insert a pipette just below the surface of the sample to collect the specimen.

BIBLIOGRAPHY

1. Guyader, M., Emerman, M., Sonigo, P., et al. Genome organization and transactivation of the human immunodeficiency virus type 2. *Nature*, 326:662-669, 1987.
2. Blattner, W., Gallo, R.C. and Temin, H.M. HIV causes AIDS. *Science*, 241:515, 1988.
3. Curran, J.W., Morgan, W.M., Hardy, A.M., et al. The epidemiology of AIDS: Current status and future prospects. *Science* 229:1352-1357, 1985.
4. Sarngadharan, M.G., Popovic, M., Bruch, L., Schupback, J., and Gallo, R.C. Antibodies reactive with human T-lymphotropic retroviruses (HTLV-III) in the serum of patients with AIDS. *Science*, 224:506-508, 1984.
5. Weber, J.N., Weiss, R.A., Roberts, C., et al. Human immunodeficiency virus infection in two cohorts of homosexual men: Neutralising sera and association of anti-gag antibody with prognosis. *Lancet* 1:118-124, 1987.
6. Clavel, F., Guetard, D., Brun-Vezinet, F., et al. Isolation of a new human retrovirus from West African patient with AIDS. *Science* 233:343-346, 1986.

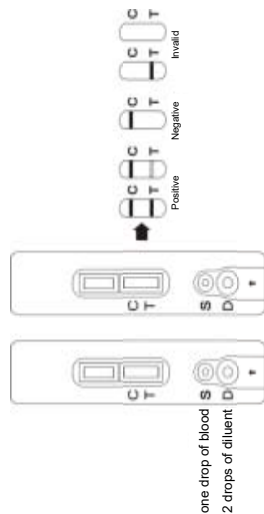


1. Push the safety lancet firmly onto the chosen site, then press trigger
2. Dispose of the lancet in a suitable container
3. Massage the site as directed to get blood flow

Note: Whole blood, serum or plasma collected following regular clinical Laboratory Procedures can be used for this test.

ASSAY PROCEDURE

1. With the plastic tube to collect blood.
2. Dispense one drop of blood to the "S" well of the test card using the plastic dropper according to the figure.
3. Add two drops of Sample Diluent to the "D" well immediately after the specimen is added.
4. Interpret test results at 15 minutes.



READING THE TEST RESULTS

1. *Positive:* Both purplish red test band and purplish red control band appear on the membrane. The lower the antibody concentration, the weaker the test band.
2. *Negative:* Only the purplish red control band appears on the membrane. The absence of a test band indicates a negative result.

A.2 Target DNA Sequence Datasheet



Inqaba Biotechnical Industries (Pty) Ltd
 P.O. Box 14356, Hatfield 0028, South Africa
 Tel: 012 343 5829
 Fax: 012 343 0287
 E-mail: info@inqaba.com

SYNTHESIS REPORT

29 Jun 2017

Client Detail: Shahieda Isaacs
 University of Stellenbosch, - Division of Medical Virology
 Floor 8
 Tygerberg
 Cape Town
 South Africa

| | | | | | |
|---|-----------------------------------|----------------|------------------|------------------|----------|
| Name: | Int-syn-standard | Barcode: | S43E6 | Length: | 33 bases |
| Sequence: | AGTGCAGGGGAAAGAATAATAGACATAATAGCA | | | | |
| OD | 17.5427 | MW min \ max | 10298.8\10298.85 | Mod | None |
| nmotes | 42.01 | GC % min \ max | 36.36\36.36 | 3' Mod | None |
| Tm min \ max | 64.66\64.66 | | Purification | Standard | |
| For a 100 μ M stock solution add 420.08 μ l water or buffer | | | | PAGE QC Image >> | |
| Comments | | | | | |

RECOMMENDATIONS FOR HANDLING AND STORAGE OF OLIGOS

- Lyophilized oligo pellets might become displaced from the bottom of the tube during shipment. Briefly centrifuge each tube before opening to prevent the loss of the pellet.
- Prepare stock solution of oligos (e.g. 100 μ M = 100 pmole per μ l) preferably with a sterile buffered solution such as TE (10 mM Tris, pH 7.5 to 8.0, 1 mM EDTA). If sterile distilled water is used, make sure that the pH is above 7.0 since acidic solutions favours oligo depurination and subsequent loss of activity.
- Working solutions might be diluted from the stock solution with sterile, nuclease-free water to prevent inhibition of enzymatic reactions (e.g. PCR) by EDTA.
- Store the oligos as concentrated stock solution or lyophilized at -20° C.
- Avoid frequent freeze-thaw cycles by dividing the stock solution into smaller aliquots for long term storage and to prevent accidental contamination.
- Dye-modified oligos are light sensitive and should always be stored in the dark.
- Re-suspend modified oligos preferably in a slightly basic solution (i.e., TE at pH 8.0). However, Cy dye modified oligos are best kept at pH 7.0 at -20° C.
- Preferably store the modified oligos as dried aliquots at -20° C.

A.3 Fluorescent DNA Probe Datasheets



| | |
|----------------------------|--|
| SPECIFICATION SHEET | www.idtdna.com |
|----------------------------|--|

27-Oct-2016

Order No. **2609535**Ref. No. **72137285**

Sequence - 4

1 umole DNA Oligo, 35 bases

5'- /5DTPA//iSpC3//iCy3/CAG GGG TGC TAT TAT GTC TAT TAT TCT TTC CCC TG/3IAbrQSp/ -3'

| Properties | Amount Of Oligo | Shipped To |
|--|-------------------------------------|--|
| T _m (50mM NaCl)*: 60.7 °C GC Content: 42.9% | 14.4 = 39 = 0.48 OD260 nmoles mg | WHITEHEAD ADMIN WHITEHEAD SCIENTIFIC UNIT 9 VAN BILJON INDUSTRIAL PARK, CAPE TOWN, 7100 SOUTH AFRICA 27219446468 207 Customer No. 4231103 PO No. 259078303 |
| Molecular Weight: 12,222.4 nmoles/OD260: 2.7 ug/OD260: 33.1 Ext. Coefficient: 368,706 L/(mole*cm) | For 100 µM: add 390 µL | |

Secondary Structure Calculations

Lowest folding-free energy (kcal/mole): -3.76 at 25 °C

Strongest Folding T_m: 51.3 °C

Secondary structure should not affect yield or purity for this oligo.

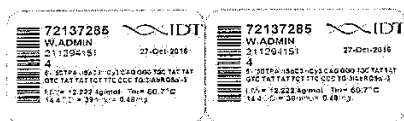
| Oligo Base Types | Quantity |
|----------------------------|----------|
| DNA Bases | 35 |
| Modifications and Services | Quantity |
| HPLC Purification | 1 |
| Level II Setup Fee | 1 |
| 3' Iowa Black® RQ-Sp | 1 |
| 5' Dithiol | 1 |
| Int C3 Spacer | 1 |
| Int Cy3™ | 1 |

Disclaimer

See on reverse page notes (i) (ii) & (iii) for usage, label license, and product warranties Also see a). Also see j). Also see p).

Mfg. ID 211294151

Labels - Peel here

**I N S T R U C T I O N S**

*Lyophilized contents may appear as either a translucent film or a white powder. This variance does not affect the quality of the oligo.

*Please centrifuge tubes prior to opening. Some of the product may have been dislodged during shipping.

*The T_m shown takes no account of Mg²⁺ and dNTP concentrations. Use the OligoAnalyzer® Program at www.idtdna.com/scitools to calculate accurate T_m for your reaction conditions.

P



WhiteSci
Whitehead Scientific (Pty) Ltd
Products. Expertise. Support.

January 2015

Advice for Resuspension of your Oligo

IDT
INTEGRATED DNA TECHNOLOGIES

Appearance of the Pellet

Always centrifuge your pellet briefly before opening the tube as oligo pellets may become dislodged during shipping.

Pure, dried oligo can be in either of **two forms**:

1. **White powder:**
The oligo froze during lyophilisation and the pellet should dissolve instantaneously.
2. **Clear film:**
The oligo didn't freeze while lyophilising, with the result that the pellet will take longer to dissolve. The tube may require vigorous vortexing to resuspend completely; heating briefly at 55°C will speed up the process, but is usually unnecessary.

Resuspending dry oligos- IDT recommends:

Dissolve your stock oligo in concentrated TE (10mM Tris pH 8.0, 1mM EDTA) rather than water.

Resuspension calculations can be made using yield information contained on IDT product specification sheets and on the oligo tube. There you will find the actual yield of the oligonucleotide synthesis in three forms: optical density units (OD); mass (in mg); and copy number (in nmole)

1. **To prepare a 100µM stock:**
µl TE needed = 10 X nanomoles of oligo (as printed on spec sheet)
example: 500µl TE + 50nmole oligo = 100µM stock
2. **To prepare working solutions:**
Dilute stock 1:10 in water = 10µM oligo
1µl working solution in 20µl reaction volume = 0.5µM = 10picomoles primer
Mass units: use milligram amounts on the spec sheet provided to make the stock solution.

Resuspension buffers:

IDT strongly recommends TE buffer (or some other pH-controlled buffer) for resuspending oligos. Resuspending oligos in water will allow the solution to become acidic, causing acid-nicking of the phosphodiester backbone, and thereby decreasing the half-life of the oligos. pH controlled buffers help maintain an ideal pH for handling oligos (pH 7.5-8.0) which will allow the oligos to remain stable and maintain their structural integrity.

Use of DEPC water is strongly discouraged for several reasons. DEPC (Diethyl Pyrocarbonate) is carcinogenic. It also has a strong affinity for adenosine, and even trace amounts will result in chemical modification of adenine residues. DEPC is reactive with primary amine groups and mercaptans. In addition, DEPC should never be added to buffers that contain TRIS (tris(hydroxymethyl)AMINOMethane). In addition, DEPC is hard to remove and interferes with PCR and other reactions.

Whitehead Scientific
Western Cape, Eastern Cape, Export • (Tel) 021 944 6460 • (fax) 021 949 5478
Gauteng, KZN, Free State, Limpopo • (Tel) 011 894 2214 • (fax) 011 894 4583
PO Box 194, Brackenfell, 7561, South Africa
whitesci@whitesci.co.za • www.whitesci.co.za

Stock solution

Make up small aliquots of stock solution rather than maintaining one large stock. Incomplete thawing of a sample can lead to inconsistent concentrations being pulled from the stock tube, so thaw the stock completely each time a working solution is made up. Repeated freeze/thaw cycles are not good for an oligo, aliquots should be small enough to not thaw the tube more than 3-4 times.

Material can be lost due to absorption of the oligo to the tube if polystyrene tubes are used. The use of polypropylene tubes is preferred.

Resuspension of hard-to-suspend Oligos

Heat the oligonucleotide at 55°C for 1–5 minutes, then vortex thoroughly. If there is still a visible precipitate in the tube, the sample may contain silica which is a by-product of oligo synthesis. It will not affect the performance of the product, and may be removed through filtration or decanting the supernatant.

Oligonucleotide Storage

Long-term storage:

If you would like to use a portion of the oligonucleotide immediately and then store the remaining mass for future use, it is best to resuspend the entire product in TE (Tris-EDTA, pH 8.0) at the desired stock solution concentration. Take a sufficient volume for immediate use from this stock and dilute it to a working stock concentration. The remaining oligonucleotide solution can be treated in one of two ways for subsequent long-term storage. The ideal situation is to dry the DNA down and store it at -20°C. If this is not practical, then the next best thing is to make small aliquots of the stock suspension and store these at -20°C. Creating aliquots will allow you to avoid potential contamination from use of a single tube. DNA kept frozen in nuclease-free environment should be stable for years.

Short-term storage:

Never store dilute solutions of DNA at 4°C for extended periods of time (ie more than one day). In dilute concentrations <1µM, the DNA can adsorb onto the plastic of the tube, changing the concentration of the solution.

Short-term storage of concentrated stock solution of oligonucleotides at 4°C is acceptable as long as this does not exceed 7 months.

Build on Quality You can Trust!



Whitehead Scientific
Western Cape, Eastern Cape, Export • (tel) 021 944 6460 • (fax) 021 949 5478
Gauteng, KZN, Free State, Limpopo • (tel) 011 894 2214 • (fax) 011 894 4583
PO Box 194, Brackenell, 7561, South Africa
whitehead@whitesci.co.za • www.whitesci.co.za

Appendix B

Electronic Component Datasheets

All electronic component datasheets can be found by following the corresponding URL provided.

B.1 ON Semiconductor, 9V Regulator, MC7800

<https://www.onsemi.com/pub/Collateral/MC7800-D.PDF>

B.2 Texas Instruments, 5V Precision Regulator, LM4120

<http://www.ti.com/lit/ds/symlink/lm4120.pdf>

B.3 Microchip, 3.3V Precision Regulator, MCP1501

<http://www.mouser.com/ds/2/268/20005474B-875837.pdf>

B.4 Texas Instruments, Adjustable Constant Current Source, LM334

<http://www.ti.com/lit/ds/symlink/lm334.pdf>

B.5 Analog Devices, Single-Supply Input/Output Operational Amplifier, AD8629

http://www.analog.com/media/en/technical-documentation/data-sheets/AD8628_8629_8630.pdf

B.6 Linear Technology, 24-bit-2 channel-Analogue to Digital Converter, LTC2402

<http://cds.linear.com/docs/en/datasheet/24012f.pdf>

B.7 Analog Devices, Programmable CMOS linear regulator, ADP123

http://www.analog.com/media/en/technical-documentation/data-sheets/ADP122_123.pdf

B.8 Texas Instruments, Precision Timers, NE555PWR

<http://www.ti.com/lit/ds/symlink/ne555.pdf>

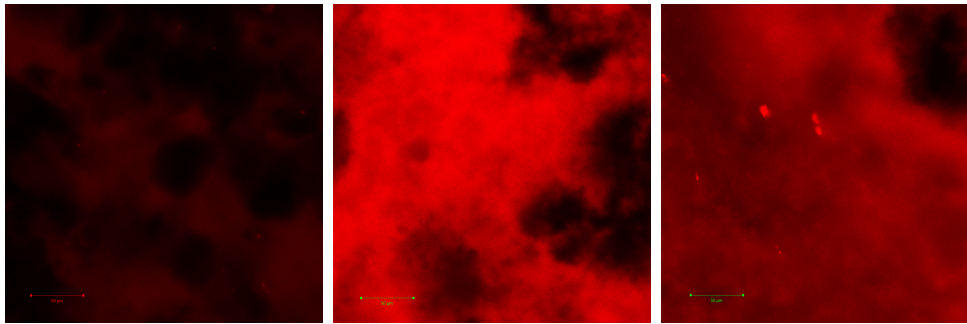
B.9 Harwin, 3mm Pitch Spring Test Probe with Concave Tip

<http://docs-europe.electrocomponents.com/webdocs/1508/0900766b81508754.pdf>

Appendix C

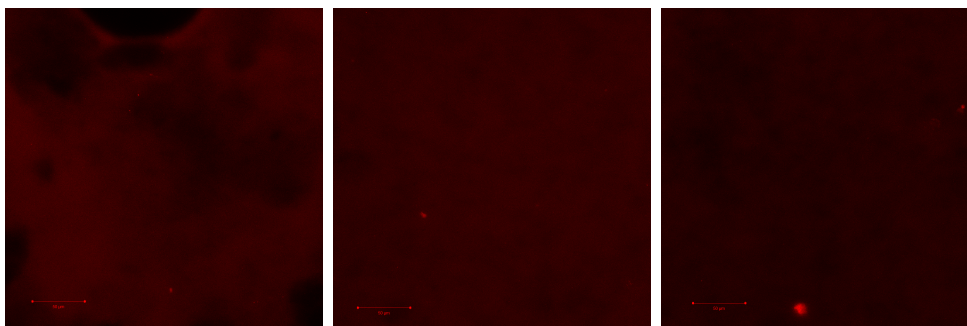
Failed Hairpin Probe Experiments

In Chapter 10, it was discussed that the FL probes began to yield unexpected results. In this chapter the failed experiments will be briefly discussed. As mentioned previously, it is expected that when there is no target DNA present, the hairpin probes should be closed and the fluorescent signal should be low. It is then expected that with an increase in temperature, the fluorescent signal should begin to increase as the hairpins begin to open. When target DNA is added it is expected that the fluorescent signal should greatly increase at any temperature in comparison to the FL probe alone. CNF samples were prepared with FL probe the day before and left overnight. Target DNA was then incubated the day of confocal imaging. The target DNA was incubated with the immobilized FL probe for 1 hour at 37°C. Confocal images were taken using a Zeiss LSM780 confocal microscopy system belonging to the CAF unit of Stellenbosch University. It was possible to obtain images at specific user defined temperatures and so images of the samples were recorded at 25°C, 37°C and 50°C. Figure C.1 and Figure C.2 show that the reverse of the expected results are seen. The experiments with FL probe and target DNA yield lower fluorescence signal than that of experiments with FL probe only. These experiments were repeated multiple times. 50°C incubation temperature was also tested with very similar results. Although the hairpin operation testing failed, these tests did confirm the positive binding of the gold-thiol reaction.



(a) Imaged at 25°C. (b) Imaged at 37°C. (c) Imaged at 50°C.

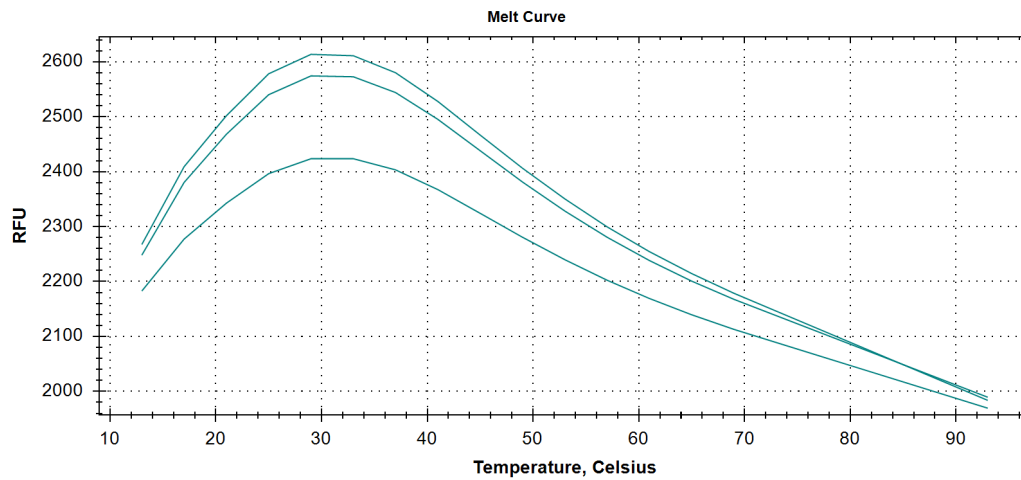
Figure C.1: Failed confocal experiment, FL probe only, incubated at 37°C.



(a) Imaged at 25°C. (b) Imaged at 37°C. (c) Imaged at 50°C.

Figure C.2: Failed confocal experiment, FL probe and target, incubated at 37°C.

Due to the above failed experiments, it was then decided to validate the hairpin probe operation in solution via qPCR. Figure C.3 shows the results of a qPCR measurement of the FL probe alone. It can be seen that the fluorescent signal reaches a maximum value at 29°C and thereafter drops dramatically. Figure C.4 shows that with the addition of target DNA, there is no significant change in fluorescent response, indicating that there is no target DNA to hairpin probe hybridization. These results are vastly different in comparison to the expected results seen in Section 10.2.3. It was determined that the initial TE buffer used for experiments were the reason for the failed experiments. The TE buffer was produced with 10mM Tris and 1mM EDTA, both of which dissolved from a solid powder. It is assumed that either the TE buffer was contaminated with nuclease or the salt concentration was not optimal. The issues seen were resolved by using specifically nuclease free solutions as well as pre-ordered tris buffer as described in the qPCR protocol (Appendix D.9). Due to the fact that the FL probe was resuspended in the initial TE buffer, the FL probe continues to degrade when aliquotes are thawed before use.



(a) Melt Curve

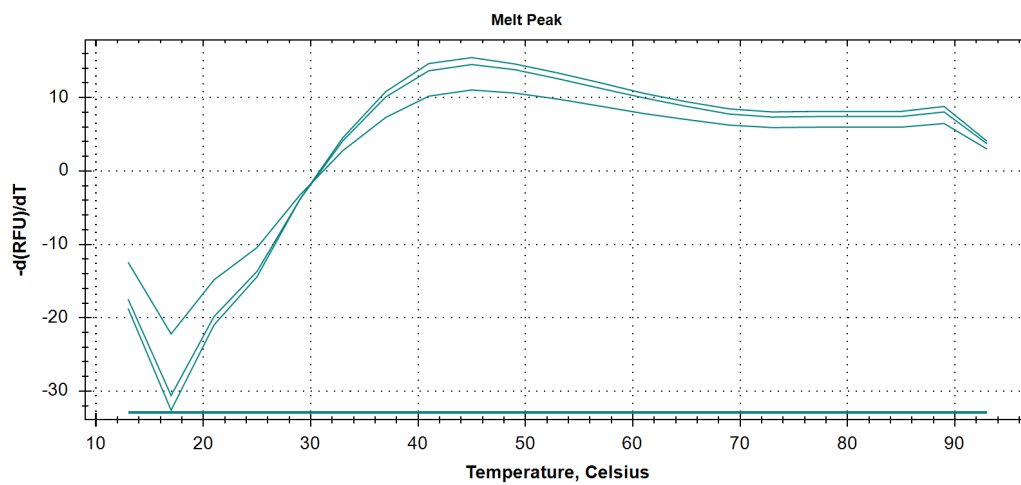
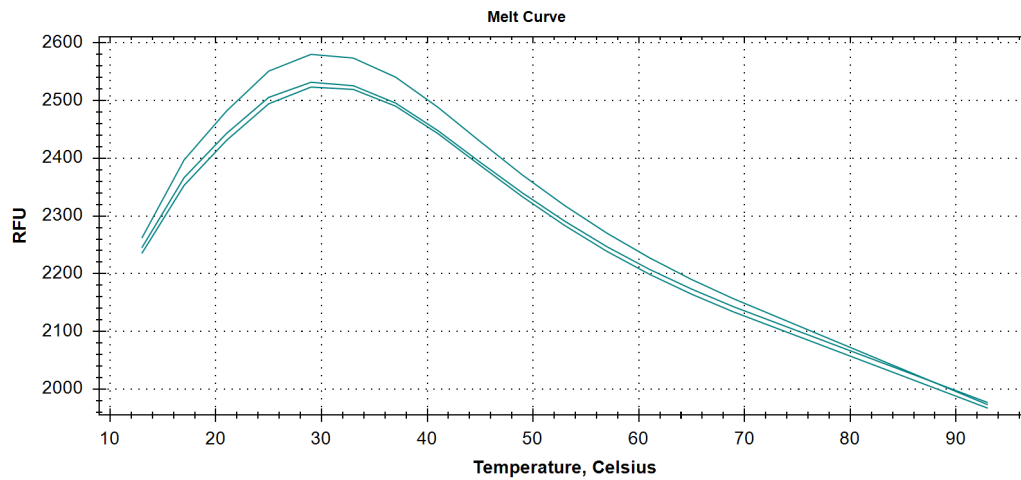
(b) Derivative curve $-d(\text{RFU})/dT$

Figure C.3: Failed qPCR experiment, FL probe only



(a) Melt Curve

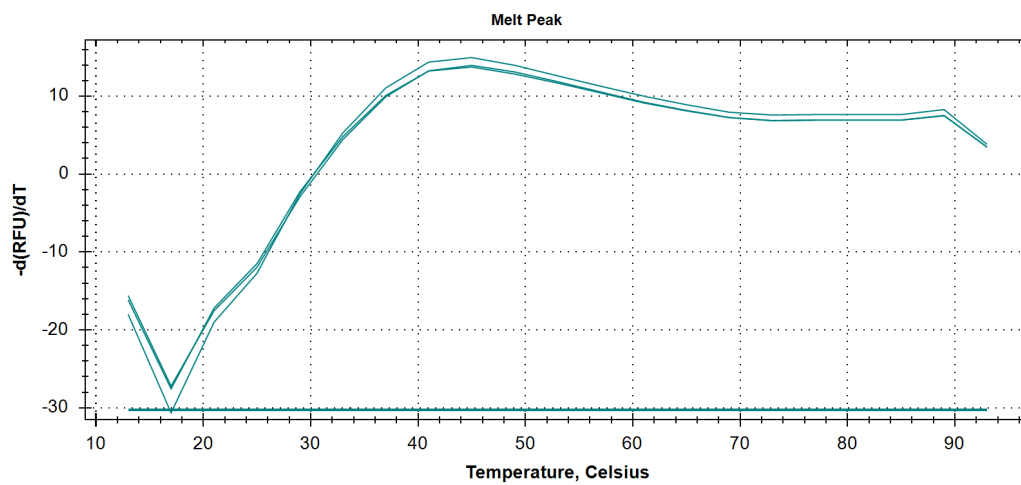
(b) Derivative curve $-d(\text{RFU})/dT$

Figure C.4: Failed qPCR experiment, FL probe and target DNA

Appendix D

Protocols

D.1 Immobilization Protocol

The basic immobilization steps are as follows:

1. Gold coated CNF samples prepared and ready for use.
2. Hairpin probe DNA resuspended in Tris buffer to produce stock solution.
3. Dilute stock solution of hairpin probe DNA to desired concentration in Tris buffer.
4. Rinse CNFs in Tris buffer three times and placed in immobilization bath.
5. 50 μL of desired probe concentration placed on individual CNFs.
6. Immobilization bath covered in foil and placed in oxidation chamber overnight (12h+) under 100% relative humidity.
7. Target DNA resuspended in Tris buffer.
8. Target DNA diluted to desired concentration in Tris buffer.
9. CNFs individually rinsed three times in Tris buffer by dipping continuously.
10. CNFs placed in clean immobilization bath or test bath.

During preparation for confocal microscopy, selected CNFs have 50 μL target DNA placed at desired concentration. The remaining CNFs are left without target or are control samples with no DNA present at all. All CNFs are left in a 30°C environment for 1.5h and thereafter taken for imaging. During electronic testing, the electronic test protocol is followed (Appendix D.8).

D.2 Stock Reagents

$$C1 \times V1 = C2 \times V2 \quad (\text{D.2.1})$$

D.2.1 Nuclease-Free Water

Nuclease-Free water from QIAGEN was used. Cat. No. 129114, 10 x 50 ml nuclease-free water was prepared without the use of diethylpyrocarbonate (DEPC); provided in 10 x 50 plastic tubes.

D.2.2 Tris Buffer Protocol

T2444 Trizma hydrochloride solution was used as the base for all tris buffer and dilutions of reagents. BioPerformance Certified, pH 7.6, 1 M, is suitable for cell culture.

Trizma is a Pre-mixed solution of TRIZMA Base and TRIZMA HCl to provide commonly used pH values for Tris buffers. The stock comes in 1mM concentration and the desired tris buffer concentration is 5mM. Using the common dilution equation seen in Equation (D.2.1), the desired volume of Trizma and nuclease free water can be calculated to dilute the tris buffer. It was decided that a diluted solution of 10mL would be required therefore from Equation (D.2.2), it can be seen that 50 μL of Trizma is required. In order to calculate the amount of nuclease free water, the Trizma volume is simply subtracted from the total desire volume (10 mL - 50 μL = 9.95 mL).

$$\begin{aligned} C1 \times V1 &= C2 \times V2 \\ 1000mM \times V1 &= 5mM \times 10mL \\ V1 &= 0.05mL \\ V1 &= 50\mu L \end{aligned} \quad (\text{D.2.2})$$

D.3 TE Buffer Protocol

500mL of 1xTE buffer was prepared with 10mM Tris (Tris Base $C_4H_{11}NO_3$, Crystals) and 1mM EDTA(Na^+). The Tris has a $Mr = 121.1$ and the EDTA a $Mr = 372.24$. Using Equation (D.3.1) and Equation (D.3.2), the desired weight of both Tris and EDTA can be calculated.

$$n = \frac{m}{Mr}$$

n = moles of substance being dissolved
 m = mass in grams (g)
 Mr = relative molecular mass

(D.3.1)

$$C = \frac{n}{V}$$

C = concentration of solution in mol (M)
 n = moles of substance being dissolved
 V = volume of solution in litres (L)

(D.3.2)

Tris calculations:

$$n = V \times C$$

$$n = 500mL \times 10mM$$

$$n = 0.005$$
(D.3.3)

$$m = n \times Mr$$

$$m = 0.005 \times 121.1$$

$$m = 0.6055g$$
(D.3.4)

EDTA calculations:

$$n = V \times C$$

$$n = 500mL \times 1mM$$

$$n = 0.0005$$
(D.3.5)

$$m = n \times Mr$$

$$m = 0.0005 \times 372.24$$

$$m = 0.18612g$$
(D.3.6)

The resulting TE buffer had an initial pH of 9.3. A concentrated HCl solution was slowly added until a pH of 8 was reached.

D.4 Fluorescent Probe DNA Resuspension

It can be seen in Appendix A.3 that a 100 μ M stock solution can be prepared by the addition of 390 μ L buffer. As mentioned, the FL probe was resuspended in TE buffer which unfortunately caused the FL probe to degrade.

D.5 Ferrocene Probe DNA Resuspension

It can be seen in Appendix A.4 that the FE probe was delivered in a 0.305 μmole yield. Using the advice for resuspension from Appendix A.3, the required Tris buffer volume can be calculated to generate a 100 μM stock concentration of FE probe.

$$\begin{aligned} \text{Tris volume}(\mu L) &= 10 \times \text{nanomoles of oligo} \\ &= 10 \times 304 \\ &= 0.05\text{mL} \\ &= 3.04\text{mL} (100\mu\text{M stock}) \end{aligned} \tag{D.5.1}$$

It was decided that a 1000 μM stock should be prepared instead. The Tris volume required was divided by 10, therefore 304 μL of Tris buffer was required.

D.6 Stock Solution Dilutions

In order to dilute stock hairpin probe and target DNA to the desired concentrations, a final solution is decided and the common dilution equation seen in Equation (D.2.1) is used. An example of a 100 μM stock dilution to a 100 μL volume at 10 μM concentration is shown in Equation (D.6.1).

$$\begin{aligned} C1 \times V1 &= C2 \times V2 \\ 100\mu\text{M} \times V1 &= 10\mu\text{M} \times 100\mu\text{L} \\ V1 &= 10\mu\text{L} \text{ (Required volume of stock solution)} \\ \text{Tris volume} &= 100\mu\text{L} - 10\mu\text{L} \\ \text{Tris volume} &= 90\mu\text{L} \end{aligned} \tag{D.6.1}$$

D.7 Bath Wash Protocol

Before every experiment, the test baths and immobilization baths were fully washed to remove all DNA and to sterilize the baths to avoid contamination during testing. The wash steps are as follows:

1. Rinse in tap water.
2. Leave in NaOH solution 10 minutes.
3. Rinse in tap water.
4. Leave in JIK solution for 10 minutes.

5. Rinse in tap water.
6. Wash with soap and hot water.
7. Rinse in tap water.
8. Rinse in 70% Ethanol.
9. Rinse in MilliQ DI water.
10. Wrap in foil.
11. Autoclave
12. Dry in 60°C oven.

NaOH is used to denature any remaining DNA left in the baths. The NaOH is prepared by adding 4g of NaOH crystals to 500ml of DI water. JIK is used to properly clean and bleach the baths. The soap and hot water are used to remove any NaOH and JIK that may have remained. Ethanol is used to remove soap and any marking made by marker pens and finally DI water is used as the last rinse step. The autoclave is used as a final sterilization step before the baths are used again.

D.8 Electronic Test Protocol

After step 10 of the immobilization protocol. The fibers are ready for electronic testing. The Electronic test protocol will be briefly described.

1. Step 10 of immobilization protocol completed (Appendix D.1).
2. Test Baths cleaned using bath wash protocol (Appendix D.7).
3. PC and electronic system setup in 30°C 20min before first test. This is to allow the test bath to reach 30°C as well.
4. 100 μL Tris buffer placed in eppendorf tube and left in 30°C with electronics.
5. Target DNA dilution prepared.
6. A single CNF with probe DNA placed in test bath.
7. 10 μL Tris buffer placed on center of CNF. This is done to ensure Tris saturation which reduces signal noise when target DNA is placed and also insured DNA hydration to avoid degradation.
8. Test bath lid is placed and fastened.

9. System is left for 10 minutes to allow CNF fibers to settle due to physical pressure of the electronic spring test probes.
10. Remaining untested CNFs are put on ice to avoid evaporation.
11. The Biosensor software is opened with all test details filled in.
12. "Base resistance" is clicked and "Read Sample" is begun directly after.
13. System reads sample and displays for 10 minutes.
14. A note is left on the software just **before** the target is added in order to post-process data with and without target.
15. 50 μ L Target DNA at desired concentration is placed in hole of test bath lid.
16. System continues to read until timer has stopped. The maximum deviance is calculated and all data saved.

D.9 qPCR Preparation Protocol

The qPCR experiment protocol will be briefly described in this section. 10 different tests were conducted all in triplicate and all simultaneously. The tests were grouped in 4 main categories labelled A-D. The tests in group A are all FL probe based tests, group B are FE probe based tests, group C are target DNA based tests and group D are control tests to ensure the SYBR Green dye was operating correctly.

| | 1 | 2 | 3 | 4 | 5 | 6 | 7 | 8 | 9 | 10 | 11 | 12 |
|---|----|----|----|----|----|----|----|----|----|----|----|----|
| A | A1 | A1 | A1 | B1 | B1 | B1 | C1 | C1 | C1 | D1 | D1 | D1 |
| B | A2 | A2 | A2 | B2 | B2 | B2 | C2 | C2 | C2 | D2 | D2 | D2 |
| C | A3 | A3 | A3 | B3 | B3 | B3 | | | | | | |
| D | | | | | | | | | | | | |
| E | | | | | | | | | | | | |
| F | | | | | | | | | | | | |
| G | | | | | | | | | | | | |
| H | | | | | | | | | | | | |

Table D.1: 96 well CFX qPCR Plate Setup.

Before the test samples were placed in the CFX plates, reagents needed to be prepared in order to make master-mixes for each test triplicate. Each of these reagents will be briefly discussed. The Tris buffer was described in Appendix D.2.2.

D.9.0.1 SYBR Green Master Mix

KAPA SYBR® FAST qPCR Master Mix (2X) kit - kk4602 was used as the detectable SYBR Green dye. Due to the fact that the master mix is already in a 2X concentration, the SYBR Green was only diluted to 1X when added to the final CFX qPCR plates.

D.9.0.2 Fluorescent Hairpin Probe DNA

The FL probe was resuspended in 100 μM stock aliquots. The stock solution was diluted to a 10 μM master mix which would then be further diluted to a 1 μM concentration in the qPCR plates. It was determined that at least 30 μL of 10 μM FL probe solution would be needed to conduct all necessary tests, this includes adjustments for pipetting error, therefore the required volume of 100 μM FL probe and tris buffer can be calculated as seen in Equation (D.9.1):

$$\begin{aligned}
 C1 \times V1 &= C2 \times V2 \\
 100\mu\text{M} \times V1 &= 10\mu\text{M} \times 30\mu\text{L} \\
 V1 &= 3\mu\text{L} \text{ (100}\mu\text{M FL probe)} \\
 \text{Tris volume} &= 30\mu\text{L} - 3\mu\text{L} \\
 &= 27\mu\text{L}
 \end{aligned} \tag{D.9.1}$$

The result is 30 μL of a 10 μM FL probe concentration.

D.9.0.3 Ferrocene Hairpin Probe DNA

The FE probe was resuspended in 1mM (1000 μM) stock aliquots. The stock solution was diluted to a 10 μM master mix which would then be further diluted to a 1 μM concentration in the qPCR plates. It was determined that at least 30 μL of 10 μM FE probe solution would be needed to conduct all necessary tests. Due to the fact that the stock concentration is relatively high, to avoid pipetting error, it was decided that at least 100 μL of 10 μM FE probe would be prepared and any unused solution would be kept for future tests, therefore the required volume of 1mM FE probe and tris buffer can be calculated as seen in Equation (D.9.2):

$$\begin{aligned}
 C1 \times V1 &= C2 \times V2 \\
 1000\mu\text{M} \times V1 &= 10\mu\text{M} \times 100\mu\text{L} \\
 V1 &= 1\mu\text{L} \text{ (1000}\mu\text{M FE probe)} \\
 \text{Tris volume} &= 100\mu\text{L} - 1\mu\text{L} \\
 &= 99\mu\text{L}
 \end{aligned} \tag{D.9.2}$$

The result is 100 μL of a 10 μM FE probe concentration.

D.9.0.4 Target DNA

The target DNA was resuspended in 100 μM stock aliquots. The stock solution was diluted to a 10 μM master mix which would then be further diluted to a 3 μM concentration in the qPCR plates to ensure that there was more than enough target DNA to hybridize to the probe DNA. It was determined that at least 36 μL of 10 μM target DNA solution would be needed to conduct all necessary tests, this includes adjustments for pipetting error, therefore the required volume of 100 μM FL probe and tris buffer can be calculated as seen in Equation (D.9.2):

$$\begin{aligned}
 C1 \times V1 &= C2 \times V2 \\
 100\mu\text{M} \times V1 &= 10\mu\text{M} \times 36\mu\text{L} \\
 V1 &= 3.6\mu\text{L} \text{ (100}\mu\text{M target DNA)} \\
 \text{Tris volume} &= 36\mu\text{L} - 3.6\mu\text{L} \\
 &= 32.4\mu\text{L}
 \end{aligned}
 \tag{D.9.3}$$

The result is 36 μL of a 10 μM target DNA concentration.

D.9.0.5 Target PCR Product

The Virology Department of Stellenbosch University provided a linear standard PCR product to also be tested as a template to the hairpin probes. Theoretically the PCR should produce a high concentration of ssDNA that is complimentary to the hairpin probes. Due to the fact that the PCR product is an amplified solution, the exact concentration is unknown but would be a relatively high concentration above 50 μM . It was decided that the linear PCR product would be 4X diluted for these tests

D.9.0.6 Genomic Control dsDNA

Random non-human genomic dsDNA was provided to be used as a control test to ensure the operation of the SYBR Green dye. This was very long dsDNA that would provide a positive SYBR Green signal after the 95°C heat step. After the test was complete, it was seen that there was a clear melt curve of the genomic dsDNA and thus the SYBR Green was operating correctly.

Bibliography

- [1] BioSure, “WHY TEST FOR HIV.” [Online]. Available: <http://www.hivselftest.co.za/why-test-for-hiv>
- [2] N. Bhalla, P. Jolly, N. Formisano, and P. Estrela, “Introduction to biosensors,” *Essays in Biochemistry*, vol. 60, pp. 1–8, 2016. [Online]. Available: <https://www.ncbi.nlm.nih.gov/pmc/articles/PMC4986445/pdf/bse0600001.pdf>
- [3] I. Palchetti and M. Mascini, “Amperometric Biosensors for Pathogenic Bacteria Detection.pdf,” in *Principles of Bacterial Detection: Biosensors, Recognition Receptors and Microsystems*, M. Zourob, A. Turner, and S. Elwary, Eds. Springer, 2008, ch. 13, pp. 299–312.
- [4] A. Dr Mandal, “Biosensor Applications,” 2017. [Online]. Available: <http://www.news-medical.net/health/Biosensor-Applications.aspx>
- [5] M. B. Maas, “Michael Benjamin Maas,” Masters, Stellenbosch University, 2015.
- [6] S. Cagnin, M. Caraballo, C. Guiducci, P. Martini, M. Ross, M. Santaana, D. Danley, T. West, and G. Lanfranchi, “Overview of electrochemical DNA biosensors: new approaches to detect the expression of life.” *Sensors*, vol. 9, no. 4, pp. 3122–48, 2009. [Online]. Available: <http://www.pubmedcentral.nih.gov/articlerender.fcgi?artid=3348825&tool=pmcentrez&rendertype=abstract>
- [7] www.merriam-webster.com, “Enzyme | Definition of Enzyme by Merriam-Webster,” 2017. [Online]. Available: <https://www.merriam-webster.com/dictionary/enzyme>
- [8] J. P. Chambers, B. P. Arulanandam, L. L. Matta, A. Weis, and J. J. Valdes, “Biosensor recognition elements,” *Current Issues in Molecular Biology*, vol. 10, no. 1, pp. 1–12, 2008.
- [9] P. Damborský, J. Švitel, and J. Katrlík, “Optical biosensors.” *Essays in biochemistry*, vol. 60, no. 1, pp. 91–100, jun 2016. [Online]. Available: <http://www.ncbi.nlm.nih.gov/pubmed/27365039>

- [10] E. Hitt, “Label-Free Methods Are Not Problem Free,” 2017. [Online]. Available: https://cml.harvard.edu/assets/DrugDiscDev_Sep04.pdf
- [11] X. Muñoz-Berbel, N. Godino, O. Laczka, E. Baldrich, F. X. Muñoz, and F. J. Del Campo, “Impedance Based Biosensors for Pathogen Detection.pdf,” in *Principles of Bacterial Detection: Biosensors, Recognition Receptors and Microsystems*, M. Zourob, A. Turner, and S. Elwary, Eds. Springer, 2008, ch. 15, pp. 341–376.
- [12] Elearning.kocw.net, “Transducers in Biosensors I,” 2017. [Online]. Available: http://elearning.kocw.net/document/wcu/2009/23/01/01/23_01_01_04_Week4_Biosensors_28Sep2009_TransducersI.pdf
- [13] M. Chaplin, “Optical biosensors,” 2017. [Online]. Available: <http://www1.lsbu.ac.uk/water/enztech/optical.html>
- [14] P. N. Patel, V. Mishra, and A. S. Mandloi, “Optical Biosensors : Fundamentals & Trends,” *Journal of Engineering Research and Studies*, vol. I, no. I, pp. 15–34, 2010.
- [15] 2009.igem.org, “Team:UAB-Barcelona/Project - 2009.igem.org,” 2017. [Online]. Available: <http://2009.igem.org/Team:UAB-Barcelona/Project>
- [16] L. Farris, M. Habteselassie, and L. Perry, “Luminescence techniques for the detection of bacterial pathogens,” in *Principles of Bacterial Detection: Biosensors, Recognition Receptors and Microsystems*, M. Zourob, A. Turner, and S. Elwary, Eds. Springer, 2008, pp. 213–230. [Online]. Available: http://link.springer.com/chapter/10.1007/978-0-387-75113-9_10
- [17] www.pharmatutor.org, “Applications of Biosensors technology : Future trends development and new intervention in biotechnology | Page 3 | PharmaTutor.” [Online]. Available: <http://www.pharmatutor.org/articles/applications-of-biosensors-technology-future-trends-development-and-new-intervention-in-biotechnology?page=2>
- [18] D. Grieshaber, R. Mackenzie, J. Vörös, and E. Reimhult, “Electrochemical Biosensors -Sensor Principles and Architectures,” *Sensors*, vol. 8, no. March, pp. 1400–1458, 2008.
- [19] D. Thevenot, K. Toth, R. Durst, G. Wilson, D. Thevenot, K. Toth, R. Durst, and G. Wilson, “Electrochemical biosensors : recommended definitions and classification To cite this version : Technical report Electrochemical biosensors : recommended definitions and,” *Biosensors and Bioelectronics*, vol. 16, pp. 121–131, 2001.

- [20] Www.kln.ac.lk, “Polarography and Voltammetry,” 2017. [Online]. Available: http://www.kln.ac.lk/science/Chemistry/Teaching_Resources/Documents/PlarographyandVoltammetry.pdf
- [21] J. Moldenhauer, “Overview of Rapid Microbiological Methods,” in *Principles of Bacterial Detection: Biosensors, Recognition Receptors and Microsystems*, M. Zourob, A. Turner, and S. Elwary, Eds. Springer, 2008, ch. 4, pp. 49–79.
- [22] P. P. Banada and A. K. Bhunia, “Antibodies and Immunoassays for Detection of Bacterial Pathogens,” in *Principles of Bacterial Detection: Biosensors, Recognition Receptors and Microsystems*, M. Zourob, A. Turner, and S. Elwary, Eds., 2008, ch. 21, pp. 567–602. [Online]. Available: http://link.springer.com/10.1007/978-0-387-75113-9_21
- [23] Www.aids.gov, “What Is HIV/AIDS?” 2017. [Online]. Available: <https://www.aids.gov/hiv-aids-basics/hiv-aids-101/what-is-hiv-aids/>
- [24] Www.avert.org, “How HIV infects the body and the lifecycle of HIV | AVERT,” 2017. [Online]. Available: <http://www.avert.org/about-hiv-aids/how-infects-body>
- [25] Aidsinfo.nih.gov, “The HIV Life Cycle | Understanding HIV/AIDS | AIDSinfo,” 2017. [Online]. Available: <https://aidsinfo.nih.gov/education-materials/fact-sheets/19/73/the-hiv-life-cycle>
- [26] Www.webmd.com, “HIV Tests for Diagnosis: Antibody Tests, Antigen Tests, and More,” 2017. [Online]. Available: <http://www.webmd.com/hiv-aids/guide/hiv-aids-screening#1>
- [27] Www.thermofisher.com, “Overview of ELISA,” 2017. [Online]. Available: <https://www.thermofisher.com/za/en/home/life-science/protein-biology/protein-biology-learning-center/protein-biology-resource-library/pierce-protein-methods/overview-elisa.html>
- [28] Hivinsite.ucsf.edu, “HIV Antibody Assays,” 2017. [Online]. Available: <http://hivinsite.ucsf.edu/InSite.jsp?page=kb-02-02-01>
- [29] —, “What kinds of HIV screening tests are available in the United States?” 2017. [Online]. Available: <http://hivinsite.ucsf.edu/insite?page=basics-01-01>
- [30] —, “HIV InSite Gateway to HIV and AIDS Knowledge,” 2017. [Online]. Available: <http://hivinsite.ucsf.edu/InSite-KB-ref.jsp?page=kb-02-02-01&ref=kb-02-02-01-fg-01&no=1>

- [31] I-base.info, “Appendix 3: How HIV tests work | Guides | HIV i-Base,” 2017. [Online]. Available: <http://i-base.info/guides/testing/appendix-3-how-hiv-tests-work>
- [32] Wwww.emedicinehealth.com, “Polymerase Chain Reaction: PCR Facts on Test and Steps,” 2017. [Online]. Available: http://www.emedicinehealth.com/pcr_polymerase_chain_reaction_test/article_em.htm
- [33] —, “PCR (Polymerase Chain Reaction) Causes, Symptoms, Treatment - How is PCR (polymerase chain reaction) done? - eMedicine-Health,” 2017. [Online]. Available: http://www.emedicinehealth.com/pcr_polymerase_chain_reaction_test/page2_em.htm
- [34] Wwww.uniteforsight.org, “Challenges and Failures of HIV Screening With Rapid Tests.” [Online]. Available: <http://www.uniteforsight.org/health-screenings/hiv>
- [35] Livescience.com, “DNA: Definition, Structure and Discovery, What Is DNA?” 2013. [Online]. Available: <https://www.livescience.com/37247-dna.html>
- [36] Thefreedictionary.com, “DNA - definition of DNA by The Free Dictionary.” [Online]. Available: <http://www.thefreedictionary.com/DNA>
- [37] B. Alberts, A. Johnson, J. Lewis, M. Raff, K. Roberts, and P. Walter, “Molecular biology of the cell,” 2002. [Online]. Available: <https://seqcore.brcf.med.umich.edu/sites/default/files/html/educ/dnapr/mbglossary/mbgloss.html>
- [38] Leslie A. Pray, “Discovery of DNA Double Helix: Watson and Crick | Learn Science at Scitable.” [Online]. Available: <https://www.nature.com/scitable/topicpage/discovery-of-dna-structure-and-function-watson-397>
- [39] Learn.genetics.utah.edu, “viruses.” [Online]. Available: <http://learn.genetics.utah.edu/content/microbiome/intro/images/viruses.jpg>
- [40] [Http://learn.genetics.utah.edu](http://learn.genetics.utah.edu), “What are Microbes?” [Online]. Available: <http://learn.genetics.utah.edu/content/microbiome/intro/>
- [41] “Melting point and thermodynamics of double-stranded DNA (practice) | Khan Academy.” [Online]. Available: <https://www.khanacademy.org/test-prep/mcat/physical-sciences-practice/physical-sciences-practice-tut/e/melting-point-and-thermodynamics-of-double-stranded-dna-1>

- [42] [Http://www.austincc.edu](http://www.austincc.edu), “MLAB 2378 Fundamentals of Molecular Diagnostics Links.” [Online]. Available: http://www.austincc.edu/mlt/mdfund/mdfund_unit9assignmentsMeltingTemperature.html
- [43] [Eu.idtdna.com](http://eu.idtdna.com), “PRODUCT.” [Online]. Available: <https://eu.idtdna.com/pages/support/technical-vault/faq/product/what-are-self--and-homo-dimers-and-how-do-i-select-primers-to-avoid-these-problems->
- [44] M. Rahman, X.-B. Li, N. Lopa, S. Ahn, and J.-J. Lee, “Electrochemical DNA Hybridization Sensors Based on Conducting Polymers,” *Sensors*, vol. 15, no. 2, pp. 3801–3829, 2015. [Online]. Available: <http://www.mdpi.com/1424-8220/15/2/3801/>
- [45] Y. Guo, J. Chen, and G. Chen, “A label-free electrochemical biosensor for detection of HIV related gene based on interaction between DNA and protein,” *Sensors and Actuators B: Chemical*, vol. 184, pp. 113–117, 2013.
- [46] Y. Fu, R. Yuan, Y. Chai, L. Zhou, and Y. Zhang, “Coupling of a Reagentless Electrochemical DNA Biosensor with Conducting Polymer Film and Nanocomposite as Matrices for the Detection of the HIV DNA Sequences,” *Analytical Letters*, vol. 39, no. 3, pp. 467–482, feb 2006. [Online]. Available: <http://www.tandfonline.com/doi/abs/10.1080/00032710500536012>
- [47] E. Skotadis, K. Voutyras, M. Chatzipetrou, G. Tsekenis, L. Patsiouras, L. Madianos, S. Chatzandroulis, I. Zergioti, and D. Tsoukalas, “Label free DNA biosensor based on resistance change of platinum nanoparticles assemblies,” *Biosensors and Bioelectronics*, vol. 81, pp. 388–394, 2016. [Online]. Available: <http://dx.doi.org/10.1016/j.bios.2016.03.028>
- [48] C. Viviers, “Development of a Resistive Microfluidic Sensing Device for Pathogen Detection by,” Undergraduate Project, University of Stellenbosch, 2015.
- [49] E. Alocilja and Z. Muhammad-Tahir, “Label-Free Microbial Biosensors Using Molecular Nanowire Transducers,” *Principles of Bacterial Detection: Biosensors, Recognition Receptors and Microsystems*, pp. 377–413, 2008.
- [50] A. Touhami, “Biosensors and Nanobiosensors: Design and Applications,” *Nanomedicine*, pp. 374–400, 2015.
- [51] D. Aussawasthien, “Electrospun Conducting Nanofiber Based Materials and Their Characterizations: Effects of Fiber Characteristics on Properties and Applications a,” Ph.D. dissertation, The University of Akron, 2006.

- [52] S. E. Baker, K. Y. Tse, E. Hindin, B. M. Nichols, T. L. Clare, and R. J. Hamers, “Covalent functionalization for biomolecular recognition on vertically aligned carbon nanofibers,” *Chemistry of Materials*, vol. 17, no. 20, pp. 4971–4978, 2005.
- [53] Pyrografproducts.com, “Pyrograf®-III Carbon Nanofiber, Stacked-Cup Carbon Nanotubes: PR-19-XT-LHT.” [Online]. Available: <http://pyrografproducts.com/carbon-nanotubes/PR-19-XT-LHT.html>
- [54] —, “Pyrograf®-III Carbon Nanofiber, Stacked-Cup Carbon Nanotubes.” [Online]. Available: http://pyrografproducts.com/Merchant5/merchant.mvc?Screen=cp_nanofiber
- [55] L. Matlock-Colangelo and A. J. Baeumner, “Recent progress in the design of nanofiber-based biosensing devices,” *Lab on a Chip*, vol. 12, no. 15, p. 2612, 2012. [Online]. Available: <http://xlink.rsc.org/?DOI=c2lc21240d>
- [56] [Http://i-base.info](http://i-base.info), “Appendix 1: Different types of HIV test | Guides | HIV i-Base.” [Online]. Available: <http://i-base.info/guides/testing/appendix-1-different-types-of-hiv-test>
- [57] [Www.trilinkbiotech.com](http://www.trilinkbiotech.com), “Custom Oligonucleotide Components by Type.” [Online]. Available: <https://www.trilinkbiotech.com/cart/Scripts/prodList.asp?idCategory=51>
- [58] A. Sassolas, B. D. Leca-Bouvier, and L. J. Blum, “DNA Biosensors and Microarrays,” *Chemical reviews*, vol. 108, pp. 109–139, 2008. [Online]. Available: <https://eng.ucmerced.edu/harmongroup/harmon.1/recently-completed-projects/iit-r-short-course-december-2011/lesson-7-water-sensors-and-emerging-sensor-technologies/biosensors-2008.pdf>
- [59] M. M. Mhlanga and S. Tyagi, “Using tRNA linked molecular beacons to image cytoplasmic mRNAs in live cells,” *Nature Protocols*, vol. 1, no. 3, pp. 1392–1398, nov 2006. [Online]. Available: <http://www.nature.com/doifinder/10.1038/nprot.2006.242>
- [60] [Www.circuitstoday.com](http://www.circuitstoday.com), “OhmMeter Circuit Using Arduino - Measure Resistance in LCD.” [Online]. Available: <http://www.circuitstoday.com/ohmmeter-using-arduino>
- [61] [Www.gebrateq.co.za](http://www.gebrateq.co.za), “About | Gebrateq cc | Advanced Engineering.” [Online]. Available: <http://www.gebrateq.co.za>
- [62] [Www.inqababiotec.co.za](http://www.inqababiotec.co.za), “Oligo Synthesis (Primers and Probes).” [Online]. Available: <http://www.inqababiotec.co.za/service/oligo-synthesis-primers-probes/>

- [63] Eu.idtdna.com, “Weblet Importer.” [Online]. Available: <https://eu.idtdna.com/calc/analyzer>
- [64] —, “Integrated DNA Technologies - Home.” [Online]. Available: <https://eu.idtdna.com/site>
- [65] Www.trilinkbiotech.com, “Dithiol Linker, DTPA.” [Online]. Available: <https://www.trilinkbiotech.com/cart/Scripts/prodView.asp?idproduct=6016>
- [66] Idtdna.com, “Integrated DNA Technologies.” [Online]. Available: <https://eu.idtdna.com/Site/Catalog/Modifications/Product/1474>
- [67] Eu.idtdna.com, “Iowa Black® Dark Quenchers.” [Online]. Available: <https://eu.idtdna.com/Site/Catalog/Modifications/Category/4>
- [68] N. Sarma, “Electrochemistry of DNA modified surfaces and sensing applications,” Masters, Indian Institute of Technology, 2006.
- [69] Www.trilinkbiotech.com, “dT-Ferrocene, 5-Ferrocene-Thymidine.” [Online]. Available: <https://www.trilinkbiotech.com/cart/Scripts/prodView.asp?idproduct=5649>
- [70] C. Fan, K. W. Plaxco, A. J. Heeger, C. Fan, K. W. Plaxco, and A. J. Heeger, “Electrochemical interrogation of conformational changes as a reagentless method for the sequence specific detection of DNA,” *PNAS*, vol. 100, no. 16, pp. 9134–9137, 2016.
- [71] S. V. John, L. S. Rotherham, M. Khati, B. B. Mamba, and O. A. Arotiba, “Towards HIV Detection: Novel Poly(propylene imine) Dendrimer-Streptavidin Platform for Electrochemical DNA and gp120 Aptamer Biosensors,” *Int. J. Electrochem. Sci. Int. J. Electrochem. Sci.*, vol. 9, no. 9, pp. 5425–5437, 2014.
- [72] Www.sciencedirect.com, “SYBR Green I - an overview | ScienceDirect Topics.” [Online]. Available: <http://www.sciencedirect.com/topics/nursing-and-health-professions/sybr-green-i>
- [73] M.blog.naver.com, “Real Time PCR Chemistry I : DNA binding fluorescent dye based Chemistry:.” [Online]. Available: <https://m.blog.naver.com/PostView.nhn?blogId=nanohelix&logNo=220418848583&proxyReferer=https%3A%2F%2Fwww.google.co.za%2F>
- [74] [Http://nptel.ac.in](http://nptel.ac.in), “Weblet Importer.” [Online]. Available: <http://nptel.ac.in/courses/102103013/module3/lec3/2.html>
- [75] Chroma.com, “Spectra Viewer | Chroma Technology Corp.” [Online]. Available: <https://www.chroma.com/spectra-viewer>

- [76] V. V. Didenko, *Fluorescent Energy Transfer Nucleic Acid Probes: Designs and Protocols*, V. V. Didenko, Ed., 2006. [Online]. Available: <http://www.springer.com/us/book/9781588293800>
- [77] W.-T. Liu, J.-H. Wu, E. S.-Y. Li, and E. S. Selamat, “Emission characteristics of fluorescent labels with respect to temperature changes and subsequent effects on DNA microchip studies.” *Applied and environmental microbiology*, vol. 71, no. 10, pp. 6453–7, oct 2005. [Online]. Available: <http://www.ncbi.nlm.nih.gov/pubmed/16204579>
- [78] Store.arduino.cc, “Arduino Nano.” [Online]. Available: <https://store.arduino.cc/arduino-nano>
- [79] Za.rs-online.com, “MAX7400ESA Maxim MAX7400ESA, Active Filter, Low Pass Filter, 8th Order Switched Capacitor 0.001 10kHz, 8 Pin SOIC Maxim.” [Online]. Available: <http://za.rs-online.com/web/p/active-filters/7861271/>
- [80] [Http://www.dropsens.com/](http://www.dropsens.com/), “...: DropSens ... Products.” [Online]. Available: <http://www.dropsens.com/>
- [81] [Http://www.dropsens.com](http://www.dropsens.com/), “Gold Nanoparticles modified Screen Printed Carbon Electrodes.” [Online]. Available: http://www.dropsens.com/en/pdfs_productos/new_brochures/110gnp-c1110gnp.pdf
- [82] —, “...: DropSens ... Screen-printed electrodes.” [Online]. Available: http://www.dropsens.com/en/screen_printed_electrodes_pag.html